

Ana Cláudia Paiva Santos

LAYER-BY-LAYER NANOPARTICLES DESIGNED TO IMPROVE THE BIOAVAILABILITY OF RESVERATROL

Tese de Doutoramento em Ciências Farmacêuticas, especialidade de Tecnologia Farmacêutica, orientada pelo Professor Doutor António José Ribeiro, pelo Professor Doutor Francisco José de Baptista Veiga e pelo Professor Doutor Carlos Alberto Fontes Ribeiro e apresentada à Faculdade de Farmácia da Universidade de Coimbra.

Novembro 2017



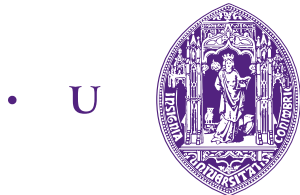
UNIVERSIDADE DE COIMBRA

LAYER-BY-LAYER NANOPARTICLES DESIGNED TO IMPROVE THE BIOAVAILABILITY OF RESVERATROL

Ana Cláudia Paiva Santos

Thesis submitted to the Faculty of Pharmacy of the University of
Coimbra for the attribution of the Doctor degree in
Pharmaceutical Sciences, in the speciality field of Pharmaceutical
Technology.

Tese apresentada à Faculdade de Farmácia da Universidade de
Coimbra para prestação de provas de Doutoramento em Ciências
Farmacêuticas, na especialidade de Tecnologia Farmacêutica.



FFUC FACULDADE DE FARMÁCIA
UNIVERSIDADE DE COIMBRA

LAYER-BY-LAYER NANOPARTICLES DESIGNED TO IMPROVE THE BIOAVAILABILITY OF RESVERATROL

The research work presented in this thesis was performed at the Laboratory of Development and Drug Technologies of the Faculty of Pharmacy of the University of Coimbra, Portugal, and at the Institute for Research and Innovation in Health Sciences (i3S), Porto, Portugal, under the supervision of Professor António Ribeiro and Professor Francisco Veiga from the Faculty of Pharmacy of the University of Coimbra, and Professor Carlos Fontes Ribeiro from the Faculty of Medicine of the University of Coimbra.

O trabalho experimental apresentado nesta tese foi elaborado no Laboratório de Desenvolvimento e Tecnologias do Medicamento da Faculdade de Farmácia da Universidade de Coimbra, Portugal, e no Instituto de Investigação e Inovação em Saúde (i3S), Porto, Portugal, sob a supervisão do Professor António Ribeiro e do Professor Francisco Veiga da Faculdade de Farmácia da Universidade de Coimbra, e do Professor Carlos Fontes Ribeiro da Faculdade de Medicina da Universidade de Coimbra.

This work was funded by national funds through the Portuguese Foundation for Science and Technology (FCT), specifically by the PhD grant SFRH/BD/109261/2015, through the QREN - POPH/FSE program.

Este trabalho foi financiado por fundos nacionais através da Fundação para a Ciência e Tecnologia (FCT), especificamente pela bolsa de doutoramento SFRH/BD/109261/2015, através do programa QREN - POPH/FSE.



Front cover:

Layer-by-Layer self-assembled poly(allylamine hydrochloride)/ dextran sulfate (respectively, orange and purple coating layers) nanoparticle of core-encapsulated resveratrol (red).

*AOS MEUS AVÔS,
Luiz (In memoriam)
e
Paiva.*

“Valeu a pena? Tudo vale a pena
Se a alma não é pequena.
Quem quer passar além do Bojador
Tem que passar além da dor.
Deus ao mar o perigo e o abismo deu,
Mas nele é que espelhou o céu.”

Fernando Pessoa

“Para ser grande, sê inteiro: nada

Teu exagera ou exclui.

Sê todo em cada coisa. Põe quanto és

No mínimo que fazes.

Assim em cada lago a lua toda

Brilha, porque alta vive.”

Odes de Ricardo Reis. Fernando Pessoa

Acknowledgments / Agradecimentos

Ao Professor Doutor António Ribeiro, gostaria de agradecer a pronta disposição com que me acolheu no primeiro dia para levar este desafio a bom porto. Não esqueço a disponibilidade com que me recebeu, muitas vezes em horários menos acessíveis, sobretudo quando eu ainda trabalhava fora da faculdade aquando do início do doutoramento. Obrigada pelo incentivo. Não tenho dúvidas de que constitui um pilar assertivo no meu crescimento ao longo deste percurso.

Ao Professor Doutor Francisco Veiga, estou e estarei inteiramente grata pela confiança depositada em mim, pelo constante incentivo e incansável acompanhamento, bem como pelos tantos e admiráveis ensinamentos e conselhos que sempre tão genuinamente, e em tempo útil, me concedeu. O Professor Francisco é uma pessoa especialmente completa, com qualidades profissionais e humanas raras e inspiradoras, que fazem dele um exemplo. Porque só com um orientador excepcional é possível chegar ao fim, a si lhe devo a exequibilidade deste percurso. Muito obrigada.

Ao Professor Doutor Carlos Fontes Ribeiro, o meu reconhecido obrigado por ter abraçado este projeto comigo. Obrigada pela sua disponibilidade em receber-me e ajudar-me sempre que necessário.

To Professor Yuri M. Lvov, I thoroughly acknowledge the valuable contribute to this work, as well as the constant encouragement. Professor Lvov holds an impressive expertise, wisdom, dedication and professionalism, and it is therefore an honor for me to have the opportunity to work with him. Thank you very much.

Ao Professor Doutor Ricardo Castro, gostaria de expressar o meu profundo agradecimento, face à sua permanente disponibilidade, simpatia e profissionalismo com que sempre me recebe. A sua vontade em partilhar o saber, e até em aprender, é absolutamente motivante. Muito obrigada.

À Professora Doutora Eliana Souto, gostaria de agradecer a confiança para levar a cabo as mais diversas tarefas. Estou verdadeiramente agradecida por todos os ensinamentos facultados, bem como as oportunidades concedidas.

Ao Professores Doutores João José Sousa e Maria Eugénia Pina, agradeço a simpatia e também a disponibilidade prestada sempre que foi necessário.

Aos meus colegas de doutoramento, colegas doutorados, investigadores, alunos e funcionários da Faculdade de Farmácia da Universidade de Coimbra que me acompanharam ao longo do meu doutoramento, desculpem-me, em primeiro lugar, a retirada dos títulos, e aceitem sinceramente o meu maior obrigado. Todos vós, das mais variadas formas, fizeram parte do pacote essencial de renovação de energia diária ao longo das imensas horas do dia passadas na faculdade. Muito obrigada.

Amélia Vieira e Célia Cabral, a vós muito agradeço a atenção e paciência que sempre amavelmente tiveram para expedita e cientificamente responder às questões que vos coloquei, bem como o apoio que me foram dando. Obrigada pela vossa competência e profissionalismo, sem nunca descurar o vosso lado amigo.

Carla Vitorino, durante algum tempo “colega de secretária”, para além do companheirismo, gostaria de agradecer-te pela integração no laboratório e apoio.

Carolina Macedo, Gustavo Costa, Eliana Simões, Joana Almeida e Sousa, Joana Bicker, João Abrantes, Margarida Miranda, Mariana Magalhães, Raquel Teixeira, Rita Figueiras, Nuno Ricardo Ferreira, Samantha Soares, Sandra Jesus e Sónia Pereira gostaria também de manifestar o meu muito obrigado pelo espírito de companheirismo.

Aos meus recentes e irrepreensíveis colegas de gabinete: Diogo Fonseca e Victoria Bell. Vocês dão vida ao espaço mais simpático da nossa faculdade! Muito obrigada.

Ana Isabel Simões, Aleksandra Zielińska, Alessandra Ribeiro, Irina Pereira, Joana Sequeira, Mar González e querida Raquel Pinho, colegas, amigas, que levo comigo na bagagem. Vocês são adoráveis; cada uma a seu jeito! (Aleksa e Mar, eu sei que não iriam gostar que escrevesse esta parte sem ser em português!).

Adryana Clementino, Andreia Santos, Gabrielle Pereira, Mariana Caldas, Markus Weis, Mayra Fedalto, Valker Feitosa, Liliana Damas, Diogo Oliveira, Myriam Lamrayah, Raquel Vieira e Rita Rodrigues, alunos com quem tive a fabulosa experiência de partilhar o que sabia. Convosco aprendi imenso, não tivessem sido vocês motivo de desafio constante!

À *D. Gina*, fonte perene de calor humano e de profissionalismo. Obrigada por ser uma segunda “mãe” fora da zona de conforto para todos nós que caímos abruptamente descalços em novo terreno. Que continue sempre assim, como é. O seu apoio e carisma foram essenciais para mim: muito obrigada.

Gostaria também de fazer um agradecimento dirigido à Joana Cunha e à Joana Loureiro do IBMC-i3S, da Faculdade de Farmácia da Universidade do Porto, pela disponibilidade e amabilidade com que me receberam.

In addition, I would like to give a special word of thanks to Pravin Pattekari, who kindly shared his knowledge and scientific visions with me during this journey. Together we've reached further.

No que diz respeito ao meu círculo de amigos próximos, gostaria manifestamente de direcionar-me:

À Filipa, amiga de TODAS as horas, e mais umas quantas incontáveis, obrigada por estares sempre comigo. És o meu “cantinho de conforto” e só consigo sentir-me verdadeiramente privilegiada por isto. Devo a Coimbra esta amizade, que consegue ficar todos os dias ainda mais forte. Obrigada por seres a pessoa especial que és, minha Fipas. À Sara, obrigada pelo cuidado e carinho com que sempre especialmente me trataste, bem como a confiança e consideração desiguais que sempre e à viva força depositaste em mim. És e serás sempre uma pessoa muito querida. À Cristina, por ser tão energeticamente positiva e singularmente motivadora. Obrigada! À Joana Ganço, obrigada por fomentares em mim o gosto pelas atividades extracurriculares, que deveriam ser obrigatórias mas infelizmente não são!, e que me salvaram muitas vezes da monotonia dos dias de semana. Amiga e colega de curso, muitos sorrisos e bons momentos a ti associo. Obrigada, Ju! À Inês, a amiga que mais quilómetros fez para vir ter comigo a Coimbra! Obrigada, Ness. Ao João Casalta e à Joana Soares, obrigada pela maravilhosa amizade e pela ajuda nos momentos de maior S.O.S.. Conto convosco para as próximas e mais diversas etapas. (Joaninha, está quase; e João... eu sei que também irá acontecer).

Por fim, e não de somenos importância, gostaria de agradecer:

À minha tia Celeste: a tua tranquilidade é impressionante. Obrigada pela tua constante preocupação e assídua presença, mesmo estando separadas pelo Atlântico.

Ao meu tio e padrinho, José Paiva, obrigada pela calma e firmeza que me foste transmitindo. A tua capacidade de lidar com os demais é um exemplo digno de ser apreciado.

Aos meus avós: Ao Luiz, *In memoriam*, esta tese é-te dedicada desde o primeiro dia. Tenho saudades tuas. Ao Paiva, que me permitiu enveredar por esta estrada. Obrigada, de coração, avô. À Cecília por todo o amor diário desde há 31 anos. À Floripes, obrigada pelo teu cuidado e constante preocupação desde sempre.

Aos Meus Pais, e também ao meu Irmão, obrigada pela vossa dedicação e apoio. Obrigada pelas ferramentas essenciais que me forneceram e que me permitiram desbravar tantos caminhos. Tanto esta, como as conquistas anteriores, são também vossas: parabéns! Agradeço-vos enquanto a memória não me falhar, pois eu sou aquilo que vocês educaram e que permitiram que eu fosse. Muito obrigada.

Ao Pedro, obrigada por teres acreditado irredutivelmente sempre em mim, bem como pela tua inteira compreensão. A tua integridade e perseverança fazem parte da minha maturação a muitos níveis. Muito obrigada, “(tu)”, por teres a coragem de continuar a impulsionar-me em direção às minhas irreverências, e por caminhares a meu lado.

Em suma, este texto surge como um conjunto coeso de palavras que, sendo certo que são profundamente sentidas, também não são menos doseadas, pois seria inexequível transmitir por escrito a gratidão que sinto neste momento. Estou muito feliz. E é isto que levo, como nos diz a canção de Coimbra, “*comigo p’rá vida*”!

MUITO OBRIGADA!

THANK YOU!

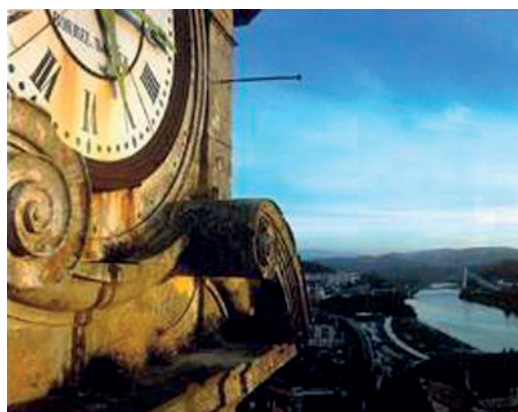


Table of contents

| | |
|--|-----------|
| List of Abbreviations | xxiii |
| List of Figures | xxvii |
| List of Tables..... | xxxii |
| List of Publications..... | xxxiii |
| Abstract..... | xxxv |
| Resumo | xxxix |
| Chapter 1 - General Introduction..... | 1 |
| 1.1. Motivation..... | 3 |
| 1.2. Objectives and outline..... | 5 |
| 1.3. Resveratrol..... | 7 |
| 1.4. Pharmacokinetics of resveratrol | 13 |
| 1.5. Evaluation of the efficacy of resveratrol..... | 23 |
| 1.6. Resveratrol delivery systems..... | 27 |
| 1.6.1. Classical pharmaceutical dosage forms..... | 28 |
| 1.6.2. New delivery systems | 28 |
| 1.6.2.1. Macromolecular drug carriers..... | 30 |
| 1.6.2.2. Particulate drug delivery | 31 |
| 1.6.2.2.1. Microencapsulation..... | 31 |
| 1.6.2.2.2. Cyclodextrins | 32 |
| 1.6.2.2.3. Solid lipid nanoparticles..... | 34 |
| 1.6.2.2.4. Liposomes | 34 |
| 1.6.2.2.5. Acoustically active lipospheres | 35 |
| 1.6.2.2.6. Nanoparticles..... | 35 |
| 1.7. Layer-by-Layer coated drug-core nanoparticles as versatile delivery platforms..... | 39 |
| 1.7.1. Drug candidates for Layer-by-Layer nanoencapsulation | 41 |
| 1.7.2. Preparation of drug nanocore templates..... | 45 |

| | |
|---|-----------|
| 1.7.2.1. Top-down approaches | 46 |
| 1.7.2.1.1. Sonication-assisted disintegration..... | 46 |
| 1.7.2.1.2. Wet media milling..... | 47 |
| 1.7.2.2. Bottom-up approaches | 48 |
| 1.7.2.2.1. Nanoprecipitation from organic solvents | 48 |
| 1.7.2.2.2. Nanoprecipitation through pH change..... | 49 |
| 1.7.2.2.3. Solvent evaporation/emulsification..... | 50 |
| 1.7.2.2.4. Spray drying | 51 |
| 1.7.2.3. Comparison between top-down and bottom-up approaches | 52 |
| 1.7.3. Layer-by-Layer coating materials..... | 52 |
| 1.7.3.1. Polyelectrolytes | 56 |
| 1.7.3.2. Advanced functional coatings..... | 57 |
| 1.7.3.3. Outermost layer functionalization..... | 57 |
| 1.7.4. Layer-by-Layer coating procedure..... | 59 |
| 1.7.4.1. Intermediate washings..... | 61 |
| 1.7.4.2. Washless approaches | 62 |
| 1.7.5. Controlled drug release | 63 |
| 1.7.5.1. Natural permeability of the LbL shells..... | 65 |
| 1.7.5.1.1. Number of layers | 65 |
| 1.7.5.1.2. Deposition conditions | 65 |
| 1.7.5.2. Stimuli-responsive permeability of the LbL shells | 66 |
| 1.7.5.2.1. pH..... | 67 |
| 1.7.5.2.2. Temperature | 67 |
| 1.7.6. Stability enhancement..... | 68 |
| 1.7.6.1. Chemical stability..... | 68 |
| 1.7.6.2. Colloidal stability | 68 |
| 1.7.7. <i>In vitro</i> studies | 69 |
| 1.7.8. <i>In vivo</i> studies..... | 73 |
| References | 77 |

| | |
|---|-----|
| Chapter 2 - Sonication-assisted Layer-by-Layer assembly for low soluble drug nanoformulation | 97 |
| 2.1. Abstract | 99 |
| 2.2. Introduction | 103 |
| 2.3. Materials and methods | 106 |
| 2.3.1. Materials..... | 106 |
| 2.3.2. Methods..... | 106 |
| 2.3.2.1. Nanoparticles preparation..... | 106 |
| 2.3.2.2. Particle size analysis..... | 106 |
| 2.3.2.3. Zeta potential analysis..... | 107 |
| 2.3.2.4. Microscopic analysis..... | 107 |
| 2.3.2.5. Determination of drug encapsulation efficiency..... | 108 |
| 2.3.2.6. Stability studies..... | 108 |
| 2.3.2.7. <i>In vitro</i> drug release assays at <i>sink</i> conditions..... | 108 |
| 2.3.2.8. Cytotoxicity MTT assay..... | 109 |
| 2.3.3. Statistical analysis..... | 109 |
| 2.4. Results and discussion | 111 |
| 2.4.1. Layer-by-Layer preparation and characterization of ibuprofen nanoparticles..... | 112 |
| 2.4.1.1. Titrations of polyelectrolytes concentrations..... | 112 |
| 2.4.1.2. Zeta potential..... | 117 |
| 2.4.1.3. Particle size..... | 118 |
| 2.4.2. Nanoparticle imaging..... | 119 |
| 2.4.3. Encapsulation efficiency..... | 121 |
| 2.4.4. Stability studies..... | 122 |
| 2.4.5. <i>In vitro</i> release studies..... | 122 |
| 2.4.6. Cytotoxicity assays..... | 126 |
| 2.5. Conclusions | 129 |
| References | 131 |

| | |
|---|-----|
| Chapter 3 - Sonication-assisted Layer-by-Layer self-assembly nanoparticles for resveratrol oral delivery | 137 |
| 3.1. Abstract | 139 |
| 3.2. Introduction | 143 |
| 3.3. Materials and methods | 147 |
| 3.3.1. Materials..... | 147 |
| 3.3.2. Methods..... | 147 |
| 3.3.2.1. Nanoparticles preparation..... | 147 |
| 3.3.2.2. Zeta potential analysis..... | 148 |
| 3.3.2.3. Particle size analysis..... | 148 |
| 3.3.2.4. Microscopic analysis..... | 148 |
| 3.3.2.5. Encapsulation efficiency | 149 |
| 3.3.2.6. Stability studies | 150 |
| 3.3.2.7. In phase solubility and <i>in vitro</i> release assays..... | 150 |
| 3.3.2.8. <i>In vitro</i> cytotoxicity assay | 151 |
| 3.3.3. Statistical analysis | 151 |
| 3.4. Results and discussion | 153 |
| 3.4.1. Layer-by-Layer resveratrol nanoparticles preparation | 154 |
| 3.4.1.1. Polyelectrolyte titrations – washless approach | 154 |
| 3.4.1.2. Zeta potential and particle size | 162 |
| 3.4.2. Nanoparticle imaging..... | 163 |
| 3.4.3. Encapsulation efficiency..... | 165 |
| 3.4.4. Stability studies | 166 |
| 3.4.4.1. Colloidal stability | 166 |
| 3.4.4.2. Chemical stability..... | 167 |
| 3.4.5. <i>In vitro</i> release studies | 168 |
| 3.4.6. <i>In vitro</i> cytotoxicity assay..... | 171 |
| 3.5. Conclusions | 175 |
| References | 177 |

| | |
|---|------------|
| Chapter 4 - Pharmacokinetic applicability of a liquid chromatographic method for first-time orally administered resveratrol-loaded Layer-by-Layer nanoparticles to rats..... | 183 |
| 4.1. Abstract..... | 185 |
| 4.2. Introduction..... | 189 |
| 4.3. Materials and methods..... | 192 |
| 4.3.1. Materials..... | 192 |
| 4.3.2. Methods..... | 192 |
| 4.3.2.1. Resveratrol stability studies under physiological gastrointestinal conditions..... | 192 |
| 4.3.2.1.1. Resveratrol solubility..... | 192 |
| 4.3.2.1.2. Chemical resveratrol stability..... | 193 |
| 4.3.2.2. Formulation of Layer-by-Layer nanoparticles..... | 194 |
| 4.3.2.3. Concentration of the Nanoparticles for <i>in vivo</i> administration..... | 194 |
| 4.3.2.4. Development and validation of the HPLC-DAD bioanalytical method..... | 195 |
| 4.3.2.4.1. Preparation of stock solutions, calibration standards and quality control samples..... | 195 |
| 4.3.2.4.2. Obtainment of blank rat plasma..... | 195 |
| 4.3.2.4.3. Sample preparation procedure..... | 196 |
| 4.3.2.4.4. HPLC-DAD instrumentation and analytical conditions..... | 196 |
| 4.3.2.4.5. Validation of the HPLC method..... | 197 |
| 4.3.2.4.5.1. Selectivity..... | 197 |
| 4.3.2.4.5.2. Linearity..... | 197 |
| 4.3.2.4.5.3. Limits of quantification and detection..... | 197 |
| 4.3.2.4.5.4. Precision and accuracy..... | 198 |
| 4.3.2.4.5.5. Recovery..... | 198 |
| 4.3.2.4.5.6. Stability..... | 198 |
| 4.3.2.5. <i>In vivo</i> pharmacokinetic studies in rat..... | 198 |
| 4.3.2.5.1. Animals..... | 199 |
| 4.3.2.5.2. Pharmacokinetic study – oral administration..... | 199 |

| | |
|---|------------|
| 4.3.2.5.3. Pharmacokinetic analysis | 200 |
| 4.3.2.6. Statistical analysis | 200 |
| 4.4. Results and discussion | 201 |
| 4.4.1. Resveratrol stability studies under physiological gastrointestinal conditions | 201 |
| 4.4.2. Optimization of the concentration of the nanoparticles for <i>in vivo</i> administration..... | 202 |
| 4.4.3. Development and validation of the HPLC-DAD bioanalytical method | 204 |
| 4.4.3.1. Development and optimization of chromatographic method..... | 204 |
| 4.4.3.2. Sample preparation procedure | 207 |
| 4.4.3.3. Validation | 208 |
| 4.4.3.3.1. Specificity, calibration, linearity, LOQ and LOD..... | 209 |
| 4.4.3.3.2. Precision and accuracy | 210 |
| 4.4.3.3.3. Recovery and matrix effects | 211 |
| 4.4.3.3.4. Stability..... | 211 |
| 4.4.4. Evaluation of the bioavailability of nanoparticles – pharmacokinetic study | 212 |
| 4.5. Conclusions | 221 |
| References | 223 |
| Chapter 5 - Concluding remarks and future perspectives | 229 |
| 5.1. Concluding remarks | 231 |
| 5.2. Future perspectives | 235 |

List of Abbreviations

| | |
|-----------------------------|---|
| AAL | Acoustically active liposphere |
| AMPK | AMP-activated protein kinase |
| AUC | Area under the concentration-time curve (plasma exposure) |
| AUC_{0-t} | Area under the concentration time-curve from time zero to the last measurable drug concentration |
| AUC_{0-∞} | Area under the concentration time-curve from time zero to infinity |
| AUC_{extrap} | Area under the concentration time-curve extrapolated from the time of the last measurable concentration to infinity |
| Aβ40 | Amyloid beta 40 |
| Aβ42 | Amyloid beta 42 |
| Aβ – β | Amyloid peptide |
| B6C3F1/J | Hybrid strain of a laboratory mouse |
| BBB | Blood brain barrier |
| BCS | Biopharmaceutical classification system |
| BSA | Bovine serum albumin |
| CAS | Chemical abstracts service registry number |
| CBZ | Carbamazepin |
| CD | Cyclodextrin |
| CI | Confidence interval |
| C_{last} | Last quantifiable drug plasma concentration |
| C_{max} | Maximum concentration |
| CMC | Carboxymethylcellulose |
| COX-1 | Cyclo-oxygenase-1 |
| COX-2 | Cyclo-oxygenase-2 |
| c-PCD | <i>Cis</i> -piceid |
| c-RSV | <i>Cis</i> -resveratrol |
| CV | Coefficient of variation |
| cβG | Cytosolic-β-glucosidase |
| DHR | Dihydroresveratrol |
| dihRSV | Dihydroresveratrol |
| DLS | Dynamic light scattering |
| DMEM | Dulbecco's modified eagle medium |
| DMSO | Dimethyl sulfoxide |
| DS | Dextran sulfate |

| | |
|---------------------------------|--|
| EGCG | Epigallocatequin-3-gallate |
| ELS | Electrophoretic light scattering |
| EPR | Enhanced permeability and retention |
| FBS | Fetal bovine serum |
| FITC | Fluorescein isothiocyanate |
| GFP | Green fluorescent protein |
| GI | Gastrointestinal |
| GMR | Geometric mean ratio |
| GRAS | Generally recognized as safe |
| HDL | High density lipoprotein |
| HPLC | High-performance liquid chromatography |
| HPLC-DAD | High-performance liquid chromatography - diode array detection |
| HP-β-CD | Hydroxypropyl- β -cyclodextrin |
| HSA | Human serum albumin |
| IBF | Ibuprofen |
| IC₅₀ | Half maximal inhibitory concentration |
| IL-4 | Interleukin-4 |
| <i>I</i>_{ERG} | Inactivating inward-rectifying current |
| <i>I</i>_{DR} | Slowly inactivating delayed rectifier current |
| <i>I</i>_{Na} | Sodium current |
| IS | Internal standard |
| <i>k</i>_e | Apparent elimination rate constant |
| LbL | Layer-by-Layer |
| LDL | Low-density lipoprotein |
| LLE | Liquid-liquid extraction |
| LOD | Limit of detection |
| logP_{o/w} | 1-octanol/water partition coefficient |
| LOQ | Limit of quantification |
| LPH | Lactase phlorizin hydrolase |
| MAP | Mitogen-activated protein |
| MMP2 | Matrix metalloproteinase-2 |
| MMP9 | Matrix metalloproteinase-9 |
| MRP3 | Multidrug resistance-associated protein 3 |
| MPS | Mononuclear phagocytic system |
| MRT | Mean residence time |

| | |
|--------------------|--|
| MTT | 3-(4,5-dimethylthiazol-2-yl)-2,5-diphenyltetrazolium bromide |
| MWCO | Molecular weight cut-off |
| NA | Not available |
| NO | Nitric oxide |
| NP | Nanoparticle |
| Nrf2 | Nuclear factor (erythroid-derived 2)-like 2 |
| NSAID | Nonsteroidal anti-inflammatory drug |
| PAA | Poly(acrylic acid) |
| PAH | Poly(allylamine hydrochloride) |
| PBS | Phosphate buffered solution |
| PCD | Piceid |
| PDDA | Poly(diallyldimethylammonium chloride) |
| PDI | Polydispersity index |
| PE | Polyelectrolyte |
| PEG | Poly(ethylene glycol) |
| PEGylated | Polyethyleneglycolated |
| PEI | Poly(ethylenimine) |
| PF 68 | Pluronic F68 |
| PK | Pharmacokinetic |
| PLA | Poly(L-arginine) |
| PLB16-5 | Block-copolymers of poly-L-lysine with polyethylene glycol |
| PLCL | Poly(lactide- <i>co</i> -epsilon-caprolactone) |
| PLGA | Poly(lactic- <i>co</i> -glycolic acid) |
| PLL | Poly(L-lysine) |
| PLL-g-PEG | Poly(ethylene glycol) grafted to poly(L-lysine) |
| PMA | Poly(methacrylic acid) |
| PNIPAM | Poly(N-isopropylacrylamide) |
| PS | Protamine sulfate |
| PSS | Poly(styrene sulfonate) |
| PSSCMA | Poly(4-styrenesulfonic acid- <i>co</i> -maleic acid) sodium salt |
| PTEN (gene) | Phosphatase and tensin homolog (gene) |
| PVA | Poly(vinyl alcohol) |
| PVP | Polyvinylpyrrolidone |
| PVP K17 | Polyvinylpyrrolidone 17 PF |
| PVS | Poly(vinyl sulfate) |

| | |
|---------------------------------|---|
| QC | Quality control |
| QC1 | Low quality control |
| QC2 | Medium quality control |
| QC3 | High quality control |
| RM-β-CD | Randomly methylated β -cyclodextrin |
| ROS | Radical oxygen species |
| RSV | Resveratrol |
| Rt | Retention time |
| SD | Standard deviation |
| SEM | Scanning electron microscopy |
| S.E.M. | Standard error of the mean |
| SGF | Simulated gastric fluid |
| SGLT1 | Sodium-glucose cotransporter 1 |
| SIF | Simulated intestinal fluid |
| SIRT1 | Silent information regulator 1 |
| SLE₂S | Sodium lauryl ethersulphate |
| SLN | Solid lipid nanoparticle |
| ST | Sulfotransferase |
| S100B | S100 calcium-binding protein B |
| TEM | Transmission electron microscopy |
| T_f | Tailing factor |
| t_{max} | Time to achieve the maximum concentration |
| TNF-α | Tumor necrosis factor- α |
| <i>t</i>-PCD | <i>Trans</i> -piceid |
| TPGS | D- α -tocopherol polyethylene glycol 400 succinate |
| TPP | Triphosphate |
| <i>t</i>-RSV | <i>Trans</i> -resveratrol |
| t_{1/2} | Apparent terminal elimination half-life |
| UGT | Uridine 5'-diphospho-glucuronosyltransferase |
| USP | United States Pharmacopeia |
| UV | Ultraviolet |
| VLDL | Very low-density lipoprotein |
| α-CDs | α - Cyclodextrin |
| β-CDs | β - Cyclodextrin |
| γ-CDs | γ - Cyclodextrin |

List of Figures

Chapter 1

- Figure 1.1:** Chemical structure of **(a)** *trans*-RSV, **(b)** *cis*-RSV, **(c)** piceid, **(d)** RSV-3-sulfate and **(e)** dihydroRSV.8
- Figure 1.2:** Oral pharmacokinetics of RSV, piceid (full arrows), and their derivatives (dashed arrows).15
- Figure 1.3:** Scheme of modular technology combination of drug nanocore-based delivery platform of LbL NPs.41
- Figure 1.4:** Top-down and bottom-up approaches used to prepare drug nanocores, prior the application of the LbL coating technology.46
- Figure 1.5:** LbL coating procedures: intermediate washings or washless approaches.61

Chapter 2

- Figure 2.1:** Schematic presentation of LbL NPs formation from low soluble drugs by washless top-down LbL PE assembly.111
- Figure 2.2:** Zeta potential against PE concentration for 0.5 mg/mL IBF NPs. Four sequential steps of polycation/polyanion deposition are shown in the stepwise addition of **(a)** PAH to IBF nanocores, **(b)** PSS to IBF-PAH NPs, **(c)** PAH to IBF-(PAH/PSS) NPs, and **(d)** PSS to IBF-(PAH/PSS)_{1.5} NPs.112
- Figure 2.3:** The particle size of IBF cores, with ca. 72 μm of initial particle size, in response to sonication time. PAH was present in solution for the first polymeric monolayer on the IBF nanocores surface and prevented particle aggregation after the removal of ultrasound.113
- Figure 2.4:** (●) Particle size and (○) zeta potential changes of IBF LbL NPs prepared with **(a)** 2.5, **(b)** 5.5 and **(c)** 7.5 bilayered coatings of PAH/PSS for 14 days at 25 °C.116
- Figure 2.5:** Zeta potential changes of IBF coated up to 7.5 coating bilayers, IBF-(PAH/PSS)_{7.5}, during process shell assembly, by top-down and washless approach.117

| | |
|--|-----|
| Figure 2.6: Particle size measurements of IBF coated up to 7.5 coating bilayers, IBF-(PAH/PSS) _{7.5} , during process shell assembly, by top-down and washless approach..... | 118 |
| Figure 2.7: SEM image of (a) IBF native micrometer-sized crystals (x220) and (b) IBF LbL NPs with a IBF-(PAH/PSS) _{5.5} coating shell (x4500). Confocal fluorescent image of an aqueous dispersion of LbL IBF NPs coated with (c) FITC-labelled PAH with a IBF-(PAH/PSS) _{5.5} coating shell and (d) with 5 min of sonication exposure, in order to obtain higher-sized particles (microparticles). | 120 |
| Figure 2.8: <i>In vitro</i> IBF release from (■) non-encapsulated crystals of IBF, and IBF LbL NPs prepared with (●) 2.5, (▲) 5.5 and (◆) 7.5 bilayered coatings of PAH/PSS in (a) simulated gastric pH 1.2 fluid and (b) simulated intestinal pH 6.8 fluid in <i>sink</i> conditions at 37 °C. Data represent mean ± SD, n = 3..... | 123 |
| Figure 2.9: Cell viability of Caco-2 cells after 24h of incubation with (●) 2.5, (■) 5.5 and (▲) 7.5 LbL bilayered coated PAH/PSS NPs for concentrations ranging from 11.7 µg/mL to 1500 µg/mL. Cell viability of each sample was determined using MTT assay. Data are expressed as mean ± S.E.M. (n = 3). *p < 0.05 for the 2.5 bilayered NPs comparing to 5.5 and 7.5 bilayered LbL NPs. | 127 |

Chapter 3

| | |
|--|-----|
| Figure 3.1: Schematic presentation of RSV-loaded LbL NPs preparation using a washless bottom-up LbL PE assembly..... | 154 |
| Figure 3.2: Zeta potential and particle size measurements against the PE concentration for 0.5 mg/mL RSV nanocores during PE titration procedures. Four sequential titrations referring to a polycation or a polyanion deposition are depicted in the stepwise addition of: (a) PAH to RSV nanocores, (b) DS to RSV-PAH NPs, (c) PAH to RSV-(PAH/DS) NPs, and (d) DS to RSV-(PAH/DS) _{1.5} NPs. | 156 |
| Figure 3.3: Diagram representing the distinct stages of a typical PE titration procedure, arising from the addition of a positively charged PE upon a negatively charged colloidal surface, emphasizing the isoelectric point and the onset point of the titration..... | 159 |

- Figure 3.4:** Zeta potential **(a)** and particle size **(b)** measurements of RSV nanocores and RSV-loaded LbL NPs with 2.5, 5.5 and 7.5 PAH/DS bilayers during the sequential build-up of the LbL shell, by the developed bottom-up and washless approach..... 160
- Figure 3.5:** Colloidal stability of **(a)** RSV nanocores and RSV-loaded LbL NPs with **(b)** 2.5, **(c)** 5.5 and **(d)** 7.5 PAH/DS bilayers. The particle size (●) and zeta potential (○) variations were assessed during 30 days at 25 °C..... 161
- Figure 3.6:** Representative image of **(a)** RSV native micrometer-sized crystals (x500) evaluated by SEM; RSV LbL NPs with a RSV-(PAH/DS)_{5.5} coating shell evidenced by **(b)** SEM (x5500) and **(c)** TEM (x98000). Confocal fluorescent image of RSV-(PAH/DS)_{5.5} NPs coated with FITC-labelled PAH **(d)**. 165
- Figure 3.7:** *In vitro* RSV release studies from non-encapsulated native crystals of RSV (■), RSV nanocores (□), and RSV-loaded LbL NPs prepared with 2.5 (●), 5.5 (▲) and 7.5 (◆) bilayered coatings of PAH/PSS in (a) simulated gastric pH 1.2 fluid and (b) simulated intestinal pH 6.8 fluid in *sink* conditions at 37 °C. Data represent mean ± SD, n = 3..... 169
- Figure 3.8:** Cell viability of Caco-2 cells after 24h of incubation with RSV native crystals (■), RSV nanocores (□) and RSV-loaded LbL NPs coated with 2.5 (●), 5.5(▲) and 7.5 (◆) PAH/DS bilayers for concentrations varying from 11.7 µg/mL to 1500 µg/mL. Cell viability of each sample was assessed by MTT assay. Data are shown as mean ± S.E.M (n = 3)..... 172

Chapter 4

- Figure 4.1:** Chemical stability of RSV in SGF **(a)** and SIF **(b)** with enzymes at 37 °C. The levels of RSV were monitored up to 24 h under the previous conditions. Results are expressed as the percentage of initial RSV ± SD (n = 3)..... 202
- Figure 4.2:** Chromatograms of RSV and IS, respectively, from left to right, both at 20 µg/mL, resulting from the use of different mobile phase mixture compositions, containing methanol – potassium dihydrogen phosphate buffer (adjusted to pH 3.8 with acetic acid 3%; 10 mM) – acetonitrile, (v/v/v)..... 207

Figure 4.3: Typical chromatograms of extracted rat plasma: **(A)** blank plasma; **(B)** plasma spiked with the IS and analyte RSV at LOQ concentration; **(C)** plasma spiked with IS and the analyte RSV at the intermediate concentration of the calibration range. 209

Figure 4.4: Representative chromatograms of plasma samples obtained from rats treated with: **(A)** free RSV; **(B)** RSV nanocores and **(C)** RSV-loaded LbL NPs after oral administration. 212

Figure 4.5: Concentration-time profiles of RSV following oral free RSV (■), nanocores (●) and RSV LbL NPs (○) administration (20 mg/kg) to rats. Symbols represent the mean values ± S.E.M. of three to five determinations per time point (n = 3-5)..... 213

List of Tables

Chapter 1

| | |
|--|----|
| Table 1.1: Biological activities of resveratrol (RSV) and respective physiological mechanisms. | 11 |
| Table 1.2: Results obtained in human pharmacokinetics studies following oral administration of RSV-based formulations (RSV administered amount (milligrams) was calculated with reference to the average adult human weight of 70 kg). | 18 |
| Table 1.3: Results obtained in studies that reported: cytotoxic properties against three breast cancer cell lines (MCF-7, ZR-75-1 and MDA-MB-231); effect on membrane potential of F-11 neuroblastoma cells line; antioxidant activity; inhibition of melanin production of RSV and its derivatives. | 25 |
| Table 1.4: Characteristics of new delivery systems for RSV, particularly with regard to stability, solubility and release of RSV. | 29 |
| Table 1.5: Drug-based nanocores, intended for subsequent LbL coating, prepared by top-down and bottom-up approaches. | 42 |
| Table 1.6: LbL-coated drug nanocore-based NPs obtained by intermediate washing or washless PE coating approaches..... | 54 |
| Table 1.7: <i>In vitro</i> studies regarding the application of LbL self-assembly nanotechnology. | 70 |
| Table 1.8: <i>In vivo</i> study regarding the application of LbL-coated drug nanocore-based NPs. | 74 |

Chapter 2

| | |
|---|-----|
| Table 2.1: Particle size, zeta potential and encapsulation efficiency of IBF crystals and IBF LbL-coated NPs. Data represent mean \pm SD, n = 3..... | 121 |
|---|-----|

Chapter 3

| | |
|---|-----|
| Table 3.1: The particle size, polydispersity index, zeta potential and encapsulation efficiency of the studied nanoformulations: RSV nanocores and LbL NPs Data represent mean \pm SD, n = 3. | 154 |
|---|-----|

Chapter 4

| | |
|---|-----|
| Table 4.1: Chemical structure and relevant physicochemical and biological properties characteristics of RSV to take into account while designing a drug delivery system. | 190 |
| Table 4.2: Values of R_t , area, height, and T_f for each chromatogram of RSV (20 $\mu\text{g}/\text{mL}$) and IS (20 $\mu\text{g}/\text{mL}$), by using different mobile phase compositions (methanol – potassium dihydrogen phosphate buffer (adjusted to pH 3.8 with acetic acid 3%; 10 mM) – acetonitrile (v/v/v)). | 206 |
| Table 4.3: Calibration parameters (mean values) of the developed HPLC-DAD method employed for the quantification of RSV in rat plasma. | 210 |
| Table 4.4: Inter- and intra-day precision (% CV) and accuracy (% Bias) of RSV in rat plasma samples at the LOQ, low (QC1), medium (QC2) and high (QC3) concentrations of the calibration ranges. | 210 |
| Table 4.5: Absolute recovery of RSV from rat plasma using the optimized sample pre-treatment and extraction protocol, by using the low (QC1), medium (QC2) and high (QC3) concentrations of the calibration ranges. | 211 |
| Table 4.6: Stability (values in percentage) of RSV under different conditions of sample handling and storage. | 212 |
| Table 4.7: Mean pharmacokinetic parameters of RSV in plasma after single oral administration of free RSV suspension, nanocores and LbL NPs to rats in the dose of 20 mg/kg. | 214 |
| Table 4.8: Point estimates and 90% confidence intervals for the comparison of the calculated pharmacokinetic parameters evaluated for the studied formulations (free RSV, nanocores and LbL NPs) administered to the animals. | 214 |

List of Publications

Santos, A.C., Veiga, F.V., Sequeira, J.A.D., Cabral, C., Collado Gonzallez, M., Fontes Ribeiro, C., Lvov, Y., Ribeiro, A.J. Sonication-assisted Layer-by-Layer self-assembly nanoparticles for resveratrol oral delivery (*Submitted to ACS Appl Mater Interfaces*).

Santos A.C., Sequeira, J.A.D., Fortuna, A., Falcão, A., Collado Gonzallez, M., Pattekari, P., Fontes Ribeiro, C., Veiga, F., Ribeiro, A.J. Pharmacokinetic applicability of a liquid chromatographic method for first-time orally administered resveratrol-loaded Layer-by-Layer nanoparticles to rats (*Submitted to Eur J Pharm Biopharm*).

Santos, A.C., Caldas, M., Pattekari, P., Fontes Ribeiro, C., Ribeiro, A.J., Lvov, Y.M., Veiga, F., Chapter 16: Layer-by-Layer coated drug-core nanoparticles as versatile delivery platforms. *Pharmaceutical nanotechnology (multi volume SET I-XXVII): Volume XI, Design and development of new nanocarriers - Core/shell nanostructures*. Grumezescu, A. M., Elsevier, Invited Chapter (2018) (*Accepted*).

Santos, A.C., Pattekari, P., Jesus, S., Veiga, F., Lvov, Y., Ribeiro, A.J. Sonication-assisted layer-by-layer assembly for low solubility drug nanoformulation. *ACS Appl Mater Interfaces* **7**, 11972–11983 (2015).

<http://pubs.acs.org/doi/abs/10.1021/acsami.5b02002?journalCode=aamick>

Santos, A.C., Costa, G., Veiga, F., Figueiredo, I.V., Batista, M.T., Ribeiro, A.J. Advance in methods studying the pharmacokinetics of polyphenols. *Curr Drug Metab* **15**, 96-115 (2014).

<http://www.eurekaselect.com/118855/article>

Santos, A.C., Veiga, F., Ribeiro, A.J., New delivery systems to improve the bioavailability of resveratrol. *Expert Opin Drug Deliv* **8**, 973-990 (2011).

<http://www.tandfonline.com/doi/abs/10.1517/17425247.2011.581655?journalCode=iedd20>

Abstract

Resveratrol (RSV) has been one of the most and extensively investigated polyphenols in the last recent years, owing to its broad-spectrum of promising therapeutic activities. It is extremely attractive for prevention or therapy where a magnitude of pathophysiological pathways is affected, making it a promising molecule for fighting cancer, diabetes and neurodegenerative diseases, amongst other targets.

However, its therapeutic potential is strongly limited by its physicochemical properties, mainly its low aqueous solubility and stability, and its poor pharmacokinetics profile, which seriously compromise its oral bioavailability.

RSV formulations, mainly available as nutritional supplements, are classic pharmaceutical dosage forms such as powders, tablets and hard gelatin capsules, to be administrated by the oral route. These formulations are often produced under uncontrolled processing procedures and using RSV with uncontrolled origin, which have shown to be not efficient.

To achieve an optimal response of RSV, new strategies are required to enhance its bioavailability and reduce its perceived toxicity. New delivery systems are sought out as valid alternatives to circumvent the limitations of the physicochemical characteristics and pharmacokinetics of RSV. An alternative formulation strategy to tackle this challenge includes the development of a safe and effective RSV formulation, using new drug delivery systems, among which nanotechnology assumes nowadays a prominent position.

Layer-by-Layer (LbL) self-assembly is an emergent nanotechnology, which is based on the design of tunable onion-like multilayered nanoarchitectures, composed of oppositely charged polyelectrolytes (PEs), upon the surface of low soluble drug nanocores, as RSV. This nanotechnology affords a versatile control over key formulation parameters, which are able to ultimately promote an improved pharmacokinetics profile.

Facing these potentialities, in this work we aim the development of RSV-loaded LbL nanoformulations capable of improving the bioavailability of this Biopharmaceutics Classification System (BCS) class II drug, by using Wistar rats as the animal model.

The research work of this thesis started with the development of a top-down LbL technique using a washless approach aiming the nanoencapsulation of ibuprofen (IBF), which was used in this stage of the work as a model BCS class II drug. For each saturated layer deposition, PE concentration was assessed by the design of PE titration curves. The LbL nanoshells were

constituted by the PEs pair cationic polyallylamine hydrochloride (PAH)/anionic polystyrene sulfonate (PSS), up to the deposition of 2.5 (IBF-(PAH/PSS)_{2.5} NPs), 5.5 (IBF-(PAH/PSS)_{5.5} NPs) and 7.5 (IBF-(PAH/PSS)_{7.5} NPs) PE bilayers. IBF LbL nanoparticles (NPs) covered with 7.5 PAH/PSS bilayers evidenced to be stable aqueous nanocolloids of this model drug, as well as biocompatible. Moreover, a controlled release of IBF from LbL NPs was accomplished under simulated intestinal conditions (from 5 h up to 7 days), according to the number of coating bilayers, which attributed to these structures the capacity to improve biopharmaceutical parameters of BCS class II drugs, as RSV.

Considering the knowledge acquired in the development of the aforementioned LbL NPs, novel LbL NPs were performed towards the nanoencapsulation of RSV. In this work, RSV nanoprecipitation followed by LbL self-assembly of PE, using a washless approach, was performed by applying the PE pair cationic PAH/anionic dextran sulfate (DS), by tracing, likewise, titration curves. Aqueous RSV nanocores and RSV LbL nanoformulations with a 2.5 (RSV-(PAH/DS)_{2.5} NPs), 5.5 (RSV-(PAH/DS)_{5.5} NPs) and 7.5 (RSV-(PAH/DS)_{7.5} NPs) bilayers were developed for the first time. Homogenous particle size distributions at the desired nanoscale interval, good colloidal and chemical stabilizations, high encapsulation efficiency, along with an excellent biocompatibility were verified. Those LbL NPs promoted a controlled release of RSV dependently of the number of PE bilayers under simulated gastrointestinal conditions, particularly in the intestine medium, which greatly highlighted their biopharmaceutical advantage. Our findings evidently pointed out that LbL PAH/DS-based NPs constitute a rational strategy for the oral administration of RSV *in vivo*.

Lastly, the bioavailability of the LbL nanoformulation composed of 5.5 bilayers of PAH and DS, previously developed, was performed using Wistar rats. We investigated the bioavailability of this LbL nanoformulation in comparison to the respective nanoformulation without LbL coatings (RSV nanocores) and the free RSV suspension, by pharmacokinetic studies following oral dosing to Wistar rats (20 mg/kg). For this study, due to the key role of the bioanalytical method in the *in vivo* data acquisition, a rapid, selective, and sensitive HPLC–DAD method has been successfully optimized and fully validated to confidently quantify RSV levels in rat plasma matrix, together with the optimization of the sample preparation procedure. Moreover, the chemical stability of RSV was assured for 24 h in simulated gastric and intestinal fluids with enzymes. Concerning the pharmacokinetic study, besides some weaknesses have been identified regarding the behaviour of the LbL shell after oral administration in Wistar rats, our results fully demonstrated, for the first time, that LbL NPs significantly enhanced the systemic exposure of RSV. Such data

emphasized thus the biopharmaceutical advantage of LbL NPs over the free drug, suggesting them as a potential oral drug delivery system for RSV.

In conclusion, with this research work we present evidence that RSV nanoencapsulation by LbL self-assembly nanotechnology constitutes a promising strategy to enhance the bioavailability of RSV after oral administration, offering great prospective to enlarge its potential preventive and therapeutic applications.

Resumo

O resveratrol (RSV) tem sido um dos polifenóis que nos últimos anos mais foi investigado devido ao seu alargado potencial terapêutico. É extremamente interessante na prevenção e terapia, quando várias vias fisiopatológicas são afetadas, tornando-a uma molécula promissora para combater, entre outras patologias, o cancro, a diabetes e as doenças neurodegenerativas.

Contudo, o seu potencial terapêutico é fortemente limitado pelas suas propriedades físico-químicas, sobretudo pela sua baixa solubilidade aquosa e instabilidade bem como pelo seu perfil farmacocinético fraco, as quais comprometem fortemente a sua biodisponibilidade oral.

As formulações de RSV, disponíveis principalmente sob a forma de suplementos nutricionais, são formas farmacêuticas clássicas, tais como pós, comprimidos e cápsulas de gelatina dura, que se destinam a ser administrados pela via oral. Estas formas farmacêuticas são frequentemente produzidas através de procedimentos de fabrico sem controlo de qualidade e com RSV de origem não controlada, o que compromete a sua eficácia.

Por forma a obter uma resposta ótima ao RSV, são necessárias novas estratégias para aumentar a sua biodisponibilidade e reduzir a sua toxicidade. Novos sistemas de libertação são necessários como alternativas válidas para ultrapassar as limitações inerentes às características físico-químicas e farmacocinéticas do RSV. Uma estratégia de formulação alternativa para responder a esse desafio inclui o desenvolvimento de uma formulação de RSV segura e eficaz, utilizando novos sistemas de libertação, entre os quais a nanotecnologia assume atualmente uma posição proeminente.

A “auto-montagem por camada-a-camada” (LbL) é uma nanotecnologia emergente, que se baseia na conceção de nanoarquitecturas em multicamadas reguláveis, semelhantes à estrutura de uma cebola, compostas por polielectrólitos (PEs) carregados com cargas opostas, sob a superfície de nanonúcleos de fármacos de baixa solubilidade, como o RSV. Esta nanotecnologia oferece um controlo versátil sobre os principais parâmetros de formulação, que são capazes de, em última instância, melhorar o perfil farmacocinético.

Face a estas potencialidades, com este trabalho pretende-se o desenvolvimento de nanoformulações de LbL carregadas com RSV capazes de melhorar a biodisponibilidade deste fármaco da classe II do Sistema de Classificação Biofarmacêutica (BCS), usando ratos Wistar como modelo animal.

O trabalho de investigação desta tese começou pelo desenvolvimento de uma técnica de LbL, sob a vertente “top-down”, realizada usando uma abordagem sem lavagens que visou a nanoencapsulação de ibuprofeno (IBF), fármaco que foi usado nesta fase do trabalho como um fármaco modelo da classe II do BCS. Para cada deposição de camada saturada, a concentração de PE foi avaliada pela conceção de curvas de titulação de PEs. As nanocápsulas de LbL foram constituídas pelo par de PEs catiónico cloridrato de polialilamina (PAH) / aniónico poliestireno sulfonato (PSS), até à deposição de 2.5 (IBF-(PAH/PSS)_{2.5}NPs), 5.5 (IBF-(PAH/PSS)_{5.5}NPs) e 7.5 (IBF-(PAH/PSS)_{7.5}NPs) bicamadas de PEs. As nanopartículas (NPs) de LbL de IBF revestidas com 7.5 bicamadas de PAH/PSS evidenciaram ser nanocolóides aquosos estáveis deste fármaco modelo, bem como serem biocompatíveis. Além disso, uma libertação controlada do IBF das NPs de LbL foi conseguida sob condições intestinais simuladas (de 5 h até 7 dias), de acordo com o número de bicamadas de revestimento, atribuindo a essas estruturas a capacidade de melhorar os parâmetros biofarmacêuticos de fármacos da classe II do BCS, como o RSV.

Considerando o conhecimento adquirido aquando do desenvolvimento das NPs anteriormente referidas, novas NPs de LbL foram concebidas com vista à nanoencapsulação de RSV. Nesta fase do trabalho, a nanoprecipitação de RSV seguida de LbL de PEs, usando a abordagem sem lavagens, foi realizada aplicando o PE catiónico PAH / PE aniónico sulfato de dextrano (DS), pelo desenho, da mesma forma, de curvas de titulação. Os nanonúcleos de RSV aquosos e as nanoformulações de LbL de RSV com 2.5 (RSV-(PAH/DS)_{2.5}NPs), 5.5 (RSV-(PAH/DS)_{5.5}NPs) e 7.5 (RSV-(PAH/DS)_{7.5}NPs) bicamadas foram desenvolvidos pela primeira vez. Verificou-se a obtenção de distribuições homogéneas de tamanho de partícula no intervalo da nanoescala desejado, boa estabilização coloidal e química, elevada eficiência de encapsulação, juntamente com uma excelente biocompatibilidade. Estas NPs de LbL promoveram uma libertação controlada do RSV, que mostrou ser dependente do número de bicamadas de PEs sob condições gastrointestinais simuladas, particularmente no meio intestinal, evidenciando fortemente a sua vantagem biofarmacêutica. Os nossos resultados apontaram, de forma evidente, que as NPs de LbL formadas por PAH/DS constituem uma estratégia racional para a administração oral de RSV *in vivo*.

Por fim, a biodisponibilidade da nanoformulação de LbL composta por 5.5 bicamadas de PAH e DS, desenvolvida anteriormente, foi realizada em ratos Wistar. A biodisponibilidade dessas nanoformulações de LbL foi investigada, em comparação com a respetiva nanoformulação sem revestimentos de LbL (nanonúcleos de RSV) e a suspensão de RSV livre, através de estudos farmacocinéticos após administração oral das nanoformulações a ratos Wistar (20 mg/kg). Para

este estudo, devido ao papel fundamental do método bioanalítico na aquisição de dados referentes ao ensaio *in vivo*, um método HPLC-DAD rápido, seletivo e sensível foi otimizado com sucesso e totalmente validado para quantificar com rigor os níveis de RSV na matriz de plasma de rato, juntamente com a otimização do procedimento de preparação da amostra. Além disso, a estabilidade química do RSV foi assegurada durante 24 h em fluidos gástrico e intestinal simulados contendo enzimas. No que diz respeito ao estudo farmacocinético, apesar de terem sido identificados alguns pontos fracos quanto ao comportamento do revestimento de LbL após a administração oral em ratos Wistar, os nossos resultados demonstraram, pela primeira vez, que as NPs de LbL aumentaram significativamente a exposição sistêmica do RSV. Tais dados enfatizaram, portanto, a vantagem biofarmacêutica das NPs de LbL sobre o fármaco livre, sugerindo-as como um potencial sistema de liberação oral para RSV.

Em conclusão, com este trabalho de investigação, apresentamos evidências de que a nanoencapsulação do RSV pela nanotecnologia de LbL constitui uma estratégia promissora para aumentar a biodisponibilidade do RSV após a administração oral, oferecendo excelente potencial para aumentar as suas potenciais aplicações preventivas e terapêuticas.

Chapter 1

General Introduction

1.1. Motivation

The relevance of natural products on health has been huge over the evolution of humankind. The history of medicine is full of outstanding reports regarding how natural products deeply impacted advances in drug discovery and therapy. This is owed to the impressive and extensive structural and chemical diversity of these compounds that is not possible to be matched by synthetic libraries of molecules, continuing to strongly influence and inspire new findings in pharmacy and medicine.

Resveratrol (3,4',5-trihydroxy-*trans*-stilbene; RSV) is a natural product especially abundant in the skin of red grapes, being presumably the most actively investigated phytochemical worldwide (Berman, Motechin *et al.* 2017, Charytoniuk, Drygalski *et al.* 2017, Hogervorst Cvejić, Atanacković Krstonošić *et al.* 2017). The research of this polyphenol started in 1992, when the presence of RSV in red wine has been curiously pointed out as the justification for the “French paradox”, which describes the unexpectedly low incidence of coronary heart diseases among French people who are heavy red wine drinkers, despite their high-fat diet (Catalgol, Batirel *et al.* 2012, Berman, Motechin *et al.* 2017). In the hope of bolstering such hypothesis, RSV has been broadly investigated ever since. Such studies lead to the recognition of a wide array of pharmacological activities exhibited by this valuable polyphenol, demonstrating great potential concerning chronic diseases, longevity (Sergides, Chirila *et al.* 2016) as well as cancer prevention and treatment (Varoni, Lo Faro *et al.* 2016).

Facing these promising beneficial activities, RSV drug supplements for oral administration have been developed in the form of several traditional dosage forms, as tablets and capsules (Li, Wong *et al.* 2017). However, those formulations have been found to fail in terms of clinical translation, emphasizing the higher hurdle related to the oral administration of RSV in its pure form: its strongly limited *in vivo* bioavailability (< 1%). This behavior is ascribed to the rapid and extensive presystemic metabolism, together to the characteristic low solubility of Biopharmaceutics Classification System (BCS) II drugs, the category to which RSV belongs, together with its low stability (Amri, Chaumeil *et al.* 2012, Singh, Pai 2015).

One strategy to overcome the inherent problems of RSV is nanotechnology, an innovative, strong and challenging tool of the contemporary Pharmaceutical Technology (Pelaz, Alexiou *et al.* 2017), by the design of novel drug delivery systems capable of improving its *in vivo* oral bioavailability (Singh, Pai 2014). Among those, multifunctional nanoscale therapies, as Layer-by-Layer (LbL) self-assembly assume relevant emphasis in modern healthcare by enabling sophisticated control over drug release (de Villiers, Lvov 2011). LbL nanoparticles (NPs) consist in

functional thin constructs, resulting from the assembly of polyelectrolytes (PEs) upon drug solid nanocores. These NPs hold a wide range of desirable features for drug delivery due to its versatility (Polomska, Gauthier *et al.* 2017).

This way, considering the actual relevance of the beneficial effects of RSV on human health and the potential of LbL assembly as formulation technology for BCS II drugs, it seems to be of great interest to explore the feasibility of this technology for the nanoencapsulation of RSV. This was thus hypothesized as a strategy to obtain RSV-loaded NPs, aiming to maximize the potential of RSV, offering, ultimately, promising avenues for further applications of this interesting natural compound.

1.2. Objectives and outline

Based on the above considerations, the central aim of this thesis was to develop drug delivery systems for RSV, specifically by the use of LbL self-assembly nanotechnology towards the obtainment of optimized LbL NPs of RSV in order to enhance its bioavailability *in vivo* following oral administration.

The specific objectives behind this thesis were as follows:

1 - Development of LbL-based NPs formulations for the first time in our laboratory, by using a BCS II class model drug (**Chapter 2**).

Ibuprofen (IBF) was chosen as the BCS II class model drug, and polyallylamine hydrochloride (PAH) and polystyrene sulfonate (PSS) as PEs. The resulting NPs, specifically with 2.5, 5.5 and 7.5 bilayered LbL shells, were obtained by a top-down LbL technique using a washless approach, and were characterized regarding morphology, particle size, zeta potential, stability under conditions of storage, drug loading, stability, *in vitro* release studies and cytotoxicity against Caco-2 cells.

2 - Application of the previously acquired LbL principles to the specific case of RSV, aiming the development of novel RSV-loaded LbL NPs (**Chapter 3**).

Uncoated RSV-loaded NPs (RSV nanocores), without adsorbed LbL coatings, and three distinct RSV-loaded PAH/dextran sulfate (DS) LbL nanoformulations, specifically with 2.5, 5.5 and 7.5 bilayered LbL shells were developed; the latter, using the nanoprecipitation of the core template RSV nanocores coupled to the LbL self-assembly of PEs, as the key nanotechnology, and by a washless approach. RSV-loaded LbL PAH/DS NPs were characterized according to morphology, particle size, zeta potential, stability under conditions of storage, drug loading/encapsulation efficiency, *in vitro* release studies and cytotoxicity against Caco-2 cells.

3 - Investigate the bioavailability of RSV when encapsulated into LbL NPs and compare the outcomes with those obtained with simple RSV-nanocores and free RSV after oral administration to Wistar rats, in the light of the scarcity of studies available concerning the immense potential of this nanotechnology regarding *in vivo* oral administration (**Chapter 4**).

In vivo pharmacokinetic studies in Wistar rats were conducted by making use of a validated, simple, sensitive and selective HPLC-DAD bioanalytical method for the

determination of RSV in rat plasma matrix after oral administration of LbL nanoformulations of RSV.

In the end, with this thesis we pretend to contribute to the development of a nanotechnology viable approach based on the LbL self-assembly for the improvement of the oral bioavailability of RSV, thus widening its promising therapeutic potential.

1.3. Resveratrol

Phenolic compounds are a large group of substances that derive from the shikimic acid or acetic metabolic pathways, belonging to secondary metabolism of plants. These polyphenols, known to grant sensorial properties to plants (ton color, astringency and some fruits' flavor), have the quality of phytoalexins – compounds that are synthesized by plants under environmental stress, such as injury, microbial (fungal), infection or UV-irradiation conditions – which are responsible for growth, reproduction and disease resistance (De La Lastra, Villegas 2007). Their chemical constitution consists of at least one aromatic ring substituted with at least one hydroxyl group, ranging from simple structures, such as phenolic acids, to complexes ones as tannins. Within the group lie stilbenes, and more specifically resveratrol (RSV, 3,4',5-trihydroxy-*trans*-stilbene), a triphenol non-flavonoid and atoxic phytoestrogen (De La Lastra CA, Villegas 2007, Martini, Del Bo *et al.* 2017). RSV is produced in higher plants through the stilbene synthase (Pervaiz 2003), which is present in at least 70 vegetal species (Kristl J, Teskac K *et al.* 2009) and has been identified as the major active compound of stilbene phytoalexins (Gülçin 2010). Like the other stilbenes, RSV is presented in nature by two isomeric forms: *trans*- (*t*-RSV in **Figure 1.1a**) and *cis*-RSV (*c*-RSV in **Figure 1.1b**). In plants, a major form of RSV is the glucosidic form called piceid (RSV-3-*O*- β -D-glucoside) or polydatin (PCD in **Figure 1.1c**) in the isomeric form *trans*-piceid (*t*-PCD) (Baur, Sinclair 2006, Jensen, Wertz *et al.* 2010). Piceid can exist as *cis*-piceid as well (*c*-PCD) (Burkon, Somoza 2008).

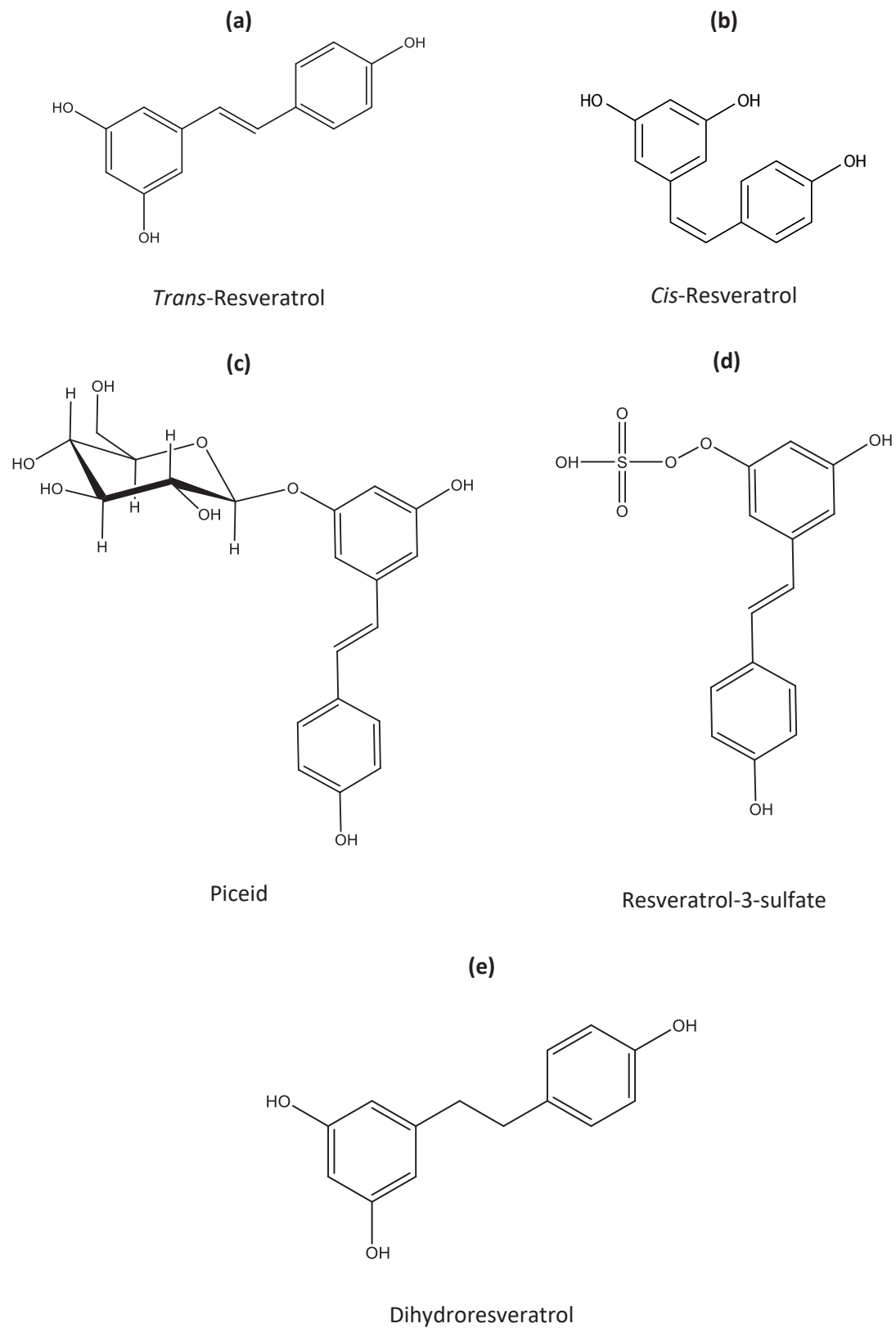


Figure 1.1: Chemical structure of (a) *trans*-RSV, (b) *cis*-RSV, (c) piceid, (d) RSV-3-sulfate and (e) dihydroRSV.

[RSV – resveratrol]

Certain physicochemical characteristics of *t*-RSV are still unknown or research findings are found to be contradictory (Zupancic, Lavric *et al.* 2015). RSV in solution shows photo-sensitivity (*trans*- to *cis*- isomerization is facilitated by UV exposure in minutes) and pH-sensitivity, being easily oxidizable (Pervaiz 2003, De La Lastra, Villegas 2007, Zupancic, Lavric *et al.* 2015). When protected from light, *t*-RSV is stable for months in acidic pH, starting to degrade significantly at pH above 6.8 (Zupancic, Lavric *et al.* 2015). These results were in agreement with Robinson *et al.*, which attributed this behavior to basic hydrolysis of the phenolic compound at neutral and basic conditions, suggesting, thus, the formulation of RSV delivery systems to be carried out in media with pH lower than 6 (Robinson, Mock *et al.* 2015). By turn, *c*-RSV was found to be stable only near neutral pH; and, in addition, when RSV and RSV glucosides are in solution, the primary degradant was encountered to be the *cis*-isomer (Jensen, Wertz *et al.* 2010). In relation to the stability of RSV in the solid state, in 2008, Shi G. *et al.*'s results claimed that solid RSV was unstable when exposed to light and elevated humidity (Shi, Rao *et al.* 2008). However, in 2010, Jensen *et al.* presented consistent data evidencing that solid *t*-RSV was not particularly sensitive to UV/fluorescent light, elevated humidity and temperature, or atmospheric oxidants at ambient concentrations. Furthermore, like RSV, PCD was considered also a stable solid (Jensen, Wertz *et al.* 2010). Those results were in agreement with more recent obtained data, emphasizing the use of crystalline *t*-RSV or *t*-RSV-incorporated solid delivery systems as the most suitable forms in terms of stability (Zupancic, Lavric *et al.* 2015).

The chemical structure of RSV, related to the synthetic lipophilic estrogen diethylstilbestrol (Kursvietiene, Staneviciene *et al.* 2016), enables it to interact with receptors and enzymes, giving rise to important biological effects (Juhasz, Varga *et al.* 2010, Berman, Motechin *et al.* 2017, Tsai, Ho *et al.* 2017) (see **Table 1.1**). Those effects comprise the prevention of many disease states that are a consequence of cell damage or death triggered by severed oxidative stress, including Alzheimer's (Kou, Chen 2017) and Parkinson's diseases (Gaballah, Zakaria *et al.* 2016), cancer (Rauf, Imran *et al.* 2016, Berman, Motechin *et al.* 2017), cardiovascular disease (Zordoky, Robertson *et al.* 2015), multiple sclerosis (Ghaiad, Nooh *et al.* 2017), colitis (Samsamikor, Daryani *et al.* 2016), severe acute pancreatitis (Wang, Zhang *et al.* 2017) and diabetes (Szkudelski, Szkudelska 2015, Zhu, Wu *et al.* 2017). Recent studies have associated as well RSV to an extension of the lifespan of a several species, owing to its capability to mimic caloric restriction (Bhullar, Hubbard 2015, Barger, Vann *et al.* 2017), which, together with the recognized aforementioned biological activities, absolutely makes it an important target of interest. Concerning mode of action, RSV reveals dual actions – cell protection or cell apoptosis – which might depend on cell type, concentration, cytosolic redox status and duration of contact (Lu, Ji *et*

al. 2009). More precisely, it shows antioxidant activity in low oral doses (10 μM); and cytotoxic action when administrated at higher concentrations (100 μM), depicted as changes in cell shape, detachment and apoptotic features (Caddeo, Teskac *et al.* 2008, Kristl, Teskac *et al.* 2009). After comparing among some of the stilbenoids, it has been concluded that the presence of different functional groups may result in derivatives with different anti-oxidative properties targeting mainly extracellular radical oxygen species (ROS) (López-Nicolás, Rodríguez-Bonilla *et al.* 2009).

Table 1.1: Biological activities of resveratrol (RSV) and respective physiological mechanisms.

| BIOLOGICAL ACTIVITIES | MECHANISM(S) |
|----------------------------------|---|
| Antioxidant | ROS scavenger, influencing the cell redox-signaling pathways (Baur, Sinclair 2006, De La Lastra, Villegas 2007) |
| | Trigger apoptosis (Kuhnle, Spencer <i>et al.</i> 2000, Pervaiz 2003) |
| | Prevent apoptosis (Kuhnle, Spencer <i>et al.</i> 2000) |
| | Modulation of NO production (De La Lastra, Villegas 2007) and cerebral blood flow variables (Kennedy, Wightman <i>et al.</i> 2010) |
| | Inhibition of membrane lipid peroxidation (De La Lastra, Villegas 2007) |
| Anti-inflammatory | Down-regulation of proinflammatory mediators: inhibition of COX-1 (Baur, Sinclair 2006), COX-2, hydroxyperoxidase activities (Marier, Vachon <i>et al.</i> 2002), MAP kinases (Liao, Ng <i>et al.</i> 2010), lipoxygenases (Kuhnle, Spencer <i>et al.</i> 2000), iNOS (Liao, Ng <i>et al.</i> 2010) |
| Neuroprotection | Inhibition of β -amyloid polymerization (Jang, Piao <i>et al.</i> 2007) |
| | Increase of heme oxygenase-1 activity (De La Lastra CA, Villegas 2007) |
| | Increase of glutamate uptake, glutathione content and trophic factor S100B secretion (Quincozes-Santos, Gottfried 2011) |
| | Reduced cerebrospinal fluid MMP9, increase IL-4, attenuated decline in A β 42 and A β 40 (Moussa, Hebron <i>et al.</i> 2017) and reduced MMP2 (Chen, Bai <i>et al.</i> 2016) |
| Cardiovascular protection | Activation of SIRT1, AMPK and endogenous anti-oxidant enzymes (Zordoky, Robertson <i>et al.</i> 2015) |
| | Modulation of lipoprotein metabolism (Increase of HDL proteins and decrease of LDL and VLDL) (Marier, Vachon <i>et al.</i> 2002, Pervaiz 2003) |
| | Inhibition of platelet aggregation (Kuhnle, Spencer <i>et al.</i> 2000, Marier, Vachon <i>et al.</i> 2002, Pervaiz 2003, Baur, Sinclair 2006, Caddeo, Teskac <i>et al.</i> 2008) |
| | Regulation of vascular smooth muscle proliferation (Liao, Ng <i>et al.</i> 2010) |
| | Inhibition of TNF- α (Zhang, Zhang <i>et al.</i> 2009) |
| | Increase of endothelial mitochondrial biogenesis (Csiszar, Labinskyy <i>et al.</i> 2009) |
| | Activation of Nrf2-driven antioxidant response (Ungvari, Bagi <i>et al.</i> 2010) |
| Anticancer | Modulation of biological pathways involved in differentiation, transformation, cell cycle regulation and cell death induction (Varoni, Lo Faro <i>et al.</i> 2016) |
| | Cancer prevention at the initiation stage (Pervaiz 2003, Walle, Hsieh <i>et al.</i> 2004) |
| | Suppression of growth of pre-neoplastic lesions (Pervaiz 2003, Walle, Hsieh <i>et al.</i> 2004) |
| | Pro-antioxidant action (disruption of intracellular redox balance which leads to apoptosis) (Marier, Vachon <i>et al.</i> 2002, De La Lastra, Villegas 2007, Kristl, Teskac <i>et al.</i> 2009) |
| | Inhibition of cell proliferation (Pervaiz 2003, Walle, Hsieh <i>et al.</i> 2004, Patel, Brown <i>et al.</i> 2010) |
| | Induction of Phase II enzymes, such as quinone reductase (Baur, Sinclair 2006) |
| | Agonist for the oestrogen receptors (Kuhnle, Spencer <i>et al.</i> 2000, Baur, Sinclair. 2006, Kristl, Teskac <i>et al.</i> 2009) |

[AMPK – AMP-activated protein kinase; A β 40 – amyloid beta 40; A β 42 – amyloid beta 42; COX-1 – cyclo-oxygenase-1; COX-2 – cyclo-oxygenase-2; HDL – high density lipoprotein; IL-4 – interleukin-4; LDL – low density lipoprotein; MAP – mitogen-activated protein; MMP2 – matrix metalloproteinase-2; MMP9 – matrix metalloproteinase-9; NO: nitric oxide; Nrf2: nuclear factor (erythroid-derived 2)-like 2; ROS: radical oxygen species; S100B: S100 calcium-binding protein B; SIRT1 – silent information regulator 1; TNF- α – tumor necrosis factor- α ; VLDL – very low-density lipoprotein]

It is not yet clear whether RSV itself, derivatives or metabolites evidence therapeutic *in vivo* effects (Kursvietiene, Staneviciene *et al.* 2016, Berman, Motechin *et al.* 2017). Recognition of the role of active metabolites of RSV will make possible the correct interpretation of the pharmacodynamic data observed in preclinical studies and extrapolation of the data to humans. Besides, the existence of RSV metabolites and quantification of their level of activity will allow a better design of a delivery system for RSV. In addition, questions about safety, dosing and clinical efficacy of RSV still remain. The design of delivery systems for RSV requires a thorough understanding of the physicochemical characteristics of RSV, specifically its low water solubility and high instability in solution, which may affect laboratory assays and formulations containing it in the dissolved form.

With the aim of contributing to the development of a proper delivery system for RSV, the pharmacokinetics of this compound as well as the experimental conditions used during formulation and assays are of utmost importance. This way, in the following sections, new drug delivery systems - such as cyclodextrins (CDs), NPs and liposomes are described and compared with classic formulations of RSV, focusing on their advantages to overcome RSV limitations, by also increasing potential to targeting and sustained delivery. A better understanding of the strength of the evidence on the effectiveness of delivery systems may contribute to increase the bioavailability of RSV.

1.4. Pharmacokinetics of resveratrol

After oral administration, and once in the small intestine, RSV and PCD are directly absorbed in the intestinal lumen, as can be seen in **Figure 1.2**, an adaptation from Ros (Ros 2008). According to studies with Caco-2 cells, the velocity of PCD absorption is four times lower than RSV's (Henry, Vitrac *et al.* 2005); however, PCD can be hydrolyzed before its absorption by lactase phlorizin hydrolase (LPH), a β -glucosidase present in the intestinal lumen. *t*-RSV crosses the intestinal epithelium by rapid trans-epithelial passive diffusion (Kuhnle, Spencer *et al.* 2000, Walle, Hsieh *et al.* 2004), whereas PCD uses the sodium-glucose cotransporter 1 (SGLT1) (**Figure 1.2**) (Henry, Vitrac *et al.* 2005). RSV and PCD are subject to a presystemic metabolism through first-pass glucuronidation and sulfate conjugation (Phase II conjugation reactions). This metabolization leads to various metabolites, fundamentally glucuronides and sulfates, abbreviated as G and S, respectively, in **Figure 1.2**. This metabolism has been described as the main cause of the trace amounts of RSV found in the systemic circulation (Das, Lin *et al.* 2008), and, consequently, for its low oral bioavailability (Kuhnle, Spencer *et al.* 2000, Walle, Hsieh *et al.* 2004, Kapetanovic, Muzzio *et al.* 2011). Once absorbed, PCD, in the enterocytes' cytoplasm, may be hydrolyzed into RSV by the local cytosolic- β -glucosidase (c β G), as shown in **Figure 1.2** (Zhou, Chen *et al.* 2007).

The remaining RSV and derivatives are transported via port towards the liver and, in hepatic microsomes, RSV is once more promptly metabolized in glucuronides and sulfates. Some results indicate that glucuronidation is preferred for the two RSV isomers, occurring the RSV sulfates only in small amounts. Other authors maintain that RSV is a better substrate for sulfotransferases (ST, **Figure 1.2**) (Miksits, Maier-Salamon *et al.* 2005, Wenzel, Somoza 2005). Sulfation of RSV in human liver cytosol in the presence of 3'-phosphoadenosine-5'-phosphosulfate converts RSV into *t*-RSV-3-*O*-sulfate (**Figure 1.1d**), *t*-RSV-4'-*O*-sulfate, and *t*-RSV-3-*O*-4'-*O*-disulfate metabolites, suggesting that these are possible sulfated metabolites, derived from liver's *in vivo* metabolism (Miksits, Maier-Salamon *et al.* 2005).

After hepatic metabolization, liver is exposed again to RSV during enterohepatic recirculation, in which RSV conjugates are excreted in bile and reabsorbed in its aglycone and/or conjugated forms, after undergoing enzymatic cleavage by the β -glucuronidase enzyme in the small intestine (Marier, Vachon *et al.* 2002, Wenzel, Somoza 2005, Boocock, Faust *et al.* 2007). The non-absorbed RSV in the small intestine addresses the colon. In fact, RSV can pass the gut without metabolic conversion, yet it can be metabolized (reduction reactions) by bacterial enzymes of the intestinal microflora (β -glucuronidases) through hydrogenation of the aliphatic double bond, resulting in dihydroresveratrol (dihRSV, in **Figure 1.1e**) (Walle, Hsieh *et al.* 2004,

Rotches-Ribalta, Andres-Lacueva *et al.* 2012). DihRSV is excreted both in the glucuronide and sulfate forms (Wenzel, Somoza 2005), and it may be absorbed and also then be combined in their glucuronide and sulfate conjugates, which agrees with their identification in plasma (Ortuno, Covas *et al.* 2010) and in urine (Walle, Hsieh *et al.* 2004). Monitoring of RSV and its metabolites in human feces indicates the existence of RSV sulfates (Walle, Hsieh *et al.* 2004) in a small quantity (<1%) (Boocock, Faust *et al.* 2007). After the liver stage, the remaining RSV and its conjugates are absorbed to the systemic circulation, where they can be transported along with the blood cells (red blood cells and platelets), lipoproteins (low density lipoprotein [LDL] both *in vitro* and in humans) (Urpí-Sardà, Jáuregui *et al.* 2005), but most travel attached to plasma proteins (Burkon, Somoza 2008).

The pharmacokinetics of RSV has been studied mainly in animal models; however, recent studies have been performed in humans. The obtained results are summarized in **Table 1.2**. Formulations used as well their total content of RSV are discriminated. Plasma concentration of RSV represents 1-15% (Urpí-Sardà, Zamora-Ros *et al.* 2007) and, in some cases, it was not detectable or quantifiable. Even when a very large dose of RSV (2.5 and 5.0 g) was given, its blood concentration failed to reach the necessary levels for systemic cancer prevention (Boocock DJ, Faust GE *et al.* 2007). However, when given in a proprietary formulation (3.0 or 5.0 g) developed by Sirtris Pharmaceuticals (Cambridge, MA, USA), RSV reached 5-8 times higher blood levels, which approached the necessary concentration to exert effects both *in vitro* and in animal experiments (Elliott, Jirousek 2008).

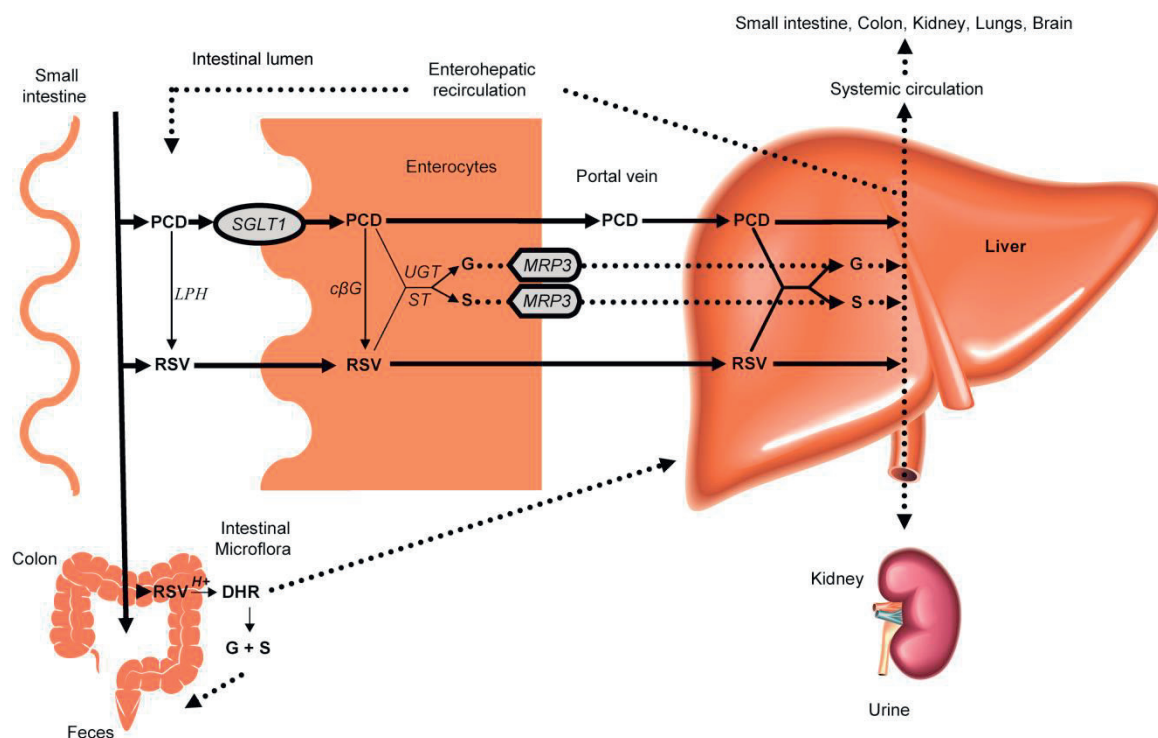


Figure 1.2: Oral pharmacokinetics of RSV, piceid (full arrows), and their derivatives (dashed arrows).

In the intestinal lumen, PCD can be hydrolyzed to RSV, which is directly absorbed by diffusion, while PCD uses a specific transporter. In the enterocytes' cytoplasm, PCD can be again hydrolyzed to RSV. RSV and PCD are metabolized in G (Derivative glucuronides) or S (Derivative sulfates). G and S derivatives cross enterocytes towards the liver through specific transport. Once in the liver, RSV and PCD can be once more metabolized into its G and S derivatives, which can undergo into enterohepatic recirculation and be reabsorbed in the small intestine. In the liver, compounds are delivered to systemic circulation and are distributed to organs. Instead, they can also be directly excreted in urine. In the intestinal tract, the non-absorbed can RSV reach the colon, where it is metabolized in DHR (dihydroresveratrol). DHR can be absorbed or excreted through G and S derivatives in feces. (Henry, Vitrac *et al.* 2005, Hu 2007)

[cβG = cytosolicβ-β-glucuronidase, LPH = lactase phlorizin hydrolase, SGLT1 = sodium-glucose transport proteins, MRP3 = multidrug resistance-associated protein 3, UGT = UDP-glucuronosyltransferase, ST = sulfotransferase]

The most abundant metabolite found in the systemic circulation by Burkon *et al.* was *t*-RSV-3,5-disulfate (Burkon, Somoza 2008), followed by *t*-RSV-3-sulfate, which, in turn, has been described by Boocock *et al.* (Boocock, Faust *et al.* 2007) as the most abundant metabolite. However, Urpí-Sardà *et al.* (Urpí-Sardà, Jáuregui *et al.* 2005, Urpí-Sardà, Zamora-Ros *et al.* 2007) and Vitaglione *et al.* (Vitaglione, Sforza *et al.* 2005) have identified two glucuronides, namely *t*-RSV-3-*O*-glucuronide and RSV-4'-*O*-glucuronide, as the most abundant forms. Glucuronides were also detected as the most abundant forms in plasma by Sergides *et al.* in relation to sulfates (Sergides, Chirila *et al.* 2016). Two new plasma metabolites of RSV were identified by Boocock *et al.*, precisely *t*-RSV-C/*O*-diglucuronide (18%) and *t*-RSV-3,4'-disulfate (11%). One RSV disulfate was also identified in plasma in the same study but it has not been quantified, leading to the

assumption that it probably coincides with the previous one (Boocock, Patel *et al.* 2007). In addition, RSV glucosides (*t*-RSV-4-*O*-glucoside and *c*-RSV-3-*O*-glucoside) were detected in human LDL samples after oral intake of red wine. These RSV glucosides are absorbed from the intestine, possibly by the same glucose transport system of phenolic compounds in rats. Once in human liver microsomes, glucosidation may serve as an alternative detoxification pathway, as aglycones can preferentially undergo glucosidation (Urpí-Sardà, Jáuregui *et al.* 2005). Overall, animal and in human studies reveal that the major components detected in plasma are the metabolites of RSV, precisely glucuronides and sulfates, being those reported to be in superior plasma levels compared with those of the parent compound (Sergides, Chirila *et al.* 2016).

RSV was identified in several organs, mostly in the small intestine, colon, kidney, liver, lungs and brain (Ros 2008). Most routes of excretion are via urine and feces; however, the percentage of excreted compounds varies according to used experimental conditions. As it can be seen in **Table 1.2**, most of the orally administered RSV is recovered in urine in highly variable amounts (Walle, Hsieh *et al.* 2004). After oral administration of formulations containing administered RSV amounts varying from 0.5-5.0 g, 1.0, 5.4 and 25 mg, the quantification of RSV in urine revealed distinct results, varying from only trace amounts, to 17% and 26-52% when compared with initial RSV. Contrary to reports in animals (Wenzel, Soldo *et al.* 2005), human studies revealed that sulfated forms are more abundant than glucuronidated ones, and RSV is present in a much smaller proportion. The most abundant RSV derivative in urine is *c*-RSV-4'-sulfate (84%), followed by *c*-RSV-3-*O*-glucuronide (8%) and other glucuronides and sulfates (Urpí-Sardà, Zamora-Ros *et al.* 2007). According to Burkon and Sumoza's studies (Burkon, Somoza 2008), the most abundant metabolite is *t*-RSV-3,5-disulfate, followed by *t*-RSV-3-sulfate, where *t*-RSV-*C/O*-diglucuronide and *t*-RSV-3,4'-disulfate were also posted. In Boocock *et al.* (Boocock, Faust *et al.* 2007) studies, RSV-3-sulfate was the predominant metabolite. RSV was detected in varying amounts in urine, from only trace amounts (Boocock, Faust *et al.* 2007, Boocock, Patel *et al.* 2007) up to 17% (Urpí-Sardà, Jáuregui *et al.* 2005) and 53-85% (Walle, Hsieh *et al.* 2004). These results point out that the administration of high doses of RSV leads to the presence of sulfate conjugates in higher amounts than the glucuronide ones. This fact must be emphasized, as a possible saturation of glucuronosyltransferases occurs following the administration of greater doses of RSV, contrarily to the sulfation pathway that evidenced a non-competitive substrate inhibition. The occurrence of this saturation might conduce to a shift from glucuronidation to sulfation in the metabolization of RSV, which justified the encountered superior amounts of sulfate metabolites in the presence of high doses of RSV (Rotches-Ribalta, Andres-Lacueva *et al.* 2012). Furthermore, to the best of author's knowledge, besides several RSV derivatives were

reported, the total recovery in urine was ca. 1-52%, which is substantially different from 53-85% reported by Walle *et al.* (Walle, Hsieh *et al.* 2004). In this case, the identity of the radioactive moiety was not taken into consideration in the recovery calculation. Thereby, considering that RSV and all metabolites were presumed to participate in radioactivity recovery, it is suggested that not all RSV metabolites have been identified yet. The same assumption is applied to feces recoveries (Cottart, Nivet-Antoine *et al.* 2010). It must also be taken into account that sulfate conjugates have some technological limitations, namely the chromatographic behavior, which prevents their correct identification (Walle, Hsieh *et al.* 2004).

Table 1.2: Results obtained in human pharmacokinetics studies following oral administration of RSV-based formulations (RSV administered amount (milligrams) was calculated with reference to the average adult human weight of 70 kg).

| Formulations | RSV (mg) | RSV and Metabolites | | | | | | Overall Recovery(%) | Ref. |
|-------------------------------|--------------------|--------------------------------------|--|-------------------|---|----------|-------------|----------------------------------|---|
| | | Plasma(%) | | Urine(%) | | Feces(%) | | | |
| | | RSV | Metabolites | RSV | Metabolites | RSV | Metabolites | | |
| Wine (with a standard meal) | 0.25 ^a | <LOD | <i>t</i> -4'-G > <i>t</i> -3-G | N.A. ^b | N.A. | N.A. | N.A. | N.A. | (Vitaglione, Sforza <i>et al.</i> 2005) |
| Wine | 1.92 ^a | <LOQ | <i>t</i> -4'-G > <i>t</i> -3-G | N.A. | N.A. | N.A. | N.A. | | |
| Wine (with a "fat" meal) | 0.48 ^a | 1-6 ng/mL ^a | <i>t</i> -3-G | N.A. | N.A. | N.A. | N.A. | | |
| Wine with a "lean" meal | | 1 ng/mL ^a | <i>t</i> -4'-G | N.A. | N.A. | N.A. | N.A. | | |
| Wine | 0.36 | N.A. | N.A. | <LOD | <i>t</i> -3- <i>O</i> -G, <i>c</i> -3- <i>O</i> -G | N.A. | N.A. | 72 nmoL/g in urine ^c | (Zamora-Ros, Urpí-Sardà <i>et al.</i> 2006) |
| | 2.56 | | | | | | | 350 nmoL/g in urine ^c | |
| | 0.40 | | | | | | | 212 nmoL/g in urine ^c | |
| Wine | 0.4 ^{d,e} | 2 | <i>t</i> -3- <i>O</i> -G > <i>t</i> -4'- <i>O</i> -G > <i>c</i> -4'- <i>S</i> = <i>c</i> -3- <i>O</i> -G > <i>c</i> -3- <i>S</i> ^{f,g} > <i>t</i> -3- <i>S</i> > <i>t</i> -4'- <i>S</i> | <LOD | <i>c</i> -4'- <i>S</i> > <i>c</i> -3- <i>O</i> -G > <i>c</i> -4'- <i>O</i> -G > <i>t</i> -3- <i>O</i> -G > <i>c</i> -3- <i>S</i> < <i>t</i> -4'- <i>O</i> -G > <i>t</i> -3- <i>S</i> > <i>t</i> -4'- <i>S</i> | N.A. | N.A. | N.A. | (Urpí-Sardà, Zamora-Ros <i>et al.</i> 2007) |
| Wine | 5.4 ^d | 1-9 ^h | <i>t</i> -3- <i>O</i> -G ↑ > <i>t</i> -4- <i>O</i> -Glucos. ⁱ > <i>c</i> -3- <i>O</i> -Glucos. | 26-52 | N.A. | N.A. | N.A. | N.A. | (Urpí-Sardà, Jáuregui <i>et al.</i> 2005) |
| Wine, grape juice and tablets | 1 ^a | <i>c</i> -RSV and <i>t</i> -RSV <LOD | dihRSV ^j | <LOD | dihRSV (↑) | N.A. | N.A. | N.A. | (Ortuno, Covas <i>et al.</i> 2010) |
| Whisky | 2 | <LOQ | N.A. | 52 | G | N.A. | N.A. | N.A. | (Meng, Maliakal <i>et al.</i> 2004) |
| | 35 | | N.A. | 34 | | | | | |
| | 70 | | G | 26 | | | | | |
| Grape juice | 1 ^k | <LOD | <LOD | <LOQ | 5 | N.A. | N.A. | N.A. | |
| | 2 | | | <LOQ | | | | | |

| Formulations | RSV (mg) | RSV and Metabolites | | | | | | Overall Recovery(%) | Ref. |
|--------------------------------------|-------------------------------|---------------------------|--|---------------------------|---|------------------------|------------------|--------------------------|--|
| | | Plasma(%) | | Urine(%) | | Feces(%) | | | |
| | | RSV | Metabolites | RSV | Metabolites | RSV | Metabolites | | |
| Wine | 25 ^a | [Conjugates]/[RSV]=30-50x | | [Conjugates]/[RSV]=20-30x | | N.A. | N.A. | 25 ^a in urine | (Soleas, Yan <i>et al.</i> 2001a) |
| Wine | 25 ^a | 10-15 | N.A. | <1 | N.A. | N.A. | N.A. | 89-97 | (Soleas, Yan <i>et al.</i> 2001b) |
| Wine, grape and vegetable juices | 25 ^a | 1.7-1.9 | G and S | 16-17 | G and S | N.A. | N.A. | N.A. | (Goldberg, Yan <i>et al.</i> 2003) |
| Ethanol solution | 25 | <5 ng/mL | G and S | 53-85 | S > G | 0-38 | S | 71-98 | (Walle, Hsieh <i>et al.</i> 2004) |
| | 100 | N.A. | N.A. | <LOQ | Two G, diHG ^l , S, diHS ^m | N.A. | N.A. | N.A. | |
| | 0.2 ⁿ | 4-16 ng/mL | 9-14ng/ml S | 42-83 | S | 1-23 | S | 54-91 | |
| Capsules | 25-150 ^a | ≤1 to <10 ng/mL | N.A. | N.A. | N.A. | N.A. | N.A. | N.A. | (Almeida, Vaz-da-Silva <i>et al.</i> 2009) |
| Ethanol solution | 50 ^{a,o} | <LOD | <i>t</i> -3,5-diS > <i>t</i> -3-S > <i>t</i> -C/O-diG ^p > <i>t</i> -3,4'-diS > <i>t</i> -4'-G > <i>t</i> -3-G | <LOD | <i>t</i> -3,5-diS, > <i>t</i> -3-S > 17 <i>t</i> -3-G > <i>t</i> -C/O-diG > <i>t</i> -3,4'-diS > <i>t</i> -4'-G | N.A. | N.A. | 14-36 in urine | (Burkon, Somoza 2008) |
| Capsules | 500-5000 | 8.4-52 ng/mL | 3-S > S, di-S, G, G-S | <0,04 | 3-S ^q and other S, 1 di-S, 2 G, G-S | 0-23 μg/g ^r | <1% ^s | 77% in urine | (Boocock, Faust <i>et al.</i> 2007) |
| Tablets | 500 ^a | 0.3 | 63 G > 23 S | N.A. | N.A. | N.A. | N.A. | N.A. | (Sergides, Chirila <i>et al.</i> 2016) |
| Capsules | 1000 | <1 ng/mL | S-G, G, di-S, S | <1 ng/mL | S-G, G, di-S, S | N.A. | N.A. | 58 in plasma and urine | (Boocock, Patel <i>et al.</i> 2007) |
| Standard food | 2000 twice daily ^a | 1274 ng/mL | N.A. | N.A. | N.A. | N.A. | N.A. | N.A. | (La Porte, Voduc <i>et al.</i> 2010) |
| High-fat food | | 689 ng/mL | N.A. | N.A. | N.A. | N.A. | N.A. | N.A. | |
| Standard food and quercetin | | 1272 ng/mL | N.A. | N.A. | N.A. | N.A. | N.A. | N.A. | |
| Standard food, quercetin and alcohol | | 1296 ng/mL | N.A. | N.A. | N.A. | N.A. | N.A. | N.A. | |

| Formulations | RSV (mg) | RSV and Metabolites | | | | | | Overall Recovery(%) | Ref. |
|--------------|----------------------------|---------------------|-------------|----------|--|----------|-------------|--------------------------|---|
| | | Plasma(%) | | Urine(%) | | Feces(%) | | | |
| | | RSV | Metabolites | RSV | Metabolites | RSV | Metabolites | | |
| Wine | Moderate daily consumption | N.A. | N.A. | N.A. | <i>t</i> -3- <i>O</i> -G, <i>c</i> -4'- <i>O</i> -G, <i>c</i> -3- <i>O</i> -G, <i>t</i> -4'- <i>O</i> -S, <i>t</i> -3- <i>O</i> -S, <i>c</i> -4'- <i>O</i> -S, <i>c</i> -3- <i>O</i> -G ^t | N.A. | N.A. | 1243 nmol/g ^u | (Zamora-Ros, Urpí-Sardà <i>et al.</i> 2009) |

^a*t*-RSV, ^bN.A.-Not Available, ^cNmol of total metabolites/g creatinine, ^dTotal RSV, ^eThe mean amount of total RSV consumed was 5.4 mg, corresponding to 2.6 mg of *t*-PCD, 2.0 mg of *c*-PCD, 0.4 *t*-RSV and 0.4 *c*-RSV, ^fPercentage values were calculated based on published results, with the expense of phase I metabolites and microflora metabolites which were detected but not quantified (<LOQ), ^gValues report to blood LDL fraction, ^hpmol *t*-RSV/mg LDL protein, ⁱRSV **Glucoside**, ^j**DihydroRSV**, ^kAlthough were administered 4 different doses (200, 400, 600 and 1200 mL) of grape juice (0,16 mg RSV/100 mL), only the two largest were considered here regarding the lack of quantifiable results, which contain 1 and 2 mg of total RSV, ^l**DihydroG**, ^m**DihydroS**, ⁿIntravenous administration, 85.5 mg PCD, ^oC/O Conjugates, ^qAt 0.5 mg dose, ^rOf dry weight feces, ^sIn respect to RSV, ^tCumulative effect of RSV repeated intake (increased concentration of metabolites), ^uNmol total RSV/g creatinine.

[*c*-PCD – *cis*-piceid; *c*-RSV – *cis*-resveratrol; dihydroRSV – dihydroresveratrol; G –derivatives glucuronides; LDL – low-density lipoprotein; LOQ – limit of quantification; PCD – piceid; RSV – resveratrol; S – derivatives sulfates; *t*-RSV – *trans*-resveratrol; *t*-PCD – *trans*-piceid]

The most abundant metabolite found in the systemic circulation by Burkon *et al.* was *t*-RSV-3,5-disulfate (Burkon, Somoza 2008), followed by *t*-RSV-3-sulfate, which, in turn, has been described by Boocock *et al.* (Boocock, Faust *et al.* 2007) as the most abundant metabolite. However, Urpí-Sardà *et al.* (Urpí-Sardà, Jáuregui *et al.* 2005, Urpí-Sardà, Zamora-Ros *et al.* 2007) and Vitaglione *et al.* (Vitaglione, Sforza *et al.* 2005) have identified two glucuronides, namely *t*-RSV-3-*O*-glucuronide and RSV-4'-*O*-glucuronide, as the most abundant forms. Glucuronides were also detected as the most abundant forms in plasma by Sergides *et al.* in relation to sulfates (Sergides, Chirila *et al.* 2016). Two new plasma metabolites of RSV were identified by Boocock *et al.*, precisely *t*-RSV-*C/O*-diglucuronide (18%) and *t*-RSV-3,4'-disulfate (11%). One RSV disulfate was also identified in plasma in the same study but it has not been quantified, leading to the assumption that it probably coincides with the previous one (Boocock, Patel *et al.* 2007). In addition, RSV glucosides (*t*-RSV-4-*O*-glucoside and *c*-RSV-3-*O*-glucoside) were detected in human LDL samples after oral intake of red wine. These RSV glucosides are absorbed from the intestine, possibly by the same glucose transport system of phenolic compounds in rats. Once in human liver microsomes, glucosidation may serve as an alternative detoxification pathway, as aglycones can preferentially undergo glucosidation (Urpí-Sardà, Jáuregui *et al.* 2005). Overall, animal and in human studies reveal that the major components detected in plasma are the metabolites of RSV, precisely glucuronides and sulfates, being those reported to be in superior plasma levels compared with those of the parent compound (Sergides, Chirila *et al.* 2016).

RSV was identified in several organs, mostly in the small intestine, colon, kidney, liver, lungs and brain (Ros 2008). Most routes of excretion are via urine and feces; however, the percentage of excreted compounds varies according to used experimental conditions. As it can be seen in **Table 1.2**, most of the orally administered RSV is recovered in urine in highly variable amounts (Walle, Hsieh *et al.* 2004). After oral administration of formulations containing administered RSV amounts varying from 0.5-5.0 g, 1.0, 5.4 and 25 mg, the quantification of RSV in urine revealed distinct results, varying from only trace amounts, to 17% and 26-52% when compared with initial RSV. Contrary to reports in animals (Wenzel, Soldo *et al.* 2005), human studies revealed that sulfated forms are more abundant than glucuronidated ones, and RSV is present in a much smaller proportion. The most abundant RSV derivative in urine is *c*-RSV-4'-sulfate (84%), followed by *c*-RSV-3-*O*-glucuronide (8%) and other glucuronides and sulfates (Urpí-Sardà, Zamora-Ros *et al.* 2007). According to Burkon and Somoza's studies (Burkon, Somoza 2008), the most abundant metabolite is *t*-RSV-3,5-disulfate, followed by *t*-RSV-3-sulfate, where *t*-RSV-*C/O*-diglucuronide and *t*-RSV-3,4'-disulfate were also posted. In Boocock *et al.* (Boocock, Faust *et al.* 2007) studies, RSV-3-sulfate was the predominant metabolite. RSV was detected in varying

amounts in urine, from only trace amounts (Boocock, Faust *et al.* 2007, Boocock, Patel *et al.* 2007) up to 17% (Urpí-Sardà, Jáuregui *et al.* 2005) and 53-85% (Walle, Hsieh *et al.* 2004). These results point out that the administration of high doses of RSV leads to the presence of sulfate conjugates in higher amounts than the glucuronide ones. This fact must be emphasized, as a possible saturation of glucuronosyltransferases occurs following the administration of greater doses of RSV, contrarily to the sulfation pathway that evidenced a non-competitive substrate inhibition. The occurrence of this saturation might conduce to a shift from glucuronidation to sulfation in the metabolization of RSV, which justified the encountered superior amounts of sulfate metabolites in the presence of high doses of RSV (Rotches-Ribalta, Andres-Lacueva *et al.* 2012). Furthermore, to the best of author's knowledge, besides several RSV derivatives were reported, the total recovery in urine was ca. 1-52%, which is substantially different from 53-85% reported by Walle *et al.* (Walle, Hsieh *et al.* 2004). In this case, the identity of the radioactive moiety was not taken into consideration in the recovery calculation. Thereby, considering that RSV and all metabolites were presumed to participate in radioactivity recovery, it is suggested that not all RSV metabolites have been identified yet. The same assumption is applied to feces recoveries (Cottart, Nivet-Antoine *et al.* 2010). It must also be taken into account that sulfate conjugates have some technological limitations, namely the chromatographic behavior, which prevents their correct identification (Walle, Hsieh *et al.* 2004).

1.5. Evaluation of the efficacy of resveratrol

Besides both RSV's isomers are considered biologically active (Orallo 2006), *t*-RSV is the isomer which exhibits higher biological activity (Sergides, Chirila *et al.* 2016). Beyond this, not much is comparatively known about *c*-RSV for reasons of lack of stability (Orallo 2006), being, for the aforementioned reasons, *t*-RSV the isomer most used in human pharmacological studies (Ortuno, Covas *et al.* 2010). The effectiveness of RSV is supported by *in vivo* testing and bioavailability studies both in animals and humans. However, in most experiments, RSV has been used at concentrations often 10-100 times greater than peak concentrations observed in human plasma after oral consumption (Gescher, Steward 2003) in a free form dissolved in different organic solvents (i.e., dimethyl sulfoxide [DMSO], acetone and ethanol) that are not suitable for drug delivery (Athar, Back *et al.* 2007, Jang, Piao *et al.* 2007, Juan, Wenzel *et al.* 2008). In addition, as it is possible to see in **Table 1.2** the bioavailability studies of RSV in humans range tremendously regarding the administered sources (red wine, grape juice, capsules, among others) and the doses applied (from 0.25 to 5000 mg of RSV).

Given the influence of the matrix type on RSV yield and presumably on its stability (Ortuno, Covas *et al.* 2010), the formulations must be analyzed before and during experiments. It is also important to take into account the contribution of RSV metabolites, assessing them as precisely as possible, by making use of highly sensitive analytical techniques. These techniques should be standardized so the obtained results may hold a degree of comparison and consequently a higher correlation, particularly with regard to the limit of detection (LOD) and the limit of quantitation (LOQ) values. Finally, it is also of relevance to evaluate the impact of RSV and metabolites' interactions with serum proteins on RSV activity to better understand the differences between *in vitro* and *in vivo* assays.

RSV formulations are available as nutritional supplements at doses ranging from 15 to 600 mg per capsule or tablet. Marketing websites recommend both low and high doses, and make claims of "high potency" formulations, yet no evidence exists for a recommended dose of RSV. In fact, despite similar *t*-RSV doses are being administered, its bioavailability from wine and grape juice was six-fold higher than from tablets (Ortuno, Covas *et al.* 2010). The absence of a therapeutic dose for RSV is a result of an inability to translate successful doses used in animal models to humans (Sharma, McNeill 2009) and to an incomplete knowledge about the biomarkers of RSV activity. Although cells that line the digestive tract are exposed to unmetabolized RSV, research in humans suggests that other tissues are exposed primarily to RSV metabolites. RSV urine metabolites have been proposed as biomarkers of moderate wine

consumption (Zamora-Ros , Urpí-Sardà *et al.* 2006, Urpí-Sardà, Zamora-Ros *et al.* 2007, Zamora-Ros, Urpí-Sardà *et al.* 2009), although noticeable inter-individual variability was observed (Zamora-Ros, Urpí-Sardà *et al.* 2009).

The therapeutic potential of certain polyphenols is similar to or higher than that of the parent molecule (Tribolo, Lodi *et al.* 2008, Suri, Liu *et al.* 2010) and it is still unclear whether RSV exerts its biological effects directly, through its metabolites (Shu, Li *et al.* 2010), or whether an *in vivo* interplay between all of them exists. Therefore, the therapeutic potential of RSV conjugates should be considered in future investigations (Wenzel, Soldo *et al.* 2005, Cottart, Nivet-Antoine *et al.* 2010) and, ideally, all the RSV metabolites should be identified and linked to the administered RSV. Several studies have reported the activity for RSV and its metabolites found *in vitro* or *in vivo* studies, as we can see in **Table 1.3**. To determine whether RSV metabolites demonstrate any cytotoxic properties, three major human sulfated conjugates of RSV (*t*-RSV-3-*O*-sulfate, *t*-RSV-4'-*O*-sulfate and *t*-RSV-3-*O*-4'-*O*-disulfate) were synthesized and their anticancer activity was evaluated against three breast cancer cell lines. In contrast to *t*-RSV, its sulfated metabolites showed poor cytotoxicity in human malignant and nonmalignant breast cancer cell lines. In fact, the conjugation of the phenolic groups with sulfuric acid strongly affects the cytotoxicity of all metabolites, which were reduced ca. 10-fold (Miksits, Wlcek *et al.* 2009). However, the *in vitro* activity of the metabolites may not necessarily reflect their *in vivo* function, given the fact that the existing human sulfatases (Miksits, Wlcek *et al.* 2009) and β -glucuronidases (Wang, Heredia *et al.* 2004) could convert the metabolites back to RSV in humans.

RSV oligomers are also proposed as therapeutic compounds. A chemical theoretical approach has shown that oligomers of *t*-RSV, *t*-RSV-3-*O*-glucuronide and glucosides exhibit a remarkably higher antioxidant activity than *t*-RSV (Mikulski, Górnjak *et al.* 2010). The structure-activity relationships obtained for the inhibitory effect of stilbene derivatives, which are RSV oligomers ranging from monomer to tetramer, against murine tyrosinase activity suggest that the double bond in the stilbene skeleton is critical for the inhibition and also that molecular size is important for inhibitory potency. The effects of some RSV derivatives were tested on the F-11 neuroblastoma cell line, which expresses sodium current (I_{Na}) and two different types of voltage-dependent potassium currents: inactivating inward-rectifying current (I_{ERG}) and a slowly inactivating delayed rectifier current (I_{DR}). RSV derivatives, which have been implicated in neuronal apoptosis, modulated voltage-gated potassium channels similarly to the parent

compound, and in some cases they showed better activity and higher specificity toward I_{DR} than I_{ERG} currents (Orsini, Verotta *et al.* 2004).

Table 1.3: Results obtained in studies that reported: cytotoxic properties against three breast cancer cell lines (MCF-7, ZR-75-1 and MDA-MB-231); effect on membrane potential of F-11 neuroblastoma cells line; antioxidant activity; inhibition of melanin production of RSV and its derivatives.

| COMPOUNDS | ACTIVITY | | |
|---|--|-----------------------|----------------------|
| | Anticancer properties (Miksits, Wlcek <i>et al.</i> 2009) | | |
| | Cells | | |
| | MCF-7 | ZR-75-1 | MDA-MB-231 |
| <i>t</i> -RSV | All three sulfated metabolites were less potent than <i>t</i> -RSV (<i>t</i> -RSV-3- <i>O</i> -sulfate < <i>t</i> -RSV-4'- <i>O</i> -sulfate < <i>t</i> -RSV-3- <i>O</i> -4'- <i>O</i> -disulfate) | | |
| <i>t</i> -RSV-3- <i>O</i> -sulfate | | | |
| <i>t</i> -RSV-4'- <i>O</i> -sulfate | | | |
| <i>t</i> -RSV-3- <i>O</i> -4'- <i>O</i> -disulfate | | | |
| | Potassium channels activity (Orsini, Verotta <i>et al.</i> 2004) | | |
| | Concentration (μ M) | I_{ERG} blocked (%) | I_{DR} blocked (%) |
| <i>t</i> -RSV | 90 | 28.9 | 42.9 |
| DihydroRSV | 90 | 39.2 | 50.0 |
| | Antioxidant properties (Mikulski, Górnjak <i>et al.</i> 2010) | | |
| <i>t</i> -RSV | ++ ^a | | |
| <i>t</i> -RSV-3- <i>O</i> -glucuronide | +++ | | |
| PCD | +++ | | |
| ^a From lower(+) to higher (+++) activity | | | |
| | Inhibition of tyrosinase activity (Ohguchi, Tanaka <i>et al.</i> 2003) | | |
| | Inhibition (%) ^b | | |
| RSV | 97 | | |
| DihydroRSV | 60 | | |
| PCD | 17 | | |
| ^b Inhibitory effects on tyrosinase activity by samples at a concentration of 100 μ M | | | |

[I_{ERG} – inactivating inward-rectifying current; I_{DR} – slowly inactivating delayed rectifier current; I_{Na} – sodium current; *t*-RSV – *trans*-resveratrol; PCD – piceid]

To determine total plasma RSV or metabolites concentrations, it is also necessary to take into account LDL and protein-bound fractions. *In vitro* assays have shown that more than > 90% of *t*-RSV is bound to human plasma lipoproteins in a non-covalent manner (Burkon, Somoza 2008), which is reinforced by a study that focused on the binding of RSV to LDL. RSV and its metabolites were recovered in the LDL fraction of healthy volunteers after consumption of 250 mL of Merlot wine (Urpí-Sardà, Jáuregui *et al.* 2005). It is also suggested that RSV levels in serum could be underestimated because of the amounts potentially contained in the cellular fraction, which are not assessed when the analysis of the whole blood is not performed, and therefore its effects and bioavailability are not accurately assessed (Cottart, Nivet-Antoine *et al.* 2010, Sergides, Chirila *et al.* 2016).

As a rational path to overcome the discrepancy between the concentration of RSV required for *in vitro* activity and the doses found to be efficacious *in vivo*, an adaptation of a previously strategy (Gescher, Steward 2003) is proposed:

- Further efficacy studies of RSV in rodents *in vivo* should, as a priority, include measurements of the parent compound and metabolites in the target tissues.
- To determine total plasma RSV or metabolites concentrations, including LDL- and protein-bound fractions.
- Mechanistic *in vitro* studies should explore the activity of RSV at nanomolar concentrations and focus on RSV metabolites, especially its conjugates and oligomers.
- Metabolites and oligomers of RSV, *c*-RSV and PCD should be characterized and quantified in humans.
- Bioavailability assays of RSV in humans need to be increased, preferably with longer testing periods and in larger groups.
- Make an allometric approach between the animal and the human RSV studies.
- Develop suitable delivery systems to provide the optimal state and concentration of RSV able to be delivered to target tissues.

1.6. Resveratrol delivery systems

RSV is targeted for long-term treatments, more properly for prevention. Oral administration of RSV is the preferred route, except for the topical application. However, it is hypothesized that administering RSV through a biodegradable drug delivery system via injection might be a potential therapeutic tool (Lu, Ji *et al.* 2009) to transpose the step taken as limiting the RSV's bioavailability: the intestinal metabolism.

Buccal delivery of RSV-loaded lozenges, which consists of, without swallowing, the direct absorption through the inside of the mouth, has revealed much higher blood levels of RSV than systemic-intended oral formulations. When 1 mg of RSV in 50 mL solution was retained in the mouth for one minute before swallowing, 37 ng/mL of RSV was measured in plasma two minutes later, similar to values achieved with 250 mg of RSV taken in a pill form (Asensi, Medina *et al.* 2002).

Administering oral higher doses to improve the efficacy may be insufficient to elicit systemic levels commensurate with given therapeutic effects (Boocock, Faust *et al.* 2007) and may not be possible as toxic effects have been observed at 1 g/kg (body weight), which would result, moreover, in very high costs (Baur, Sinclair 2006). In this sense, no dose effect in the absorption of RSV was found; therefore, it is not worthwhile to increase RSV content in oral formulations (Walle, Hsieh *et al.* 2004).

Glycosylation can represent an alternative soluble form for RSV administration (Burkon, Somoza 2008, Cottart, Nivet-Antoine *et al.* 2010, Lepak, Gutmann *et al.* 2015), whereas it protects RSV from deleterious oxidation, increasing its solubility in the cell cytoplasm (Regev-Shoshani, Shoseyov *et al.* 2003). Another approach is to modify the RSV structural determinants, such as the number and the position of the hydroxyl groups, intramolecular hydrogen bonding, stereoisomerism and the double bond (Cottart, Nivet-Antoine *et al.* 2010). Methylated RSV has been proposed to circumvent RSV's high degree of metabolism, as it is metabolized slower, a property that has been exploited in drug development of RSV analogues (Pervaiz, Holme 2009, Kapetanovic, Muzzio *et al.* 2011). However, methylation often can change the activity of polyphenols, so it cannot be a solution (Hu 2007).

To achieve an optimum response, RSV should be delivered to its site of action at a rate and concentration that both maximize its therapeutic effects and minimize its side effects, which implies the development of an appropriate RSV delivery system. Strategies of formulations for RSV are presented and explained in terms of pharmaceutical dosage forms, which are: classical

dosage forms and new delivery systems. Classical dosage forms are established drug delivery systems, and new drug delivery systems are drug carriers that aim to deliver RSV to the target or receptor site in a manner that provides the maximum therapeutic activity, prevents degradation or inactivation during transit to target sites, and protects the body from adverse reactions because of inappropriate disposition. Examples include macromolecular drug carriers (protein drug carriers), particulate drug delivery systems (e.g., microparticles, NPs and liposomes), monoclonal antibodies and cells. Over the last two decades, a variety of nanoscale vehicles, including gelatin (Fuchs 2010, Karthikeyan, Hoti *et al.* 2015), ceramic (Peter, Binulal *et al.* 2010), liposomes (Kristl, Teskac *et al.* 2009, Vijayakumar, Vajanthri *et al.* 2016) and micelles (Atanacković, Posa *et al.* 2009) have been under development for therapeutic use.

1.6.1. Classical pharmaceutical dosage forms

These are formulations often based on uncontrolled processing procedures and sources of RSV, of which the most common are tablets, capsules and powders. The tablets and hard gelatin capsules, because of their greater accuracy of drug content, are the most popular. They are available as nutritional supplements, so data about RSV accurate content are often scarce.

Stability of polyphenols is a major concern, so powders, often micronized, are preferred to liquid RSV solutions, and their formulations include surface agents in order to improve RSV absorption following oral administration.

1.6.2. New delivery systems

The slow progress in the efficacy of the treatment of severe diseases suggested a growing need for new ideas on controlling the pharmacokinetics, pharmacodynamics, nonspecific toxicity, immunogenicity, biorecognition and efficacy of drugs. These new strategies, often called drug delivery systems, are based on interdisciplinary approaches that combine polymer science, pharmaceutics, bioconjugate chemistry and molecular biology.

Targeting of drugs to specific sites in the body can be achieved by linking particulate systems or macromolecular carriers to monoclonal antibodies or to cell-specific ligands (e.g., asialofetuin, glycoproteins or immunoglobulins) or by alterations in the surface characteristics of carriers so that they are not recognized by the reticuloendothelial system. To gain an insight about the development of new delivery systems for RSV, the next subsections cover targeted delivery systems that have been proven to be effective for RSV, including a comparison of available results related to stability, solubility and pharmacokinetics of RSV, as shown in **Table 1.4**.

Table 1.4: Characteristics of new delivery systems for RSV, particularly with regard to stability, solubility and release of RSV.

| Delivery System | Effect on RSV properties | | |
|--|--|---|---|
| | Stability | Solubility | Release |
| Casein-RSV Complex | <ul style="list-style-type: none"> • Long shelf-life (Chen 2008) | <ul style="list-style-type: none"> • 2-fold increase of RSV's solubility (Chen 2008) | N.A. |
| Multi-particulate calcium-pectinate carrier | <ul style="list-style-type: none"> • Resistance to stomach's acid-base (Das, Ng 2010) • Stability at 4 °C (>99%) for 6 months, but poorly stable at 40 °C (>90%) (Das, Ng 2010) | N.A. | <ul style="list-style-type: none"> • Gradual drug release (Das, Ng 2010) • Colon-specific delivery (Das, Ng 2010) |
| Chitosan microspheres | <ul style="list-style-type: none"> • More resistance after irradiation and higher thermal stability in relation to RSV (Peng, Xiong <i>et al.</i> 2010) • Stability of encapsulated RSV kept constant (Altiok 2009) | N.A. | <ul style="list-style-type: none"> • Two stages release: first burst release and the second, slower, occurs at higher pH (Peng, Xiong <i>et al.</i> 2010) • Controlled RSV release, with reduction of the initial burst release after enhancement in the cross-linking agent TPP concentration (Cho, Chun <i>et al.</i> 2014) |
| Cyclodextrins (CD's) | <ul style="list-style-type: none"> • Stabilization at pH 5.5-8.5 • HP-β-CD-<i>t</i>-RSV exhibits high stability (López-Nicolás, Rodríguez-Bonilla <i>et al.</i> 2009) | <ul style="list-style-type: none"> • High solubility of resulting complexes (López-Nicolás, Rodríguez-Bonilla <i>et al.</i> 2009, Duarte, Martinho <i>et al.</i> 2015) • Solubility of RSV-CD complex at least 100 times greater (Souto, A. 2009) | <ul style="list-style-type: none"> • Controlled release of RSV (López-Nicolás, Rodríguez-Bonilla <i>et al.</i> 2009) |
| Solid Lipid Nanoparticles (SLN) | <ul style="list-style-type: none"> • Partition of <i>t</i>-RSV into the SLN sphere (Teskač, Kristl 2010) • Physical stability (zeta potential: -38 mV), stable for at least 4 weeks (Teskač, Kristl 2010) • Stability (zeta potential ranging from -29.1 to -34.5 mV) for 3 months at 4 °C (Pandita, Kumar <i>et al.</i> 2014) • Protection from light (Pandita, Kumar <i>et al.</i> 2014) | <ul style="list-style-type: none"> • Lutrol[®] enhance RSV's solubility (Teskač, Kristl 2010) | <ul style="list-style-type: none"> • Two-stage model controlled release of RSV (Teskač, Kristl 2010) • Fast delivery of RSV to the nuclear region (Teskač, Kristl 2010) • Prolonged RSV release up to ca. 120 h, following an Higuchi kinetics model (Pandita, Kumar <i>et al.</i> 2014) |

| Delivery System | Effect on RSV properties | | |
|---|---|---|---|
| | Stability | Solubility | Release |
| Liposomes | <ul style="list-style-type: none"> ●Protection from light and other degradative processes (Caddeo, Teskac <i>et al.</i> 2008, Kristl, Teskac <i>et al.</i> 2009) | <ul style="list-style-type: none"> ●Enhancement of the RSV's solubility (Basavaraj, Betageri 2014) | <ul style="list-style-type: none"> ●Slow and sustained release of RSV (Caddeo, Teskac <i>et al.</i> 2008, Kristl, Teskac <i>et al.</i> 2009, Vijayakumar, Vajanthri <i>et al.</i> 2016) ●Targeting to multiple intracellular sites (Kristl, Teskac <i>et al.</i> 2009) ●Rapid cellular internalization (Kristl, Teskac <i>et al.</i> 2009) |
| Acoustically active lipospheres (AALs) | <ul style="list-style-type: none"> ●12-hour stability (Fang, Hung <i>et al.</i> 2007) | <ul style="list-style-type: none"> ●RSV's solubility water enhanced to 130- and 10-fold comparatively to pH 7.4 buffer and coconut oil, respectively (Fang, Hung <i>et al.</i> 2007) | <ul style="list-style-type: none"> ●Abrupt RSV release upon ultrasound pressure (Fang, Hung <i>et al.</i> 2007) ●Retarded RSV-release profile (compared to aqueous one) (Fang, Hung <i>et al.</i> 2007) |
| Nanoparticles (NPs) | <ul style="list-style-type: none"> ●NPs with improved stability (Jung, Lee <i>et al.</i> 2015, Geng, Zhao <i>et al.</i> 2017) ●Stable loaded biodegradable NPs (Lu, Ji <i>et al.</i> 2009, Penalva, Esparza <i>et al.</i> 2015) ●LbL NPs with physical stability (zeta potential: 35-45 mV) (Lvov, Pattekari <i>et al.</i> 2011) | <ul style="list-style-type: none"> ●Enhancement of the RSV's solubility (Jung, Lee <i>et al.</i> 2015, Zu, Zhang <i>et al.</i> 2016, Geng, Zhao <i>et al.</i> 2017) | <ul style="list-style-type: none"> ●Controlled release of RSV (Lu, Ji <i>et al.</i> 2009, Shao, Li <i>et al.</i> 2009, Lvov, Pattekari <i>et al.</i> 2011, Bu, Gan <i>et al.</i> 2013, Penalva, Esparza <i>et al.</i> 2015, Zu, Zhang <i>et al.</i> 2016, Geng, Zhao <i>et al.</i> 2017) |

[AAL – acoustically active liposphere; CD – cyclodextrin; NP – nanoparticle; RSV – resveratrol; SLN – solid lipid nanoparticle]

1.6.2.1. Macromolecular drug carriers

Both, natural and synthetic water-soluble polymers, have been used as macromolecular drug carriers. A casein-RSV complex makes RSV available in stable forms and formulations having long shelf-life and improved solubility, preferably in aqueous media. The complex is present in the form of discrete powder particles, with an average particle diameter of 5-2000 μm , or in the form of dispersion. The compositions containing the complex are administered to human adult (body weight ca. 70 kg) in the form of capsule, tablet or liquid formulation. Dosage is 0.5-2000 (preferably 5-500) mg/day (Chen 2008).

1.6.2.2. Particulate drug delivery

1.6.2.2.1. Microencapsulation

Encapsulating RSV in a matrix or inside a capsule can reduce its degradation with light and heat and make possible a slow release pattern, which could improve its absorption. RSV was immobilized in polymeric microspheres and the antioxidant activity was found to be preserved for aged samples in ethanolic media (Nam, Ryu *et al.* 2005), thus demonstrating to be a viable a strategy to stabilize RSV in solution. Recently, encapsulation within yeast cells was also described as a technique for stabilizing solid RSV (Shi, Rao *et al.* 2008).

When together, pectins and calcium divalent ions (Ca^{2+}) hardened with PEI (polyethyleneimine) constitute suitable carriers for colon-specific delivery system, called a multi-particulate calcium-pectinate carrier. Pectins (natural polysaccharides) are resistant to the stomach and intestine enzymes, but sensitive to the colonic bacterial enzymes enabling them to transverse the stomach and to be degraded in the colon. However, their solubility and swellability in the basic/neutral fluids (such as intestine) prevent them for being used as efficient colon-specific drugs. These pectin microspheres can encapsulate > 80% of RSV without altering the RSV-retention pattern in simulated (gastrointestinal) GI conditions. The formation of a strong matrix and hard surface layer slows down the release of RSV, which is stable when stored at 4 °C and room temperature. Indeed, microspheres in simulated conditions are able to prevent the release of RSV in simulated upper GI conditions and release in simulated colonic conditions. As a matter of fact, multiple-unit dosage forms, such as multi-particulate calcium-pectinate bead formulations, seem to have advantage over single-unit dosage forms owing to their reproducible and predictable GI transit time, more reliable drug release profile and less local irritation than single-unit forms (Das, Ng 2010).

Chitosan is a natural polysaccharide derived from chitin, which has good properties of non-toxicity, good biocompatibility and mechanical film-forming ability. Its potential is exploited as a delivery system of active agents in the format of microspheres or nanospheres. To increase the time frame and controlled release property of active agents, chitosan microspheres usually need to be cross-linked. RSV-loaded chitosan microspheres showed high stability in relation to light and heat. Precisely, these microspheres showed > 16% of resistance after 60 min of irradiation and thermal stability rose from 72 to 84% at 60 °C and from 48 to 75% at 70 °C for 15 days, in relation to reference samples of RSV (Peng H, Xiong H *et al.* 2010). Peng *et al.* (Peng, Xiong *et al.* 2010) used vanillin, a natural and non-toxic cross-linker, to obtain microspheres with a compacted and continuous network, however with many voids, the voids probably being related

to the mechanisms of air bubbles or entrapped fluid formed during the cross-linking and solidification process. The encapsulation efficiency was very high, 94% (Peng, Xiong *et al.* 2010), and exceeded the values obtained so far with liposomes (76%) (Caddeo, Teskac *et al.* 2008, Kristl, Teskac *et al.* 2009), NPs (91%) (Lu, Ji *et al.* 2009) and additional RSV delivery systems. Release of RSV from chitosan or derivative microspheres involves three different mechanisms: release from the surface of particles, diffusion through the swollen rubbery matrix and release due to polymer erosion. Controlled release of RSV was dependent on pH value of media conditions, with slower release kinetics at higher pH conditions. The release pattern of RSV from chitosan microspheres was divided into two stages. The first stage was initially rapid (burst release), which may be result of the rapid diffusion of RSV onto the surface of microspheres from the initial swelling of the spheres. Latter, the second stage of release from the microspheres was slow (controlled release). The burst release helps to reach the effective RSV concentration rapidly in plasma, whereas the controlled release maintains the effective concentration of RSV in plasma for a long time. These results suggest that the poor bioavailability of RSV could be supplemented by this encapsulation method, thus prolonging its biological half-life *in vivo* (Peng, Xiong *et al.* 2010). Similar results were obtained more recently by using chitosan–sodium tripolyphosphate (TPP) microspheres ranging between 160 and 206 μm , with high encapsulation efficiency values equal or above 94%. A controlled RSV release pattern was encountered at basic pH (7.4), characterized by a lower initial burst of *in vitro* release when using higher TPP solution concentrations. These results emphasized the role of the concentration of the cross-linking agent TPP in the swelling and permeability features of chitosan coated vehicles, pointing them as viable carriers for the delivery of RSV (Cho, Chun *et al.* 2014).

1.6.2.2.2. Cyclodextrins

Cyclodextrins (CDs) are a group of naturally occurring cyclic oligosaccharides composed of glucopyranose derived from starch, which are constituted by variable glucose residues linked by glycosidic bonds. These systems consist of a truncated cone structure with an hydrophobic cavity and are well known for their ability to form inclusion complexes with a wide range of guest molecules (Marier, Vachon *et al.* 2002, Lu, Cheng *et al.* 2009). CDs are divided into two groups: naturals, obtained with higher yield, namely α -, β - and γ -CD, and chemically modified CDs. Unmodified or unsubstituted β -CD has poor water solubility and is unsafe due to its nephrotoxicity, therefore several modified and relatively safe semi-synthetic CDs with higher capacity of molecular recognition and aqueous solubility have been made, such as HP- β -CDs

(hydroxypropyl- β -cyclodextrins) and sulfobutyl ether β -CD. In comparison, it was also found that HP- β -CDs have larger inclusion ability than β -CDs (Lu, Cheng *et al.* 2009).

CDs act as a controlled dosage reservoir that protects RSV against rapid oxidation by free radicals, increasing its antioxidant activity (Marier, Vachon *et al.* 2002). This effect may be due to the formation of inclusion complexes between RSV and HP- β -CDs, where intervenes the -OH group of monophenolic ring of RSV. The RSV's antioxidant activity is prolonged in time and reaches its maximum when all of it is complexed (Marier, Vachon *et al.* 2002). In practice, RSV-HP- β -CD complex shows a higher scavenging capacity than RSV- β -CD complex. However, the inclusion process has little influence on the antioxidant activity of RSV (Lu, Cheng *et al.* 2009). It has also been concluded that *t*-RSV presents a higher stability when complexed by HP- β -CD, comparing to pterostilbene and pinosylvin, two stilbenoid compounds (López-Nicolás, Rodríguez-Bonilla *et al.* 2009).

Possible alterations which may interfere in RSV's bioavailability are on RSV's dissolution capacity, stability, and the slowing of its rapid metabolism and elimination (Marier, Vachon *et al.* 2002). In addition to the scavenging capacity of β -CD and HP- β -CD increase with increasing concentration of CDs (Lu, Cheng *et al.* 2009), RSV was 38% bioavailable after oral administration in a solution of HP- β -CD in rats, which, besides being a significantly higher value than its bioavailability alone, has shown to be insignificant (Marier, Vachon *et al.* 2002). The solubility of RSV increases with increasing CDs concentration in the order β -CD < HP- β -CD, which implies that the cavity of modified CDs provides a better protective microenvironment (Lu, Cheng *et al.* 2009). However, it was suggested that RSV's poor solubility is not the main cause of the maintenance of its low oral bioavailability while carried by RM- β -CDs (randomly methylated β -CD) in suspension. RSV might be rapidly crashing out of the complexes following immediate dilution in the GI tract by binding to the plasma proteins (this explains why the enhanced solubility by means of CDs complexation did not result in increased oral bioavailability of RSV). However, the poor solubility of RSV in aqueous environment coupled with its rapid occurrence in the plasma refutes such a possibility. Alternatively, it is possible that solubility of RSV is pH-dependent, its absorption in the GI tract no longer being just an issue of solubility, but a pH concern as well. The involved data clearly indicated a pH-dependent effect (Das, Lin *et al.* 2008).

López-Nicolás *et al.* reported that HP- β -CDs, including the protonated form of pinosylvin, were more stable than the interaction with the deprotonated form. Therefore, it is necessary to control the pH in the RSV's inclusion formulations because its protonated structures (low pH)

have important beneficial effects for human health to the detriment of higher pH values (López-Nicolás, Rodríguez-Bonilla *et al.* 2009).

1.6.2.2.3. Solid lipid nanoparticles

Solid lipid nanoparticles (SLNs) are endowed with a lipophilic nature, and consequently function as carrier systems for hydrophobic drugs, such as RSV. The affinity between RSV and the SLN is satisfied, leading to the preferential partition of RSV into the SLN sphere instead of staying in the aqueous media (Lu, Ji *et al.* 2009, Shao, Li *et al.* 2009, Teskač, Kristl 2010). The release profile of RSV from the SLNs into dialysis medium, composed of a phosphate buffer saline (pH=7.4), correlates with the RSV loading distribution into the latter. The physicochemical characteristics of RSV favor its localization near the SLNs' shell, enabling its rapid release from the NPs (5h) during one first stage (Shao J, Li X *et al.* 2009, Teskač, Kristl 2010). This happens because, beyond RSV lipophilic nature, it has three-OH groups with a tendency to localize at the interface in the SLN's hydrophilic area. In the following stage, the adsorbed RSV on the particle surface is steadily released over a long period in a sustained manner (Teskač K,J. 2010). The authors underlined additionally that SLNs have the capacity to be transdermally delivered by crossing the keratinocytes membrane (<1 min), transversing the cytoplasm and concentrating near the nucleus. The rate and efficiency of RSV uptake by these cells depend of the NP's surface properties (Teskač, Kristl 2010). In addition, Pandita *et al.* realized pharmacokinetic studies in male Wistar rats and came to the conclusion that, in comparison to its pure suspension, SLNs were able to enhance 8.035-fold the oral bioavailability of RSV, thus acting as promising sustained release system for RSV oral administration (Pandita, Kumar *et al.* 2014).

1.6.2.2.4. Liposomes

Liposomes are small and spherical vesicles that consist of amphiphilic lipids enclosing an aqueous core. The constituent lipids are predominantly phospholipids that form bilayers similar to those found in biomembranes. In most cases, the major component is phosphatidyl choline. Depending on the processing conditions and the chemical composition, liposomes are formed with one or several concentric bilayers. Liposomes are considered an appropriate delivery system for RSV (Kristl, Teskac *et al.* 2009, Vijayakumar, Vajanthri *et al.* 2016). This molecule, once into liposomes, prefers localizing at the liposome surface, where it remains biologically effective in *trans*-conformation by the prevention of transformation into the *cis*-form (Caddeo, Teskac *et al.* 2008, Kristl, Teskac *et al.* 2009). The liposomal bilayers store RSV, preventing overloading of the cells' membranes by the slow and sustained release of RSV to the biological

domains, avoiding cytotoxicity. For this, it is required that liposomes contain an amount of RSV that would be toxic in its unloaded state to maintain therapeutic-free concentration. These bilayers further promote the stimulation of cell-defense system and RSV long-term stability (Caddeo, Teskac *et al.* 2008, Kristl, Teskac *et al.* 2009).

1.6.2.2.5. Acoustically active lipospheres

Microbubbles are a class of oily parenteral formulations constituted by spherical voids filled by a gas that function as lipophilic drug carriers sensitive to ultrasounds waves. Acoustically active lipospheres (AALs) constitute a kind of microbubbles and comprise perfluorocarbons and coconut oil as the cores of inner phase, stabilized with coconut and phospholipid coatings, and the co-emulsifier Pluronic F68 (PF68) (which lowers interfacial tension, adds rigidity, and impedes gas escape and coalescence). As ultrasound pressure waves interact with microbubbles, they begin to oscillate or resonate, which triggers collapse and abrupt drug release in a specific location. These precise locations can be determined by focusing ultrasound energy. Upon insonation of sufficient energy from ultrasound, however, they may convert to a gas, in turn increasing the acoustic reactivity and the potential for localized drug release. Cavitation of AALs with ultrasound can be used to reach the cardiovascular system and treat vascular thromboses by the drugs' delivery. In AAL formulations, RSV shows a sustained release profile. This profile can be well modulated by the alteration of the microbubbles' oil and perfluorocarbon percentages. Formulations with high oil (18%) and perfluorocarbon (32%) percentages have low drug release. On the other hand, ultrasound at 1 MHz showed a more efficient ability to accelerate the amount of drug delivered from AALs with high oil and perfluoropentane compared with the opposite concentrations. The larger droplet size may contribute to increasing the acoustic reflectivity, thus increasing the ultrasound efficacy. PF68 was shown to be effective to slightly but further slowing down RSV release (Fang, Hung *et al.* 2007).

The chosen microbubbles' components with high ratios in AALs may be feasible because of their small size, acceptable safety, sustained drug release and high sensitivity to ultrasound treatment. One of the possible applications of these systems is parenteral injection. As phospholipids are known to cause hemolysis, the formulation of AALs with high oil contents decreases this phenomenon substantially, making it negligible (Fang, Hung *et al.* 2007).

1.6.2.2.6. Nanoparticles

Recent progress in drug delivery has focused on improving it by nanomedicine and polymer techniques (Pelaz, Alexiou *et al.* 2017). New drug delivery systems may be desirable and useful

for the therapeutic use of antioxidants in human diseases. The structure and tunable surface functionality of nanoparticulate systems allows them to encapsulate/conjugate single or multiple entities, either in the core or on the surface, rendering them ideal carriers for various drugs.

Poly(lactide-*co*-epsiloncaprolactone) (PLCL) was successfully developed as epigallocatechin-3-gallate (EGCG) eluting polymeric stent, which could be utilized for preventing thrombosis, inflammation and in-stent restenosis (Han, Lee *et al.* 2009). In another study, Italia *et al.* also suggested the potential of biodegradable NPs in improving the therapeutic efficacy of EGCG (Italia, Datta *et al.* 2008). Sahu *et al.* (Sahu, Bora *et al.* 2008) and Thangapazham *et al.* (Thangapazham, Puri *et al.* 2008), in two separate studies, have demonstrated that curcumin can be delivered by means of nanotechnology-based carriers for prevention and cancer therapy. Curcumin was also nanoformulated with three biocompatible polymers – alginate, chitosan and pluronic – by ionotropic pre-gelation followed by polycationic crosslinking. In detail, pluronic F127 was used to enhance the solubility of curcumin in the alginate-chitosan NPs. This study demonstrated additionally the cellular internalization of curcumin-loaded composite NPs (Das, Kasoju *et al.* 2010). Other study demonstrated that a curcumin-loaded poly(caprolactone) nanofiber matrix is bioactive and has potential as a wound dressing with inflammatory induction and increased rate of wound closure (Merrell, McLaughlin *et al.* 2009). In a different study, PEGylated curcumin conjugate was demonstrated to have much more potent effects on pancreatic cancer cell growth inhibition than free curcumin (Li, Wang *et al.* 2009).

Amphiphilic block copolymer-based polymeric micelles receive most attention because they can self-assemble into NPs with hydrophilic outer shells and hydrophobic inner cores, which capture the hydrophobic drug in the cores and easily disperse in solution with the protection of the hydrophilic shells (Xu, Yang *et al.* 2016). These drug-loaded polymeric micelles are not bigger than 100 nm, being easy to be internalized by cells (Kabanov, Gendelman 2007). By incorporation in these NPs, drugs are prevented from being quickly degraded (Hu, Jiang *et al.* 2003, Zhang, Hu *et al.* 2004) and a sustained release is enabled at the expected site. The hydrophobic characteristics of nanodelivery systems based on polymeric micelles also enable the crossing of blood-brain barrier, where these systems release the drug, as RSV, by a water-soluble controlled release (Lu, Ji *et al.* 2009).

As a matter of fact, a stimulating outlook on the prospective of polymeric NPs as an efficient approach to deliver RSV for cancer therapy has been noticeably offered over the last ten years. RSV-loaded NPs at lower concentration were recently observed to lead to significantly higher cell

death compared with an equivalent dose of free RSV, and this difference of cytotoxicity was not found to be abrogated by the antioxidant vitamin E (Shao, Li *et al.* 2009). In a separate study (Lu, Ji *et al.* 2009), a 12h pre-incubation of RSV-loaded NPs was found to protect cells from A β -induced damage in a dose-dependent manner by attenuating intracellular oxidative stress and caspase-3 activity. Naraynan *et al.* (Narayanan, Nargi *et al.* 2009), recently used liposome-encapsulated curcumin and RSV individually and in combination in male B6C3F1/J and prostate-specific PTEN knockout mice. *In vitro* assays using PTEN-CaP8 cancer cells were also performed to investigate the combined effects of curcumin with RSV. In this study, HPLC analysis of serum and prostate tissues showed a significant increase in curcumin levels when liposome-encapsulated curcumin was co-administered with liposomal RSV. Combination of liposomal forms of curcumin and RSV significantly decreased prostatic adenocarcinoma *in vivo* in PTEN mice, and the *in vitro* studies revealed that curcumin plus RSV effectively inhibited cell growth and induced apoptosis. Findings from this study provided evidence for the first time that phytochemicals in combination are able to enhance the chemopreventive efficacy in prostate cancer.

RSV-loaded chitosan NPs with a modification of the surface using biotin and avidin were suggested as a potent drug delivery system particularly targeting to hepatic carcinoma. Those structures exhibited RSV sustained release *in vitro* profiles, which were confirmed further by their *in vivo* pharmacokinetic profiles in tumor-bearing mice, evidencing as well a dramatic improvement of RSV bioavailability and liver targeting index after injection. Moreover, those NPs were proved to significantly improve the anticancer activity using an inhibitory study on HepG2 cells (Bu, Gan *et al.* 2013).

Recently, RSV-loaded human serum albumin (HSA) spherically-shaped NPs conjugating arginine–glycine–aspartate via a poly(ethylene glycol) (PEG) “bridge” were efficiently designed with an homogeneous particle size distribution with ca. 120 nm of particle size for targeted pancreatic tumor therapy. NPs were shown to be physically stable, while enabling an excellent *in vivo* anti-cancer activity in tumor-bearing mice. In addition, a meritorious feature of high biocompatibility was found to those NPs, with no significant systemic toxicity *in vivo* over 35 days treatment (Geng, Zhao *et al.* 2017). Additional NPs based on proteins consisted in the use of zein, a corn protein. A controlled release of RSV was obtained from RSV-loaded zein NPs, and the bioavailability of RSV was markedly improved after their oral administration in rats. Those NPs offered sustained and prolonged levels of RSV in the plasma, providing a great advantage for the oral delivery of RSV (Penalva, Esparza *et al.* 2015).

RSV-loaded poly (lactic-co-glycolic acid) (PLGA) NPs conjugated with KIM-1 antibody successfully improved the pharmacokinetic profile of RSV and lowered creatinine and protected against tubulointerstitial injury in chronic kidney disease-bearing mice (Lin, Lee *et al.* 2017). In another case, RSV-loaded PEG–poly(lactic acid) improved the stability and controlled delivery of RSV. After intravenous administration into tumor bearing-mice, a retardation of tumor growth in conjunction with an improvement in survival were successfully accomplished, which emphasized the strong beneficial potential of those NPs (Jung, Lee *et al.* 2015).

In the past three decades, Layer-by-Layer (LbL) self-assembly was implemented as a well-established technique to generate films of nanometer sized thickness for various applications including pharmaceutical research, tissue engineering, biosensors, and biomimetics research (Lvov, Decher *et al.* 1993). Drug reservoirs coated with LbL, namely drug NPs, are presented in the next section of this thesis with emphasis, due to the inherent versatility and potential of this technique with personalized drug release profile capabilities which fulfill the criteria imposed for novel drug delivery applications, as for low soluble drug delivery (de Villiers, Lvov 2011, Lvov, Pattekari *et al.* 2011), precisely as RSV.

1.7. Layer-by-Layer coated drug-core nanoparticles as versatile delivery platforms

The assembly of multiple films by LbL assembly consists of depositing alternatively charged PEs on any surface. The interaction between two layers of oppositely charged PEs occurs through electrostatic interaction and ionic bonds (Lvov, Decher *et al.* 1993). Recent studies on LbL assembly published comprise the inclusion of hydrogen bonding, covalent bonding, and biologically specific interaction in addition to electrostatic interaction (Borges, Mano 2014). LbL assembly of ultrathin films was developed on a wide range of substrates. Particularly for biomedical application, substrates include biomedical implants, micrometer sized capsules, metal micro- and NPs, microneedles and lyotropic liquid crystalline NPs (De Geest, Sukhorukov *et al.* 2009, Correa, Dreaden *et al.* 2016, Freag, Elnaggar *et al.* 2016).

LbL assembly is a versatile technique which was used to coat both water soluble and insoluble drugs. Multilayer coatings using LbL assembly have developed on water soluble drug crystals. In this case, the drug crystals were coated under pH condition which makes the drug crystals insoluble in water. Researchers showed controlled release of fluorescein crystals, as the model drug, using LbL assembly based on PAH and PSS (Antipov, Sukhorukov *et al.* 2001).

A promising treatment to cure cancer is still quite challenging for the researchers and physicians worldwide. Various treatments have been carried out for cancer treatment with limited success rate, which include surgery, chemotherapy, hormonal therapy, immunotherapy, and radiation. Among the aforementioned treatments, numerous research teams are focusing on pharmacological studies of many drug molecules still under investigation. Based on previous studies, the majority of the failures in new drug development have been attributed to poor water solubility of the drugs. About 40% of drugs with market approval and nearly 90% of molecules in the discovery pipeline are poorly water soluble. Issues associated with poor solubility can lead to low drug bioavailability, impairing successful drug delivery and thus their clinical application (Kalepu, Nekkanti 2015).

For many poorly soluble compounds, as RSV, the specific surface area created by micronization is not sufficiently large to adequately enhance the dissolution velocity and increase the bioavailability, thus requiring further decrease of the drug particles' size to the nanometer scale. Due to the particular characteristics of constituent particles, nanosuspensions show the capacity of enhancing the saturation solubility of the drug dissolved from NPs. This phenomenon is explained by the Ostwald–Freundlich equation which correlates the small radius and the increased surface interfacial tension with the improved saturation solubility (Van Eerdenbrugh,

Vermant *et al.* 2010). These characteristics allow NPs to be administered intravenously as aqueous suspensions, broadening their potential applications compared to drug microparticles. Nevertheless, the process of drug nanosizing implies additional challenges comparing to micronization and also requires more energy input and more efficient stabilizers (Muller, Gohla *et al.* 2011).

Whereas development of LbL-encapsulated insoluble drug delivery have unique challenge of size restriction for certain treatments. Here we will be discussing aspects of improving existing drug delivery systems for these drugs which are restricted its bioavailability due to less solubility in water. A transition of submicron size particles to NPs size under 200 nm based formulations showed an advantage of greater accumulation at the desired tumoral target due to the enhanced permeation and retention effect (Cui, Wang *et al.* 2016). Another key fact to remember is that LbL assembly can be easily developed by incorporating multilayer films with targeted molecules or ligands specifically towards cell surface receptors. Here we are focusing on LbL assembly on nanometer sized drug capsules.

LbL assembly has shown formation of thin polymer film on core substrate, as small as 10 nm in diameter (Correa, Choi *et al.* 2016). Traditional LbL assembly on colloidal dispersion was based on centrifugation to eliminate PEs in excess. Over the time drug formulations shifted from microparticles to NPs, the process transfer for centrifugation could require long time and speed to separate out NPs. The process becomes very cumbersome in order to achieve NPs based formulation requirements. Many researchers come up with an alternative to replace centrifugation by introducing washless LbL process (Pattekari, Zheng *et al.* 2011, Shutava, Pattekari *et al.* 2012, Santos, Pattekari *et al.* 2015).

The development of micro/NPs using LbL assembly proved efficient delivery mechanisms for hydrophobic and hydrophilic drugs. A wide range of synthetic and biological polymeric materials can be coated on the substrates, such as PAH, PSS, protamine sulfate (PS), alginate, dextran sulfate (DS), chitosan, and bovine serum albumin (BSA) (Lvov, Pattekari *et al.* 2011).

Given the broad range of LbL applications, only the research in exclusively LbL NPs which are specifically composed of pure drug in the core is addressed. To that end, a comprehensive exposition will include the drug nanocore production, used coating materials and associated techniques, multilayer shell permeability control, stability concerns, and *in vitro* and *in vivo* outcomes. **Figure 1.3** depicts the modular technology combination of drug nanocore-based delivery platform of LbL NPs.

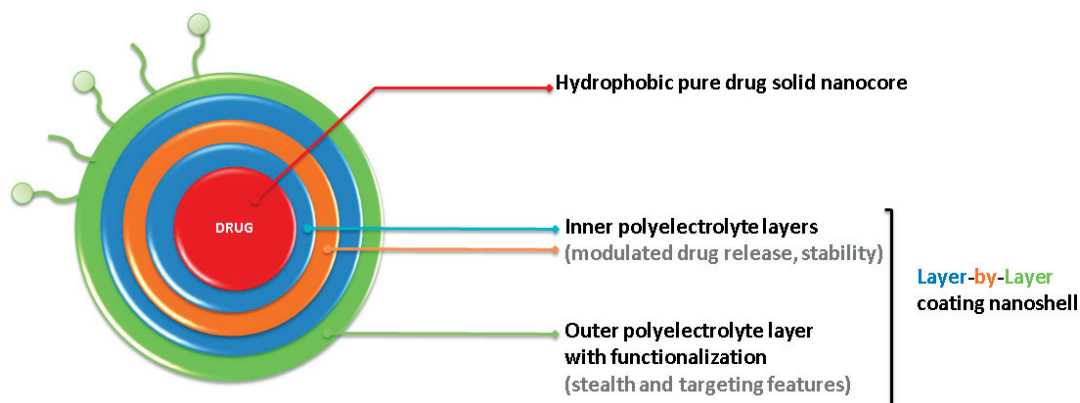


Figure 1.3: Scheme of modular technology combination of drug nanocore-based delivery platform of LbL NPs.

[LbL – Layer-by-Layer; NP – nanoparticle]

1.7.1. Drug candidates for Layer-by-Layer nanoencapsulation

As previously referred, only the LbL NPs performed upon pure drug nanocores will be addressed. These nanocores are constituted by pure hydrophobic drugs, characterized, thus, by a low solubility in water, aiming the enhancement of its water solubility by nanoencapsulation. Among the many physicochemical characteristics to be considered in the whole LbL process production of NPs, the drug solubility is of pivotal relevance.

Several drugs have been employed for LbL drug nanocores encapsulation, more precisely: artemisinin (Chen, Lin *et al.* 2009), camptothecin (Shutava, Pattekari *et al.* 2012, Parekh, Pattekari *et al.* 2014), curcumin (Zheng, Zhang *et al.* 2010, Lvov, Pattekari *et al.* 2011), dexamethasone (Zahr, De Villiers *et al.* 2005, Zhou, Pishko *et al.* 2014), docetaxel (Singh, Banala *et al.* 2015), furosemide (Strydom, Otto *et al.* 2014), IBF (Santos, Pattekari *et al.* 2015), indomethacin (Milkova, Kamburova *et al.* 2013), isoxyl (Strydom, Otto *et al.* 2014), lornoxicam (Pandey, Singh *et al.* 2015), meloxicam (Dev, Toster *et al.* 2013), nifedipine (Strydom, Otto *et al.* 2014), paclitaxel (Zahr, Pishko 2007, Lvov, Pattekari *et al.* 2011, Pattekari, Zheng *et al.* 2011, Yu, Pishko 2011, Shutava, Pattekari *et al.* 2012, Vergara, Bellomo *et al.* 2012, Strydom, Otto *et al.* 2014, Polomska, Gauthier *et al.* 2016), prednisolone (Patil, Ramani *et al.* 2013), RSV (Lvov, Pattekari *et al.* 2011) and tamoxifen (Agarwal, Lvov *et al.* 2008, Lvov, Pattekari *et al.* 2011). Great attention has been devoted to anticancer drugs, due to the large interest and challenge devoted to these therapeutics nowadays.

The methods employed for the preparation of drugs nanocores for LbL further assembly are listed in **Table 1.5**, depicting their characteristics and composition, including the nature of the drug encapsulated into the core.

Table 1.5: Drug-based nanocores, intended for subsequent LbL coating, prepared by top-down and bottom-up approaches.

| Nanonization approach | Drug | Excipients (surfactants, stabilizers, polymers) | Drug nanocore particle size (nm) | Drug nanocore polydispersity index (PDI) | Drug nanocore zeta-potential (mV) | Ref. |
|---|--------------|---|----------------------------------|--|-----------------------------------|---|
| <i>Top-down</i> | | | | | | |
| Sonication-assisted disintegration | Curcumin | PAH, PS | 100-220 | N.A. | ca. – 25-30 | (Lvov, Pattekari <i>et al.</i> 2011) |
| | Docetaxel | Chitosan | ca. 300 | N.A. | ca. + 35 | (Singh, Banala <i>et al.</i> 2015) |
| | Ibuprofen | PAH | 122 | 0.24 | ca + 80 | (Santos, Pattekari <i>et al.</i> 2015) |
| | Indomethacin | Chitosan | 140-200 | N.A. | N.A. | (Milkova, Kamburova <i>et al.</i> 2013) |
| | Lornoxicam | Gelatin-A | 231-265 | N.A. | +0.83 | (Pandey, Singh <i>et al.</i> 2015) |
| | Paclitaxel | PAH, Chitosan | 100-220 | N.A. | ca. – 25-30 | (Lvov, Pattekari <i>et al.</i> 2011) |
| | Paclitaxel | PAH | 200 | N.A. | ca. – 20 | (Pattekari, Zheng <i>et al.</i> 2011) |
| | Paclitaxel | , Chitosan | 150 | N.A. | + 26 | (Vergara, Bellomo <i>et al.</i> 2012) |
| | Paclitaxel | PAH | ca. 100 | N.A. | ca. + 30 | (Agarwal, Lvov <i>et al.</i> 2008) |
| | Prednisolone | Gelatin-A | 220 | N.A. | + 20 | (Patil, Ramani <i>et al.</i> 2013) |
| | Resveratrol | Chitosan | 100-220 | N.A. | ca. – 25-30 | (Lvov, Pattekari <i>et al.</i> 2011) |
| | Tamoxifen | PAH, PDDA | 100-220 | N.A. | ca. – 25-30 | (Lvov, Pattekari <i>et al.</i> 2011) |
| | Tamoxifen | PDDA | 100 | N.A. | ca. + 45 | (Agarwal, Lvov <i>et al.</i> 2008) |
| Wet media milling | Paclitaxel | PSS | 173 | 0.25 | – 58 | (Polomska, Gauthier <i>et al.</i> 2016) |

| Nanonization approach | Drug | Excipients (surfactants, stabilizers, polymers) | Drug nanocore particle size (nm) | Drug nanocore polydispersity index (PDI) | Drug nanocore zeta-potential (mV) | Ref. |
|--|---------------|---|----------------------------------|--|-----------------------------------|---|
| Bottom-up | | | | | | |
| Nanoprecipitation from organic solvents | Camptothecin | PVP and BSA in PBS | 140 | N.A. | + 15 | (Parekh, Pattekari <i>et al.</i> 2014) |
| | Camptothecin | PVP and BSA in PBS | < 150 | N.A. | N.A. | (Shutava, Pattekari <i>et al.</i> 2012) |
| | Curcumin | PAH | N.A. | N.A. | + 30 | (Zheng, Zhang <i>et al.</i> 2010) |
| | Curcumin | PS | N.A. | N.A. | + 30 | (Zheng, Zhang <i>et al.</i> 2010) |
| | Paclitaxel | PAH | ca. 100 | N.A. | + 20 | (Pattekari, Zheng <i>et al.</i> 2011) |
| | Paclitaxel | PVP, sodium docusate and Polysorbate 80 in PBS | 170-180 | N.A. | ca. – 25 | (Shutava, Pattekari <i>et al.</i> 2012) |
| | Paclitaxel | GRAS surfactant calcium alginate | 153 | 0.22 | – 35 | (Zahr, Pishko 2007) |
| Nanoprecipitation through pH change | Meloxicam | Alkaline solution, citric acid | 100 | 0.02 | – 23 | (Dev, Toster <i>et al.</i> 2013) |
| Solvent evaporation/emulsification | Dexamethasone | N-heptane | ca. 150 | N.A. | – 22 | (Zahr, De Villiers <i>et al.</i> 2005) |
| | Dexamethasone | N-heptane | ca. 200 | N.A. | – 16 | (Zhou, Pishko <i>et al.</i> 2014) |
| | Furosemide | Eucalyptol | 174 | N.A. | + 22 | (Strydom, Otto <i>et al.</i> 2014) |
| | Isoxyl | Eucalyptol | 65 | N.A. | + 35 | (Strydom, Otto <i>et al.</i> 2014) |
| | Nifedipine | Eucalyptol | 110 | N.A. | – 32 | (Strydom, Otto <i>et al.</i> 2014) |
| | Paclitaxel | PVA | 100 | N.A. | – 40 | (Yu, Pishko 2011) |

| Nanonization approach | Drug | Excipients (surfactants, stabilizers, polymers) | Drug nanocore particle size (nm) | Drug nanocore polydispersity index (PDI) | Drug nanocore zeta-potential (mV) | Ref. |
|-----------------------|-------------|---|----------------------------------|--|-----------------------------------|------------------------------------|
| | Paclitaxel | Eucalyptol | 156 | N.A. | - 39 | (Strydom, Otto <i>et al.</i> 2014) |
| Spray drying | Artemisinin | Chitosan | 766-806 | N.A. | + 35 | (Chen, Lin <i>et al.</i> 2009) |

[BSA – bovine serum albumin; GRAS – generally recognized as safe; LbL – Layer-by-Layer; NA – not available; PAH – poly(allylamine hydrochloride); PBS –phosphate buffered solution; PDI – polydispersity index; PDDA – poly(diallyldimethylammonium chloride); PS – protamine sulfate; PSS – poly(styrene sulfonate); PVA – poly(vinyl alcohol); PVP – polyvinylpyrrolidone]

1.7.2. Preparation of drug nanocore templates

The production of well-dispersed template drug-based nanocores constitutes the first and the crucial step in the obtainment of LbL-coated drug nanosuspensions. The LbL nanoarchitecture starts to be formed during or immediately after the drug nanocores production, consisting in the second step of this process. The main forces involved in LbL nanoarchitecture establishment are electrostatic interactions, allowing not only for the adsorption of the subsequent PE layers of the nanoshell but also for further electrostatic forces between the charged layers and the NP surface. Some poorly water soluble drugs bear a sufficient intrinsic surface charge in water capable of promoting the adsorption of the first PE coating layer, which can be accomplished during or immediately after the initial size reduction step. In the case of drugs with insufficient surface intrinsic charge, it can be used an ionic stabilizer to provide charge after its strong interactions with the NPs surface by electrostatic interactions. The LbL coating, which is exposed later in this chapter, is performed sequentially after these drug nanocores obtainment, by the alternated adsorption of polycations and polyanions to the system up to the attainment of the desired numbers of PE layers (Santos, Pattekari *et al.* 2015).

This section discusses the two general experimental manufacturing approaches that allow a high degree of drug dispersion used for the obtainment of LbL self-assembly NPs: the top-down and bottom-up approaches, which are graphically represented in **Figure 1.4**.

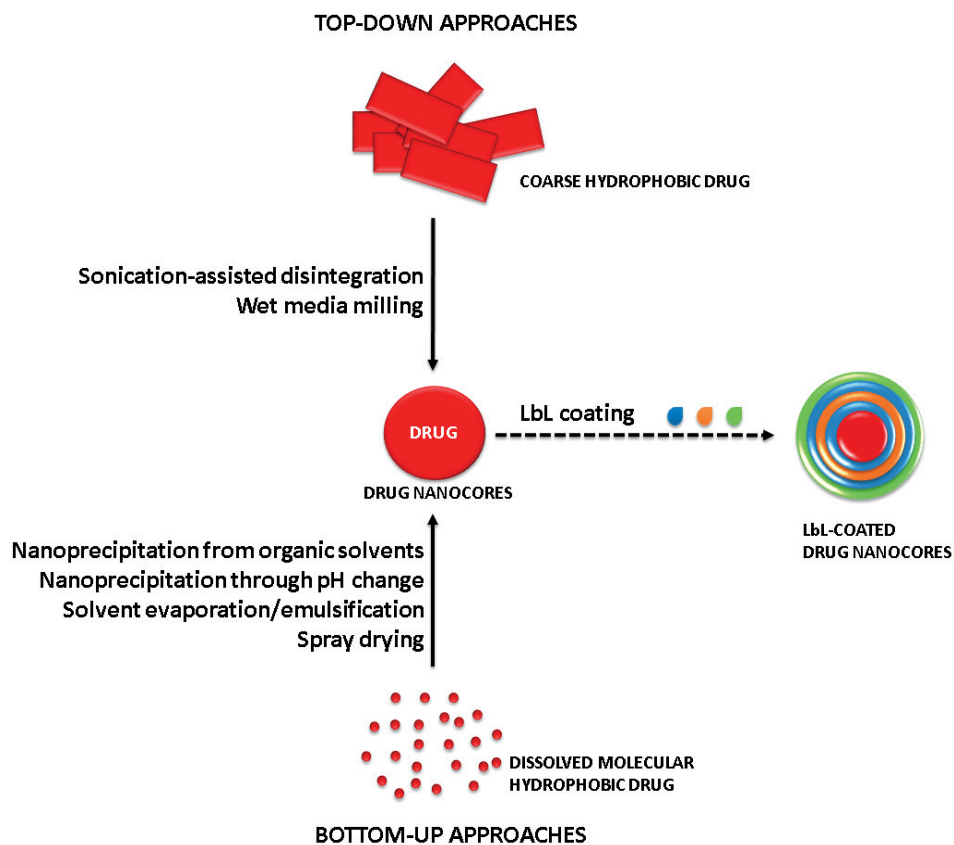


Figure 1.4: Top-down and bottom-up approaches used to prepare drug nanocores, prior the application of the LbL coating technology.

[LbL – Layer-by-Layer]

1.7.2.1. Top-down approaches

Top-down approaches refer to particle size drug reduction techniques into the nanoscale, promoting the direct nanoencapsulation of the drug (Santos, Pattekari *et al.* 2015). Top-down approaches involve sonication-assisted disintegration, and wet media milling of a coarse material in a liquid (aqueous or non-aqueous).

1.7.2.1.1. Sonication-assisted disintegration

The application of ultrasounds has enhanced over the last decades. The most often used top-down approach for the preparation of nanocores for LbL assembly is, in fact, the sonication-assisted powder disintegration. In this method, the drug powder is dispersed in water and submitted to sonication. During sonication, the ultrasound cavitation bubbles expand and collapse in the liquid. This gives origin to very high temperatures and pressure exceeding one thousand atmospheres in the confined volume of a collapsing cavitation bubble, breaking down drug particles into smaller pieces (Shutava, Lvov 2012). The addition of the oppositely charged

PE can be performed before or just immediately after the sonication starts, whose function is to provide sufficient charge in order to promote the stabilization of the system by preventing aggregation. The deposition of this layer allows, thereby, the formation of NPs, conferring a high surface zeta-potential, constituting the first coating layer of drug nanocores (Agarwal, Lvov *et al.* 2008, Lvov, Pattekari *et al.* 2011, Pattekari, Zheng *et al.* 2011, Vergara, Bellomo *et al.* 2012, Milkova, Kamburova *et al.* 2013, Patil, Ramani *et al.* 2013, Pandey, Singh *et al.* 2015, Santos, Pattekari *et al.* 2015, Singh, Banala *et al.* 2015).

The optimization of the process consists in increasing the time and the power of sonication, which allows for particle size reduction. Besides, the use of gas releasing agents, as NH_4HCO_3 , in the dispersing medium proved to enhance the efficient intensity of ultrasounds and facilitate drug powder disintegration, conducting to smaller particles (Lvov, Pattekari *et al.* 2011, Vergara, Bellomo *et al.* 2012).

1.7.2.1.2. Wet media milling

Wet media milling (also called nanomilling) consists in the placing of drug powder in a milling chamber along with the milling media, a stabilizer and an aqueous or non-aqueous liquid medium. Several materials are used as milling media, including glass (yttrium-stabilized), ceramics, zirconium oxide or highly cross-linked polystyrene resins (Patravale, Date *et al.* 2004). The mechanical attrition and impaction of the drug powder in suspension triggered by the milling media unleash vigorous disruptive forces – as shearing, collision and cavitation – which break down the coarse drug into NPs, while the stabilizer is adsorbed alongside (Loh, Samanta *et al.* 2015). Surfactants or amphiphilic block copolymers are commonly applied as stabilizers. The particle size of nanocrystals is influenced by the amount of drug compound, the stabilizer, as well as the technological factors of the processing material, which are strongly determined by used instruments (as the duration of milling, material feed rate and additional operational conditions) (Shutava, Lvov 2012).

In a new research work, several positively charged PEs were used for paclitaxel milling. However, even though the intrinsic expected bare negative surface charge for paclitaxel nanocores, none of the screened polycations allowed for the obtainment of a stable nanosuspension. By contrast, the presence of PSS polyanion in the milling process gave rise to nanocrystals with particle size close to 170 nm. This result pointed out for hydrophobic interactions or specific interactions establishment between the aromatic groups of paclitaxel and repeating units of PSS instead of electrostatic interactions (Polomska, Gauthier *et al.* 2016).

In the last decade, much attention has been paid to wet milling media owed to its robust processing, ease of scale-up, economic benefits and approval by regulatory authorities (Loh, Samanta *et al.* 2015). In fact, wet milling provides many advantages like the absence of organic solvents, possibility of tunable and high drug loadings, possibility of a continuous processing, as well as the applicability low soluble drugs majority (Li, Azad *et al.* 2016). However, in spite of the recognized advantages, this technique has not been widely used to prepare template drug nanosuspensions for LbL, most likely due to the difficulty of implementation on limited drug amount situations.

1.7.2.2. Bottom-up approaches

Bottom-up approaches are based on the drug nucleation in the co-solvent after its previous dissolution in organic solvent (Santos, Pattekari *et al.* 2015).

1.7.2.2.1. Nanoprecipitation from organic solvents

Nanoprecipitation consists in the obtainment of drug NPs in the crystalline or semicrystalline state through the nucleation of drug nanocrystals. This technique starts from high concentrated drug solutions – in which the drug is in a dissolved molecular state – prepared in an appropriate organic solvent (such as acetone, ethanol, tetrahydrofuran, dimethyl sulfoxide, N-methyl-2-pyrrolidone). The drug seed development – which means the conversion of the dissolved molecular drug into drug fine particles in suspension – is initiated following the addition of the organic drug solution to a miscible antisolvent (often water) in the presence of surfactants, and by the slowly enhancement of the antisolvent amount in the mixture. The addition of the organic drug solution to the antisolvent creates a supersaturation state which is followed by drug nucleation and crystal growing. The latter process can be performed by means of an additional effect of powerful sonication, which avoids the formation of larger particles. Due to elevated temperatures of the reaction media, in these cases, the evaporation of the organic solvent is enhanced, and, as consequence, the percentage of water in the media increases, leading to slow oversaturation, multiple seeds, and, ultimately, to nanocrystals formation. It is necessary to take into account that it should be achieved an equilibrium between the low PE solubility in organic solvent/water mixtures (with higher than 60% of organic solvent) and the lowering solubility of low soluble drugs, facing the water content increase. Hence, the choice of the conditions of the LbL assembly should be cautiously made, being difficulty to predict for the majority of the natural PEs (Shutava, Lvov 2012). During the process, the growth of nanocrystals

is controlled by the adsorption of surfactants, giving origin to 100–200 nm drug nanocores (Chen, Khemtong *et al.* 2011, Pattekari, Zheng *et al.* 2011, Parekh, Pattekari *et al.* 2014).

Thereby, the choice of solvents and stabilizers and the mixing process play a key role in the size and stability control of the drug nanocrystals. In fact, surfactants are required in the aqueous phase for the minimization of the high surface energy of incipient nanocores, preventing uncontrolled crystal growth or re-aggregation processes. Ionic (e.g., sodium docusate, sodium lauryl sulfate) and non-ionic (e.g., polyethylene glycols, polysorbates, polyvinylpyrrolidone (PVP)) surfactants can be used. In the case of ionic polymeric surfactants, several consist on PEs, among which are carboxymethylcellulose (CMC), chitosan and its quaternized derivatives, amine derivatives of dextran, carrageenans and proteins (like BSA). Non-ionic and ionic surfactants are usually applied in a combination for better performance, providing both steric and electrostatic repulsions. In addition, the presence of surfactants allows for the enhancement of the viscosity and density of the medium, enhancing ultimately the colloidal stability during drug nanocores generation. Typical formulations contain up to 5–10% (w/w) of stabilizers that cannot be removed or exchanged, under the risk of colloidal stability loss. (Shutava, Lvov 2012, Shutava, Pattekari *et al.* 2012, Parekh, Pattekari *et al.* 2014).

The mixing (also designated by micromixing) phase is essential to enable a fast and uniform supersaturated solution, facilitating the formation of small and homogenous drug NPs. Not least, other important factors of nanoprecipitation process consist on the drug concentration, volume ratio of antisolvent to solvent, temperature and viscosity (Chen, Khemtong *et al.* 2011). The use of sonication avoids agglomeration processes, enabling the obtainment of lower-sized NPs (Zheng, Zhang *et al.* 2010, Pattekari, Zheng *et al.* 2011, Shutava, Pattekari *et al.* 2012, Parekh, Pattekari *et al.* 2014).

1.7.2.2.2. Nanoprecipitation through pH change

Nanoprecipitation can also be induced by pH manipulation when considered drugs show pH-dependent solubility. This approach avoids the concern over the use of organic solvents, which is strongly desirable (Herranz-Blanco, Shahbazi *et al.* 2016). NPs produced by this approach are although curiously instable with regard to dissolution and/or regrowth into microparticles. The surface modification by further drug coatings using LbL PEs suppresses this tendency, while guaranteeing a carrier capable of drug controlled release. Crystalline meloxicam-loaded NPs of close to 100 nm with a polydispersity index (PDI) of 0.015 were obtained by this approach using

a microfluidic continuous flow rotating tube processor along with subsequent LbL oppositely charged PEs coatings (Dev, Toster *et al.* 2013).

1.7.2.2.3. Solvent evaporation/emulsification

In solvent evaporation/emulsification, the hydrophobic drug is dissolved firstly in an organic solvent (e.g., acetone) and it is subject to emulsification – by, e.g., ultrasounds, microfluidizer – into a nonmiscible continuous phase, giving origin to emulsion organic solvent nanodroplets. These nanodroplets, after further evaporation of the solvent, enable the formation of solid NPs. If the continuous phase consists in water, the stabilizer may be dissolved on it (Nicolas, Mura *et al.* 2013). In cases of using other immiscible organic solvents as the continuous phase (e.g., *n*-hexane, eucalyptol), the formed particles can be isolated by using centrifugation and subsequent resuspension in an aqueous phase without the need for stabilizers (Strydom, Otto *et al.* 2014, Zhou, Pishko *et al.* 2014).

Zhou *et al.* prepared dexamethasone nanocores with 200 nm of particle size and zeta potential of – 16 mV of by using solvent evaporation/emulsification technique without using surfactants. The LbL coating of nanocores allowed for the obtainment of a thermoresponsive drug delivery system of solid dexamethasone NPs. This formulation with tunable permeability depending on temperature was proposed to presumably offer an option approach for localized drug delivery, with reduced toxic effects (Zhou, Pishko *et al.* 2014). In parallel, Strydom *et al.* prepared hydrophobic drugs nanocores with a particle size ranging between 75 and ca. 270 nm, with highly different surface characteristics, namely of furosemide, isoxyl, rifampin and paclitaxel. For the nanocores preparation, the authors used eucalyptol as the oil phase and no stabilizers were necessary. These nanocores were further coated with LbL, ensuring for a long-term physical stability, as well as practically ideal zero-order controlled release profiles, which notoriously improved the performance of formulated poorly water-soluble drugs (Strydom, Otto *et al.* 2014).

Besides the nanoencapsulation of hydrophobic drugs is performed frequently by solvent evaporation/emulsification to obtain polymeric NPs (Nicolas, Mura *et al.* 2013), it is, in fact, relatively underutilized to produce drug nanocores. This may occur by the dependence upon the use of significant amounts of organic solvents, capable of compromising drug bioactivity, imparting toxicity and lasting counteractive outcomes.

1.7.2.2.4. Spray drying

Spray drying begins by atomizing/spraying the precursor colloidal suspension or solution in a suspension of droplets, which are following submitted to a drying process that conducts to solvent evaporation, converting them finally into solid particles. The concentration of the precursor suspension or solution, and the atomization step constitute key parameters in defining particle size (Nandiyanto, Okuyama 2011). When the suspension of droplets is sprayed into the drying chamber, it is already warmed to a temperature above the vaporization temperature of the solvent in order to evaporate it. Evaporation of the solvent, diffusion of the solute, the drying process, and the precipitation may take place inside the drying chamber to give origin to the solid product, which are also important factors impacting on final particle size. The involved dry time relies on the residence time of the droplet in the gas phase, that, in turn, is given by several processing factors, such as the geometry of the chamber, carrier gas flow rates, temperature and pressure. The drying method is very effective on account of the high surface area accessible for heat and mass transfer, as a result of the liquid atomization into very small droplets. Spray-drying can be used to produce submicron-sized powders comprised of drug NPs, while preserving the properties of NPs. The transformation into a powder form by spray-drying avoids unexpected chemical reactions, capable of occurring in the surface of NPs due to their characteristic high surface area (Okuyama, Abdullah *et al.* 2006). This stabilizing effect can be strengthened by following coatings at the surface, as the ones achieved by LbL assembly.

In a work performed by Chen *et al.*, for the obtainment of artemisinin nanocrystals, the artemisinin powder was dissolved firstly in ethanol and the transformation into nanocrystals of 766 nm was performed by using a spray-drying method. LbL-coated artemisinin nanocrystals were obtained after the assembly of chitosan, gelatin and alginate as PE coating multilayers (Chen, Lin *et al.* 2009).

Spray drying is, in fact, a well-established technique first and foremost in the drying process of aqueous nanosuspensions to obtain solid dosage forms, as those are definitely more acceptable in regard of their long-term stability, controlled drug release, and patient compliance. However, the obtainment of pure drug nanocrystals directly and solely by spray-drying is not common, probably due to the difficulties arising on the obtainment of 100-200 nm-sized NPs by the conventional spray-drying technique, as well as the costs of processing. New improvements coupled to the conventional spray-drying technique may be considered to obtain drug nanocrystals with a desired particle morphology and with industrial potential applications by

using, e.g., rapid-solvent evaporation, additive-assisted spraying and electro-spray spray-drying (Gao, Liu *et al.* 2013).

1.7.2.3. Comparison between top-down and bottom-up approaches

For the purpose of initial drug nanocores preparation, some differences are emphasized among the two previous presented approaches, concerning essentially the characteristics of obtained nanocores which highly depend on the chosen approach. Top-down approaches do not make use of harsh solvents, however a high energy input is necessary. Moreover, significant amount of heat is created during these protocols, hampering the processing of thermolabile materials (Verma, Gokhale *et al.* 2009). This approach has showed to be more effective for the obtainment of large amounts of close to 200 nm NPs. Distinctly, the bottom-up approach was shown to be more efficient in producing smaller NPs, close to 100 nm, however with lower product yield and the need of organic solvents use, which raises environmental and human safety concerns over residual solvent contents (Pattekari, Zheng *et al.* 2011, Shutava, Lvov 2012, Santos, Pattekari *et al.* 2015). A careful choice and optimization of the preparation approach should be performed in order to obtain the desired characteristics of the final formulation, including the particle size, the zeta potential and the physical stability.

1.7.3. Layer-by-Layer coating materials

The prerequisite for successful LbL surface coating establishment is the existence of surface charge, even if minimal, of drug nanocores. In this context, upon nanocores preparation the concern of charge necessity arises. To that end, when present, apart from preventing drug nanocrystals from coalescence, surfactants serve also as anchors for the polycation/polyanion shell attachment. In the cases of no surfactants use, the first PE layer pursues the stabilizer function by conferring a high surface zeta potential. The deposition of the second charged layer exhibits an opposite surface charge magnitude, able to tie the chains of the first PE layer together and thus hindering their disengagement from the surface (Shutava, Lvov 2012). Thereby, for all cases, the LbL shell performs a dual task in the stabilization of NP. Inner layers further enhance nanocore inaccessibility for recrystallization into larger particles, whilst the outermost shell layers enhance the colloidal stability attributed to the high hydrophilicity of PEs (Shutava, Pattekari *et al.* 2012). These PE multilayers together provide long colloidal stability to the nanoparticulate system and chemical stability of the encapsulated drug, by preventing it from degradation. These layers play additionally a key role on the control of drug release. All these aspects will be further discussed over this chapter.

The composition and characteristics of final LbL NPs are showed in **Table 1.6**. Those NPs consist of the drug nanocores present in **Table 1.5** after the deposition of the LbL coating materials at their surface.

Table 1.6: LbL-coated drug nanocore-based NPs obtained by intermediate washing or washless PE coating approaches.

| Drug-based nanocore | Polycation | Polyanion | Number of bilayers | LbL-coated NPs particle size (nm) | LbL-coated NPs polydispersity index (PDI) | LbL-coated NPs zeta-potential (mV) | Encapsulation Efficiency (%) | Ref. |
|---------------------------------------|-------------------|-----------------------|--------------------|-----------------------------------|---|------------------------------------|------------------------------|---|
| Intermediate washings approach | | | | | | | | |
| Artemisinin | Chitosan | Alginate | 6 | 806 | N.A. | ca. – 30 | 96 | (Chen, Lin <i>et al.</i> 2009) |
| Curcumin | PAH, PS | PSS,BSA | 2 | 107 | N.A. | ca. – 40 | N.A. | (Lvov, Pattekari <i>et al.</i> 2011) |
| Curcumin | PAH | PSS | 2 | 80 | N.A. | ca. – 50 | 80-90 | (Zheng, Zhang <i>et al.</i> 2010) |
| Curcumin | PS | BSA | 2 | 80 | N.A. | ca. – 50 | 80-90 | (Zheng, Zhang <i>et al.</i> 2010) |
| Dexamethasone | PAH | PSS | 2 | ca. 150 | N.A. | < + 5 | N.A. | (Zahr, de Villiers <i>et al.</i> 2005) |
| Dexamethasone | PDDA | PSS | 2 | ca. 200 | N.A. | ca. – 50 | 35 | (Zhou, Pishko <i>et al.</i> 2014) |
| Docetaxel | Chitosan | Alginate | 2-2.5 | 336-354 | 0.172-0.193 | – 32 / + 36 | 94-97 | (Singh, Banala <i>et al.</i> 2015) |
| Furosemide | PDDA | PSS | 2.5 | 186 | N.A. | ca. – 30 | N.A. | (Strydom, Otto <i>et al.</i> 2014) |
| Indomethacin | Chitosan | Pectin | 3 | ca. 275 | N.A. | N.A. | N.A. | (Milkova, Kamburova <i>et al.</i> 2013) |
| Isoxyl | PDDA | PSS | 2.5 | 151 | N.A. | ca. – 30 | N.A. | (Strydom, Otto <i>et al.</i> 2014) |
| Lornoxicam | Gelatin-A | PSS | 2 | 265 | N.A. | ca. + 2 | 57 | (Pandey, Singh <i>et al.</i> 2015) |
| Meloxicam | PAH | Polyprotomine sulfate | 2 | 127 | N.A. | ca. – 40 | 63 | (Dev, Toster <i>et al.</i> 2013) |
| Nifedipine | PDDA | PSS | 2 | 136 | N.A. | ca. – 30 | N.A. | (Strydom, Otto <i>et al.</i> 2014) |
| Paclitaxel | PAH, chitosan | PSS, alginate | 2 | 211 | N.A. | ca. – 40 | N.A. | (Lvov, Pattekari <i>et al.</i> 2011) |
| Paclitaxel | PAH, PS, chitosan | BSA, alginate, PSS | 2 | 100 | N.A. | ca. – 45 | N.A. | (Pattekari, Zheng <i>et al.</i> 2011) |
| Paclitaxel | PAH | PSS | 2 | ca. 120 | N.A. | ca. – 40 | N.A. | (Agarwal, Lvov <i>et al.</i> 2008) |

| Drug-based nanocore | Polycation | Polyanion | Number of bilayers | LbL-coated NPs particle size (nm) | LbL-coated NPs polydispersity index (PDI) | LbL-coated NPs zeta-potential (mV) | Encapsulation Efficiency (%) | Ref. |
|--------------------------|---------------------|--------------------|--------------------|-----------------------------------|---|------------------------------------|------------------------------|---|
| Paclitaxel | PAH | PSS | 1.5 | 166 | N.A. | < + 5 | N.A. | (Zahr, Pishko 2007) |
| Paclitaxel | PDDA | PSS | 2 | 185 | N.A. | ca. – 30 | N.A. | (Strydom, Otto <i>et al.</i> 2014) |
| Paclitaxel | PAH, chitosan | PSSCMA, dextran | 2.5 | ca. 110 | N.A. | ca. – 28 | 98 | (Yu, Pishko 2011) |
| Prednisolone | Gelatin-A | PSS | 2 | 260 | N.A. | – 20 | 58 | (Patil, Ramani <i>et al.</i> 2013) |
| Resveratrol | Chitosan | Alginate | 2 | 200 | N.A. | ca. – 40 | N.A. | (Lvov, Pattekari <i>et al.</i> 2011) |
| Tamoxifen | PAH, PDDA | PSS, PAA | 2 | 220 | N.A. | ca. – 40 | N.A. | (Lvov, Pattekari <i>et al.</i> 2011) |
| Tamoxifen | PDDA | PSS | 3 | 120 | N.A. | ca. – 20 | N.A. | (Agarwal, Lvov <i>et al.</i> 2008) |
| Washless approach | | | | | | | | |
| Camptothecin | Heparin | PLB16-5 | 7.5 | 123 | N.A. | ca. – 15 | 60 | (Parekh, Pattekari <i>et al.</i> 2014) |
| Camptothecin | Heparin | PLB16-5 | 8.5 | 150 | N.A. | ca. + 10 | 70 | (Shutava, Pattekari <i>et al.</i> 2012) |
| Ibuprofen | PAH | PSS | 7.5 | 128 | 0.24 | + 33 | 72 | (Santos, Pattekari <i>et al.</i> 2015) |
| Paclitaxel | Heparin | PLB16-5 | 7.5 | 200 | N.A. | ca. + 20 | 60-70 | (Shutava, Pattekari <i>et al.</i> 2012) |
| Paclitaxel | PAH, PS, chitosan | BSA, alginate, PSS | 2 | 220 | N.A. | ca. – 45 | N.A. | (Pattekari, Zheng <i>et al.</i> 2011) |
| Paclitaxel | Chitosan, lapatinib | Alginate | 4 | ca. 230 | N.A. | – 35 | ca. 70 | (Vergara, Bellomo <i>et al.</i> 2012) |
| Paclitaxel | PLA | PSS | 3.5 | ca. 220 | N.A. | ca. – 5 | N.A. | (Polomska, Gauthier <i>et al.</i> 2016) |

[BSA – bovine serum albumin; LbL – Layer-by-Layer; NA – not available; NP – nanoparticle; PAA – Poly(acrylic acid); PAH – poly(allylamine hydrochloride); PE – polyelectrolyte; PBS – phosphate buffered solution; PDI – polydispersity index; PDDA – poly(diallyldimethylammonium chloride); PLA – Poly(L-arginine); PLB 16-5 – block-copolymers of poly-L-lysine with polyethylene glycol; PS – protamine sulfate; PSS – poly(styrene sulfonate)]

1.7.3.1. Polyelectrolytes

Among the several charged materials introduced for LbL assembly onto the surface of drug nanocores, PEs have been the most frequently applied. In all cases, coating materials can be categorized according to their origin, namely: synthetic (non- and biodegradable) or natural.

A range of different PEs has been used. Standard synthetic PEs include PSS, poly(diallyldimethylammonium chloride) (PDDA), PEI, poly(N-isopropyl acrylamide) (PNIPAM), poly(acrylic acid) (PAA), poly(methacrylic acid) (PMA), poly(vinyl sulfate) (PVS) and PAH (Bertrand, Jonas *et al.* 2000). Natural PEs include polysaccharides, including commonly alginic acid, chitosan, cellulose sulfate, dextran sulfate (DS), heparin, PS and CMC (De Villiers, Otto *et al.* 2011, Lvov, Pattekari *et al.* 2011). **Table 1.6** depicts employed polycation-polyanion pairs (or vice versa) for LbL coating and encapsulation of drug nanocores.

The choice of coating materials for LbL shell assembly is confined to low molecular weight PEs (less than 65 kDa), due to the restricted space for polymer chain adsorption available for NPs. This behaves in contrast to the case of microparticles, that are larger, exhibiting approximate characteristics to a flat surface (Shutava, Pattekari *et al.* 2012). The peculiarity of the LbL assembly process on small NP pertains to the confined space available for PE chain adsorption on the surface of NPs, as well as the extreme influence of the ionic strength of the solution. As a consequence, the tails of PEs protrude into solution (Chodanowski, Stoll 2001), promoting aggregation. Recently, a work of our research group revealed that low molecular weight polymers promoted a decrease in aggregation. In fact, the use of a PSS endowed with a higher molecular weight led to enhanced aggregation, which was reversed in the following layer by using lower molecular weight PAH. This originated, thus, a particle size oscillation during LbL assembly, depending on the PE nature of the outer layer of the LbL shell (Santos, Pattekari *et al.* 2015).

A very interesting fact of LbL assembly upon nanocores is the possibility and, in many cases, the demand for charged PEs adsorption from solutions containing an overload of uncharged, occasionally polymeric, pharmaceutical excipients used for preparation and/or stabilization of NPs, as PVP, glycerol, PEG and sucrose. Thereby, the presence of water-soluble polymers when performing LbL multilayers adsorption onto the surface on NPs can markedly contribute for modification and stabilization of the formulations (Shutava, Lvov 2012, Shutava, Pattekari *et al.* 2012).

1.7.3.2. Advanced functional coatings

Additionally to usual PEs, other components can also be used in the LbL shell composition for precise functionalities either in the external and interior layers of the LbL film. This is possible due to the aqueous nature and the simplicity of the LbL assembly method. An important example of these different LbL shell components are drugs, focusing the obtainment of combination therapy, capable of improving the efficacy or the minimization of the side effects of the nanocore-composed drug. Intermediate LbL bilayers can serve, thus, not only as drug release controllers, but also as drug carriers, capable to incorporate high drug loadings (Correa, Dreaden *et al.* 2016). A study performed by Vergara *et al.* employed negatively charged lapatinib, an epidermal growth factor inhibitor that is able to revert multidrug resistance (by the inhibition of P-gp pump), within the PE multilayer while encapsulating paclitaxel nanocrystals in the core. This nanoformulation has successfully enhanced the cytotoxic efficacy of paclitaxel in OVCAR-3, a multidrug-resistant ovarian cancer cell line, in comparison to the isolated administration of the drug. Thus, these results emphasized the important role of drugs used as components of the LbL shell, enabling for an optimal synergy, and diminishing possible differences in the pharmacokinetics and tumor accumulation of the different employed drugs (Vergara, Bellomo *et al.* 2012).

Several biological drugs have been incorporated into LbL shells, including proteins (Al-Saadi, Yu *et al.* 2009), peptides (Yoshida, Sato *et al.* 2010), and nucleic acids (namely RNAi (Deng, Morton *et al.* 2013), DNA and oligonucleotide sequences) that determine immune response (Shopsowitz, Wu *et al.* 2016), gene transcription (Roh, Deng *et al.* 2016) or gene editing. Notwithstanding, limited efforts have been dedicated to advanced functional LbL shell coatings on the surface of drug-based nanocores until now. The majority of research focuses essentially on the physicochemical characterization of the LbL-coated system. The advantage of enforcing these differentiated materials upon drug nanocores is a field which needs to be developed, facing its potential activities mainly in biological meaningful environments.

1.7.3.3. Outermost layer functionalization

LbL provides a strong tool to engineer NP systems that are able to control drug release while containing dynamic, protein-resistive, and molecularly targeted materials, coming as efficient systemic diseases treatments candidates (Morton, Poon *et al.* 2013). In this context, the outer layer of the LbL shell has been target of particular focus due to its crucial function on the establishment of specific interactions of NPs with tissues/cells, and at last their guiding within the body (Poon, Lee *et al.* 2011, Morton, Poon *et al.* 2013, Hammond 2015, Correa, Dreaden *et*

al. 2016). Thereby, in recent years, widely research has been devoted to specific coating materials for the outer LbL shell layer of drug nanocores-based LbL NPs, specially focusing on two specific attributed and described features, namely the assignment of “stealth” characteristics and the enhancement of the adhesiveness, that are described next.

During LbL assembly processing, depending on the degree of ionization of the adsorbed polyion and the underlying polymer it is possible to attain dense, brush-like layers with high charge density. These conformations can yield hydrated and highly charged systems that regulate protein opsonization and monocyte uptake in the bloodstream, providing key “stealth” characteristics for systemic delivery (Correa, Dreaden *et al.* 2016). Thus, after intravenous administration, LbL-coated NPs can be subjected to opsonization and rapid clearance from the bloodstream by the mononuclear phagocytic system (MPS). This triggers for short biological half-lives and accumulation in the liver and spleen, compromising the desired therapeutic effects. It is, thus, necessary to mask these charged NP coatings with flexible hydrophilic polymers capable of sterically avoid opsonization process, as PEG, improving bioavailability. PEGylation offers additional electrostatic repulsion of PE shells through the interactions with the tails of PEG, preventing aggregation phenomena of NPs mainly under conditions when NPs exhibit low surface charge, and ultimately contributing for colloidal stability enhancement (Shutava, Pattekari *et al.* 2012, Polomska, Gauthier *et al.* 2016). In this context, the surface chemical functionalization of the outer layer of the LbL film of drug nanocore-based LbL NPs with PEG has been performed by several authors (Zahr, De Villiers *et al.* 2005, Zahr, Pishko 2007, Yu, Pishko 2011, Shutava, Pattekari *et al.* 2012, Parekh, Pattekari *et al.* 2014). To this end, after terminating the LbL assembly of the shell, the PEGylation was performed by the covalent attachment of the polymer used as the outer layer to specific reactive groups, e.g., via carboxylic or amine groups, like (Zahr, Pishko 2007, Yu, Pishko 2011, Parekh, Pattekari *et al.* 2014). PEG of high density can be incorporated by electrostatic interactions be the use of copolymers with PEs.

The data obtained by Shutava *et al.* pointed to a higher stability of concentrated paclitaxel LbL-NPs in phosphate buffer solution using the assembly of a PEGylated PE, rather than using it only in the outermost layer of the LbL shell. In addition, higher degree of PEGylation for both of the used polyanions induced further stabilization if applied in the outermost layers (Shutava, Pattekari *et al.* 2012). Polomska *et al.* used a copolymer composed of PEG grafted to PLL, PLL-g-PEG, as the final layer of LbL-coated paclitaxel nanocores. However, the applied electrostatic interactions were not sufficient and/or appropriate to keep the PEGylated layer in the presence of complex serum components, compromising *in vivo* outcomes (Polomska, Gauthier *et al.* 2016). This study calls for the thoroughly *in vitro* evaluation of the stability of PEGylated layers

adsorbed upon LbL shells prior to *in vivo* applications, in order to better predict their capacity of opsonization reduction. Naturally derived and biomimetic, high molecular weight polysaccharides – like hyaluronic acid or alginate – can constitute feasible and promising alternatives to the use of PEG to minimize protein adsorption and opsonization, due to their reported “steath” properties for quantum dots and other polymeric NPs. In fact, hyaluronic acid is a ligand for CD44 receptors, that are typically overexpressed in several cancer cell types, enclosing triple-negative breast cancer. Alginate constitutes a vital protective coating of pathogenic bacteria to escape host immune responses (Poon, Lee *et al.* 2011, Morton, Poon *et al.* 2013). A stringent choice of the outer layer of the LbL film is able to promote, thus, intrinsic molecular targeting, or the option to control targeting of the NP by taking advantage of the inherent *in vivo* properties as, e.g., the tumor microenvironment (Correa, Dreaden *et al.* 2016).

Additionally to “stealth” characteristics, drug nanocore-based LbL NPs are distinguished by enhanced adhesiveness properties due to their high surface area. This assumes special relevance for the cases of NPs intended to oral and pulmonary administration, since the mucoadhesion can boost the bioavailability of drugs. Specific mucoadhesive polymers with valuable biodegradability and biocompatibility characteristics, as chitosan, can be used as the outer layer of the LbL film of drug-nanocore-based LbL NPs aiming the maximization of this effect (Fan, Wang *et al.* 2006).

Furthermore, advanced PE layers can also assume additional functions, as antifouling properties, salt and buffer long-time stability, as well as decreased toxicity and immunogenicity (Shutava, Lvov 2012).

1.7.4. Layer-by-Layer coating procedure

The LbL coating technology was first indicated for the coating of colloidal PE “onion-like” architectures by Mallouk *et al.* (Keller, Johnson *et al.* 1995), and it was elaborated for PE microsized shells coating using washing and centrifugation intermediate steps in the Max Planck Institute (Germany), by Sukhorukov, Caruso, Möhwald, among others (Caruso, Caruso *et al.* 1998, Sukhorukov, Donath *et al.* 1998a, Sukhorukov, Donath *et al.* 1998b). The importance of the development of structures at the nanoscale called for the extension of LbL coating application at the surface of NPs, that on the whole follows the same assumptions as that of microparticles (Bantchev, Lu *et al.* 2009, De Geest, Sukhorukov *et al.* 2009). Therefore, for the preparation of LbL-coated drug-nanocore-based formulations, the drug nanocores obtainment, by the previous listed techniques, is followed by the application of the LbL coating technology at the surface level.

The LbL coating technology consists in the alternating adsorption from an aqueous medium of two or more polymers (usually oppositely charged PEs) or other multivalent species with complementary interactions, including electrostatic and hydrogen bond association, assembling thin PE shells onto the surface of substrate (Iler 1966, Decher, Hong 1991, Decher, Hong *et al.* 1992), the drug nanocores. To that end, for a successful LbL coating it is demanded that the surface of nanocores exhibit a minimal charge (De Villiers, Otto *et al.* 2011). For each PE-based layer deposition of the LbL coating, a non-stoichiometric excess of charge from the PE is absorbed relative to the previous deposited layer on the shell. This is due to the strong linear surface charge density which PEs possess. This charge excess enables the step-wise mechanism necessary for the surface charge polarity reversal, promoting a receptive surface for the next layer adsorption (Decher 1997, Ochs, Such *et al.* 2010). All of the interactions responsible for the LbL process pursuit can be explored and optimized to control the stability, morphology, LbL film thickness, nanocore-polymer molecule depositions and permeation characteristics of the shells (De Villiers, Otto *et al.* 2011). In addition, in order to prevent drug losses throughout the process, the deposition of the multilayers should be conducted in conditions which ensure either the active compound at its lowest solubility and also at the highest stability. To give an illustration, camptothecin nanocrystals should be coated at low pH to avoid the hydrolysis to carboxylate at neutral and moderately alkaline conditions (Shutava, Pattekari *et al.* 2012, Parekh, Pattekari *et al.* 2014).

Two to three PE pair bilayers have proven to be sufficient to promote good colloidal stability for NPs. This occurs in contrast to microparticles, where the LbL shell works as a regulable diffusion barrier, requiring for thick LbL shells. For encapsulation of low soluble drugs is solely necessary a thin LbL shell, since the nanocore drug shows characteristically a low solubility. In fact, two PE bilayers in the shell promote a long time for complete dissolution in sink conditions, e.g. 4-20 h (Lvov, Pattekari *et al.* 2012). Further coatings in the shell are aimed to be specific advanced features as, e.g., targeting as it has already been exposed in the previous section.

The LbL coating of NP templates can be achieved by using also different methods, as, e.g., fluidized bed, electrophoresis or microfluidics devices (Kantak, Beyer *et al.* 2011, Richardson, Ejima *et al.* 2013, Noi, Roozmand *et al.* 2015, Richardson, Bjornmalm *et al.* 2015), being expected as well as to be feasible to perform for the present case of drug nanocores.

The LbL assembly technology presents notorious advantages compared to more conventional coating methods, comprising: the simplicity of the process and equipment; the suitability for most surfaces coating, including NPs surfaces; the flexible aptness to objects of irregular shapes

and sizes; the obtainment of stabilizing coatings; and the control offered over the desired and appropriate multilayer shell thickness (De Villiers, Lvov 2011).

Purification steps are usually necessary for the removal of the excess of nonadsorbed PEs by using intermediate washings. In addition, more recently, non-washings techniques between PE adsorption cycles have been adopted, shortening the duration of the LbL process (Santos, Pattekari *et al.* 2015). These particularities are discussed below. **Figure 1.5** represents graphically the both LbL coating procedures, namely by the use of intermediate washings or by a non-washing approach.

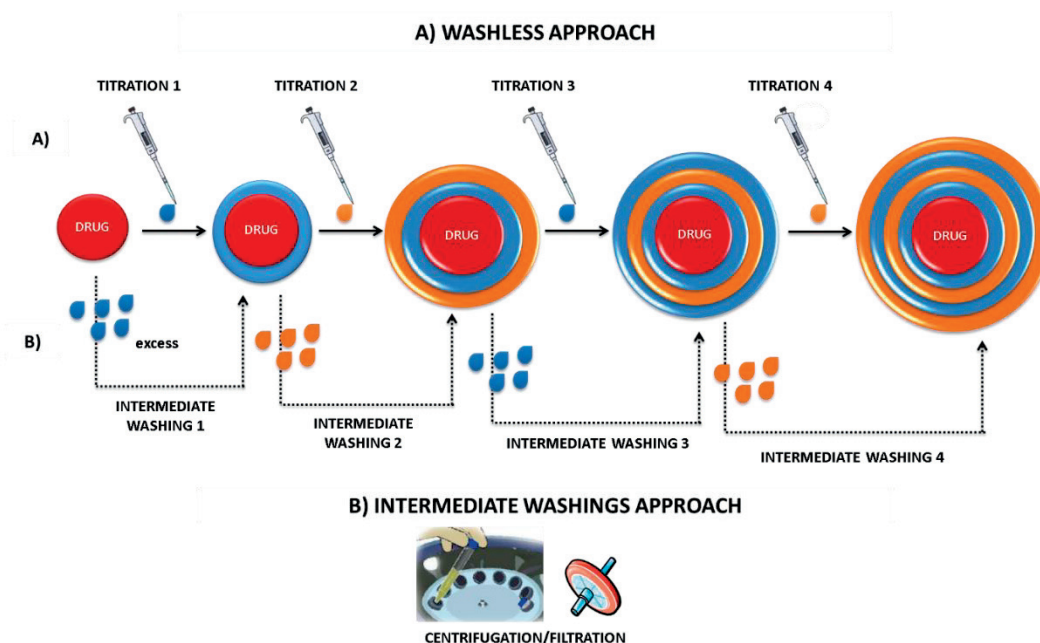


Figure 1.5: LbL coating procedures: intermediate washings or washless approaches.

[LbL – Layer-by-Layer]

1.7.4.1. Intermediate washings

Conventionally, LbL assembly involves the use of intermediate washings to ensure the removal of free PEs in excess after the adsorption of each layer or each adsorption cycle (i.e., two-step polycation/polyanion coating). The non-removal of PEs excesses can conduct to the formation of undesired drug-free PE complexes and to aggregation (Santos, Pattekari *et al.* 2015). Intermediate washings are achieved by means of centrifugation, washing and re-suspension cycles in water. Yet, this procedure demands for significant hands-on-time and are particularly unfeasible in situations of very small NPs which are strongly difficult to pelletize (Bantchev, Lu *et al.* 2009, Richardson, Bjornmalm *et al.* 2015). Besides being more suited for microparticles preparation, the majority of works performed intermediate washings for drug-core LbL NPs obtainment (Zahr, De Villiers *et al.* 2005, Zahr, Pishko 2007, Agarwal, Lvov *et al.* 2008, Chen, Lin

et al. 2009, Zheng, Zhang *et al.* 2010, Yu, Pishko 2011, Dev, Toster *et al.* 2013, Milkova, Kamburova *et al.* 2013, Patil, Ramani *et al.* 2013, Strydom, Otto *et al.* 2014, Zhou, Pishko *et al.* 2014, Pandey, Singh *et al.* 2015, Singh, Banala *et al.* 2015, Polomska, Gauthier *et al.* 2016). In addition, filtration is another possible method that has been used for intermediate washings purposes. However, obtained precipitates by centrifugation and the application of filtration processes lead to significant losses and aggregation along the LbL process (Shutava, Lvov 2012), demanding for alternative washing or non-washing processes for LbL NPs production.

1.7.4.2. Washless approaches

Facing previous stated disadvantages and concerns associated with the use of intermediate washings in preparation of NPs, the necessity for non-washing LbL assembly approaches to obtain a consistent number of layers in the shell was claimed. An alternative approach designated “washless” or “titration” was first studied in detail and developed by Bantchev *et al.* for the coating of TiO₂ nanocores template. Here, the coating species is added to the system in the final amount that is completely adsorbed on the NP template, eradicating intermediate washing steps for the surplus removal of PEs that are used in the conventional methods and are responsible for process losses (Bantchev, Lu *et al.* 2009).

This way, the minimal quantity of PE necessary to reverse the surface charge of NPs is determined from the plateau onset of zeta potential, which is given by the titration graph of zeta potential versus PE added quantity for the layer in hand. The plateau onset corresponds to the moment when surface charge saturation is reached. Each titration graph is, thus, constructed for each layer of the LbL shell by the permanent monitoring of zeta potential during the coating process after each PE fraction addition. In addition, the particle size is stepwise and alongside evaluated since the plateau onset has to consist not only to the reversal of the surface charge, but also to the maintenance of the particle size at the nanoscale, indicating the absence of aggregation. Once the plateau onset is established by the titration curve, the amount of PE necessary for the coating of each layer can be added to the system at one time when performing the preparation of the optimized formulation.

In this regard, one disadvantage of the titration approaches resides on the careful required titration process for each layer of the LbL shell at the specific used conditions (e.g., pH, ionic strength). Conventional methods, on the contrary, involve a weaker optimization and enable the screening of a great number of PE pairs in a relatively short period. Notwithstanding, the use of titrations implies the threat of aggregation when the surface is poorly charged and electrostatic stabilization is not present. This situation can be successfully overcome by using sonication

during the whole LbL coating process (Santos, Pattekari *et al.* 2015); and/or by using block copolymers of PLL and PEG capable of reducing NP aggregation in the presence of low surface charges thanks to the steric stabilization conferred by the chains of PEG (Shutava, Pattekari *et al.* 2012, Parekh, Pattekari *et al.* 2014). Another key fact to remember is that the washless approach enables the scale-up of the LbL-process using highly concentrated nanosuspensions, notably facilitating the process. This approach is more affordable not also because the separation and washings steps are annulled, but also due to the lower amount of PEs used. This assumes particular relevance in the cases of expensive and/or limited available materials, as modified PEs (e.g., PEGylated). To give an illustration, while it is only necessary 2.5 mg PSS per 1 g TiO₂ to reverse completely the surface charge of the particles, for the case of changing the surface charge after centrifugation and re-dispersion the amount of PSS is much higher, namely close to 20 mg. This assumes even a higher emphasis knowing that both centrifugation and washless methods enable the obtainment of the same thickness of PE LbL shells upon nanocores (Bantchev, Lu *et al.* 2009).

Due to the high potential of the LbL approach, recently, a highly versatile and continuous and washless approach for the preparation of multilayered polymeric NPs was developed using a tubular flow type reactor. The adsorption of the PEs occurs in the tubing where particles and PE solution is mixed, promoting the adsorption of the PE upon the surface. Next, NPs pass into the next segment of tubing, where they are mixed with the oppositely charged PE. This process is repeated incessantly until the desired number of layers is adsorbed. The authors pointed out for the necessity of a careful monitoring of the amount of used polymer, in order to avoid any presence of PE in excess in the tubing. This method gives origin to stable NPs during the whole LbL adsorption process at a rate of tens of milligrams of NPs per hour. This method substantially reduced the preparation time and the amount of material, whilst handling to produce a relatively large amount of NPs. The authors claim, thus, for further research by using this washless approach, focusing on further scalability by using higher concentrated NPs, as well as faster flow rates (Elizarova, Luckham 2016).

1.7.5. Controlled drug release

One of the most important goals of LbL assembly of PEs on drug nanocores is to modulate the drug release profiles under the intended conditions of the administration route of interest. Regarding the most attractive and widespread administration route – the oral route – the main aim is to essentially conserve the drug integrity, guarantee the colloidal stability and significantly reduce the drug dissolution rate at gastric conditions, which exhibit a very low pH (Santos,

Pattekari *et al.* 2015, Dilnawaz 2016). These factors assume additional relevance for the case of drugs which cause gastric secondary irritation effects, like, e.g., most of nonsteroidal anti-inflammatory drugs (NSAIDs) (Dev, Toster *et al.* 2013, Milkova, Kamburova *et al.* 2013, Pandey, Singh *et al.* 2015). It is, thus, strongly desirable that a controlled drug release in intestinal conditions promoted by LbL shell coatings, which consequently controls the systemic absorption of drug, and ultimately maintains drug concentrations at therapeutic levels for extended periods of time. Likewise, the LbL coating assembly may also be applied for the controlled dissolution and absorption of drugs administered by other routes, e.g., pulmonary route, in addition to the possibility of sustained locally drug release, e.g., for topical administration. Do to their capacity of reduction of the drug dissolution rate, the LbL coatings can also be implemented to extend the circulation bloodstream time of NPs of anticancer drugs after intravenous administration. The extension of the circulation time is a requirement for the drug passive accumulation in the tumor tissues via the enhanced permeability and retention (EPR) effect (Peer, Karp *et al.* 2007, Fuhrmann, Gauthier *et al.* 2014). Several works have been performed towards this aim, namely the nanoencapsulation of paclitaxel, tamoxifen and camptothecin coated by LbL shells, presented as chemotherapeutics candidates (Zahr, De Villiers *et al.* 2005, Zahr, Pishko 2007, Yu, Pishko 2011, Shutava, Pattekari *et al.* 2012, Parekh, Pattekari *et al.* 2014). For those cases, the PEGylation is unavoidably required to anulate the opsonization and rapid clearance by the MPS of these nanostructures, as it is exposed in section 1.7.3.3.

The diffusion-controlled drug release mechanism from LbL-coated nanocores involves two different steps. Firstly, solvent molecules diffuse across the LbL shell, triggering, secondly, the diffusion of the dissolved drug molecules out of the multilayer shell. The LbL shell permeability is, therefore, responsible for the overall drug release rate. The permeation through water filled pores created within the multilayers, as well as the permeation through the multilayer LbL shell, constitute two mechanisms of permeation that occur in parallel. Due to these facts, the shell permeability is influenced by its thickness and by the particle size and the concentration of the pores. It is necessary to take into account that the drug nanocore dissolution may origin to a strong concentration gradient across the multilayer, triggering for an enhanced osmotic pressure inside the LbL shell. A rearrangement of the PEs may occur under these circumstances leading to larger multilayer pores, boosting the drug diffusion to out of the shell in the initial steps of the dissolution process (Antipov, Sukhorukov 2004, Mansouri, Winnik *et al.* 2009).

Both, the shell thickness as well as the size and the concentration of the pores inside the multilayers, can be subjected to modification, for instance, by changing the type and the number of deposited layers and the deposition media – called bellow as “Natural permeability of the LbL

shells”, or by changing the medium when the coating is finished – titled below as “Stimuli-responsive permeability of the LbL shells”.

1.7.5.1. Natural permeability of the LbL shells

1.7.5.1.1. Number of layers

Increasing the number of deposited layers on the LbL shell is the most linear approach to reduce the permeability of the shell. The lower permeability of thicker LbL shells is attributed to the higher diffusional path that the dissolved drug has to surpass, as well as the consecutive closure of the pores devoted by additional layers deposition (Antipov, Sukhorukov 2004). In fact, while the consecutive closing of the multilayer pores may offer a further barrier to drug diffusion for the inner layers, the reduction in the permeability for the outer layers is mostly attributed to the higher diffusional pathway (Antipov Sukhorukov *et al.* 2001, Antipov, Sukhorukov 2004). Several examples of enhancing the number of layers in the LbL shell have shown to promote prolonged drug dissolution from the nanocore (Agarwal, Lvov *et al.* 2008, Chen, Lin *et al.* 2009, Pattekari, Zheng *et al.* 2011, Yu, Pishko 2011, Patil, Ramani *et al.* 2013, Strydom, Otto *et al.* 2014, Zhou, Pishko *et al.* 2014, Singh, Banala *et al.* 2015, Polomska, Gauthier *et al.* 2016). In our previous work, after 2 h in simulated intestinal conditions, the nanoencapsulation of ibuprofen by using 7.5 bilayered LbL NPs allowed for only 50.6% ibuprofen release as compared with of 59.7% of the 5.5-bilayered LbL NPs, and 88.5% of the 2.5-bilayered NPs. These results are consistent with the previous explanations, depicting an increasing effect of the number of coating bilayers on drug delayed release, as well the notorious decrease of the initial drug burst release (Santos, Pattekari *et al.* 2015). It should be taken into account a detail that is emphasized in some of these works, precisely the need of a minimum number of layers in the LbL for a significant delayed drug release in comparison to the free drug (Santos, Pattekari *et al.* 2015, Polomska, Gauthier *et al.* 2016).

1.7.5.1.2. Deposition conditions

The impact factors on the structure of the PEs during the LbL deposition process and the successive permeability of the obtained shell are discussed below, distinguishing essentially between the ionic strength and pH, and the temperature and organic solvents.

The conformational structure taken by PEs is typically dependent of the ionization state, which can be changed by the alteration of pH for the case of weak PEs, or by the enhancement of the ionic strength to counterbalance charges. In fact, at lower ionization states, PEs assume a more globular than extended conformation, attending to lower interchain repulsions; in addition, the

lateral electrostatic repulsions between the PEs exhibiting the same charge are weaker, yielding to LbL thicker shells. In these cases, the shell thickness enhances exponentially with the number of layers, due to the interpenetration of PEs within the multilayers shell (Guzman, Ritacco *et al.* 2009, De Villiers, Otto *et al.* 2011, Elźbieciak-Wodka, Kolasińska-Sojka *et al.* 2015).

Due to the fact that thicker layers promote lesser permeation, in a study performed by Chen *et al.*, the presence of 0.5 M NaCl in the medium of LbL deposition promoted a tenfold enhancement of the half-time release of artemisinin encapsulated in a chitosan/alginate LbL shell, in comparison to the LbL process deposition without salts (Chen, Lin *et al.* 2009). Notwithstanding, reports of LbL shells composed exclusively of strong PEs showed to be more permeable in higher ionic strengths conditions, regarding their “spongy” structure, which is richer of water-filled pores that expedite the diffusion (Quinn, Pas *et al.* 2012, Elźbieciak-Wodka, Kolasińska-Sojka *et al.* 2015). An example of these findings was the quicker dexamethasone release from PDDA/PSS shells, whose assembly was performed in higher ionic strength conditions in comparison to water (Zhou, Pishko *et al.* 2014).

Another key fact to remember is the temperature as well as the presence of organic solvents in the LbL deposition medium, which also impact on the permeability of the shell. High temperatures in the presence of ethanol gave origin to exponentially growing PE LbL shells. The explanation beyond this effect was close to the influence of ionic strength, specifically by a more globular conformation taken by the PEs, ultimately resulting in the obtainment of interpenetrated PE chains (Poptoshev, Schoeler *et al.* 2004, Salomaki, Vinokurov *et al.* 2005). In agreement with this, the half-time of artemisinin release from chitosan/alginate LbL shells was shown to be enhanced by two to six-fold when the PE layers were deposited in the presence of high temperatures and also in the presence of ethanol in the PE coating solution (Chen, Lin *et al.* 2009).

1.7.5.2. Stimuli-responsive permeability of the LbL shells

The permeability of the LbL shell may also be stimulated by manipulating the conditions of the medium after the assembly is finalized, allowing the design of stimuli-responsive LbL systems. In these cases, the drug release can be manipulated for occurring in targeted body locations or upon external stimuli applications. Much emphasis has been engaged to the development of LbL shells capable of being responsive to several factors, as pH, temperature, solvent, ionic strength, redox potential, glucose, electric, magnetic, light or ultrasounds (Delcea, Mohwald *et al.* 2011, Correa, Dreaden *et al.* 2016). These stimuli have shown to contribute to numerous functionalities of LbL shells, although just a few applications are already available for specific

drug nanocores. The potential of a stimuli-responsive drug release fashion for LbL NPs gives respect to the special interest on controlling or gating drug release depending on the situation of interest.

1.7.5.2.1. pH

The LbL assembly of PEs involves the formation of interpolyelectrolyte complexes, which are obtained in a stoichiometric ratio of charge. Any disturbance on the previous referred stoichiometry due to any change on the absorption conditions, like pH or ionic strength, can induce structural multilayers changes. Thus, the permeability of LbL shells should be susceptible to pH, when they are constituted by at least one weak PE (e.g., PAH/PSS, chitosan/DS). Usually, the accumulation of charges with the same sign origins to enhanced PEs repulsions, leading to swelling and the creation of additional volume cavities that, ultimately, enhance the permeability of the shell. The pH change can reverse this process to reduce the interpolyelectrolyte repulsion, shrinking the LbL shell and consequently closing pores and decreasing the shell permeability. Although, this process occurs just within a specific pH interval, due to the possibility of shell disassembly as a consequence of high interpolyelectrolytes charge imbalance (Antipov, Sukhorukov 2004, Delcea, Mohwald *et al.* 2011, Santos, Pattekari *et al.* 2015).

The pH-dependent release of orally administered drugs has been reported facing the implementation of pH-sensitive LbL shells, including our recent work with ibuprofen (Santos, Pattekari *et al.* 2015). It has to be considered that in the previous situations the differences in the drug release rates is not due to the pH-responsive permeability, but from the natural permeability of the LbL shells of the nanocore drugs, as previously referred.

1.7.5.2.2. Temperature

Thermally-responsive drug release is another inviting approach for a targeted therapeutic action. The LbL PEs architecture rearrangement under high temperatures triggers the creation of higher concentration of free volume cavities within the assemblies, allowing for quicker drug diffusion through the shell. In fact, the LbL shell is highly ion paired and dense in the absence of salts, and, upon heating the film swells gently (Vidyasagar, Sung *et al.* 2012). Zhou *et al.* assisted to a cumulative dexamethasone release from PDDA/PSS LbL-coated NPs enhancement close to 40%, in 8 h, when temperature increased from 37 to 60 °C (Zhou, Pishko *et al.* 2014).

1.7.6. Stability enhancement

The implementation of the LbL technology on the surfaces on NPs impart from several gains, which include the enhancement of chemical stability of the encapsulated drugs, just as well the increase of the stability of the drug –encased nanosuspensions.

1.7.6.1. Chemical stability

LbL allows for the maintenance of the encapsulated drug in the solid form in the nanocore, or even in the shell, making it less susceptible to chemical and/or enzymatic degradation. As an example, the LbL encapsulation of camptothecin prevented the rapid hydrolysis of its active lactone form into its inactive carboxylate form, when it is exposed to neutral and slightly alkaline aqueous solutions, which is of high priority. The chemical stability was preserved for a prolonged period, even in the presence of albumin in the media that turns this formulation more active than free camptothecin and with a lower toxicity due to a lower camptothecin administered dose. Specifically, LbL NPs preserved the camptothecin lactone form at pH 7.4, leading in triple action of the encapsulated drug towards CRL2303 glioblastoma cell (Shutava, Pattekari *et al.* 2012, Parekh, Pattekari *et al.* 2014).

1.7.6.2. Colloidal stability

One challenge implicit to NPs is maintaining their physical or colloidal stability in suspension against particle growth. In fact, very small particles, like NPs, are prone to aggregation while in suspension. In another hand, on account of their high solubility and the surface energy, NPs may suffer an enhancement orders of magnitude in their particle size grow due to Ostwald ripening (Noyes, Whitney 1897, Thanh, Maclean *et al.* 2014). This effect can be successfully overcome by coating these surfaces.

The coating LbL shell promotes the colloidal stability by preventing NP growth through electrostatic stabilization and to offer an impediment for dissolution, that antagonize aggregation and Ostwald ripening, respectively (Parekh, Pattekari *et al.* 2014, Strydom, Otto *et al.* 2014). For instance, LbL coated NPs of paclitaxel, isoxy, furosemide and nifedipine showed to be stable for a long time period of 120 days, contrary to their nonencapsulated forms which suffered an increase in the particle size up to the microscale after 5 days. The authors pointed out that LbL coating shell of NPs prevented crystal growth and aggregation in suspension, showing a sufficient storage period prior to the dosage form formulation, and also to the proper dosage form (Strydom, Otto *et al.* 2014). In accordance to the previous results, other LbL coated shells were adsorbed upon the surface of poorly soluble drugs nanocores (namely curcumin,

paclitaxel, tamoxifen and RSV) by using different biodegradable PEs, showing clearly to promote high colloidal stability (Zheng, Zhang *et al.* 2010, Lvov, Pattekari *et al.* 2011, Pattekari, Zheng *et al.* 2011).

The introduction of PEG in the outer layer of the LbL shell, or even within the inner multilayer layers, improved, as previously referred, the colloidal stability via steric repulsion. This type of conferred stabilization is much less influenced by ionic strength than electrostatic stabilization, which is particularly relevant to obtain colloidal stability in physiologically significant media (Parekh, Pattekari *et al.* 2014, Polomska, Gauthier *et al.* 2016). In fact, in the work of Shutava *et al.*, a 72 h support of colloidal stability of a paclitaxel NPs formulation in phosphate buffer saline was the prerequisite for further *in vivo* testing (Shutava, Pattekari *et al.* 2012).

1.7.7. *In vitro* studies

In vitro assays constitute meaningful agents to firstly predict about the performance, efficacy and safety of emerging developed drug delivery systems. **Table 1.7** lists the *in vitro* studies performed so far with LbL-coated drug nanocores formulations.

LbL-encapsulated NPs of noncytotoxic drugs proved to be nontoxic in a vast range of concentrations and also to be independent of the shell thickness (Milkova, Kamburova *et al.* 2013, Santos, Pattekari *et al.* 2015). For the case of LbL NPs encasing cytotoxic drugs, the materials didn't trigger any cytotoxic response beyond the drug itself (Yu, Pishko 2011). Regarding the importance of PEs in the LbL architectures, it should be taken into account a careful selection should be made in order to use PEs with high stability, efficiency as well low cytotoxicity. In a study performed to assess the cytotoxicity of PEs used for LbL assembly, positively charged PAH was a significantly more toxic than negatively charged PAA on rat smooth muscle A7r5 and human osteosarcoma U-2 OS cells. Although both PEs presented toxicity, their combined use within PE multilayers neutralized isolated cytotoxic effects due to the formation of stable polyvalent interpolyelectrolyte interactions, preventing interactions of these components with membranes or cell uptake (Martinez, Keller *et al.* 2011). Besides very high concentrations of NPs can origin cytotoxicity, probably due to the agglomeration effect and subsequent deposition onto the cells, we have confirmed significantly the safety of the multilayered shell used in a LbL formulation developed by our group (Santos, Pattekari *et al.* 2015). Similar results of no cytotoxicity of the LbL shell were also achieved by Polomska *et al.* on human colon adenocarcinoma HT-29 cell line (Polomska, Gauthier *et al.* 2016), and by Dev *et al.* on mouse fibroblasts NIH 3T3 and neuronal PC12 cells (Dev, Toster *et al.* 2013).

Table 1.7: *In vitro* studies regarding the application of LbL self-assembly nanotechnology.

| Drug | LbL shell composition | Concentration | Target cells | Outcomes | Ref. |
|---------------------|--|------------------|------------------|--|---|
| Cytotoxicity | | | | | |
| Camptothecin | (Heparin/PLB16-5) ₇ - mPEG | 0.01 – 10 μM | <i>CRL2303</i> | 3-fold drug activity enhancement | (Parekh, Pattekari <i>et al.</i> 2014) |
| Meloxicam | (PAH/Polyprotomine sulfate) ₂ | 10 – 500 μM | NIH 3T3 and PC12 | No cytotoxicity induced by the LbL NPs | (Dev, Toster <i>et al.</i> 2013) |
| Paclitaxel | (Chitosan/Dextran) ₂ -PEG | N.A. | Caco-2 | No cytotoxicity induced by the LbL NPs | (Yu, Pishko 2011) |
| Docetaxel | (Chitosan/Alginate) ₂ | 1 – 20 nM | MCF-7 | Higher cytotoxicity observed for LbL NPs compared to the plain drug | (Singh, Banala <i>et al.</i> 2015) |
| Ibuprofen | (PAH/PSS) _{7.5} | 11.7 – 1500 μg/L | Caco-2 | No cytotoxicity, except for higher concentrations | (Santos, Pattekari <i>et al.</i> 2015) |
| Paclitaxel | (PAH/PSS) ₂ -mAb 2C5 | Up to 200 ng/mL | MCF-7 and BT-20 | Higher cytotoxicity for targeted drug LbL NPs than the non-targeted counterparts | (Agarwal, Lvov <i>et al.</i> 2008) |
| Paclitaxel | (PLA/PSS) ₃ - PEG | 0.1 – 100 nM | HT-29 | No cytotoxicity induced by the LbL PE shell | (Polomska, Gauthier <i>et al.</i> 2016) |
| Paclitaxel | (Chitosan/Alginate) ₃ - PEG | 1.5 – 5000 ng/mL | OVCAR-3 | Higher cytotoxicity observed for LbL NPs compared to the plain drug | (Vergara, Bellomo <i>et al.</i> 2012) |
| Paclitaxel | (PAH/PSS) _{1.5} - PEG | 22 μg/mL | MCF-7 | Block of cell growth induced by the drug at the G2/M phase, uninfluenced by LbL PE shell | (Zahr, Pishko 2007) |

| Drug | LbL shell composition | Concentration | Target cells | Outcomes | Ref. |
|---------------------------|--------------------------------------|--|------------------------|--|---|
| Cellular uptake | | | | | |
| Docetaxel | (Chitosan/Dextran-FITC) ₂ | N.A. | MCF-7 | ≥ 1.2-fold higher uptake of positive charged LbL NPs in comparison to negative charged LbL NPs | (Singh, Banala <i>et al.</i> 2015) |
| Hemolytic activity | | | | | |
| Docetaxel | (Chitosan/Alginate) ₂ | N.A. | Wistar rat blood cells | Non-hemolytic potential of LbL NPs, with a safety profile as compared to plain drug | (Singh, Banala <i>et al.</i> 2015) |
| Paclitaxel | (PLA/PSS) ₃ - PEG | Similar concentrations to those present in the blood after the intravenous administration of LbL NPs | Red blood cells | Non-hemolytic potential of LbL NPs | (Polomska, Gauthier <i>et al.</i> 2016) |

[FITC – fluorescein isothiocyanate; LbL – Layer-by-Layer; NA – not available; NP – nanoparticle; PAH – poly(allylamine hydrochloride); PE – polyelectrolyte; PEG – poly(ethylene glycol); PLA – Poly(L-arginine); PLB 16-5 – block-copolymers of poly-L-lysine with polyethylene glycol; PSS – poly(styrene sulfonate)]

In vitro hemolytic assays were performed to evaluate the hemolytic activity of the LbL formulations intended for intravenous administration. The red blood cells exposed to the LbL formulations did not show significant hemolytic activity, evidencing once more that the PEs do not exhibit deleterious effects when exposed to red blood cells (Polomska, Gauthier *et al.* 2016). Singh *et al.* also performed an *in vitro* hemolytic assay and the results suggested for a safety administration, having no significant hemolytic effects in red blood cells (Singh, Banala *et al.* 2015).

Besides the positive feedback of the previous studies regarding the safety of the multilayers LbL shells, more research will be needed to better confirm whether these assumptions are transversal to *in vivo* conditions. In fact, a toxicity response may be triggered after their degradation. It is known, for instance, that positively charged PEs can foster cell death by the interactions with negatively charged cell membranes (Martinez, Keller *et al.* 2011). Above all, it seems pertinent to remember that, when using drug nanocores, the whole PE-to-drug mass ratio is reduced compared with drug-loaded matrices, mitigating thus the toxicity risk of LbL shells.

In order to test the targeting capacity of functionalized LbL shells, Agarwal *et al.* successfully showed that the cytotoxicity of the tamoxifen and paclitaxel induced in human epithelial breast cancer MCF-7 and BT-20 cancer cells was greater for the targeted tumor-specific mAb 2C5-LbL drug-loaded NPs than the non-targeted analogues. With that, it was proved that the LbL approach allows the addition of other relevant functions than the drug itself without changing the activity of the drug (Agarwal, Lvov *et al.* 2008). Parekh *et al.* observed that after several hours of culture using rat brain glioblastoma cells, camptothecin-loaded LbL NPs provoked necrosis unlike the free camptothecin of controls that continued to grow, evidencing the delayed effect of the LbL NPs compared to the free drug, and, ultimately in the greater inhibition effect of the tumor cell growth (Parekh, Pattekari *et al.* 2014). The LbL formulations of Singh *et al.* showed higher cytotoxicity efficiency in MCF-7 cells compared to the plain docetaxel. In addition, cell uptake studies indicated the positively charged formulation had more cytotoxicity than the negatively charged, suggesting an improved uptake of the positive charged formulation (Singh, Banala *et al.* 2015). Other study using MCF-7 breast cancer cells lead to the conclusion that the LbL paclitaxel-loaded NPs were able to block MCF-7 cells at the G2/M phase, appealing to the advantageous use of those formulations in the treatment of metastatic breast cancer (Zahr, Pishko 2007). Regarding these PEGylation approaches targeting the reduction of opsonization, it should be emphasized that, to the best of our knowledge, no reports exist considering the uptake of NPs by phagocytic cells, the essential cells encompassed in their

clearance. However, reduced uptake of LbL-coated modified fluorescent polystyrene nanobeads was already registered by those cells, underlining the strong potential *in vivo* application of NPs with hydrophilic surfaces and a low negative charge (Zahr, Davis *et al.* 2006).

Multi-drug loading systems constitute an attractive concept that is simplified by the implementation of LbL coatings. Vergara *et al.* formulated paclitaxel-loaded LbL NPs with co-encapsulation of lapanitib within the shells. Exposure of the resistant ovary adenocarcinoma OVCAR-3 cells to the LbL paclitaxel and lapanitib-loaded NPs resulted in increased cell death as compared with the treatment with free paclitaxel and free of lapanitib LbL NPs. Using this approach, both drugs can be temporally co-localized in tumor cells for optimum synergy, restricting eventual differences in the pharmacokinetics and tumor accumulation of the two drugs as well as the reduction of systemic toxicity. These results pointed out, thus, the importance of LbL shells in the fight against multidrug-resistant cancers by considering combination therapy (Vergara, Bellomo *et al.* 2012).

In this context, researchers tried to go further and aimed for novel drug delivery platforms capable of new combination therapies. Deng *et al.* developed doxorubicin-nanocore loaded phospholipid liposomes coated by a LbL shell loading siRNA into the outer shell layers. For this, the siRNA was intercalated with poly-L-arginine (PLA) as the polycation in the LbL shell. To assess gene silencing efficiency and cytotoxicity of the NPs, green fluorescent protein (GFP)-expressing MDA-MB-468 cells were used. The present NPs showed to be efficient regarding the gene silencing, while exhibiting no signs of cytotoxicity at a concentration 20-fold higher to the reference PEI/siRNA shell. Thereby, this work constituted a significant development of the LbL approach onto drug nanocores by the combination of a chemotherapy agent with siRNA in a single delivery vehicle, focusing the obtainment of synergic effects and tumor targeting, with the minimum toxicity (Deng, Morton *et al.* 2013). Besides this specific case does not consist properly as a solely drug-core, attending to its liposomal core structure, it constitutes a valuable example of possible and future applications for pure drug cores. All things considered, the administration of multi-drug delivery systems by using LbL core-shell NPs may promote synergistic effects with higher therapeutic efficacy and lower toxicity, representing viable avenues to address aggressive and worrying cancer pathologies.

1.7.8. *In vivo* studies

In vivo studies correspond to a crucial stage addressing the clinical translation of novel developed nanosized drug delivery systems. The assessment of the integrity of the interactions

under *in vivo* conditions is of utmost relevance with respect to LbL drug-loaded NPs. **Table 1.8** shows the *in vivo* study carried out so far with LbL-coated drug nanocores formulations. A very recent study, which consists, to the best of our knowledge, to the unique research study involving LbL drug-nanocore administration *in vivo*, pointed out exactly for this concern and importance (Polomska, Gauthier *et al.* 2016). In this work, PEGylated PE multilayer coated nanocrystals were administered intravenously in subcutaneous HT-29 tumor xenografts bearing mice. Results were compared with approved nanoformulation Abraxane®. LbL NPs demonstrated to be mostly distributed in tissues and/or body organs relatively to plasma. However, their pharmacokinetic and biodistribution profile pointed revealed a rapid clearance followed by accumulation in the MPS organs. This was justified by a destabilization, namely by the shedding of the PEGylated PE from the surface of NPs by the serum components. The authors proposed that electrostatic complexation solely may be insufficient to keep PEGylated PEs after *in vivo* administration, emphasizing the possibility of using covalent bonds between the PEs. With this, the stealth properties of a high developed formulation for anticancer drugs *in vivo* administration could be retained, aiming for higher drug efficacies (Polomska, Gauthier *et al.* 2016).

Table 1.8: *In vivo* study regarding the application of LbL-coated drug nanocore-based NPs.

| Drug | LbL shell composition | Animal model | Administration route | Dosage (mg/kg) | Outcomes | Ref. |
|------------|------------------------------|--|-------------------------|----------------|--|---|
| Paclitaxel | (PLA/PSS) ₃ - PEG | Mice (bearing subcutaneous HT-29 tumor xenografts) | Intravenous (tail vein) | 15 | Higher distribution in the tissue or organs of the body relatively to plasma; however, PEGylation did not prevent adsorption of serum components | (Polomska, Gauthier <i>et al.</i> 2016) |

[LbL – Layer-by-Layer; NP – nanoparticle; PEG – poly(ethylene glycol); PLA – Poly(L-arginine); PSS – poly(styrene sulfonate)]

In this context, to assess *in vivo* gene silencing capacity, Deng *et al.* injected intratumorally doxorubicin co-loaded in PLA/siRNA LbL NPs into the luciferase-expressing MDA-MB468 subcutaneous xenografts of NCR nude mice. These NPs attained extended serum half-lives of up to 28 h, much higher than commonly exhibited half-lives of siRNA delivery NPs. Moreover, a 2-

fold decrease in the luciferase activity in treated tumors after two days was observed, compared to the ones injected with scrambled-siRNA LbL NPs. In addition, the authors assessed the capacity of targeting and of reduction of the specific tumors by LbL NPs. After five days, a 4-fold reduction in luciferase mRNA levels with a clearly sustained release and a cumulative effect of siRNA in tumors was observed. The final study assessment consisted in the treatment of NCR nude mice bearing subcutaneous xenograft tumors of luciferase-expressing MDA-MB-468 cells with intravenous administration of MRP1-siRNA/doxorubicin liposomes. The results of the triple combination therapy exhibited significant regression of the tumor and, in some animals, a complete regression (Deng, Morton *et al.* 2013). This work, besides using liposomes, as previously referred, supported the potential of LbL NPs as combination multitherapeutic platforms for increased efficacy in the fight against aggressive cancers.

This way, and to the best of our knowledge, few studies exist in the literature regarding the oral administration of LbL NPs, calling for the performance of new studies in order to better exploit these interesting platforms under *in vivo* conditions.

References

- Agarwal, A., Lvov, Y., Sawant, R., Torchilin, V. Stable nanocolloids of poorly soluble drugs with high drug content prepared using the combination of sonication and layer-by-layer technology. *J Control Release* **128**, 255-260 (2008).
- Al-Saadi, A., Yu, C. H., Khutoryanskiy, V. V., Shih, S. J., Crossley, A., Tsang, S. C. Layer-by-layer electrostatic entrapment of protein molecules on superparamagnetic nanoparticle: A new strategy to enhance adsorption capacity and maintain biological activity. *J Phys Chem C* **113**, 15260-15265 (2009).
- Almeida, L., Vaz-da-Silva, M., Falcão, A., Soares, E., Costa, R., Loureiro, A.I., et al. Pharmacokinetic and safety profile of trans-resveratrol in a rising multiple-dose study in healthy volunteers. *Mol Nutr Food Res* **53**, 7-15 (2009).
- Altıok, D., Altıok, E., Bayraktar, O., Tihminlioglu, F. Stability of trans-resveratrol incorporated in chitosan microspheres. *Biyomut: 2009 14th National Biomedical Engineering Meeting*, 360-363 (2009).
- Amri, A., Chaumeil, J. C., Sfar, S., Charrueau, C. Administration of resveratrol: What formulation solutions to bioavailability limitations? *J Control Release* **158**, 182-193 (2012).
- Antipov, A. A., Sukhorukov, G. B. Polyelectrolyte multilayer capsules as vehicles with tunable permeability. *Adv Colloid Interface Sci* **111**, 49-61 (2004).
- Antipov, A. A., Sukhorukov, G. B., Donath, E., Möhwald, H. Sustained release properties of polyelectrolyte multilayer capsules. *J Phys Chem B* **105**, 2281-2284 (2001).
- Souto, A. Resveratrol complex and process for the preparation. World Patent WO2009012551. *Eurofarma Laboratórios Ltda; Uniaeo Brasileira de Educacao E Assitencia-Mantedora Da Pucrs* (2009-03-12).
- Asensi, M., Medina, I., Ortega, A., Carretero, J., Baño, M.C., Obrador, E., et al. Inhibition of cancer growth by resveratrol is related to its low bioavailability. *Free Radic Biol Med* **33**, 387-398 (2002).
- Atanacković, M., Posa, M., Heinle, H., Gojković-Bukarica, L., Cvejić, J. Solubilization of resveratrol in micellar solutions of different bile acids. *Colloids Surf B Biointerfaces* **72**, 148-154 (2009).

- Athar, M., Back, J.H., Tang, X., Kim, K.H., Kopelovich, L., Bickers, D.R., *et al.* Resveratrol: a review of preclinical studies for human cancer prevention. *Toxicol Appl Pharmacol* **224**, 274-283 (2007).
- Bantchev, G., Lu, Z., Lvov, Y. Layer-by-layer nanoshell assembly on colloids through simplified washless process. *J Nanosci Nanotechnol* **9**, 396-403 (2009).
- Barger, J. L., Vann, J. M., Cray, N. L., Pugh, T. D., Mastaloudis, A., Hester, S. N., *et al.* Identification of tissue-specific transcriptional markers of caloric restriction in the mouse and their use to evaluate caloric restriction mimetics. *Aging Cell* **16**, 750-760 (2017).
- Basavaraj, S., Betageri, G. V. Improved oral delivery of resveratrol using proliposomal formulation: investigation of various factors contributing to prolonged absorption of unmetabolized resveratrol. *Expert Opin Drug Deliv* **11**, 493-503 (2014).
- Baur, J.A., Sinclair, D.A. Therapeutic potential of resveratrol: the *in vivo* evidence. *Nat Rev Drug Discov* **5**, 493-506 (2006).
- Berman, A. Y., Motechin, R. A., Wiesenfeld, M. Y., Holz, M. K. The therapeutic potential of resveratrol: a review of clinical trials. *NPJ Precis Oncol* **1** 35 (2017).
- Bertrand, P., Jonas, A., Laschewsky, A., Legras, R. Ultrathin polymer coatings by complexation of polyelectrolytes at interfaces: suitable materials, structure and properties. *Macromol Rapid Commun* **21**, 319-348 (2000).
- Bhullar, K. S., Hubbard, B. P. Lifespan and healthspan extension by resveratrol. *Biochim Biophys Acta* **1852**, 1209-1218 (2015).
- Boocock, D.J., Faust, G.E., Patel, K.R., Schinas, A.M., Brown, V.A., Ducharme, M.P., *et al.* Phase I dose escalation pharmacokinetic study in healthy volunteers of resveratrol, a potential cancer chemopreventive agent. *Cancer Epidemiol Biomarkers Prev* **16**, 1246-1252 (2007).
- Boocock, D.J., Patel, K.R., Faust, G.E., Normolle, D.P., Marczylo, T.H., Crowell, J.A., *et al.* Quantitation of trans-resveratrol and detection of its metabolites in human plasma and urine by high performance liquid chromatography. *J Chromatogr B Analyt Technol Biomed Life Sci* **848**, 182-187 (2007).
- Borges, J., Mano, J. F. Molecular interactions driving the layer-by-layer assembly of multilayers. *Chem Rev* **114**, 8883-8942 (2014).

- Bu, L., Gan, L. C., Guo, X. Q., Chen, F. Z., Song, Q., Qi, Z., *et al.* Trans-resveratrol loaded chitosan nanoparticles modified with biotin and avidin to target hepatic carcinoma. *Int J Pharm* **452**, 355-362 (2013).
- Burkon A., Somoza, V. Quantification of free and protein-bound trans-resveratrol metabolites and identification of trans-resveratrol-C/O-conjugated diglucuronides - two novel resveratrol metabolites in human plasma. *Mol Nutr Food Res* **52**, 549-557 (2008).
- Caddeo C, Teskac K, Sinico, C., Kristl, J. Effect of resveratrol incorporated in liposomes on proliferation and UV-B protection of cells. *Int J Pharm* **363**, 183-191 (2008).
- Caruso, F., Caruso, R. A., Möhwald, H. Nanoengineering of inorganic and hybrid hollow spheres by colloidal templating. *Science* **282**, 1111-1114 (1998).
- Catalgol, B., Batirel, S., Taga, Y., Ozer, N. K. Resveratrol: French paradox revisited. *Front Pharmacol* **3**, 141 (2012).
- Charytoniuk, T., Drygalski, K., Konstantynowicz-Nowicka, K., Berk, K., Chabowski, A. Alternative treatment methods attenuate the development of NAFLD: A review of resveratrol molecular mechanisms and clinical trials. *Nutrition* **34**, 108-117 (2017).
- Chen, C. Casein complexes. World Patent WO2008017415. *DSM IP ASSETS BV* (2008-02-14).
- Chen, H., Khemtong, C., Yang, X., Chang, X., Gao, J. Nanonization strategies for poorly water-soluble drugs. *Drug Discov Today* **16**, 354-360 (2011).
- Chen, J., Bai, Q., Zhao, Z., Sui, H., Xie, X. Resveratrol improves delayed r-tPA treatment outcome by reducing MMPs. *Acta Neurol Scand* **134**, 54-60 (2016).
- Chen, Y., Lin, X., Park, H., Greever, R. Study of artemisinin nanocapsules as anticancer drug delivery systems. *Nanomed Nanotechnol* **5**, 316-322 (2009).
- Cho, A. R., Chun, Y. G., Kim, B. K., Park, D. J. Preparation of chitosan-TPP microspheres as resveratrol carriers. *J Food Sci* **79**, E568-E576 (2014).
- Chodanowski, P., Stoll, S. Polyelectrolyte adsorption on charged particles: ionic concentration and particle size effects—a Monte Carlo approach. *J Chem Phys* **115**, 4951-4960 (2001).
- Correa, S., Choi, K. Y., Dreaden, E. C., Renggli, K., Shi, A., Gu, L., *et al.* Highly scalable, closed-loop synthesis of drug-loaded, layer-by-layer nanoparticles. *Adv Funct Mater* **26**, 991-1003 (2016).

- Correa, S., Dreaden, E. C., Gu, L., Hammond, P. T. Engineering nanolayered particles for modular drug delivery. *J Control Release* **240**, 364-386 (2016).
- Cottart, C.H., Nivet-Antoine, V., Laguillier-Morizot, C., Beaudoux, J.L. Resveratrol bioavailability and toxicity in humans. *Mol Nutr Food Res* **54**, 7-16 (2010).
- Csiszar, A., Labinsky, N., Pinto, J.T., Ballabh, P., Zhang, H., Losonczy, G., *et al.* Resveratrol induces mitochondrial biogenesis in endothelial cells. *Am J Physiol Heart Circ Physiol* **297**, H13-H20 (2009).
- Cui, W., Wang, A., Zhao, J., Li, J. Biomacromolecules based core/shell architecture toward biomedical applications. *Adv Colloid Interface Sci* **237**, 43-51 (2016).
- Cvejić, J. H., Krstonošić, M. K., Bursać, M., Miljić, U. Chapter 7: Polyphenols. *Nutraceutical and functional food components - effects of innovative processing techniques*. Galanakis, Charis M., Chania, Academic Press: 203-258 (2017).
- Das, R.K., Kasoju, N., Bora, U. Encapsulation of curcumin in alginate-chitosan-pluronic composite nanoparticles for delivery to cancer cells. *Nanomedicine* **6**, 153-160 (2010).
- Das, S., Lin, H.S., Ho, P.C., Ng, K.Y. The impact of aqueous solubility and dose on the pharmacokinetic profiles of resveratrol. *Pharm Res* **25**, 2593-2600 (2008).
- Das, S., Ng, K.Y. Colon-specific delivery of resveratrol: optimization of multi-particulate calcium-pectinate carrier. *Int J Pharm* **385**, 20-28 (2010).
- De Geest, B. G., Sukhorukov, G. B., Mohwald, H. The pros and cons of polyelectrolyte capsules in drug delivery. *Expert Opin Drug Deliv* **6**, 613-624 (2009).
- De la Lastra C.A., Villegas, I. Resveratrol as an antioxidant and pro-oxidant agent: mechanisms and clinical implications. *Biochem Soc Trans* **35**, 1156-1160 (2007).
- De Villiers, M. M., Lvov, Y. M. Layer-by-layer self-assembled nanoshells for drug delivery. *Adv Drug Deliv Rev* **63**, 699-700 (2011).
- De Villiers, M. M., Otto, D. P., Strydom, S. J., Lvov, Y. M. Introduction to nanocoatings produced by layer-by-layer (LbL) self-assembly. *Adv Drug Delivery Rev* **63**, 701-715 (2011).
- Decher, G. Fuzzy nanoassemblies: toward layered polymeric multicomposites. *Science* **277**, 1232-1237 (1997).

- Decher, G., Hong, J. D. Buildup of ultrathin multilayer films by a self-assembly process .1. Consecutive adsorption of anionic and cationic bipolar amphiphiles on charged surfaces. *Makromol Chem, Macromol Symp* **46**, 321-327 (1991).
- Decher, G., Hong, J. D., Schmitt, J. Buildup of Ultrathin Multilayer Films by a Self-Assembly Process .3. Consecutively Alternating Adsorption of Anionic and Cationic Polyelectrolytes on Charged Surfaces. *Thin Solid Films* **210**, 831-835 (1992).
- Delcea, M., Mohwald, H., Skirtach, A. G. Stimuli-responsive LbL capsules and nanoshells for drug delivery. *Adv Drug Delivery Rev* **63**, 730-747 (2011).
- Deng, Z. J., Morton, S. W., Ben-Akiva, E., Dreaden, E. C., Shopsowitz, K. E., Hammond, P. T. Layer-by-layer nanoparticles for systemic codelivery of an anticancer drug and siRNA for potential triple-negative breast cancer treatment. *ACS Nano* **7**, 9571-9584 (2013).
- Dev, S., Toster, J., Prasanna, S. V., Fitzgerald, M., Iyer, K. S., Raston, C. L. Suppressing regrowth of microfluidic generated drug nanocrystals using polyelectrolyte coatings. *RSC Adv* **3**, 695-698 (2013).
- Dilnawaz, F. Polymeric biomaterial and lipid based nanoparticles for oral drug delivery. *Curr Med Chem* (2016).
- Duarte, A., Martinho, A., Luís, Â., Figueiras, A., Oleastro, M., Domingues, F. C., *et al.* Resveratrol encapsulation with methyl- β -cyclodextrin for antibacterial and antioxidant delivery applications. *LWT--Food Sci Technol* **63**, 1254-1260 (2015).
- Elizarova, I. S., Luckham, P. F. Fabrication of polyelectrolyte multilayered nano-capsules using a continuous layer-by-layer approach. *J. Colloid Interface Sci* **470**, 92-99 (2016).
- Elliott, P.J., Jirousek, M. Sirtuins: novel targets for metabolic disease. *Curr Opin Investig Drugs* **9**, 371-378. (2008).
- Elźbieciak-Wodka, M., Kolasińska-Sojka, M., Nowak, P., Warszyński, P. Comparison of permeability of poly(allylamine hydrochloride)/and poly(diallyldimethylammonium chloride)/poly(4-styrenesulfonate) multilayer films: linear vs. exponential growth. *J Electroanal Chem* **738**, 195-202 (2015).
- Fan, Y. F., Wang, Y. N., Fan, Y. G., Ma, J. B. Preparation of insulin nanoparticles and their encapsulation with biodegradable polyelectrolytes via the layer-by-layer adsorption. *Int J Pharm* **324**, 158-167 (2006).

- Fang, J.Y., Hung, C.F., Liao, M.H., Chien, C.C. A study of the formulation design of acoustically active lipospheres as carriers for drug delivery. *Eur J Pharm Biopharm* **67**, 67-75 (2007).
- Freag, M. S., Elnaggar, Y. S., Abdelmonsif, D. A., Abdallah, O. Y. Layer-by-layer-coated lyotropic liquid crystalline nanoparticles for active tumor targeting of rapamycin. *Nanomedicine (Lond)* **11**, 2975-2996 (2016).
- Fuchs S, K. M., Hertel T, Winter G, Pietzsch M, Coester C. Transglutaminase: new insights into gelatin nanoparticle cross-linking. *J Microencapsul* **27**, 747-754. (2010).
- Fuhrmann, K., Gauthier, M. A., Leroux, J. C. Targeting of injectable drug nanocrystals. *Mol Pharmaceutics* **11**, 1762-1771 (2014).
- Gaballah, H. H., Zakaria, S. S., Elbatsh, M. M., Tahooun, N. M. Modulatory effects of resveratrol on endoplasmic reticulum stress-associated apoptosis and oxido-inflammatory markers in a rat model of rotenone-induced Parkinson's disease. *Chem Biol Interact* **251**, 10-16 (2016).
- Gao, L., Liu, G., Ma, J., Wang, X., Zhou, L., Li, X., et al. Application of drug nanocrystal technologies on oral drug delivery of poorly soluble drugs. *Pharm. Res.* **30**, 307-324 (2013).
- Geng, T., Zhao, X., Ma, M., Zhu, G., Yin, L. Resveratrol-loaded albumin nanoparticles with prolonged blood circulation and improved biocompatibility for highly effective targeted pancreatic tumor therapy. *Nanoscale Res Lett* **12**, 437 (2017).
- Gescher, A.J., Steward, W.P. Relationship between mechanisms, bioavailability, and preclinical chemopreventive efficacy of resveratrol: a conundrum. *Cancer Epidemiol Biomarkers Prev.* **12**, 953-957 (2003).
- Ghaiad, H. R., Nooh, M. M., El-Sawalhi, M. M., Shaheen, A. A. Resveratrol promotes remyelination in cuprizone model of multiple sclerosis: biochemical and histological study. *Mol Neurobiol* **54**, 3219-3229 (2017).
- Goldberg, D.M., Yan, J., Soleas, G.J. Absorption of three wine-related polyphenols in three different matrices by healthy subjects. *Clin Biochem* **36**, 79-87 (2003).
- Gülçin, İ. Antioxidant properties of resveratrol: A structure–activity insight. *Innovative Food Sci Emerging Technol* **11**, 210-218 (2010).

- Guzman, E., Ritacco, H., Rubio, J. E. F., Rubio, R. G., Ortega, F. Salt-induced changes in the growth of polyelectrolyte layers of poly(diallyl-dimethylammonium chloride) and poly(4-styrene sulfonate of sodium). *Soft Matter* **5**, 2130-2142 (2009).
- Hammond, P. T. Layer-by-Layer Approaches to Staging Medicine from Surfaces. *AIChE J* **61**, 1106-1117 (2015).
- Han, D.W., Lee, J.J., Jung, D.Y., Park, J.C., Hyon, S.H. Development of epigallocatechin gallate-eluting polymeric stent and its physicochemical, biomechanical and biological evaluations *Biomed Mater* **4**, 044104. (2009).
- Henry, C., Vitrac, X., Decendit, A., Ennamany, R., Krisa, S., Mérillon, J.M. Cellular uptake and efflux of trans-piceid and its aglycone trans-resveratrol on the apical membrane of human intestinal Caco-2 cells. *J Agric Food Chem* **53**, 798-803 (2005).
- Herranz-Blanco, B., Shahbazi, M. A., Correia, A. R., Balasubramanian, V., Kohout, T., Hirvonen, J., *et al.* pH-switch nanoprecipitation of polymeric nanoparticles for multimodal cancer targeting and intracellular triggered delivery of doxorubicin. *Adv Healthc Mater* **5**, 1904-1916 (2016).
- Hu, M. Commentary: bioavailability of flavonoids and polyphenols: call to arms. *Mol Pharm* **4**, 803-806 (2007).
- Hu Y, Jiang X, Ding Y, Zhang L, Yang C, Zhang J, *et al.* Preparation and drug release behaviors of nimodipine-loaded poly(caprolactone)-poly(ethylene oxide)-polylactide amphiphilic copolymer nanoparticles. *Biomaterials* **24**, 2395-2404 (2003).
- Iler, R. K. Multilayers of colloidal particles. *J Colloid Interface Sci* **21**, 569-594 (1966).
- Italia JL, Datta P, Ankola DD, Ravi, K. M. Nanoparticles enhance per oral bioavailability of poorly available molecules: epigallocatechin gallate nanoparticles ameliorates cyclosporine induced nephrotoxicity in rats at three times lower dose than oral solution. *J Biomed Nanotechnol* **4**, 304-312 (2008).
- Jang MH, Piao XL, Kim HY, Cho EJ, Baek SH, Kwon SW, *et al.* Resveratrol oligomers from *Vitis amurensis* attenuate beta-amyloid-induced oxidative stress in PC12 cells. *Biol Pharm Bull* **30**, 1130-1134 (2007).
- Jensen, J.S., Wertz, C.F., O'Neill, V.A. Preformulation stability of trans-resveratrol and trans-resveratrol glucoside (Piceid). *J Agric Food Chem* **58**, 1685-1690 (2010).

- Juan, M.E., Wenzel, U., Daniel, H., Planas, J.M. Resveratrol induces apoptosis through ROS-dependent mitochondria pathway in HT-29 human colorectal carcinoma cells. *J Agric Food Chem* **56**, 4813-4818 (2008).
- Juhasz, B., Varga, B., Gesztelyi, R., Kemeny-Beke, A., Zsuga, J., Tosaki, A. Resveratrol: a multifunctional cytoprotective molecule. *Curr Pharm Biotechnol* **11**, 810-818 (2010).
- Jung, K. H., Lee, J. H., Park, J. W., Quach, C. H., Moon, S. H., Cho, Y. S., *et al.* Resveratrol-loaded polymeric nanoparticles suppress glucose metabolism and tumor growth *in vitro* and *in vivo*. *Int J Pharm* **478**, 251-257 (2015).
- Kabanov, A.V., Gendelman, H.E. Nanomedicine in the diagnosis and therapy of neurodegenerative disorders. *Prog Polym Sci* **32**, 1054-1082 (2007).
- Kalepu, S.,Nekkanti, V. Insoluble drug delivery strategies: review of recent advances and business prospects. *Acta Pharm Sin B* **5**, 442-453 (2015).
- Kantak, C., Beyer, S., Yobas, L., Bansal, T.,Trau, D. A 'microfluidic pinball' for on-chip generation of Layer-by-Layer polyelectrolyte microcapsules. *Lab Chip* **11**, 1030-1035 (2011).
- Kapetanovic, I. M., Muzzio, M., Huang, Z., Thompson, T. N.,McCormick, D. L. Pharmacokinetics, oral bioavailability, and metabolic profile of resveratrol and its dimethylether analog, pterostilbene, in rats. *Cancer Chemother Pharmacol* **68**, 593-601 (2011).
- Karthikeyan, S., Hoti, S. L.,Prasad, N. R. Resveratrol loaded gelatin nanoparticles synergistically inhibits cell cycle progression and constitutive NF-kappaB activation, and induces apoptosis in non-small cell lung cancer cells. *Biomed Pharmacother* **70**, 274-282 (2015).
- Keller, S. W., Johnson, S. A., Brigham, E. S., Yonemoto, E. H.,Mallouk, T. E. Photoinduced charge separation in multilayer thin films grown by sequential adsorption of polyelectrolytes. *J Am Chem Soc* **117**, 12879–12880 (1995).
- Kennedy, D.O., Wightman, E.L., Reay, J.L., Lietz, G., Okello, E.J., Wilde, A., *et al.* Effects of resveratrol on cerebral blood flow variables and cognitive performance in humans: a double-blind, placebo-controlled, crossover investigation. *Am J Clin Nutr* **91**, 1590-1597 (2010).
- Kou, X.,Chen, N. Resveratrol as a natural autophagy regulator for prevention and treatment of alzheimer's disease. *Nutrients* **9** (2017).

- Kristl J, Teskac K, Caddeo C, Abramović Z, M., S. Improvements of cellular stress response on resveratrol in liposomes. *Eur J Pharm Biopharm* **73**, 253-259 (2009).
- Kuhnle, G., Spencer, J.P., Chowrimootoo, G., Schroeter, H., Debnam, E.S., Srai, S.K., *et al.* Resveratrol is absorbed in the small intestine as resveratrol glucuronide. *Biochem Biophys Res Commun* **272**, 212-217 (2000).
- Kursvietiene, L., Staneviciene, I., Mongirdiene, A., Bernatoniene, J. Multiplicity of effects and health benefits of resveratrol. *Medicina (Kaunas)* **52**, 148-155 (2016).
- La Porte, C., Voduc, N., Zhang, G., Seguin, I., Tardiff, D., Singhal, N., *et al.* Steady-State pharmacokinetics and tolerability of trans-resveratrol 2000 mg twice daily with food, quercetin and alcohol (ethanol) in healthy human subjects. *Clin Pharmacokinet* **49**, 449-454 (2010).
- Lepak, A., Gutmann, A., Kulmer, S. T., Nidetzky, B. Creating a water-soluble resveratrol-based antioxidant by site-selective enzymatic glucosylation. *Chembiochem* (2015).
- Li, J., Wang, Y., Yang, C., Wang, P., Oelschlager, D.K., Zheng, Y., *et al.* Polyethylene glycosylated curcumin conjugate inhibits pancreatic cancer cell growth through inactivation of Jab1. *Mol Pharmacol* **76**, 81-90. (2009).
- Li, M., Azad, M., Davé, R., Bilgili, E. Nanomilling of drugs for bioavailability enhancement: a holistic formulation-process perspective. *Pharmaceutics* **8**, 17 (2016).
- Li, T. P., Wong, W. P., Chen, L. C., Su, C. Y., Chen, L. G., Liu, D. Z., *et al.* Physical and pharmacokinetic characterizations of trans-resveratrol (t-resv) encapsulated with self-assembling lecithin-based mixed polymeric micelles (saLMPMs). *Sci Rep* **7**, 10674 (2017).
- Liao, P. C., Ng, L. T., Lin, L. T., Richardson, C. D., Wang, G. H., Lin, C. C. Resveratrol arrests cell cycle and induces apoptosis in human hepatocellular carcinoma Huh-7 cells. *J Med Food* **13**, 1415-1423 (2010).
- Lin, Y. F., Lee, Y. H., Hsu, Y. H., Chen, Y. J., Lin, Y. F., Cheng, F. Y., *et al.* Resveratrol-loaded nanoparticles conjugated with kidney injury molecule-1 as a drug delivery system for potential use in chronic kidney disease. *Nanomedicine (Lond)* **12**, 2741-2756 (2017).
- Loh, Z. H., Samanta, A. K., Heng, P. W. S. Overview of milling techniques for improving the solubility of poorly water-soluble drugs. *Asian J Pharm Sci (Amsterdam, Neth)* **10**, 255-274 (2015).

- López-Nicolás, J.M., Rodríguez-Bonilla, P., García-Carmona, F. Complexation of pinosylvin, an analogue of resveratrol with high antifungal and antimicrobial activity, by different types of cyclodextrins. *J Agric Food Chem* **57**, 10175-10180 (2009).
- Lu, X., Ji, C., Xu, H., Li, X., Ding, H., Ye, M., *et al.* Resveratrol-loaded polymeric micelles protect cells from Abeta-induced oxidative stress. *Int J Pharm* **37**, 89-96. (2009).
- Lu, Z., Cheng, B., Hu, Y., Zhang, Y., Zou, G.. Complexation of resveratrol with cyclodextrins: Solubility and antioxidant activity. *Food Chem* **113**, 17-20 (2009).
- Lvov, Y., Decher, G., Moehwald, H. Assembly, structural characterization, and thermal behavior of layer-by-layer deposited ultrathin films of poly(vinyl sulfate) and poly(allylamine). *Langmuir* **9**, 481-486 (1993).
- Lvov, Y., Pattekari, P., Shutava, T. Chapter 8: Making aqueous nanocolloids from low solubility materials: Lbl shells on nanocores. *Multilayer Thin Films*. Decher, G., Schlenoff, J. B., Weinheim, Wiley-VCH Verlag GmbH & Co. KGaA: 151-170 (2012).
- Lvov, Y. M., Pattekari, P., Zhang, X., Torchilin, V. Converting poorly soluble materials into stable aqueous nanocolloids. *Langmuir* **27**, 1212-1217 (2011).
- Mansouri, S., Winnik, F. M., Tabrizian, M. Modulating the release kinetics through the control of the permeability of the layer-by-layer assembly: a review. *Expert Opin Drug Deliv* **6**, 585-597 (2009).
- Marier, J.F., Vachon, P., Gritsas, A., Zhang, J., Moreau, J.P., Ducharme, M.P. Metabolism and disposition of resveratrol in rats: extent of absorption, glucuronidation, and enterohepatic recirculation evidenced by a linked-rat model. *J Pharmacol Exp Ther* **302**, 369-373 (2002).
- Martinez, J.S., Keller, T.C., III, Schlenoff, J.B. Cytotoxicity of free versus multilayered polyelectrolytes. *Biomacromolecules* **12**, 4063-4070 (2011).
- Martini, D., Del Bo, C., Porrini, M., Ciappellano, S., Riso, P. Role of polyphenols and polyphenol-rich foods in the modulation of PON1 activity and expression. *J Nutr Biochem* **48**, 1-8 (2017).
- Meng, X., Maliakal, P., Lu, H., Lee, M.J., Yang CS. Urinary and plasma levels of resveratrol and quercetin in humans, mice, and rats after ingestion of pure compounds and grape juice. *J Agric Food Chem* **52**, 935-942 (2004).

- Merrell, J.G., McLaughlin, S.W., Tie, L., Laurencin, C.T., Chen, A.F., Nair, L.S. Curcumin-loaded poly(epsilon-caprolactone) nanofibres: diabetic wound dressing with anti-oxidant and anti-inflammatory properties. *Clin Exp Pharmacol Physiol* **36**, 1149-1156 (2009).
- Miksits, M., Maier-Salamon, A., Aust, S., Thalhammer, T., Reznicek, G., Kunert, O., *et al.* Sulfation of resveratrol in human liver: evidence of a major role for the sulfotransferases SULT1A1 and SULT1E1. *Xenobiotica* **35**, 1101-1119 (2005).
- Miksits, M., Wlcek, K., Svoboda, M., Kunert, O., Haslinger, E., Thalhammer, T., *et al.* Antitumor activity of resveratrol and its sulfated metabolites against human breast cancer cells. *Planta Med* **75**, 1227-1230. (2009).
- Mikulski, D., Górnjak, R., Molski M. A theoretical study of the structure-radical scavenging activity of trans-resveratrol analogues and cis-resveratrol in gas phase and water environment. *Eur J Med Chem.* **45**, 1015-1027 (2010).
- Milkova, V., Kamburova, K., Radeva, T. Nanocolloids of indomethacin prepared using sonication and subsequent encapsulation with polysaccharide films. *Colloids Surf., B* **108**, 279-284 (2013).
- Morton, S. W., Poon, Z., Hammond, P. T. The architecture and biological performance of drug-loaded LbL nanoparticles. *Biomaterials* **34**, 5328-5335 (2013).
- Moussa, C., Hebron, M., Huang, X., Ahn, J., Rissman, R. A., Aisen, P. S., *et al.* Resveratrol regulates neuro-inflammation and induces adaptive immunity in Alzheimer's disease. *J Neuroinflammation* **14**, 1 (2017).
- Muller, R. H., Gohla, S., Keck, C. M. State of the art of nanocrystals--special features, production, nanotoxicology aspects and intracellular delivery. *Eur. J. Pharm. Biopharm.* **78**, 1-9 (2011).
- Nam J.-B., Ryu J.-H., Kim J.-W., Chang I.-S., K.-D., S. Stabilization of resveratrol immobilized in monodisperse cyano-functionalized porous polymeric microspheres *Polymer* **46**, 8956-8963 (2005).
- Nandiyanto, A. B. D., Okuyama, K. Progress in developing spray-drying methods for the production of controlled morphology particles: From the nanometer to submicrometer size ranges. *Adv Powder Technol* **22**, 1-19 (2011).

- Narayanan, N.K., Nargi, D., Randolph, C., Narayanan, B.A. Liposome encapsulation of curcumin and resveratrol in combination reduces prostate cancer incidence in PTEN knockout mice. *Int J Cancer* **125**, 1-8. (2009).
- Nicolas, J., Mura, S., Brambilla, D., Mackiewicz, N., Couvreur, P. Design, functionalization strategies and biomedical applications of targeted biodegradable/biocompatible polymer-based nanocarriers for drug delivery. *Chem Soc Rev* **42**, 1147-1235 (2013).
- Noi, K. F., Roozmand, A., Bjornmalm, M., Richardson, J. J., Franks, G. V., Caruso, F. Assembly-controlled permeability of layer-by-layer polymeric microcapsules using a tapered fluidized bed. *ACS Appl Mater Interfaces* **7**, 27940-27947 (2015).
- Noyes, A. A., Whitney, W. R. The rate of solution of solid substances in their own solutions. *J Am Chem Soc* **19**, 930-934 (1897).
- Ochs, C. J., Such, G. K., Yan, Y., van Koeverden, M. P., Caruso, F. Biodegradable click capsules with engineered drug-loaded multilayers. *ACS Nano* **4**, 1653-1663 (2010).
- Ohguchi, K., Tanaka, T., Ito, T., Iinuma, M., Matsumoto, K., Akao, Y., *et al.* Inhibitory effects of resveratrol derivatives from dipterocarpaceae plants on tyrosinase activity. *Biosci Biotechnol Biochem* **67**, 1587-1589 (2003).
- Okuyama, K., Abdullah, M., Wuled Lenggoro, I., Iskandar, F. Preparation of functional nanostructured particles by spray drying. *Adv Powder Technol* **17**, 587-611 (2006).
- Orallo, F. Comparative studies of the antioxidant effects of cis- and trans-resveratrol. *Curr Med Chem* **13**, 87-98 (2006).
- Orsini, F., Verotta, L., Lecchi, M., Restano, R., Curia, G., Redaelli, E., *et al.* Resveratrol derivatives and their role as potassium channels modulators. *J Nat Prod* **67**, 421-426 (2004).
- Ortuno, J., Covas, M.I., Farre, M., Pujadas, M., Fito, M., Khymenets, O., *et al.* Matrix effects on the bioavailability of resveratrol in humans. *Food Chem* **120**, 1123-1130 (2010).
- Pandey, A. P., Singh, S. S., Patil, G. B., Patil, P. O., Bhavsar, C. J., Deshmukh, P. K. Sonication-assisted drug encapsulation in layer-by-layer self-assembled gelatin-poly(styrenesulfonate) polyelectrolyte nanocapsules: process optimization. *Artif Cells Nanomed Biotechnol* **43**, 413-424 (2015).

- Pandita, D., Kumar, S., Poonia, N., Lather, V. Solid lipid nanoparticles enhance oral bioavailability of resveratrol, a natural polyphenol. *Food Res Int* **62**, 1165-1174 (2014).
- Parekh, G., Pattekari, P., Joshi, C., Shutava, T., DeCoster, M., Levchenko, T., *et al.* Layer-by-layer nanoencapsulation of camptothecin with improved activity. *Int J Pharm* **465**, 218-227 (2014).
- Patel, K. R., Brown, V. A., Jones, D. J., Britton, R. G., Hemingway, D., Miller, A. S., *et al.* Clinical pharmacology of resveratrol and its metabolites in colorectal cancer patients. *Cancer Res* **70**, 7392-7399 (2010).
- Patil, G. B., Ramani, K. P., Pandey, A. P., More, M. P., Patil, P. O., Deshmukh, P. K. Fabrication of layer-by-layer self-assembled drug delivery platform for prednisolone. *Polym-Plast Technol Eng* **52**, 1637-1644 (2013).
- Patravale, V. B., Date, A. A., Kulkarni, R. M. Nanosuspensions: a promising drug delivery strategy. *J Pharm Pharmacol* **56**, 827-840 (2004).
- Pattekari, P., Zheng, Z., Zhang, X., Levchenko, T., Torchilin, V., Lvov, Y. Top-down and bottom-up approaches in production of aqueous nanocolloids of low solubility drug paclitaxel. *Phys Chem Chem Phys* **13**, 9014-9019 (2011).
- Peer, D., Karp, J. M., Hong, S., Farokhzad, O. C., Margalit, R., Langer, R. Nanocarriers as an emerging platform for cancer therapy. *Nat Nanotechnol* **2**, 751-760 (2007).
- Pelaz, B., Alexiou, C., Alvarez-Puebla, R. A., Alves, F., Andrews, A. M., Ashraf, S., *et al.* Diverse applications of nanomedicine. *ACS Nano* **11**, 2313-2381 (2017).
- Penalva, R., Esparza, I., Larraneta, E., Gonzalez-Navarro, C. J., Gamazo, C., Irache, J. M. Zein-based nanoparticles improve the oral bioavailability of resveratrol and its anti-inflammatory effects in a mouse model of endotoxic shock. *J Agric Food Chem* **63**, 5603-5611 (2015).
- Peng H, Xiong H, Li J, Xie M, Liu Y, Baiand C, *et al.* Vanillin cross-linked chitosan microspheres for controlled release of resveratrol. *Food Chem* **121**, 23-28 (2010).
- Pervaiz, S. Resveratrol: from grapevines to mammalian biology. *FASEB J.* **17**, 1975-1985 (2003).
- Pervaiz, S., Holme, A.L. Resveratrol: its biologic targets and functional activity. *Antioxid Redox Signal* **11**, 2851-2897 (2009).

- Peter, M., Binulal, N.S., Nair, S.V., Selvamurugan, N., Tamura, H., Jayakumar, R. Novel biodegradable chitosan–gelatin/nano-bioactive glass ceramic composite scaffolds for alveolar bone tissue engineering. *Chem Eng J (Amsterdam, Neth)* **158**, 353-361 (2010).
- Polomska, A., Gauthier, M. A., Leroux, J. C. *In vitro* and *in vivo* evaluation of PEGylated layer-by-layer polyelectrolyte-coated paclitaxel nanocrystals. *Small* **13** (2017).
- Poon, Z., Lee, J. B., Morton, S. W., Hammond, P. T. Controlling *in vivo* stability and biodistribution in electrostatically assembled nanoparticles for systemic delivery. *Nano Lett* **11**, 2096-2103 (2011).
- Poptoshev, E., Schoeler, B., Caruso, F. Influence of solvent quality on the growth of polyelectrolyte multilayers. *Langmuir* **20**, 829-834 (2004).
- Quincozes-Santos, A., Gottfried, C. Resveratrol modulates astroglial functions: neuroprotective hypothesis. *Ann N Y Acad Sci* **1215**, 72-78 (2011).
- Quinn, J. F., Pas, S. J., Quinn, A., Yap, H. P., Suzuki, R., Tuomisto, F., *et al.* Tailoring the chain packing in ultrathin polyelectrolyte films formed by sequential adsorption: nanoscale probing by positron annihilation spectroscopy. *J Am Chem Soc* **134**, 19808-19819 (2012).
- Rauf, A., Imran, M., Butt, M. S., Nadeem, M., Peters, D. G., Mubarak, M. S. Resveratrol as an anticancer agent: a review. *Crit Rev Food Sci Nutr* 1-20 (2016).
- Regev-Shoshani G, Shoseyov O, Bilkis I, Z., K. Glycosylation of resveratrol protects it from enzymatic oxidation. *Biochem J* **374**, 157–163 (2003).
- Richardson, J. J., Bjornmalm, M., Caruso, F. Multilayer assembly. Technology-driven layer-by-layer assembly of nanofilms. *Science* **348**, 411 (2015).
- Richardson, J. J., Ejima, H., Lorcher, S. L., Liang, K., Senn, P., Cui, J., *et al.* Preparation of nano- and microcapsules by electrophoretic polymer assembly. *Angew Chem, Int Ed Engl* **52**, 6455-6458 (2013).
- Robinson, K., Mock, C., Liang, D. Pre-formulation studies of resveratrol. *Drug Dev Ind Pharm* **41**, 1464-1469 (2015).
- Roh, Y. H., Deng, J. Z., Dreaden, E. C., Park, J. H., Yun, D. S., Shopsowitz, K. E., *et al.* A multi-RNAi microsphere platform for simultaneous controlled delivery of multiple small interfering RNAs. *Angew Chem, Int Ed* **55**, 3347-3351 (2016).

- Ros, R. Z. Resveratrol: Marcador biològic i dietètic de consum de vi. Doctoral Thesis, Universitat de Barcelona, Facultat de Farm Barcelona, 3-30 (2008).
- Rotches-Ribalta, M., Andres-Lacueva, C., Estruch, R., Escribano, E., Urpi-Sarda, M. Pharmacokinetics of resveratrol metabolic profile in healthy humans after moderate consumption of red wine and grape extract tablets. *Pharmacol Res* **66**, 375-382 (2012).
- Sahu, A., Bora, U., Kasoju, N., Goswami, P. Synthesis of novel biodegradable and self-assembling methoxy poly(ethylene glycol)-palmitate nanocarrier for curcumin delivery to cancer cells. *Acta Biomater* **4**, 1752-1761. (2008).
- Salomaki, M., Vinokurov, I. A., Kankare, J. Effect of temperature on the buildup of polyelectrolyte multilayers. *Langmuir* **21**, 11232-11240 (2005).
- Samsamikor, M., Daryani, N. E., Asl, P. R., Hekmatdoost, A. Resveratrol supplementation and oxidative/anti-oxidative status in patients with ulcerative colitis: a randomized, double-blind, placebo-controlled pilot study. *Arch Med Res* **47**, 304-309 (2016).
- Santos, A. C., Pattekari, P., Jesus, S., Veiga, F., Lvov, Y., Ribeiro, A. J. Sonication-assisted layer-by-layer assembly for low solubility drug nanoformulation. *ACS Appl Mater Interfaces* **7**, 11972-11983 (2015).
- Sergides, C., Chirila, M., Silvestro, L., Pitta, D., Pittas, A. Bioavailability and safety study of resveratrol 500 mg tablets in healthy male and female volunteers. *Exp Ther Med* **11**, 164-170 (2016).
- Shao, J., Li, X., Lu, X., Jiang, C., Hu, Y., Li, Q., *et al.* Enhanced growth inhibition effect of resveratrol incorporated into biodegradable nanoparticles against glioma cells is mediated by the induction of intracellular reactive oxygen species levels. *Colloids Surf B Biointerfaces* **72**, 40-47 (2009).
- Sharma, V., McNeill, J.H. To scale or not to scale: the principles of dose extrapolation. *Br J Pharmacol* **157**, 907-921 (2009).
- Shi, G., Rao, L., Yu, H., Xiang, H., Yang, H., Ji, R. Stabilization and encapsulation of photosensitive resveratrol within yeast cell. *Int J Pharm* **349**, 83-93 (2008).
- Shopsowitz, K. E., Wu, C., Liu, G. N., Dreaden, E. C., Hammond, P. T. Periodic-shRNA molecules are capable of gene silencing, cytotoxicity and innate immune activation in cancer cells. *Nucleic Acids Res.* **44**, 545-557 (2016).

- Shu, X.H., Li, H., Sun, Z., Wu, M.L., Ma, J.X., Wang, J.M., *et al.* Identification of metabolic pattern and bioactive form of resveratrol in human medulloblastoma cells. *Biochem Pharmacol* **79**, 1516-1525 (2010).
- Shutava, T. G., Lvov, Y. M. Chapter 9: Encapsulation of natural polyphenols with antioxidant properties in polyelectrolyte capsules and nanoparticles. *Natural compounds as inducers of cell death: volume 1*. Diederich, M., Noworyta, K., Dordrecht, Springer: 215-235 (2012).
- Shutava, T. G., Pattekari, P. P., Arapov, K. A., Torchilin, V. P., Lvov, Y. M. Architectural layer-by-layer assembly of drug nanocapsules with PEGylated polyelectrolytes. *Soft Matter* **8**, 9418-9427 (2012).
- Singh, G., Pai, R. S. Optimized PLGA nanoparticle platform for orally dosed trans-resveratrol with enhanced bioavailability potential. *Expert Opin Drug Deliv* **11**, 647-659 (2014).
- Singh, G., Pai, R. S. Trans-resveratrol self-nano-emulsifying drug delivery system (SNEDDS) with enhanced bioavailability potential: optimization, pharmacokinetics and in situ single pass intestinal perfusion (SPIP) studies. *Drug Deliv* **22**, 522-530 (2015).
- Singh, S. K., Banala, V. T., Gupta, G. K., Verma, A., Shukla, R., Pawar, V. K., *et al.* Development of docetaxel nanocapsules for improving in vitro cytotoxicity and cellular uptake in MCF-7 cells. *Drug Dev Ind Pharm* **41**, 1759-1768 (2015).
- Soleas, G.J., Yan, J., Goldberg, D.M. Ultrasensitive assay for three polyphenols (catechin, quercetin and resveratrol) and their conjugates in biological fluids utilizing gas chromatography with mass selective detection. *J Chromatogr B Biomed Sci Appl* **757**, 161-172 (2001a).
- Soleas, G.J., Yan, J., Goldberg, D.M. Measurement of trans-resveratrol, (+)-catechin, and quercetin in rat and human blood and urine by gas chromatography with mass selective detection. *Methods Enzymol* **335**, 130-145 (2001b).
- Strydom, S. J., Otto, D. P., Stieger, N., Aucamp, M. E., Liebenberg, W., de Villiers, M. M. Self-assembled macromolecular nanocoatings to stabilize and control drug release from nanoparticles. *Powder Technol* **256**, 470-476 (2014).
- Sukhorukov, G. B., Donath, E., Davis, S., Lichtenfeld, H., Caruso, F., Popov, V. I., *et al.* Stepwise polyelectrolyte assembly on particle surfaces: a novel approach to colloid design. *Polym Adv Technol* **9**, 759-767 (1998a).

- Sukhorukov, G. B., Donath, E., Lichtenfeld, H., Knippel, E., Knippel, M., Budde, A., *et al.* Layer-by-layer self assembly of polyelectrolytes on colloidal particles. *Colloids Surf, A* **137**, 253-266 (1998b).
- Suri, S., Liu, X.H., Rayment, S., Hughes, D.A., Kroon, P.A., Needs, P.W., *et al.* Quercetin and its major metabolites selectively modulate cyclic GMP-dependent relaxations and associated tolerance in pig isolated coronary artery. *Br J Pharmacol* **159**, 566-575 (2010).
- Szkudelski, T.,Szkudelska, K. Resveratrol and diabetes: from animal to human studies. *Biochim Biophys Acta* **1852**, 1145-1154 (2015).
- Teskač K, Kristl, J. The evidence for solid lipid nanoparticles mediated cell uptake of resveratrol. *Int J Pharm* **390**, 61-69 (2010).
- Thangapazham, R.L., Puri, A., Tele, S., Blumenthal, R., Maheshwari, R.K. Evaluation of a nanotechnology-based carrier for delivery of curcumin in prostate cancer cells. *Int J Oncol* **32**, 1119-1123 (2008).
- Thanh, N. T., Maclean, N.,Mahiddine, S. Mechanisms of nucleation and growth of nanoparticles in solution. *Chem Rev* **114**, 7610-7630 (2014).
- Tribolo, S., Lodi, F., Connor, C., Suri, S., Wilson, V.G., Taylor, M.A., *et al.* Comparative effects of quercetin and its predominant human metabolites on adhesion molecule expression in activated human vascular endothelial cells. *Atherosclerosis* **197**, 50-56 (2008).
- Tsai, H. Y., Ho, C. T.,Chen, Y. K. Biological actions and molecular effects of resveratrol, pterostilbene, and 3'-hydroxypterostilbene. *J Food Drug Anal* **25**, 134-147 (2017).
- Ungvari, Z., Bagi, Z., Feher, A., Recchia, F. A., Sonntag, W. E., Pearson, K., *et al.* Resveratrol confers endothelial protection via activation of the antioxidant transcription factor Nrf2. *Am J Physiol Heart Circ Physiol* **299**, H18-H24 (2010).
- Urpí-Sardà M, Jáuregui O, Lamuela-Raventós RM, Jaeger W, Miksits M, Covas MI, *et al.* Uptake of diet resveratrol into the human low-density lipoprotein. Identification and quantification of resveratrol metabolites by liquid chromatography coupled with tandem mass spectrometry. *Anal Chem* **77**, 3149-3155 (2005).
- Urpí-Sardà, M., Zamora-Ros, R., Lamuela-Raventós, R., Cherubini, A., Jauregui, O., de la Torre, R., *et al.* HPLC-tandem mass spectrometric method to characterize resveratrol metabolism in humans. *Clin Chem* **53**, 292-299 (2007).

- Van Eerdenbrugh, B., Vermant, J., Martens, J. A., Froyen, L., Humbeeck, J. V., Van den Mooter, G., *et al.* Solubility increases associated with crystalline drug nanoparticles: methodologies and significance. *Mol Pharmaceutics* **7**, 1858-1870 (2010).
- Varoni, E. M., Lo Faro, A. F., Sharifi-Rad, J., Iriti, M. Anticancer molecular mechanisms of resveratrol. *Front Nutr* **3**, 8 (2016).
- Vergara, D., Bellomo, C., Zhang, X., Vergaro, V., Tinelli, A., Lorusso, V., *et al.* Lapatinib/Paclitaxel polyelectrolyte nanocapsules for overcoming multidrug resistance in ovarian cancer. *Nanomedicine* **8**, 891-899 (2012).
- Verma, S., Gokhale, R., Burgess, D. J. A comparative study of top-down and bottom-up approaches for the preparation of micro/nanosuspensions. *Int J Pharm* **380**, 216-222 (2009).
- Vidyasagar, A., Sung, C., Gamble, R., Lutkenhaus, J. L. Thermal transitions in dry and hydrated layer-by-layer assemblies exhibiting linear and exponential growth. *ACS Nano* **6**, 6174-6184 (2012).
- Vijayakumar, M. R., Vajanthri, K. Y., Balavigneswaran, C. K., Mahto, S. K., Mishra, N., Muthu, M. S., *et al.* Pharmacokinetics, biodistribution, in vitro cytotoxicity and biocompatibility of Vitamin E TPGS coated trans resveratrol liposomes. *Colloids Surf B Biointerfaces* **145**, 479-491 (2016).
- Vitaglione, P., Sforza, S., Galaverna, G., Ghidini, C., Caporaso, N., Vescovi, P.P., *et al.* Bioavailability of trans-resveratrol from red wine in humans. *Mol Nutr Food Res* **49**, 495-504 (2005).
- Walle, T., Hsieh, F., DeLegge, M.H., Oatis, J.E. Jr., Walle, U.K. High absorption but very low bioavailability of oral RSV. *Drug Metab Dispos* **32**, 1377-1382 (2004).
- Wang, L.X., Heredia, A., Song, H., Zhang, Z., Yu, B., Davis, C., *et al.* Resveratrol glucuronides as the metabolites of resveratrol in humans: characterization, synthesis, and anti-HIV activity. *J Pharm Sci* **93**, 2448-2457 (2004).
- Wang, N., Zhang, F., Yang, L., Zou, J., Wang, H., Liu, K., *et al.* Resveratrol protects against L-arginine-induced acute necrotizing pancreatitis in mice by enhancing SIRT1-mediated deacetylation of p53 and heat shock factor 1. *Int J Mol Med* **40**, 427-437 (2017).

- Wenzel, E., Soldo, T., Erbersdobler, H., Somoza V. Bioactivity and metabolism of trans-resveratrol orally administered to Wistar rats. *Mol Nutr Food Res* **49**, 482-494 (2005).
- Wenzel, E., Somoza, V. Metabolism and bioavailability of *trans*-resveratrol. *Mol Nutr Food Res* **49**, 472-481 (2005).
- Xu, H., Yang, P., Ma, H., Yin, W., Wu, X., Wang, H., *et al.* Amphiphilic block copolymers-based mixed micelles for noninvasive drug delivery. *Drug Deliv* **23**, 3063-3071 (2016).
- Yoshida, K., Sato, K., Anzai, J. Layer-by-layer polyelectrolyte films containing insulin for pH-triggered release. *J Mater Chem* **20**, 1546-1552 (2010).
- Yu, X., Pishko, M. V. Nanoparticle-based biocompatible and targeted drug delivery: characterization and *in vitro* studies. *Biomacromolecules* **12**, 3205-3212 (2011).
- Zahr, A. S., Davis, C. A., Pishko, M. V. Macrophage uptake of core-shell nanoparticles surface modified with poly(ethylene glycol). *Langmuir* **22**, 8178-8185 (2006).
- Zahr, A. S., De Villiers, M., Pishko, M. V. Encapsulation of drug nanoparticles in self-assembled macromolecular nanoshells. *Langmuir* **21**, 403-410 (2005).
- Zahr, A. S., Pishko, M. V. Encapsulation of paclitaxel in macromolecular nanoshells. *Biomacromolecules* **8**, 2004-2010 (2007).
- Zamora-Ros, R., Urpí-Sardà, M., Lamuela-Raventós, R.M., Estruch, R., Martínez-González, M.A., Bulló, M., *et al.* Resveratrol metabolites in urine as a biomarker of wine intake in free-living subjects: The PREDIMED Study. *Free Radic Biol Med* **46**, 1561 (2009).
- Zamora-Ros, R., Urpí-Sardà, M., Lamuela-Raventós, R.M., Estruch, R., Vázquez-Agell, M., Serrano-Martínez, M., *et al.* Diagnostic performance of urinary resveratrol metabolites as a biomarker of moderate wine consumption. *Clin Chem* **52**, 1373-1380 (2006).
- Zhang, H., Zhang, J., Ungvari, Z. Resveratrol improves endothelial function: role of TNF α and vascular oxidative stress. *Arterioscler Thromb Vasc Biol* **29**, 1164-1171 (2009).
- Zhang, L., Hu, Y., Jiang, X., Yang, C., Lu, W., Yang, Y.H. Camptothecin derivative-loaded poly(caprolactone-co-lactide)-b-PEG-b-poly(caprolactone-co-lactide) nanoparticles and their biodistribution in mice. *J Control Release* **96**, 135-148 (2004).
- Zheng, Z., Zhang, X., Carbo, D., Clark, C., Nathan, C., Lvov, Y. Sonication-assisted synthesis of polyelectrolyte-coated curcumin nanoparticles. *Langmuir* **26**, 7679-7681 (2010).

- Zhou, J., Pishko, M. V., Lutkenhaus, J. L. Thermoresponsive layer-by-layer assemblies for nanoparticle-based drug delivery. *Langmuir* **30**, 5903-5910 (2014).
- Zhou, M. J., Chen, X. Y., Zhong, D. F. Simultaneous determination of trans-resveratrol-3-O-glucoside and its two metabolites in rat plasma using liquid chromatography with ultraviolet detection. *J Chromatogr B Analyt Technol Biomed Life Sci* **854**, 219-223 (2007).
- Zhu, X., Wu, C., Qiu, S., Yuan, X., Li, L. Effects of resveratrol on glucose control and insulin sensitivity in subjects with type 2 diabetes: systematic review and meta-analysis. *Nutr Metab (Lond)* **14**, 60 (2017).
- Zordoky, B. N., Robertson, I. M., Dyck, J. R. Preclinical and clinical evidence for the role of resveratrol in the treatment of cardiovascular diseases. *Biochim Biophys Acta* **1852**, 1155-1177 (2015).
- Zu, Y., Zhang, Y., Wang, W., Zhao, X., Han, X., Wang, K., *et al.* Preparation and *in vitro/in vivo* evaluation of resveratrol-loaded carboxymethyl chitosan nanoparticles. *Drug Deliv* **23**, 981-991 (2016).
- Zupancic, S., Lavric, Z., Kristl, J. Stability and solubility of trans-resveratrol are strongly influenced by pH and temperature. *Eur J Pharm Biopharm* **93**, 196-204 (2015).

Chapter 2

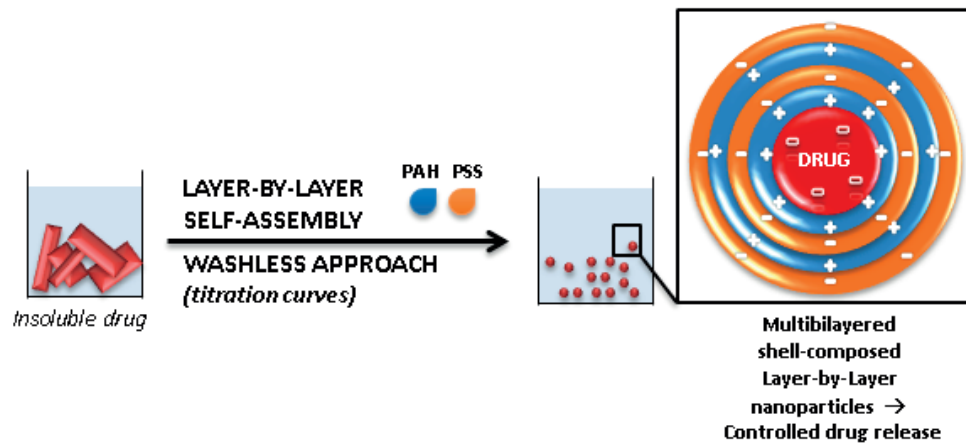
Sonication-assisted Layer-by-Layer assembly for low soluble drug nanoformulation

2.1. Abstract

Sonication-assisted Layer-by-Layer (LbL) self-assembly is a nanoencapsulation technique based on the alternate adsorption of oppositely charged polyelectrolytes (PEs), enabling the encapsulation of low soluble drugs. In this work, a top-down LbL technique was performed using a washless approach and ibuprofen (IBF) as a model class II drug. For each saturated layer deposition, PE concentration was determined by titration curves. The first layer was constituted by cationic polyallylamine hydrochloride (PAH), given the IBF negative surface charge, followed by anionic polystyrene sulfonate (PSS). This PE sequence was made up with 2.5, 5.5 and 7.5 bilayer nanoshells. IBF nanoparticles (NPs) coated with 7.5 bilayers of PAH/PSS showed 127.5 ± 38.0 nm of particle size, a PDI of 0.24 and a high zeta potential ($+32.7 \pm 0.6$ mV), allowing for a stable aqueous nanocolloid of the drug. IBF entrapment efficiency of $72.1 \pm 5.8\%$ was determined by HPLC quantification. *In vitro* MTT assay showed that LbL NPs were biocompatible. According to the number of coating layers, a controlled release of IBF from LbL NPs was achieved under simulated intestinal conditions (from 5 h up to 7 days). PAH/PSS-LbL NPs constitutes a potential delivery system to improve biopharmaceutical parameters of water low soluble drugs.

Keywords: Layer-by-Layer self-assembly; washless; colloid; electrostatic interactions; controlled release; oral delivery.

Graphical abstract



LbL NPs allow for controlled drug release depending on shell architecture and composition.

[LbL – Layer-by-Layer; NP – nanoparticle; PAH – poly(allylamine hydrochloride); PSS – poly(styrene sulfonate)]

2.2. Introduction

The development of versatile and efficient nanoparticulate drug carriers for low soluble drugs is of outmost interest, due to the significant increase of the dissolution rate, which in turn can lead to increases in the drug bioavailability (Kesisoglou, Panmai *et al.* 2007).

Several nanoparticulate delivery systems have been recently developed, however some limitations still have to be overcome. Micelles offer appropriate nanoparticle (NP) size, but for low water soluble drugs low loading capacities are achieved (Torchilin 2006, Szczepanowicz, Hoel *et al.* 2010). On the other side, drug-loaded polymeric coacervates show larger particle sizes and low drug loading capacities (Shutava, Balkundi *et al.* 2009). Synthetic polymer-drug conjugates have concerns related to lack of stability, low drug-holding capacity and absence of controlled drug delivery (Zhang, Gu *et al.* 2008).

Layer-by-Layer (LbL) self-assembly is a promising approach that assembles polyelectrolyte (PE) multilayer shells into drug-loaded particles (Wang, Hosta-Rigau *et al.* 2011, Yan, Björnmalm *et al.* 2014). LbL coating is obtained by the alternated addition of polycations and polyanions to the system under sonication, assembling thin PEs shells on drug particles surface. After the first PE deposition, the highly charged polymeric layer is formed on the drug NP surface, preventing aggregation when the sonication stops (Agarwal, Lvov *et al.* 2008). These particles can display different properties based on the nature of the PEs and the architecture of the charged PE shell or the number of coating cycles (Balabushevich, Izumrudov *et al.* 2012). These systems allow for high low soluble drug content and high aqueous physical stability (De Villiers, Lvov 2011). The appropriate design of shell architecture at nanometer level enables the control of drug release (Agarwal, Lvov *et al.* 2008).

LbL fabricated-PE particles have successfully modified the solubility of drugs, however in most cases these systems showed with a diameter of a few micrometers (De Villiers, Lvov 2011), which is too large to increase drug dissolution velocity. Reducing particle size into the nanoscale leads to a surface area increase and, consequently, increases the drug dissolution velocity (Nokhodchi, Amire *et al.* 2010). These formulation improvements together with the versatility of formed nanoparticulate carriers resulted in a growing interest on the application of LbL drugs delivery systems into the nanoscale (Hammond 2012). Therefore, LbL NPs can be successfully employed if the dissolution velocity is the rate-limiting step for absorption of Biopharmaceutics Classification System (BSC) II drugs intended for the oral route (Junyaprasert, Morakul 2015).

The production of LbL self-assembly NPs can be achieved using sonication by a top-down or a bottom-up approach. A top-down approach refers to a particle size reduction technique for drug direct nanoencapsulation. In this case, aqueous suspensions of micron sized drugs are submitted to sonication to decrease the size of drug to the nanoscale. The continuous sonication prevents fast agglomeration of smaller particles and the application of the LbL technology promotes suspension stabilization. On the other hand, the bottom-up approach is based on the drug nucleation in the co-solvent after its dissolution in organic solvent. Comparatively, the top-down approach has been shown to be more efficient in the preparation of large amounts of ca. 200 nm capsules. The bottom-up approach, in turn, has shown to be more efficient in producing smaller capsules of ca. 100 nm, but with lower product yield (Pattekari, Zheng *et al.* 2011). Moreover, the use of organic solvents used in bottom-up approaches raises environmental and human safety concerns over residual solvent. For these reasons, a top-down approach was chosen for this work.

The traditional LbL technique uses intermediate washings to remove the excess of PE after each layer deposition. These repetitive washings are time and PE consuming, conduct to process losses and are less adaptable to common manufacturing processes (Agarwal, Lvov *et al.* 2008). Newly and detailed characterization of LbL shell compositions produced without using intermediate washings are being reported to avoid these drawbacks. Using simultaneous sonication-assisted breakup of native micro-sized hydrophobic drugs into nanocrystals with PE adsorption yields coated nanocrystals in a process without intermediate centrifugations (Hammond 2012). Thus, nanocoating layers formed in equilibrium or reduced PE concentrations are emerging towards the simplification and maximization of NPs production (Pattekari, Zheng *et al.* 2011, Shutava, Pattekari *et al.* 2012).

Multiple works used 3-5 μm multilayer LbL shells to encase highly soluble proteins and drugs using sacrificial templates (Qiu, Loporatti *et al.* 2001, Trau, Renneberg 2003, De Geest, Sanders *et al.* 2007, De Geest, Sukhorukov *et al.* 2009). Nowadays, many efforts are directed toward the encapsulation of low soluble drugs and perform drug direct encapsulation, avoiding the use of sacrificial cores (De Villiers, Lvov 2011).

The design of LbL nanovehicle systems only recently reached the desirable level of properties for efficient systemic delivery such as minimum toxicity, due to biodegradable materials, nanocolloidal stability using isotonic formulations and prolonged *in vitro* and *in vivo* release of encased drugs (Hammond 2012, Torchilin 2012).

The LbL nanoencapsulation increased the solubility of curcumin (Zheng, Zhang *et al.* 2010), tamoxifen (Agarwal, Lvov *et al.* 2008), paclitaxel (Agarwal, Lvov *et al.* 2008, Pattekari, Zheng *et al.* 2011, Shutava, Pattekari *et al.* 2012), resveratrol (RSV) (Lvov, Pattekari *et al.* 2010) and camptothecin (Shutava, Pattekari *et al.* 2012, Parekh, Pattekari *et al.* 2014). This technique has been successful by making use of either synthetic polymers such as polyallylamine hydrochloride (PAH) (Lvov, Pattekari *et al.* 2010, Pattekari, Zheng *et al.* 2011), polystyrene sulfonate (PSS) (Lvov, Pattekari *et al.* 2010, Pattekari, Zheng *et al.* 2011, Parekh, Pattekari *et al.* 2014), poly(diallyldimethylammonium chloride) (PDDA) (Lvov, Pattekari *et al.* 2010) or natural polymers such as bovine serum albumin (BSA) (Pattekari, Zheng *et al.* 2011, Shutava, Pattekari *et al.* 2012, Parekh, Pattekari *et al.* 2014), protamine sulfate (PS) (Lvov, Pattekari *et al.* 2010, Pattekari, Zheng *et al.* 2011), chitosan (Lvov, Pattekari *et al.* 2010, Pattekari, Zheng *et al.* 2011), alginate (Lvov, Pattekari *et al.* 2010, Pattekari, Zheng *et al.* 2011), poly(ethylenimine) (PEI) (Shutava, Pattekari *et al.* 2012, Parekh, Pattekari *et al.* 2014), poly-L-lysine (PLL) (Shutava, Pattekari *et al.* 2012) and heparin (Parekh, Pattekari *et al.* 2014). The application of the LbL nanoencapsulation to increase the solubility of drugs to be administered orally requires a fully physicochemical characterization of the nanoparticulate system, a biopharmaceutical characterization through gastrointestinal (GI) simulating dissolution tests, biocompatibility and biodegradability studies.

The novelty of the present work was to prepare low soluble drug-loaded NPs for oral delivery by sonication-assisted LbL top-down nanotechnology without intermediate washings. New architected PE coated shells were constructed. Ibuprofen (IBF) was chosen as a low soluble model drug, and PAH and PSS as PEs with low molecular weight, regarding their high surface charge, stability and biocompatibility (Agarwal, Lvov *et al.* 2008). The resulting IBF NPs were characterized with regard to morphology, particle size, zeta potential, drug loading, stability, *in vitro* release and cytotoxicity.

2.3. Materials and methods

2.3.1. Materials

PAH (M_w ca. 15 kDa), PSS (M_w ca. 75 kDa), fluorescein isothiocyanate (FITC), gel chromatography Sephadex PD10 columns (Amersham Biosciences, Wikströms, Sweden), 3-(4,5-dimethylthiazol-2-yl)-2,5-diphenyltetrazolium bromide (MTT) reagent and Dulbecco's Modified Eagle Medium (DMEM) were purchased from Sigma-Aldrich (Steinheim, Germany). Fetal bovine serum (FBS) supplemented with PenStrep and trypsin were acquired from Life Technologies Corporation (Paisley, UK). IBF was kindly donated from Medinfar - Amadora, Portugal. Milli-Q water was used at pH 7.0-7.2. All other reagents were of analytical grade and were used as received.

2.3.2. Methods

2.3.2.1. Nanoparticles preparation

IBF was dispersed at 0.5 mg/mL in 1 – 5 mL of Milli-Q water. For initial dispersion, IBF was sonicated 5 min using an ultrasound bath sonicator (Bandelin *Sonorex* Super, Bandelin, Berlin, Germany). IBF particle size and zeta potential were periodically measured during the sonication-assisted LbL procedure. Polycation PAH was used under continuous sonication to form the first surface layer, since the IBF nanocores were found to bear the intrinsic negative charge. To determine the PE concentration to completely coat IBF nanocores surface, PE titrations depending on zeta potential and particle size of NPs were made through the dropwise addition of PAH at 1 mg/mL to IBF NPs. After the first PAH layer addition, the LbL process was continued with the use of the titrated concentration of the oppositely charged PSS at 1 mg/mL. The LbL assembly was carried up to 7.5 bilayers of PAH/PSS shell, through the following alternately addition of PEs PAH and PSS. The formulations with 2.5, 5.5 and 7.5 LbL bilayers were considered for further studies that are discussed below.

2.3.2.2. Particle size analysis

The particle size and polydispersity index (PDI) was investigated by dynamic light scattering (DLS) using a particle size analyser (DelsaNano C Submicron, Beckman Coulter Delsa™, Krefeld, Germany). Mean diameter, size distribution and PDI of aqueous NPs suspensions were determined for 5 min in triplicate at 25 °C with an angle measurement of 60°, after an equilibration time of 3 min. For each measurement, the NPs suspension was diluted in Milli-Q water to an appropriate concentration to avoid multiple scattering. Results are presented as

mean \pm standard deviation (SD), extracted from the Cumulants algorithm (ISO13321 1996, ISO22412 2008). The instrument was checked and calibrated using standard latex nanoparticles (Beckman Coulter, Inc.).

2.3.2.3. Zeta potential analysis

Zeta potential measurements were taken by electrophoretic light scattering (ELS) using a Nano Zeta Potential Analyser (DelsaNano C Submicron, Beckman Coulter Delsa™, Krefeld, Germany). Measurements were taken in a Flow Cell (Beckman Coulter Delsa™) at 25 ° C and Milli-Q water (pH 7.0-7.2) was used as diluent to proper concentration. The zeta potential was calculated using the Helmholtz–Smoluchowski equation. Values are presented as means of triplicate runs per sample. The instrument was routinely checked and calibrated using a mobility standard (Beckman Coulter, Inc.).

2.3.2.4. Microscopic analysis

An optical microscope equipped with a Digital Sight DS-U2 microscope camera controller was used to evaluate IBF crystals size and to check for IBF crystals presence in LbL NPs formulations. The sample preparation was made by placing a 10 μ L-drop of diluted NPs suspensions between glass slides.

The shape and surface morphology of NPs was monitored using Jeol SM-6010LV/3010LA scanning electron microscope. For scanning electron microscopy (SEM) analysis a 10 μ L-drop of diluted NPs suspension was placed onto a metal plate and kept overnight at room temperature inside a desiccator.

To control and confirm the deposition of the polycation layers in the LbL shell formation, PAH was labelled with FITC and NPs were monitored by using a Laser Scanning Confocal Microscope, Zeiss LSM 510 Meta (Carl Zeiss Inc., Göttingen, Germany), equipped with a 63x oil immersion objective Plan-ApoChromat with numerical aperture of 1.4. To obtain FITC labelled-NPs, PAH was tagged with FITC, based on a method described elsewhere (Hiller, Leporatti *et al.* 2004). FITC was covalently bound to PAH by the slowly addition of FITC dissolved in dimethyl sulfoxide (DMSO) to the PAH buffered solution in excess, using a proportion of 0.05:1 (v/v). The FITC not utilized in the coupling reaction was removed by gel chromatography in a Sephadex PD10 column. The purified FITC-labelled PAH was stored in the dark at 4 °C until further use.

2.3.2.5. Determination of drug encapsulation efficiency

Non-encapsulated IBF was separated from NPs suspension by centrifugation (1000 rpm, 10 min) using an Eppendorf® Mini Spin centrifuge (Hamburg, Germany). The IBF LbL NPs collected in the supernatant were analyzed for IBF and the encapsulation efficiency of IBF is defined as the following equation (Equation 2.1):

$$\text{Encapsulation Efficiency (\%)} = \frac{\text{Actual amount of IBF loaded in NPs}}{\text{Theoretical amount of IBF loaded in NPs}} \times 100$$

For IBF quantification, IBF NPs were submitted to an extraction with the high-performance liquid chromatography (HPLC) mobile phase 1:5 (v/v) followed by vortex agitation for 1 min and sonication for 5 min. IBF assay was performed with a HPLC column by using a previously HPLC reported method (Fernandez-Carballido, Herrero-Vanrell *et al.* 2004). The HPLC analysis was carried out by a Shimadzu LC-2010CHT apparatus equipped with a quaternary pump, an autosampler unit, and a L2450 UV/visible dual wavelength detector. A RP18 (4.6 mm × 125 mm) Lichrospher® 100 analytical column (Merck KGaA, Germany), with a pre-column, was employed for the analysis. Mobile phase consisted of a 60:40 (v/v) mixture of acetonitrile/water adjusted to pH 2.5 with orthophosphoric acid with a flow rate 1.0 mL/min, an injection volume of 20 µL and detection at 264 nm at 30 °C.

2.3.2.6. Stability studies

LbL NPs formulations stability was evaluated by particle size and zeta potential measurements at specified time point over a total of 14 days period. All measurements were carried out at room temperature (25 °C).

2.3.2.7. *In vitro* drug release assays at sink conditions

The release tests of IBF from NPs were performed in simulated gastric (pH 1.2) and intestinal (pH 6.8) fluids without enzymes, according to United States Pharmacopeia (USPXXIV).

In order to comply with *sink* conditions during *in vitro* release studies, the saturation solubility was determined. Excess IBF powder (60 mg) was added to both 10 mL of both media and the samples were kept under agitation for 24 h (37 °C/100 rpm). Aliquots of 2 mL each were withdrawn every 2 h and immediately centrifuged (13400 rpm/10 min). The supernatant was filtered using a 0.45 µm syringe filter (GHP Acrodisc, Pall Gelman Laboratory) and the filtered samples after suitable dilution were assayed for IBF by HPLC, as described above. All syringes,

pipettes, filters and vials used were preheated to 37 °C in an oven. The solubility experiments were performed in triplicate (n = 3).

For the release studies, 1.5 mL of purified IBF-loaded NPs suspension was sealed into a dialysis membrane bag (Tsai, Jan *et al.* 2011) with a molecular weight cut-off (MWCO) of 3500 Da. The membrane was immersed into 50 mL of each media at 37 °C and stirred at 100 rpm. At fixed intervals, 0.5 mL of medium was withdrawn and filtered using a 0.45 µm syringe filter. At the same time, the same volume of fresh medium was added to the release medium. The concentration of released IBF was determined by HPLC, using the previous described method. *In vitro* IBF release studies were performed in triplicate (n = 3).

2.3.2.8. Cytotoxicity MTT assay

The cytotoxicity of LbL NPs against Caco-2 cells was studied using a MTT assay. Caco-2 cells were obtained from European Collection of Cell Cultures and were used after 71-74 passages. The cells were cultured at 37 °C and 5% CO₂, in DMEM with 10% FBS supplemented with 1% PenStrep. Subcultures were performed by detaching the cells with trypsin. These studies were performed after 18 h incubation of 100 µL of a Caco-2 cell suspension seeded in a 96-well plate at a density of 10⁵ cells/mL. Prior to the addition of the NPs, the medium was removed and 100 µL of new complete medium was added. Serial dilutions of the LbL NPs were prepared in DMEM free of serum at a concentration range between 11.7 µg/mL and 1500 µg/mL. 100 µL of each NPs sample were added and incubated with the cells for 24 h, at 37 °C and 5% CO₂. After 24 h, the MTT cytotoxicity assay was performed. The cell viability (%) related to control (cells in culture medium without NPs) was calculated by the following equation (Equation 2.2):

$$\text{Cell viability (\%)} = \frac{OD \text{ sample (540 nm)} - OD \text{ sample (630 nm)}}{OD \text{ control (540 nm)} - OD \text{ control (630 nm)}} \times 100$$

2.3.3. Statistical analysis

Statistical analysis was performed using SPSS Statistics version 20.0; for curve fitting, Origin Pro Software was used. Data regarding PE concentration *versus* zeta potential were fitted to one of two models, namely an exponential response curve (Equation 2.3):

$$y = y_0 + A_1 \cdot e^{\frac{x}{t_1}}$$

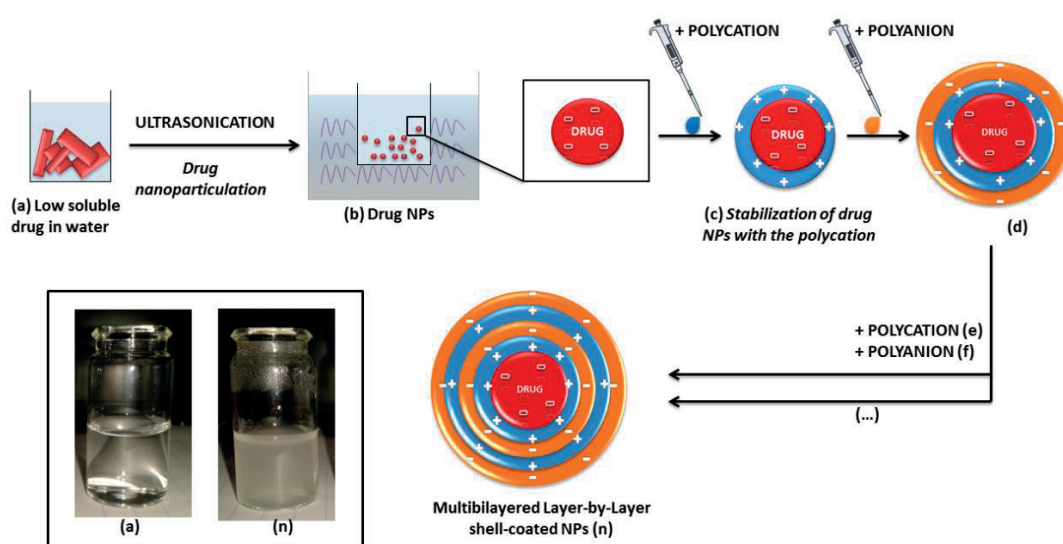
where y_0 represents the plateau for higher PE concentrations, $y_0 + A_1$ represents baseline zeta potential (no PE added) and t_1 is a kinetic parameter. Other model used to fit the data was a sigmoidal response curve (Boltzmann model) (Equation 2.4):

$$y = A_2 + \frac{A_1 - A_2}{1 + e^{\frac{x - x_0}{dx}}}$$

where A_1 and A_2 represent the upper and lower asymptotes, respectively. Data related to sonication time versus particle size was fitted to sigmoidal curve, according to Boltzmann equation (described above). Zeta potential and particle size were compared between particles with different number of coating bilayers by using Kruskal-Wallis' non parametric test, with pairwise comparisons using Bonferroni correction. In order to assess stability studies, particle size and zeta potential were analyzed across time, and a Friedman's non parametric test for paired samples was used. For *in vitro* release profiles at pH 6.8, data was fitted to the above mentioned exponential model. Cell viability results were analyzed using two-way ANOVA and Bonferroni post-test. The IC_{50} values were calculated by plotting the log concentration of the NPs *versus* inhibition percentage of Caco-2 cell viability. A significance of 0.05 was considered for all comparisons.

2.4. Results and discussion

Sonication process showed to be able to promote the reduction of IBF native micron ranged crystals (**Figure 2.1a**) to the nanometer scale (**Figure 2.1b**). Keeping these IBF NPs under sonication prevented their fast agglomeration. Subsequently, the application of LbL coating, by the adsorption of successive alternated charged PE coatings of PAH and PSS, allowed for colloidal stabilization (**Figure 2.1c-n**). Sufficient PE concentrations for each shell layer saturated deposition were determined by tracing titration curves (**Figure 2.2**), thus avoiding unwanted intermediate washings. A top-down approach using washless LbL technique produced successfully PAH/PSS-constituted multilayer shell NPs containing IBF. These NPs are proposed as potential oral delivery systems for a low soluble drug. NPs process formulation and characterization are described below in detail.



WASHLESS TOP-DOWN LAYER-BY-LAYER POLYELECTROLYTE ASSEMBLY

Figure 2.1: Schematic presentation of LbL NPs formation from low soluble drugs by washless top-down LbL PE assembly.

Drug native microcrystals are firstly dispersed in water (**a**), and subjected to ultrasonication up to the attainment of drug NPs (**b**), following by adsorption of a polycation layer (**c**) and polyanion layer (**d**) and so on (**e-f**, ...) up to the desired number (**n**) of PE bilayers upon the LbL shell, showing a characteristic naked eye Tyndal Effect (**n**).

[LbL – Layer-by-Layer; NP – nanoparticle; PE – polyelectrolyte]

2.4.1. Layer-by-Layer preparation and characterization of ibuprofen nanoparticles

2.4.1.1. Titrations of polyelectrolytes concentrations

Initially, intrinsic magnitude charge of IBF nanocores was determined by a zeta potential measurement. A value of -15.1 ± 2.1 mV reflected the IBF nanocores negative surface charge, as showed in the first point of **Figure 2.2a** titration. Since the LbL process is based upon electrostatic interactions between the core drug and the PEs, its surface charge determination was crucial to know the order of addition of the PAH/PSS PE pair to cover its surface. In this study, the first added PE was the PAH polycation, followed by the second addition of the PSS polyanion.

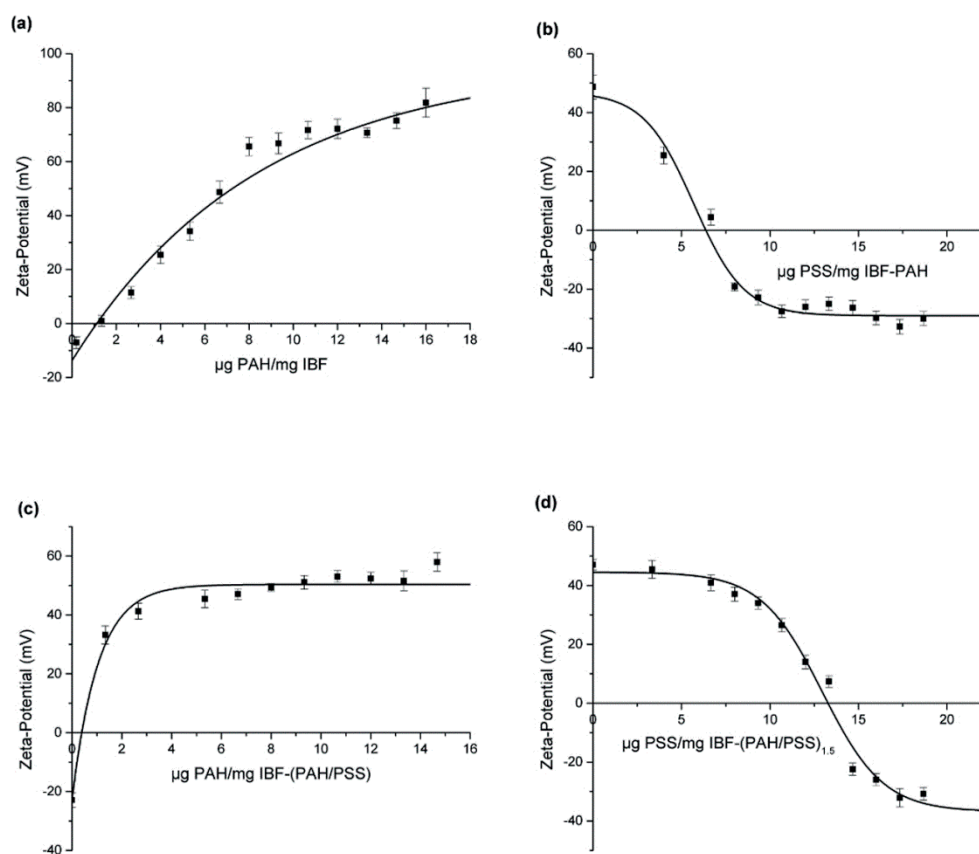


Figure 2.2: Zeta potential against PE concentration for 0.5 mg/mL IBF NPs. Four sequential steps of polycation/polyanion deposition are shown in the stepwise addition of **(a)** PAH to IBF nanocores, **(b)** PSS to IBF-PAH NPs, **(c)** PAH to IBF-(PAH/PSS) NPs, and **(d)** PSS to IBF-(PAH/PSS)_{1.5} NPs.

[IBF – ibuprofen; NP – nanoparticle; PAH – poly(allylamine hydrochloride); PE – polyelectrolyte; PSS – poly(styrene sulfonate)]

In order to establish an optimal sonication-time condition, the sonication time required to achieve the first PE coating layer (which corresponded to the IBF nanocores' surface coating with PAH) was tested for particle size. As it can be seen in **Figure 2.3**, sonication time strongly influenced particle size, and a 20-min sonication of initially low soluble IBF microcrystals in the presence of PAH allowed the attainment of IBF-PAH NPs with a particle size of 122.0 ± 37.6 nm and a PDI of 0.24. NPs formation was confirmed by suspension opalescence associated with the Tyndall effect as depicted in the **Figure 2.1n**. Further increase in the sonication time beyond 20 min did not decrease particle size, and after 40 min particle size started slightly enhancing. This was probably a consequence of the bridging of larger drug particles with the PE (Pattekari, Zheng *et al.* 2011). After the coating layer deposition of PAH over IBF nanocores, the strongly positive charge prevented aggregation and maintained colloidal stability to continue LbL shell formation with more coating PE layers.

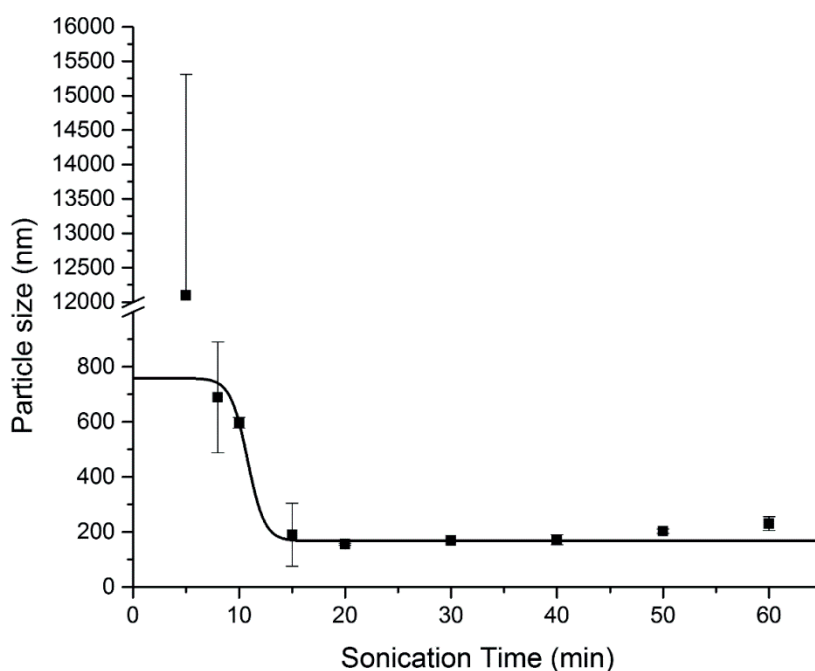


Figure 2.3: The particle size of IBF cores, with ca. $72 \mu\text{m}$ of initial particle size, in response to sonication time. PAH was present in solution for the first polymeric monolayer on the IBF nanocores surface and prevented particle aggregation after the removal of ultrasound.

[IBF – ibuprofen; PAH – poly(allylamine hydrochloride)]

After optimization of the sonication time, the ideal PE concentration for each coating layer was examined. Regarding this, a range of PE concentrations were investigated for each layer and the resulting zeta potentials were measured. The stepwise PE addition enabled the construction of

the respective titration graphs, depicted in **Figure 2.2**. In practice, this corresponds to the complete PE deposition on the NPs surface for each LbL coating layer determined by the recharging point in each titration curve. This point was the requisite to proceed for the next PE coating layer deposition.

Starting with IBF nanocores, the titration curve regarding to the PAH surface deposition is depicted in **Figure 2.2a**. As it can be seen, the point of plateau for the zeta potential started at $6.7 \pm 4.1 \mu\text{g PAH /mg IBF}$. After PAH addition and complete surface coating, the PE was switched to negative polyanion PSS, which titration corresponds to **Figure 2.2b**. The titration of IBF-PAH NPs enabled the determination of the point of the plateau at $9.3 \pm 2.5 \mu\text{g PSS /mg IBF}$. In the third step, PAH was added to IBF-(PAH/PSS) NPs, and the point of plateau was $6.7 \pm 1.8 \mu\text{g PAH /mg IBF}$, as shown in **Figure 2.2c**. The fourth titration graph, **Figure 2.2d**, shows the addition of PSS to IBF-(PAH/PSS)_{1.5} NPs, and the corresponding value was $14.7 \pm 2.1 \mu\text{g PSS /mg IBF}$. Thus, it is noteworthy that the addition of the following coating PE layer was only performed after adding the previously determined ideal concentration.

The analysis of the titration curves of IBF nanocores when using cationic PAH and anionic PSS enabled the observation of differences. Upon PAH addition, an increasing effect on zeta potential value along with a more gradual plateau onset were verified, following an exponential fitting model ($r^2 > 0.97$ for both titrations, **Figure 2.2a** and **Figure 2.2c**). On the other hand, PSS originated a clear plateau onset point, approaching to a sigmoid fitting model ($r^2 > 0.95$ for both titrations, **Figure 2.2b** and **Figure 2.2d**). This difference could be explained to the difference in charge density of the used PEs. PAH shows more molecular loops and tails than PSS (Bantchev, Lu *et al.* 2009), and it was only partially charged at the pH assay (neutral, pH=7), giving origin to thicker layers that can have hidden negatively charged patches. Furthermore, when PAH constituted the outermost layer, the highly positively charged molecules adhered to the previous layers and also protruded into the dispersion medium. This phenomenon increased PAH density and charge, which directly influenced zeta potential but in parallel created a lack of complete PE saturation, as it is visible in the titration curves of **Figure 2.2a** and **Figure 2.2c**. On the other hand, the addition of PSS to positive surfaces had just a little influence on the surface charge values, initially. This was due to the adsorption of PSS in the interior PAH loops. After overcoming PAH tails and loops, PE molecules started to form negative patches on the surface until all surface coverage, when occurred a steep change in zeta potential values, contrary to the PAH behavior (Bantchev, Lu *et al.* 2009). This fact is related to the washless LbL technique which

allows the achievement of thinner PE coating layers, more encompassed layers and thus more PE chains interpenetration (Losche, Schmitt *et al.* 1998).

As it can be seen in **Figure 2.2**, titrations were only depicted for the first four PE coatings, as previously discussed. However, titrations were performed and analysed up to the two and a half PEs bilayers, namely IBF-(PAH/PSS)_{2.5}. The two and a half PE bilayered nanoformulation (IBF-(PAH/PSS)_{2.5}) was the less complex studied nanoformulation. For this reason, it was considered for physical stability evaluation before addition of further LbL coatings, and consequently before the preparation of more complex nanoformulations. These NPs were shown to be physical stable during at least one week, as it is depicted in **Figure 2.4a**. Once acquiring physical stability with 2.5 PE bilayers was acquired, the complete titration procedure for each next coating step, which was shown to be a tedious and slow protocol, was therefore avoided. The addition of the PE layers after the 2.5 PE bilayers was done just until sufficiently physical stability was obtained. This was attained without precisely determining the critical plateau point as before, namely by the determination of the PE concentration that allowed for charge reversal without aggregation. In practice, it corresponded to the attainment of +20 and -15 mV zeta potential magnitudes without significant changes in particle size for PAH and PSS coatings.

After all the LbL coatings were done through the determination of necessary PE concentrations for each PE layer coating, IBF LbL-coated NPs were produced by ensuring no PE excess for the LbL successive coatings. A washless technique was developed for PAH/PSS coating up to 7.5 bilayers with homogenous particle size populations at the desired nanoscale interval (100-200 nm).

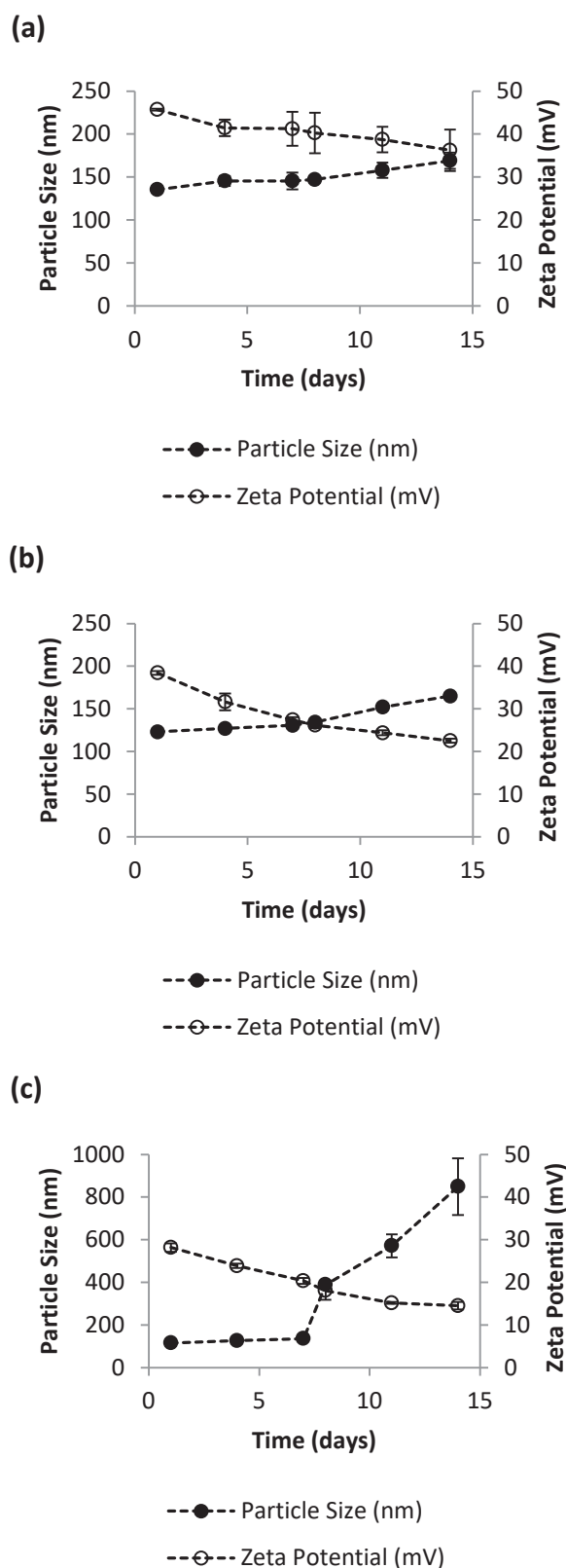


Figure 2.4: (●) Particle size and (○) zeta potential changes of IBF LbL NPs prepared with (a) 2.5, (b) 5.5 and (c) 7.5 bilayered coatings of PAH/PSS for 14 days at 25 °C.

[IBF – ibuprofen; LbL- Layer-by-Layer; NP – nanoparticle; PAH – poly(allylamine hydrochloride); PSS – poly(styrene sulfonate)]

Three different nanoformulations of IBF NPs were studied, namely with 2.5, 5.5 and 7.5 PE LbL bilayers.

2.4.1.2. Zeta potential

The values of zeta potential magnitudes monitored during the process of sequential PAH/PSS adsorption upon IBF nanocores are present in **Figure 2.5**. The results showed that after adsorption of PAH to IBF nanocores with negative surface under sonication, drug NPs were recharged to high positive surface charge ($+60.0 \pm 4.1$ mV). These values revealed that the first PAH layer conferred high physical stability to the IBF nanocores. LbL assembly proceeded with the addition of the polyanion PSS and the surface charge was again reversed to negative values (-22.8 ± 2.5 mV). The addition of the PAH constituted-third shell layer (1.5 PE coating bilayer) promoted again a charge reversal, by the formation of a highly positive charged layer. The LbL assembly was proceeded by consecutively alternating both PE additions. The most complex performed formulation corresponded to the IBF NPs coated with a multilayer shell of 7.5 PAH/PSS bilayers, showing zeta potential higher than +30 mV.

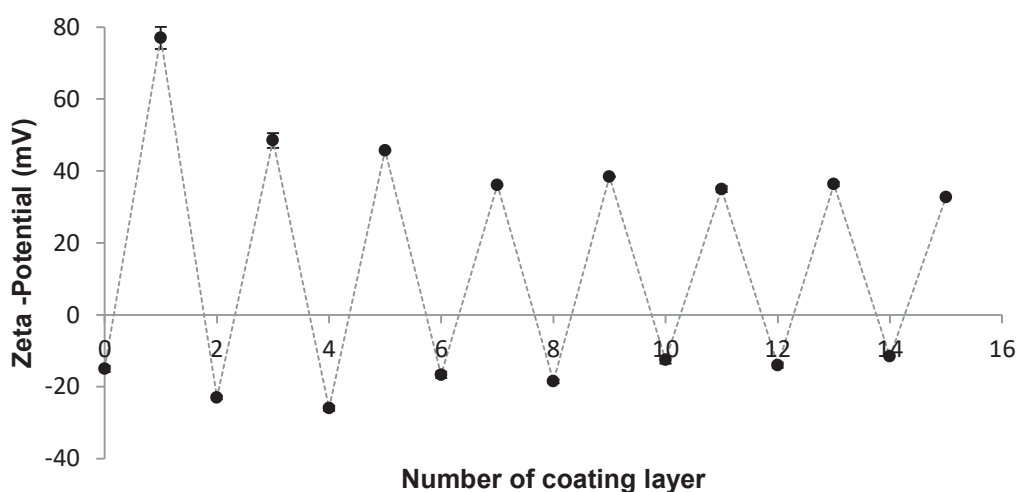


Figure 2.5: Zeta potential changes of IBF coated up to 7.5 coating bilayers, IBF-(PAH/PSS)_{7,5}, during process shell assembly, by top-down and washless approach.

[IBF – ibuprofen; NP – nanoparticle; PAH – poly(allylamine hydrochloride); PSS – poly(styrene sulfonate)]

As shown in **Figure 2.5**, the high surface potential remained constant during all the studied PE layer depositions up to the 2.5-3.0 bilayers. After this point a slight reduction on the magnitude of zeta potential was observed, depicted in the «shrinkage» of the final part of the graph. Furthermore, the values showed significant differences between initial and final LbL shell coatings-corresponding zeta potential values either for PAH and PSS layers. This happened due

to the partial PE coating of the outermost layers, as well as the existence of secondary interactions between PEs of different bilayers, which triggered a decrease in the surface charge density (Diez-Pascual, Wong 2010). Given the higher zeta potential magnitude of PAH layers (around +40 mV) comparing to PSS layers (close to -20 mV), PAH was the chosen PE for the last layer, providing higher stability to these nanoformulations.

The evaluation of zeta potential values during LbL assembly demonstrated alternation of the surface potential due to sequential polycation/polyanion deposition steps, confirming the surface recharging – the driving force of the process. This recharging, in turn, led to the conclusion that PE attachment to the NPs surface occurred and the complete coating was formed after each PE deposition step.

2.4.1.3. Particle size

Particle size of NPs was evaluated after each layer deposition during the LbL assembly technique, and the results are depicted in **Figure 2.6**.

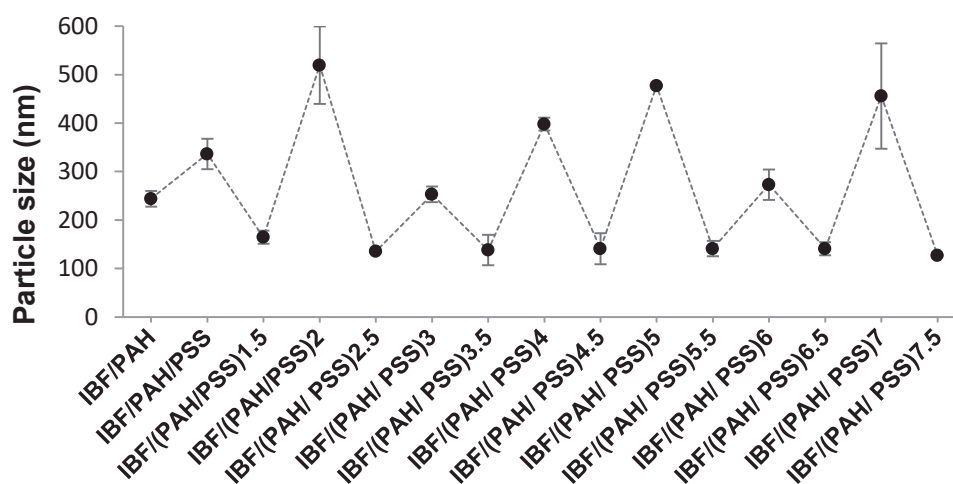


Figure 2.6: Particle size measurements of IBF coated up to 7.5 coating bilayers, IBF-(PAH/PSS)_{7.5}, during process shell assembly, by top-down and washless approach.

[IBF – ibuprofen; PAH – poly(allylamine hydrochloride); PSS – poly(styrene sulfonate)]

LbL technique allowed for homogenous size distributions of 100-150 nm with PDI values around 0.2 for all LbL nanoformulations. This suggested that NPs had an acceptable monodispersity distribution, without aggregation. Focusing on **Figure 2.6**, it is possible to see that during LbL assembly particle size suffered oscillation, which depended on the PE nature of the outermost layer. Particle size was significantly higher than 200 nm when PSS was used as the outermost coating layer of the LbL shell. The difference on the particle size, together with the previous

discussed corresponding zeta potential analysis, suggested a slight aggregation process when using PSS. This behavior was reversible by the addition of the next PAH layer. Observed NPs re-stabilization was caused by the phenomenon of NPs collapse in the presence of oppositely charged PEs able of decrease their interparticle bridging activity. Also, this occurred due to the increase particle surface charge, which led to higher electrostatic repulsion and decrease of the area occupied by single polymer molecules. In fact, when using PSS as the outermost coating layer in the LbL coating shell, zeta potential values were dominated by the anionic PE charge. However, the surface was still patching with protruding positive PAH chains which could have attached to negatively charged regions of other particles and have caused higher aggregation (Bantchev, Lu *et al.* 2009). Thus, as PAH conferred higher physical stability to the NPs, this PE was used at the outermost layer of the LbL shell architecture in all of the three present studied nanoformulations.

2.4.2. Nanoparticle imaging

The morphology and particle size of IBF NPs samples formulated by the LbL technology into nanocolloidal state were evaluated by SEM and Confocal Microscopy. **Figure 2.7** shows SEM images of native IBF crystals (**Figure 2.7a**) and prepared IBF LbL NPs (**Figure 2.7b**).

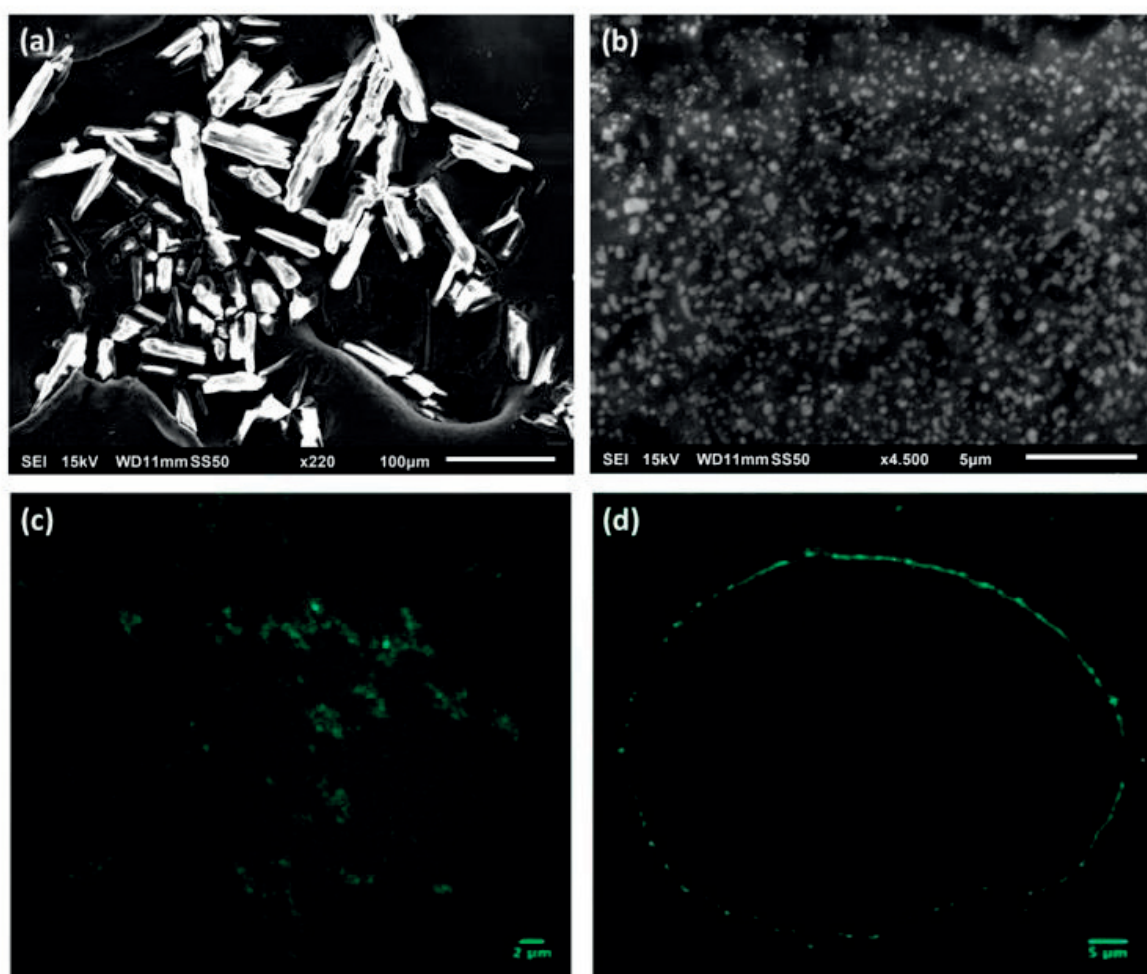


Figure 2.7: SEM image of (a) IBF native micrometer-sized crystals (x220) and (b) IBF LbL NPs with a IBF-(PAH/PSS)_{5.5} coating shell (x4500). Confocal fluorescent image of an aqueous dispersion of LbL IBF NPs coated with (c) FITC-labelled PAH with a IBF-(PAH/PSS)_{5.5} coating shell and (d) with 5 min of sonication exposure, in order to obtain higher-sized particles (microparticles).

[FITC – fluorescein isothiocyanate; IBF – ibuprofen; LbL- Layer-by-Layer; NP – nanoparticle; PAH – poly(allylamine hydrochloride); PE – polyelectrolyte; PSS – poly(styrene sulfonate); SEM – scanning electron microscopy]

These images showed the reduction of characteristic needle-like shaped original IBF micro-sized crystals ($73 \pm 46 \mu\text{m}$) to the nanoscale (100-150 nm), by the formation of square-like shaped NPs. Probably, this shape of NPs reflected IBF crystalline structures after LbL coating under sonication (Lvov, Pattekari *et al.* 2010).

It can be seen also that particle size analysis by SEM results (even without a high resolution) are in agreement with the submicron-sized colloidal particles obtained by DLS, depicted in **Figure 2.6** and **Table 2.1**.

Table 2.1: Particle size, zeta potential and encapsulation efficiency of IBF crystals and IBF LbL-coated NPs. Data represent mean \pm SD, n = 3.

| Formulation | Particle Size (nm) | Polydispersity index (PDI) | Zeta Potential (mV) | Encapsulation efficiency (%) |
|--------------------------------------|--------------------|----------------------------|---------------------|------------------------------|
| Non-encapsulated IBF native crystals | 73000 \pm 46000 | Not applicable | -15.1 \pm 2.1 | Not applicable |
| IBF-(PAH/PSS) _{2,5} NPs | 135.3 \pm 1.9 | 0.20 | +45.7 \pm 0.2 | 78.1 \pm 3.9 |
| IBF-(PAH/PSS) _{5,5} NPs | 141.1 \pm 16.0 | 0.20 | +34.9 \pm 0.8 | 74.4 \pm 4.3 |
| IBF-(PAH/PSS) _{7,5} NPs | 127.5 \pm 38.0 | 0.24 | +32.7 \pm 0.6 | 72.1 \pm 5.8 |

[IBF – ibuprofen; LbL- Layer-by-Layer; NP – nanoparticle; PAH – poly(allylamine hydrochloride); PDI – polydispersity index; PSS – poly(styrene sulfonate); SD – standard deviation]

FITC-labelled PAH was prepared in order to formulate fluorescent LbL NPs (**Figure 2.7c**). Although the resolution of confocal microscope (close to 100 nm) did not allow for detailed structure visualization, it was possible to see well-dispersed fluorescent green dots, which color is due to FITC labelling. This fluorescence of NPs confirmed the attachment of the fluorescent PAH to NPs LbL shell. In order to overcome the confocal microscopy resolution limit and better confirm the presence of the PAH PE layer upon IBF nanocores surface, larger particles (microparticles) were prepared. These NPs were achieved using a shorter sonication time (5 min) with just one PAH-labelled FITC layer adsorbed on surface cores of IBF (**Figure 2.7d**). It can be seen that there is a micrometer-sized LbL capsule cross-section which provides evidence for the capsule wall, and therefore there is evidence of the successful adsorption of PEs during the LbL technique.

2.4.3. Encapsulation efficiency

Encapsulation efficiency of the drug is an important index for drug delivery systems. The number of coating layers did not affect the encapsulation efficiency of IBF, which was higher than 70% for all the studied nanoformulations (**Table 2.1**). It can be concluded that IBF was attached to PAH with high efficiency in the first step of LbL coatings. As the encapsulation process was conducted by electrostatic interactions, the first used PE in the LbL shell was PAH that has many amine groups (Jachimska, Jasiński *et al.* 2010), which binded negatively charged IBF in pH 7. The main loss was due to the process, namely the occurrence of splashed out particles of the container under powerful sonication during LbL process. The present LbL NPs allowed the solubilization of IBF in water, and therefore this delivery system can be applied for encapsulation of other BCS class II drugs.

2.4.4. Stability studies

One of the major aims of a nanoformulation is to maintain the colloidal stability in order to preserve its inherent physicochemical properties. Stability studies of the LbL coated NPs with 2.5, 5.5 and 7.5 PE bilayers were performed during 14 days at room temperature (**Figure 2.4**). In these conditions, particle size was not affected during the first 7 days for all the nanoformulations. After 7 days, all nanoformulations showed a particle size enhancement, which could be caused by a zeta potential decrease, that could lead to aggregation phenomena. This effect was more pronounced for the most complex formulation (7.5 PE bilayers), whose particle size values were significantly different in relation to the other two nanoformulations (2.5 and 5.5 bilayers). This was probably due to the enhancement of the LbL shell complexity, which triggered the existence of more bridging interactions between neighbouring particles. For 5.5 and 7.5 bilayered-nanoformulations, changes were slighter in particle size and zeta potential during the same period. Given these results, it was possible to conclude that aqueous LbL coated NPs were stable for 7 days at room temperature. However, after this period of time, stability was significantly decreased when the complexity of the shell was enhanced. These results were in accordance with heparin/PLB16-5-coated LbL NPs, that had showed higher particle size values when the shell was composed with 7 bilayers comparing to 5 bilayers after 7 days at room temperature (Parekh, Pattekari *et al.* 2014).

2.4.5. *In vitro* release studies

As IBF is a weak acidic drug, the release from LbL NPs may be pH-dependent. In order to assess the potential of the LbL NPs to be used in drug delivery systems, release studies of IBF native crystals (non-encapsulated IBF) and IBF LbL NPs with different number of layered PAH/PSS shells were carried out in simulated gastric and intestinal fluids without enzymes at pH 1.2 (**Figure 2.8a**) and 6.8 (**Figure 2.8b**), respectively, maintaining body *sink* conditions.

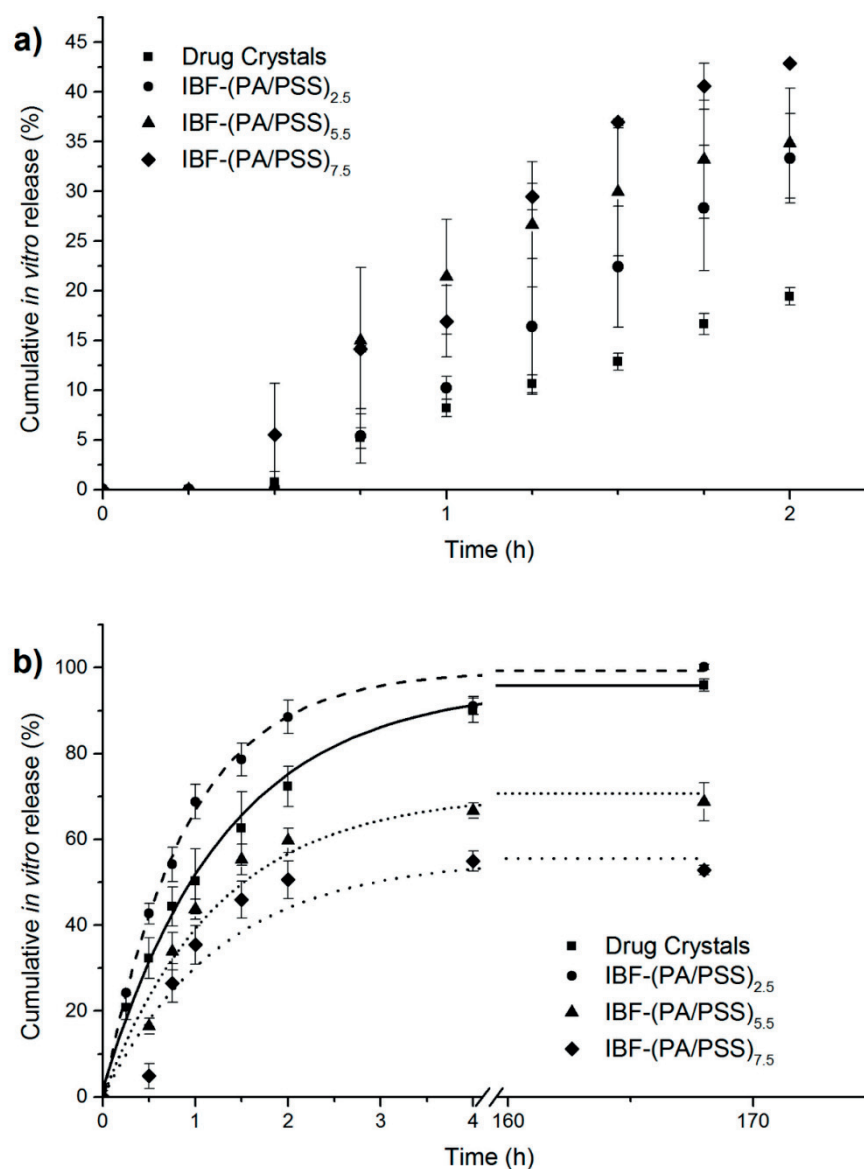


Figure 2.8: *In vitro* IBF release from (■) non-encapsulated crystals of IBF, and IBF LbL NPs prepared with (●) 2.5, (▲) 5.5 and (◆) 7.5 bilayered coatings of PAH/PSS in (a) simulated gastric pH 1.2 fluid and (b) simulated intestinal pH 6.8 fluid in *sink* conditions at 37 °C. Data represent mean \pm SD, n = 3.

[IBF – ibuprofen; LbL – Layer-by-Layer; NP – nanoparticle; PAH – poly (allylamine hydrochloride); PSS – poly(styrene sulfonate)]

As it can be seen in **Figure 2.8a**, IBF native crystals showed a lower dissolution profile in simulated gastric fluid in relation to LbL NPs due to its higher-sized crystals in relation to the NPs size (Shutava, Pattekari *et al.* 2012, Strydom, Otto *et al.* 2014), concomitantly with the low IBF solubility in this medium (Masum, Sharmin *et al.* 2012). On the other hand, no effect on dissolution rate of encapsulated IBF was observed among the studied nanoformulations of LbL NPs. Thus, no effect of shell wall thickness on IBF dissolution was detected. Drug release was overall faster for encapsulated IBF in relation to IBF native crystals, and no correlation of IBF

release with a release kinetics model was found to be satisfactory in this release medium. Regarding studied nanoformulations of LbL NPs, at simulated gastric pH PAH/PSS capsule membranes were destabilized due to the pKa of the PEs, affecting their integrity, and membrane permeability was increased due to the pore formation (Antipov, Sukhorukov *et al.* 2002), allowing for drug release. However, it is noteworthy that after 2 h of *in vitro* simulated gastric incubation, most IBF remained associated to LbL NPs (ca. 60%).

In simulated intestinal fluid (**Figure 2.8b**), it can be observed that LbL NPs allowed for a biphasic drug release pattern, with an initial burst release followed by a controlled drug release phase, showing a very good fit ($r^2 > 0.99$ for all nanoformulations) with the exponential kinetic model following an apparent first-order behavior. The release pattern of these NPs revealed initially high release rate of IBF in the first 1.5 h, which can be attributed to the diffusion of some adsorbed IBF molecules onto the NPs external surface. It was followed by a controlled IBF release phase attaining a plateau at 4 h in release medium, without significant changes in the IBF release up to 170 h (7 days). In a comparison of the different LbL studied nanoformulations, in 2 h, only 50.6% of IBF in 7.5-bilayered LbL NPs was released as compared with 59.7% of the 5.5-bilayered LbL NPs, and 88.5% of the 2.5-bilayered NPs. An increasing effect of the number of coating bilayers on delayed release of IBF was observed. This effect was probably due to the enhancement of shell wall thickness of NPs, which increased diffusional path for the encapsulated IBF and, thus, conducted for a IBF diffusion delay from the core to the LbL net-like structure of oppositely charged PE-composed shell (Fu, Kao 2010). These factors resulted in a decrease of the IBF release rate and also in a decrease of the initial IBF burst release. Similar results were found using other low water soluble drugs, like paclitaxel and isoxyl from nanocapsules (Pattekari, Zheng *et al.* 2011, Strydom, Otto *et al.* 2014). Like in the present LbL NPs, the dissolution rate was found to decrease almost linearly with increasing shell thickness. A prolongation of drug release through the use of three coating PE bilayers were already effective (Strydom, Otto *et al.* 2014). Thus, an effect of LbL shell thickness on the dissolution enhancement was found also for those low soluble drugs. In another case, under *sink* conditions in PBS buffer pH 7.2, 40% of paclitaxel was released from (PAH/BSA)₃ coated NPs in 8 h as compared with 80% for one layer coated NPs (Pattekari, Zheng *et al.* 2011). It must be emphasized that IBF delayed release from LbL NPs was much higher when compared to IBF release from chitosan/dextran sulfate LbL microcapsules with 30 PE layers (Qiu, Leporatti *et al.* 2001). In 2 h at pH 1.4, previous microcapsules released close to 100% of the IBF while in the present NPs less than 40% of IBF was released at similar conditions. In higher pH the difference was even higher, whereas microcapsules released all the encapsulated IBF in less than 1 min at

pH 7.4 comparing to 4 h of delayed release from NPs at similar conditions (pH 6.8). Theoretically, when comparing LbL systems with similar PE coating shells composition, lower-sized particles could conduce to dissolution rate and thus higher drug release (Hammond 2012). However, other factors are present in LbL formulations which influence drug release pattern besides particle size, and it was verified a higher capacity of drug delayed release in LbL NPs when compared to LbL microcapsules. As pore radius decrease with decreasing particle size (Patil, Paradkar 2006), the lower pore size distribution of the nanopores of the NPs LbL shell and their pore-matrix structure probably allowed for a lower displacement of the drug through the pores, decreasing PE shell permeability (Civan 2001), and thus delaying drug release in relation to micropores present in microcapsules. The nature of the PEs could also have contributed to this behavior, since synthetic PEs show more resistance to environmental changes than the natural PEs (Teo, Kaur *et al.* 2010).

The previous described increase in the LbL film thickness effect was also responsible for incomplete IBF release from the 5.5 and 7.5 PE bilayered-nanoformulations. Non-released IBF was confirmed to be inside LbL NPs through IBF quantification inside *in vitro* release dialysis membranes, which was shown to be in accordance to the maximum IBF released percentage (the asymptotic value of the release model fitting), namely ca. 30% and ca. 50% of non-released IBF for 5.5 and 7.5 LbL bilayers. The high electrostatic-based linkage of the PEs web around the drug core seemed to enhance the strength with the number of LbL PE bilayers. With the increase of the complexity of the LbL shell, a lower fraction of free IBF was capable to diffuse to the exterior. In addition, the non-degradable nature of the used PEs can also have contributed for this behavior. Non-complete drug release from LbL PE bilayered shells was also exhibited for higher layers number-composed LbL shells in previous reported release profiles (Pattekari, Zheng *et al.* 2011, Shutava, Pattekari *et al.* 2012).

2.5-bilayered LbL NPs, which corresponded to the less complex LbL nanoformulation, led to IBF slightly faster release in relation to non-encapsulated IBF. This was caused to NPs smaller size and higher surface area in the nanoformulation compared to micrometer size and lower surface area of the non-encapsulated IBF crystals. According to the Kelvin equation, the increase in the curvature of the particle surface triggers the increase in the dissolution pressure of the substance, being solubility substantially increased as particle size decreases up to the nanoscale (Junghanns, Muller 2008). The increased solubility (or saturation solubility) of the drug is correlated to a faster dissolution rate by the Noyes-Whitney equation (Nokhodchi, Amire *et al.* 2010). These results were in accordance to PLB16-5/Hep bilayered LbL NPs which did not show

significant influences on the drug release rate for LbL shells thinner than 3.5 bilayers (Shutava, Pattekari *et al.* 2012).

PAH/PSS composed-shell LbL NPs showed a pH-dependent drug release behavior, as previously reported (De Geest, Sanders *et al.* 2007). A suitable gastro-resistant approach should be used to avoid drug release in acidic medium, like gelatinous gastro-resistant capsules or the use of an enteric coating polymer with a molecular weight lower than 65 kDa to prevent colloidal aggregation (Schneider, Decher 2004).

2.4.6. Cytotoxicity assays

In vitro cytotoxicity evaluation can be performed to screen pharmaceutical formulations before testing in animals (Al-Qubaisi, Rasedee *et al.* 2013). MTT assay was chosen because is one of the well-established cell viability assays, which is based on the capacity of the cellular mitochondrial dehydrogenase enzyme in living cells to reduce the yellow water-soluble MTT into a purple formazan (Gerlier, Thomasset 1986), therefore not evaluating the cell but its mitochondrial activity (Kharlampieva, Kozlovskaya 2014). Caco-2 cells were used considering the intended oral route of the NPs.

Previous studies had shown a good cytotoxic profile for PAH/PSS capsules on different cell lines, which depended on the dosage and also on the capsules size (Lewinski, Colvin *et al.* 2008, Wattendorf, Kreft *et al.* 2008). The outermost membrane layer effect on the toxicity had also been reported before on L929 cell line, and results indicated comparable results for PAH and PSS (Luo, Neu *et al.* 2012). In this work, the choice of PAH as the outermost layer was previously explained with formulation aspects. The potential cytotoxicity of PAH/PSS-constituted LbL IBF NPs was evaluated with different number of coating bilayers (2.5, 5.5 and 7.5 bilayers) by determining the viability of the Caco-2 cells when exposed to NPs formulations (**Figure 2.9**).

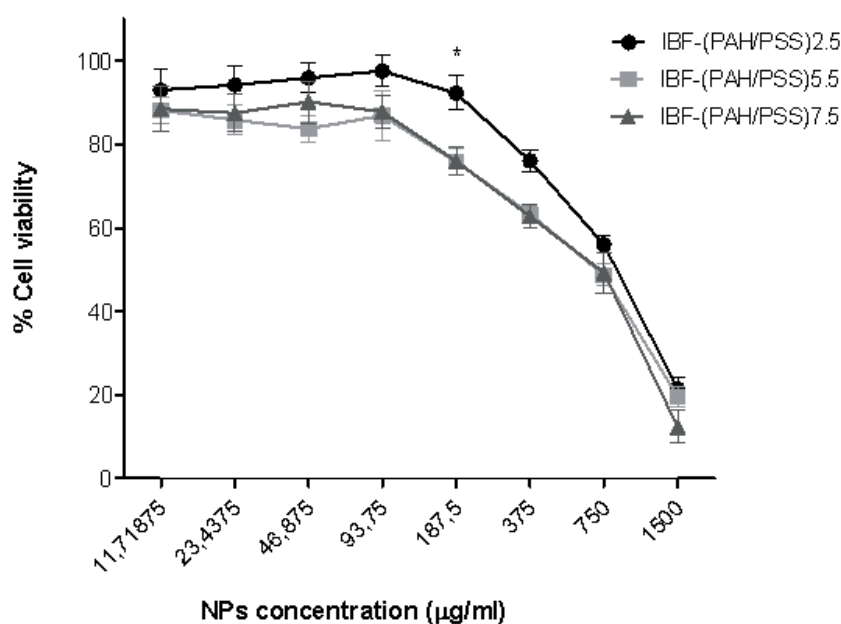


Figure 2.9: Cell viability of Caco-2 cells after 24h of incubation with (●) 2.5, (■) 5.5 and (▲) 7.5 LbL bilayered coated PAH/PSS NPs for concentrations ranging from 11.7 µg/mL to 1500 µg/mL. Cell viability of each sample was determined using MTT assay. Data are expressed as mean ± S.E.M. (n = 3). *p < 0.05 for the 2.5 bilayered NPs comparing to 5.5 and 7.5 bilayered LbL NPs.

[IBF – ibuprofen; LbL- Layer-by-Layer; MTT – 3-(4,5-dimethylthiazol-2-yl)-2,5-diphenyltetrazolium bromide; NP – nanoparticle; PAH – poly(allylamine hydrochloride); PSS – poly(styrene sulfonate; S.E.M. – standard error of the mean)]

A very good cytotoxicity profile was observed, indicating an *in vitro* cytocompatibility of the LbL NPs in this cell culture system. The concentrations where the cell viability decreased to 50% (half maximal inhibitory concentration, IC_{50}) were 845.1 ± 1.1 , 771.2 ± 1.1 and 698.9 ± 1.1 µg/mL for 2.5, 5.5 and 7.5-bilayered NPs, respectively. In the presence of higher concentrations, the three mentioned nanoformulations promoted a considerable increase in cytotoxicity, wherein almost no cell viability was achieved at 1500 µg/mL. This concentration-dependent toxicity can be caused by the instability obtained with higher NPs concentrations. Higher concentrations led to agglomeration on the cell culture medium and consequently sedimentation over the adherent cells causing their death. For lower concentrations, the electrostatically induced repulsive bilayered LbL coatings of the NPs were probably responsible for NPs suspension stability in the *in vitro* testing conditions, favouring NPs-cell interactions (Horie, Nishio *et al.* 2010). Beyond this, comparing the cytotoxicity between the three different nanoformulations, it was possible to see that no statistical differences were observed along tested concentrations excluding the 187.5 µg/mL, where the 2.5 bilayered-coated LbL NPs showed statistically significant higher cell viability comparing to the other two nanoformulations. In consideration of the zeta potential values for the 3 systems, this result could be attributed to the more cationic profile of the 2.5-

bilayered NPs that leads to a stronger interaction with the negatively charged cell membrane (Goodman, McCusker *et al.* 2004). The positive surface charge of PAH/PSS LbL shells may have caused cell membrane pore formation followed by cell damage and death (Veerabadran, Price *et al.* 2007). Nevertheless, considering the range of the whole experiment, these results demonstrated that the present LbL NPs system has a large range of no toxic *in vitro* concentrations, constituting a promising nanocarrier for low soluble drugs and enabling *in vitro/in vivo* further applications.

2.5. Conclusions

A sonication-assisted top-down approach along with a washless LbL technique was applied for nanoencapsulation of low water soluble drug IBF by using PAH/PSS-constituted shell up to 7.5 bilayers NPs. Modification of the traditional LbL-coating technique using a washless protocol allowed the use of smaller amounts of PEs, avoiding excessive washed out PEs. Less material was used and often complicated procedure of centrifugations, filtrations and intermediate PE washings were avoided, allowing for the process scale-up.

With this we changed a traditional LbL microencapsulation approach for well soluble drugs encased in PE multilayer shells which slowed down dissolution, to nanoarchitectural design of well dispersed low soluble drug nanocolloids stabilized with strongly charged PE shells.

LbL NPs presented important characteristics necessary for improved drug delivery related to nanotechnology. The attainment of a tunable PE LbL multilayer shell offered structural control over the size and surface charge, high encapsulation efficiency, controlled drug release and absence of *in vitro* toxicity. This technique was shown also to be a simple coating technique at nanoscale, without the use of any special equipment, harsh chemicals or extreme temperature. It does not require stabilizers and the medium is water, absent the use of organic solvents.

Thus, LbL-nanocoating technology offers promising scaling-up perspectives in the obtainment of an effective delivery system for low aqueous soluble drugs. For an effective oral drug delivery, further work is being developed in order to optimize controlled drug release.

References

- Agarwal, A., Lvov, Y., Sawant, R., Torchilin, V. Stable nanocolloids of poorly soluble drugs with high drug content prepared using the combination of sonication and layer-by-layer technology. *J Control Release* **128**, 255-260 (2008).
- Al-Qubaisi, M. S., Rasedee, A., Flaifel, M. H., Ahmad, S. H., Hussein-Al-Ali, S., Hussein, M. Z., *et al.* Cytotoxicity of nickel zinc ferrite nanoparticles on cancer cells of epithelial origin. *Int J Nanomedicine* **8**, 2497-2508 (2013).
- Antipov, A. A., Sukhorukov, G. B., Leporatti, S., Radtchenko, I. L., Donath, E., Möhwald, H. Polyelectrolyte multilayer capsule permeability control. *Colloids Surf A Physicochem Eng Asp.* **198**, 535-541 (2002).
- Balabushevich, N. G., Izumrudov, V. A., Larionova, N. I. Protein microparticles with controlled stability prepared via layer-by-layer adsorption of biopolyelectrolytes. *J Polym Sci A* **54**, 540-551 (2012).
- Bantchev, G., Lu, Z., Lvov, Y. Layer-by-layer nanoshell assembly on colloids through simplified washless process. *J Nanosci Nanotechnol* **9**, 396-403 (2009).
- Civan, F. Scale effect on porosity and permeability: Kinetics, model, and correlation. *AIChE J* **47**, 271-287 (2001).
- De Geest, B. G., Sanders, N. N., Sukhorukov, G. B., Demeester, J., De Smedt, S. C. Release mechanisms for polyelectrolyte capsules. *Chem Soc Rev* **36**, 636-649 (2007).
- De Geest, B. G., Sukhorukov, G. B., Möhwald, H. The pros and cons of polyelectrolyte capsules in drug delivery. *Expert Opin Drug Deliv* **6**, 613-624 (2009).
- De Villiers, M. M., Lvov, Y. M. Layer-by-layer self-assembled nanoshells for drug delivery. *Adv Drug Deliv Rev* **63**, 699-700 (2011).
- Diez-Pascual, A. M., Wong, J. E. Effect of layer-by-layer confinement of polypeptides and polysaccharides onto thermoresponsive microgels: a comparative study. *J Colloid Interface Sci* **347**, 79-89 (2010).
- Fernandez-Carballido, A., Herrero-Vanrell, R., Molina-Martinez, I. T., Pastoriza, P. Biodegradable ibuprofen-loaded PLGA microspheres for intraarticular administration. Effect of Labrafil addition on release in vitro. *Int J Pharm* **279**, 33-41 (2004).

- Fu, Y.,Kao, W. J. Drug release kinetics and transport mechanisms of non-degradable and degradable polymeric delivery systems. *Expert Opin Drug Deliv* **7**, 429-444 (2010).
- Gerlier, D.,Thomasset, N. Use of MTT colorimetric assay to measure cell activation. *J Immunol Methods* **94**, 57-63 (1986).
- Goodman, C. M., McCusker, C. D., Yilmaz, T.,Rotello, V. M. Toxicity of gold nanoparticles functionalized with cationic and anionic side chains. *Bioconjug Chem* **15**, 897-900 (2004).
- Hammond, P. T. Polyelectrolyte multilayered nanoparticles: using nanolayers for controlled and targeted systemic release. *Nanomedicine (Lond)* **7**, 619-622 (2012).
- Hiller, S., Leporatti, S., Schnackel, A., Typlt, E.,Donath, E. Protamine assembled in multilayers on colloidal particles can be exchanged and released. *Biomacromolecules* **5**, 1580-1587 (2004).
- Horie, M., Nishio, K., Kato, H., Shinohara, N., Nakamura, A., Fujita, K., *et al.* *In vitro* evaluation of cellular responses induced by stable fullerene C60 medium dispersion. *J Biochem* **148**, 289-298 (2010).
- ISO13321. Methods for determination of particle size distribution part 8: photon correlation spectroscopy, International Organisation for Standardisation (ISO) (1996).
- ISO22412. Particle Size Analysis — Dynamic Light Scattering, International Organisation for Standardisation (ISO) (2008).
- Jachimaska, B., Jasiński, T., Warszyński, P.,Adamczyk, Z. Conformations of poly(allylamine hydrochloride) in electrolyte solutions: Experimental measurements and theoretical modeling. *Colloids Surf A Physicochem Eng Asp* **355**, 7-15 (2010).
- Junghanns, J. U.,Muller, R. H. Nanocrystal technology, drug delivery and clinical applications. *Int J Nanomedicine* **3**, 295-309 (2008).
- Junyaprasert, V. B.,Morakul, B. Nanocrystals for enhancement of oral bioavailability of poorly water-soluble drugs. *Asian J Pharm Sci* **10**, 13-23 (2015).
- Kesisoglou, F., Panmai, S.,Wu, Y. Nanosizing--oral formulation development and biopharmaceutical evaluation. *Adv Drug Deliv Rev* **59**, 631-644 (2007).

- Kharlampieva, E., Kozlovskaya, V. Chapter 6: Cytocompatibility and toxicity of functional coatings engineered at cell surfaces. *Cell surface engineering: fabrication of functional nanoshells*. Fakhruллин R., Choi I., Lvov Y., Cambridge, The Royal Society of Chemistry: 98-125 (2014).
- Lewinski, N., Colvin, V., Drezek, R. Cytotoxicity of nanoparticles. *Small* **4**, 26-49 (2008).
- Losche, M., Schmitt, J., Decher, G., Bouwman, W. G., Kjaer, K. Detailed structure of molecularly thin polyelectrolyte multilayer films on solid substrates as revealed by neutron reflectometry. *Macromolecules* **31**, 8893-8906 (1998).
- Luo, R., Neu, B., Venkatraman, S. S. Surface functionalization of nanoparticles to control cell interactions and drug release. *Small* **8**, 2585-2594 (2012).
- Lvov, Y. M., Pattekari, P., Zhang, X., Torchilin, V. Converting poorly soluble materials into stable aqueous nanocolloids. *Langmuir* **27**, 1212-1217 (2010).
- Masum, A. M., Sharmin, F., Ashraful, I. S. M., Reza, S. Enhancement of solubility and dissolution characteristics of ibuprofen by solid dispersion technique. *Dhaka Univ J Pharm Sci* **11**, 1-6 (2012).
- Nokhodchi, A., Amire, O., Jelvehgari, M. Physico-mechanical and dissolution behaviours of ibuprofen crystals crystallized in the presence of various additives. *Daru* **18**, 74-83 (2010).
- Parekh, G., Pattekari, P., Joshi, C., Shutava, T., DeCoster, M., Levchenko, T., *et al.* Layer-by-layer nanoencapsulation of camptothecin with improved activity. *Int J Pharm* **465**, 218-227 (2014).
- Patil, P., Paradkar, A. Porous polystyrene beads as carriers for self-emulsifying system containing loratadine. *AAPS PharmSciTech* **7**, E199-E205 (2006).
- Pattekari, P., Zheng, Z., Zhang, X., Levchenko, T., Torchilin, V., Lvov, Y. Top-down and bottom-up approaches in production of aqueous nanocolloids of low solubility drug paclitaxel. *Phys Chem Chem Phys* **13**, 9014-9019 (2011).
- Qiu, X., Leporatti, S., Donath, E., Möhwald, H. Studies on the drug release properties of polysaccharide multilayers encapsulated ibuprofen microparticles. *Langmuir* **17**, 5375-5380 (2001).

- Schneider, G., Decher, G. From functional core/shell nanoparticles prepared via Layer-by-Layer deposition to empty nanospheres. *Nano Lett.* **4**, 1833-1839 (2004).
- Shutava, T. G., Balkundi, S. S., Vangala, P., Steffan, J. J., Bigelow, R. L., Cardelli, J. A., *et al.* Layer-by-Layer-coated gelatin nanoparticles as a vehicle for delivery of natural polyphenols. *ACS Nano* **3**, 1877-1885 (2009).
- Shutava, T. G., Pattekari, P. P., Arapov, K. A., Torchilin, V. P., Lvov, Y. M. Architectural layer-by-layer assembly of drug nanocapsules with PEGylated polyelectrolytes. *Soft Matter* **8**, 9418-9427 (2012).
- Strydom, S. J., Otto, D. P., Stieger, N., Aucamp, M. E., Liebenberg, W., de Villiers, M. M. Self-assembled macromolecular nanocoatings to stabilize and control drug release from nanoparticles. *Powder Technol* **256**, 470-476 (2014).
- Szczepanowicz, K., Hoel, H. J., Szyk-Warszynska, L., Bielańska, E., Bouzga, A. M., Gaudernack, G., *et al.* Formation of biocompatible nanocapsules with emulsion core and pegylated shell by polyelectrolyte multilayer adsorption. *Langmuir* **26**, 12592-12597 (2010).
- Teo, W. E., Kaur, S., Ramakrishna, S. Chapter 18: Electrospun polymer nanocomposite fibers: fabrication and physical properties. *Physical properties and applications of polymer nanocomposites*. Tjong, S. C., Mai, Y. W., Cambridge, Woodhead Publishing: 616-637 (2010).
- Torchilin, V. P. Multifunctional nanocarriers. *Adv Drug Deliv Rev* **58**, 1532-1555 (2006).
- Torchilin, V. P. Chapter 5: Multifunctional pharmaceutical nanocarriers: promises and problems. *Nanotechnologies for the life sciences: volume 10*. Kumar, C. S. S. R., Weinheim, Wiley-VCH Verlag GmbH & Co. KGaA: 121-155 (2012).
- Trau, D., Renneberg, R. Encapsulation of glucose oxidase microparticles within a nanoscale layer-by-layer film: immobilization and biosensor applications. *Biosens Bioelectron* **18**, 1491-1499 (2003).
- Tsai, Y. M., Jan, W. C., Chien, C. F., Lee, W. C., Lin, L. C., Tsai, T. H. Optimised nano-formulation on the bioavailability of hydrophobic polyphenol, curcumin, in freely-moving rats. *Food Chem* **127**, 918-925 (2011).
- Veerabadran, N. G., Price, R. R., Lvov, Y. M. Clay nanotubes for encapsulation and sustained release of drugs. *Nano* **02**, 115-120 (2007).

-
- Wang, Y., Hosta-Rigau, L., Lomas, H., Caruso, F. Nanostructured polymer assemblies formed at interfaces: applications from immobilization and encapsulation to stimuli-responsive release. *Phys Chem Chem Phys* **13**, 4782-4801 (2011).
- Wattendorf, U., Kreft, O., Textor, M., Sukhorukov, G. B., Merkle, H. P. Stable stealth function for hollow polyelectrolyte microcapsules through a poly(ethylene glycol) grafted polyelectrolyte adlayer. *Biomacromolecules* **9**, 100-108 (2008).
- Yan, Y., Björnalm, M., Caruso, F. Assembly of layer-by-layer particles and their interactions with biological systems. *Chem Mater* **26**, 452-460 (2014).
- Zhang, L., Gu, F. X., Chan, J. M., Wang, A. Z., Langer, R. S., Farokhzad, O. C. Nanoparticles in medicine: therapeutic applications and developments. *Clin Pharmacol Ther* **83**, 761-769 (2008).
- Zheng, Z., Zhang, X., Carbo, D., Clark, C., Nathan, C., Lvov, Y. Sonication-assisted synthesis of polyelectrolyte-coated curcumin nanoparticles. *Langmuir* **26**, 7679-7681 (2010).

Chapter 3

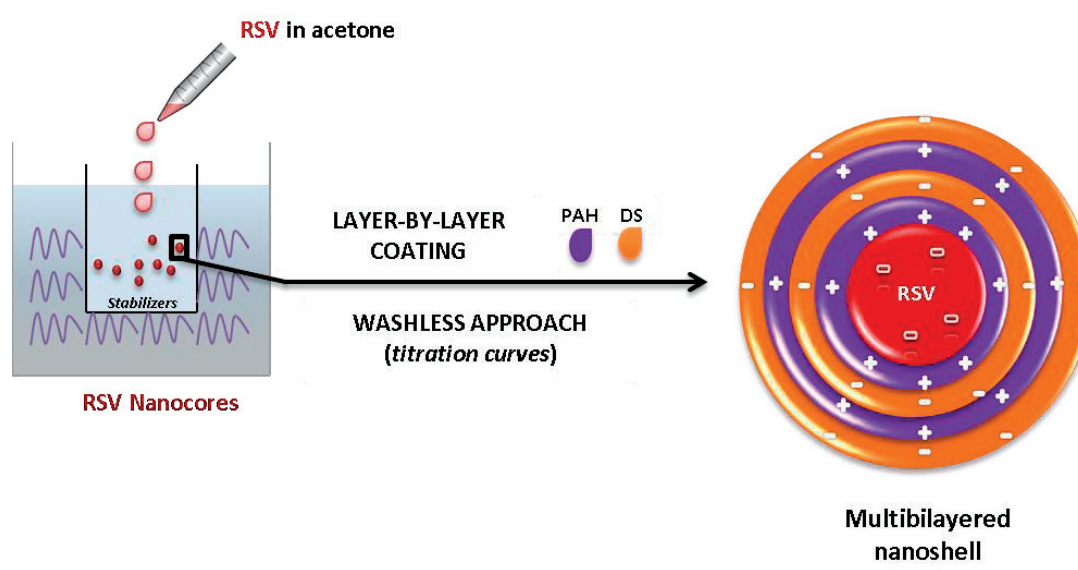
Sonication-assisted Layer-by-Layer self-assembly nanoparticles for resveratrol oral delivery

3.1. Abstract

This paper advances the development of a novel drug nanodelivery solution to the oral administration of resveratrol (RSV), a low soluble drug whose recognized therapeutic applications are circumscribed when administered in the free compound form. Layer-by-Layer (LbL) self-assembly is an emergent nanotechnology proposed to address this concern with means to afford control over key formulation parameters, which are able to ultimately promote an improved pharmacokinetics. LbL self-assembly consists in the sequential adsorption of oppositely charged polyelectrolytes (PEs) upon a low soluble drug nanoparticle (NP) template, giving rise to onion-like multilayered nanoarchitectures. In this work, RSV nanoprecipitation followed by LbL self-assembly of PEs, led by a washless approach, was carried out by using the cationic poly(allylamine hydrochloride) (PAH) and the anionic dextran sulfate (DS) as PEs towards the nanoencapsulation of RSV. Each saturated PE layer deposition involved the rigorous PE concentration assessment which was accomplished by tracing titration curves. This way, aqueous RSV nanocores and RSV LbL nanoformulations with a distinct number of PAH/DS bilayers were developed, including 2.5 (RSV-(PAH/DS)_{2.5} NPs), 5.5 (RSV-(PAH/DS)_{5.5} NPs) and 7.5 (RSV-(PAH/DS)_{7.5} NPs) bilayered nanoformulations. Homogenous particle size distributions at the desired nanoscale interval (ca. 116-220 nm; polydispersity index below 0.15), good colloidal (zeta potential magnitudes ca. \pm 20-30 mV) and chemical stabilizations, high encapsulation efficiency (above 90%) together with an excellent cytocompatibility with Caco-2 cells (cell viability above 90%) were observed for all the nanoformulations. Eventually, LbL NPs promoted a controlled release of RSV pursuant to the number of PE bilayers under simulated gastrointestinal conditions, particularly in the intestine medium, emphasizing their biopharmaceutical advantage. Our findings manifestly pinpoint that LbL PAH/DS NPs constitute a promising nanodelivery system for the oral delivery of RSV, providing a rational strategy to enlarge the implementation range of this interesting polyphenol, which is possibly the most actively investigated phytochemical worldwide.

Keywords: Layer-by-Layer self-assembly; resveratrol; washless; colloid; nanoparticle; controlled release; biocompatibility; oral delivery.

Graphical abstract



LbL NPs promote a controlled RSV release in GI simulated media, being presented as a potential oral nanodelivery system for RSV.

[DS – dextran sulfate; GI – gastrointestinal; LbL – Layer-by-Layer; NP – nanoparticle; PAH – polyallylamine hydrochloride; RSV – resveratrol]

3.2. Introduction

Over recent years, the exponential growth in the economic burden towards developing novel drugs has been calling for the use of natural compounds which are actively sought as potential therapeutic agents. Resveratrol (RSV), 3,5,4'-trihydroxystilbene, a naturally occurring non-flavonoid polyphenol and bioactive phytoalexin produced naturally by several plants when under attack by pathogens, occupies a prominent place in the interest of the research community. RSV is found in red wine, legumes, berries, peanuts, and pistachios and is a possible contributor to the cardiovascular protection conferred by red wine consumption, the so-called French Paradox (Santos, Veiga *et al.* 2011). RSV exists in *cis* and *trans* structural isoforms endowed with distinct activity profiles. The *trans* isomer corresponds to the more biologically active form, which is converted into its *cis* isomer, a less active form, upon light exposure (Charytoniuk, Drygalski *et al.* 2017). The most abundant and consistently used isoform consists in *trans*-RSV, which displays wide recognized beneficial activities, as anti-inflammatory (Gordon, Delgado Diaz *et al.* 2013), antidiabetic and sirtuin activation outcomes (Bonkowski, Sinclair 2016), and cardioprotective (Sung, Byrne *et al.* 2017) effects. RSV exerts, as well, a preventive action on numerous relevant pathologies, such as neurodegenerative processes (Ethemoglu, Seker *et al.* 2017), viral infections, vascular diseases (Sanna, Roggio *et al.* 2012), and several kinds of human cancers (Rauf, Imran *et al.* 2016), being currently a topic of several animal and human studies (Charytoniuk, Drygalski *et al.* 2017).

In spite of promising achievements in preclinical settings, the extensive use of RSV, which belongs to the Biopharmaceutical Classification System (BCS) II class, is hampered by its low favourable physicochemical and pharmacokinetics properties, including a poor water solubility and chemical instability which contributes to a dissolution-limited absorption (Amri, Chaumeil *et al.* 2012). In parallel with this concern, RSV is subject of a large phase II metabolization in the gastrointestinal (GI) tract, which together with the aforementioned factors, contribute to an inefficient systemic delivery, culminating in a reduced low bioavailability *in vivo*, thus hindering its immense therapeutic potential (Santos, Veiga *et al.* 2011). Against this backdrop, the development of new technologies capable of improving the delivery of RSV is imposed, of which nanotechnology, by the development of nanoparticles (NPs), constitutes a powerful and well-based encapsulation strategy with ascribed merits of stabilization, protection, interaction with the environment, efficient and controlled delivery, as well as the improvement of bioavailability and intracellular uptake of RSV (Sanna, Siddiqui *et al.* 2013, Singh, Pai 2014a).

Plenty of work has been performed with respect to the development of RSV-loaded nanodelivery systems, including solid lipid nanoparticles (SLNs) (Ramalingam, Ko 2016, Yadav, Sunkaria *et al.* 2017), liposomes (Joraholmen, Skalko-Basnet *et al.* 2015, Ethemoglu, Seker *et al.* 2017) and cyclodextrins (CDs) inclusion (Mantegna, Binello *et al.* 2012, Venuti, Cannava *et al.* 2014). Notwithstanding, a vast array of problems arises from the use of such vehicles, including, e.g., the poor stability of liposomes and the demand for complex equipment regarding the fabrication of SLNs (Summerlin, Soo *et al.* 2015). This way, multifunctional nanoscale technologies have gained increasing interest facing their inherent granted versatility and their capacities to change modern healthcare by supplying superior control over the release of drugs (Correa, Choi *et al.* 2016).

Layer-by-Layer (LbL) self-assembly constitutes a promising drug delivery platform which consists in the sequential fashion deposition of stabilizing polyelectrolyte (PE) coatings upon oppositely charged substrates, driven particularly by electrostatic interactions (Polomska, Gauthier *et al.* 2017). These substrates comprised microsized sacrificial templates in several works (De Villiers, Otto *et al.* 2011), however, currently, formulation improvements have been made towards the use of drug NPs (described herein as drug nanocores) as the template to directly perform the LbL assembly at nanoscale dimension, avoiding the use of sacrificial templates (Shutava, Pattekari *et al.* 2012, Parekh, Pattekari *et al.* 2014, Santos, Pattekari *et al.* 2015). This way, by using this recent nanotechnology, modular nanocapsule-type constructs (shells) are obtained in solution with nanometer scale precision, chiefly consisting of a drug NP coated with a multilayered PE shell made of a set number of PE pairs or bilayers (De Villiers, Otto *et al.* 2011). In essence, each bilayer is the result of the combination of a polycation layer with a polyanion layer, consisting of the fundamental building block of a multilayer film structure (Santos, Pattekari *et al.* 2015).

Distinct PEs may be incorporated into the LbL shell, comprising synthetic PEs as poly(allylamine hydrochloride) (PAH) (Pattekari, Zheng *et al.* 2011, Santos, Pattekari *et al.* 2015, Polomska, Gauthier *et al.* 2017), poly(diallyldimethylammonium chloride) (PDDA) (Lvov, Pattekari *et al.* 2011), poly(styrene sulfonate) (PSS) (Pattekari, Zheng *et al.* 2011, Santos, Pattekari *et al.* 2015, Polomska, Gauthier *et al.* 2017), poly(L-arginine) (PLA) (Deng, Morton *et al.* 2013, Gu, Deng *et al.* 2017, Polomska, Gauthier *et al.* 2017) or natural PEs just like chitosan (Pattekari, Zheng *et al.* 2011), alginate (Lvov, Pattekari *et al.* 2011, Pattekari, Zheng *et al.* 2011, Morton, Poon *et al.* 2013), poly-L-lysine, (PLL) (Shutava, Pattekari *et al.* 2012, Morton, Poon *et al.* 2013, Parekh, Pattekari *et al.* 2014, Correa, Choi *et al.* 2016), bovine serum albumin (BSA) (Pattekari, Zheng *et al.* 2011, Shutava, Pattekari *et al.* 2012, Parekh, Pattekari *et al.* 2014), poly(ethylenimine) (PEI)

(Shutava, Pattekari *et al.* 2012, Parekh, Pattekari *et al.* 2014), heparin (Parekh, Pattekari *et al.* 2014, Correa, Choi *et al.* 2016) and protamine sulfate (PS) (Lvov, Pattekari *et al.* 2011, Pattekari, Zheng *et al.* 2011). Owing to such hierarchical assembly, LbL self-assembly NPs exhibit a multifunctional structure gifted with a strong versatility, bestowing various desirable traits, as a high degree of particle size control, high drug encapsulation efficiency, increased *in vivo* colloidal stability, improved biocompatibility, reduced off-target toxicity and the possibility of surfaces tuning (Gu, Deng *et al.* 2017, Polomska, Gauthier *et al.* 2017). Importantly, the thickness design of the LbL shell architecture promotes additionally the controlled release of low soluble drugs, as ibuprofen (IBF) (Santos, Pattekari *et al.* 2015), curcumin (Lvov, Pattekari *et al.* 2011), paclitaxel (Agarwal, Lvov *et al.* 2008, Lvov, Pattekari *et al.* 2011, Polomska, Gauthier *et al.* 2017) and tamoxifen (Agarwal, Lvov *et al.* 2008, Lvov, Pattekari *et al.* 2011), representing a prominent platform towards the improvement of the *in vivo* bioavailability of these problematic drugs, as RSV. LbL self-assembly is effectively more appealing than additional methods as spin-coating, solution casting and thermal deposition in view of the precise control over the multilayer thickness and the surface charge (Nayef, Castiello *et al.* 2017). Furthermore, the versatility of coating upon nearly any surface or shape and its simplicity, which does not demands for sophisticated equipment, is viewed as an enforceable technology for large-scale fabrication (De Villiers, Otto *et al.* 2011).

The conventional approach for obtaining LbL NPs implies the incubation of NPs with PE amounts in excess to ensure maximum PE coverages, requiring the prosecution of several intermediate washing steps to remove these PE excesses between sequential layers deposition, which consist usually in the application of centrifugation and filtration processes (Santos, Pattekari *et al.* 2015). These repetitive washings, besides being time intensive, conduct usually to aggregation phenomena, which assumes a stronger problematic expression when transitioning from micro- to NPs formulations, facing the need of higher forces application for NPs isolation, strongly limiting the yield, efficiency, scale-up and the potential for clinical translation (Correa, Choi *et al.* 2016). Research has, thus, leaned towards to newly LbL shell characterizations eliminating the need for intermediate washing or purification steps by using a washless approach (Bantchev, Lu *et al.* 2009). This approach consists in the performance of the deposition of PE coating layers in equilibrium, by the assessment of only the necessary PE amount for each layer of the multilayered shell, by the use of detailed PE titration curves and, thus, simplifying the LbL fabrication process (Santos, Pattekari *et al.* 2015, Nayef, Castiello *et al.* 2017).

In the current work, a novel nano-scaled drug delivery system was developed using the nanoprecipitation of the core template RSV nanocores coupled to the LbL self-assembly of PEs, as the key nanotechnology, and by a washless approach, to obtain RSV-loaded LbL NPs. The multilayered shell of NPs was thoroughly designed and developed using PAH and dextran sulfate (DS) PEs, being proposed to protect RSV under gastric conditions and to allow for a controlled RSV release under intestinal conditions in order to improve its oral bioavailability. Herein, RSV nanocores, without adsorbed LbL coatings, and three distinct RSV-loaded PAH/DS LbL nanoformulations, specifically with 2.5, 5.5 and 7.5 bilayered LbL shells were considered to explore and modulate the properties of the polymeric LbL shell. To our knowledge, no studies exist within the literature reporting the encapsulation of RSV into LbL nanocapsules with this constitution. The developed RSV-loaded LbL PAH/DS NPs were characterized according to their surface charge (zeta potential), particle size, polydispersity index (PDI), morphology, stability under conditions of storage, encapsulation efficiency, *in vitro* release studies and cytotoxicity studies.

3.3. Materials and methods

3.3.1. Materials

PAH (MW ca. 15 kDa), DS dextran sulfate sodium salt from *Leuconostoc* species (MW ca. 5 kDa), fluorescein isothiocyanate (FITC), *ortho*-phosphoric acid, gel chromatography Sephadex PD10 columns (Amersham Biosciences, Wikströms, Sweden), 3-(4,5-dimethylthiazol-2-yl)-2,5-diphenyltetrazolium bromide (MTT) reagent, dulbecco's modified eagle medium (DMEM), fetal bovine serum (FBS), PenStrep and trypsin were purchased from Sigma-Aldrich (Steinheim, Germany).

RSV was acquired from Abatra Technology Co., Ltd. - Xi'an, China. Polyvinylpyrrolidone (PVP 17 PF, 7-11 kDa) were kindly supplied from BASF - The Chemical Company (Ludwigshafen, Germany) and sodium lauryl ether sulfate (Texapon® NSO, SLE₂S, 28% (w/w); Cognis) was provided by the Department of Chemistry of the University of Coimbra. Methanol of HPLC grade was supplied by Chem-Lab NV (Zedelgem, Belgium). Extra pure acetone and hydrochloric acid (HCl) 37% were obtained from Sharlau (Barcelona, Spain). Ultra-pure water (18.2 MΩ·cm at 25 °C) used was obtained from a Milli-Q ultra-pure water system from Millipore (Milford, MA, USA). All other reagents were of analytical grade and were used as received.

3.3.2. Methods

3.3.2.1. Nanoparticles preparation

RSV powder was dissolved in extra pure acetone at 20 mg/mL. A 60 µL volume of the previously referred prepared solution was added to an aqueous solution containing 1 mg/mL PVP 17 PF and 0.005 mg/mL SLE₂S at pH 3.5. This procedure was performed under sonication by using an ultrasound bath sonicator (Bandelin Sonorex Super; Bandelin, Berlin, Germany), conducting to the formation of NPs of RSV (RSV nanocores). In order to obtain LbL-coated NPs, reduced aliquots of cationic PAH and anionic DS 1-4 mg/mL were sequentially added to RSV nanosuspensions, always kept under sonication, until the deposition of 7.5 bilayers, at maximum, during a time-period of 20-50 min. The necessary amount of PE to cover and, thus, recharge the surface of NPs was investigated for each nanolayer assembly by performing PE titrations according to our previous work (Santos, Pattekari *et al.* 2015). The LbL assembly was, thereby, performed through the alternately addition of PAH and DS, obtaining three distinct LbL nanoformulations comprising 2.5, 5.5 and 7.5 bilayers of PAH/DS nanoshell.

3.3.2.2. Zeta potential analysis

Zeta potential measurements were assessed by electrophoretic light scattering (ELS) using a Nano Zeta Potential Analyser (DelsaNano C Submicron, Beckman Coulter Delsa™, Krefeld, Germany). Each sample was properly diluted using Milli-Q water pH 3.5 as diluent. Measurements were performed in a Flow Cell (Beckman Coulter Delsa™) at 25 °C. The zeta potential was extracted from the Helmholtz–Smoluchowski equation. Those values are listed as means of triplicate runs per sample. The apparatus was routinely verified and calibrated by the use of a mobility standard (Beckman Coulter, Inc.).

3.3.2.3. Particle size analysis

The mean particle size, polydispersity index (PDI) and the size distribution of aqueous NPs suspensions were assessed by dynamic light scattering (DLS) using the particle size analyser DelsaNano C Submicron, Beckman Coulter Delsa™ (Krefeld, Germany). Results were acquired for 5 min in triplicate at 25 °C using an angle measurement of 60°, after an equilibration period of 3 min. For each run, NPs suspensions were previously diluted with Milli-Q water to proper concentration to avoid multiple scattering. Results are introduced as mean ± standard deviation (SD), obtained from the Cumulants algorithm (ISO13321 1996, ISO22412 2008). The instrument was verified and calibrated using standard latex NPs (Beckman Coulter, Inc.).

3.3.2.4. Microscopic analysis

Morphological examination of NPs was carried out using transmission electron microscopy (TEM). Diluted samples of NPs (5 µL) were placed onto formvar/carbon-coated grids for 30 s to origin a thin film. Before drying, those were counterstained with 1% phosphotungstic acid for 5 min. The excess solution was removed with filter paper and grids were allowed to dry at room temperature. Samples were afterwards observed under FEI-Tecnaï G2 Spirit Bio Twin apparatus at 100 kV.

Towards the same objective, the shape and surface morphology of NPs was additionally investigated by using Jeol SM-6010LV/3010LA scanning electron microscopy operating at a voltage set at 15 kV. To conduct scanning electron microscopy (SEM) analysis, a 5 µL-drop of diluted NPs nanosuspension was placed onto a metal plate and kept overnight at room temperature inside a desiccator.

The deposition of the polycation layers during the LbL process was controlled and confirmed by using FITC-labelled PAH in the production of NPs. PAH was tagged with FITC using a technique

described elsewhere (Hiller, Leporatti *et al.* 2004). To do so, FITC was covalently bound to PAH by the slowly addition of FITC, previously dissolved in dimethyl sulfoxide (DMSO), to the PAH buffered solution in excess, using a proportion of 0.05:1 (v/v). Unspent FITC in the coupling reaction was extracted by gel chromatography through Sephadex PD10 columns (Sephadex™ G-25 M, Amersham Bioscience, UK). Purified FITC-labelled PAH was stored at 4 °C and in the dark until further use. Labelled NPs were monitored using a Laser Scanning Confocal Microscope, Zeiss LSM 510 Meta (Carl Zeiss Inc., Göttingen, Germany), equipped with a 63x oil immersion objective Plan-ApoChromat with numerical aperture of 1.4.

3.3.2.5. Encapsulation efficiency

To determine the encapsulation efficiency, 0.5 mL of NPs were added into a Centrifugal Concentrator Vivaspin® 2 (molecular weight cut off (MWCO)): 3 kDa, polyethersulfone membrane) reservoir for centrifuging at 4000 g for 20 min. The encapsulation efficiency was determined indirectly, after filtrate analysis by high-performance liquid chromatography - diode array detection (HPLC-DAD). The amount of RSV loaded in the NPs (actual amount) was determined by subtracting the free RSV amount from the theoretical RSV amount. In order to confirm the encapsulation efficiency values obtained by the previous indirect quantification, the direct quantification of RSV was performed by directly using the concentrate sample, in which the NPs remain after centrifugation. In this case, NPs concentrate samples were extracted using the HPLC mobile phase 1:20 (v/v), followed by vortex agitation during 1 min, sonication for 5 min and finally centrifugation (13,400 rpm/10 min). The encapsulation efficiency of RSV was defined as the following equation (Equation 3.1):

$$\text{Encapsulation Efficiency (\%)} = \frac{\text{Actual amount of RSV loaded in NPs}}{\text{Theoretical amount of RSV loaded in NPs}} \times 100$$

RSV assay by HPLC-DAD was conducted by using a reversed-phase LiChrospher® 100 C₁₈ column (5 µm particle size, 125 mm length and 3 mm internal diameter), fitted with a pre-column, acquired from MZ-Analysentechnik GmbH (Mainz, Germany). The analysis was performed by a Shimadzu apparatus (Kyoto, Japan) equipped with a LC-20AD quaternary pump, a DGU-20A5 degasser unit, a SIL-20 AHT auto-sampler unit, a CTO-10AS oven and an UV/VIS photodiode array detector (SPD-M20A). Data acquisition and instrumentation control were performed by Shimadzu LC-solution version 1.25 software. The mobile phase mixture consisted of water at pH 2.5, adjusted with *ortho*-phosphoric acid (A) and methanol (B). The chromatographic separation was carried out by a two-stage linear gradient: from 70% to 37% A in 10 min, and 3 min to achieve 70% A in order to restore the initial conditions. The run time was 13 min, with a flow

rate of 1.0 mL/min, an injection volume of 20 μ L and a temperature of 25 $^{\circ}$ C. Chromatographic separations were monitored at 306 nm.

3.3.2.6. Stability studies

NPs formulations stability was evaluated by particle size and zeta potential measurements at predetermined time points over a total of 30 days period. All measurements were carried out in triplicate (n = 3) at room temperature (25 $^{\circ}$ C).

3.3.2.7. In phase solubility and *in vitro* release assays

In order to fulfil *sink* conditions during *in vitro* release studies, the saturation solubility of RSV in each of the following used media was assessed. In order to conduct such assessment, excess RSV powder was added separately to 6 mL of simulated gastric (SGF, pH 1.2) and intestinal (SIF, pH 6.8) fluids without enzymes, in accordance with United States Pharmacopeia (USPXXIV), and those were maintained under agitation for 24 h (37 $^{\circ}$ C/100 rpm). Experiments were conducted in the dark and flasks were covered with aluminium foil to minimise photochemical degradation. 0.5 mL aliquots were collected after 12 h and 24 h, and were immediately centrifuged (13,400 rpm/10 min). The supernatant was filtered through a 0.45 μ m syringe filter (GHP Acrodisc, Pall Gelman Laboratory) and the obtained filtered samples, after proper dilution in each corresponding medium, were quantified by HPLC-DAD, using the chromatographic conditions exposed above. All syringes, pipettes, filters and vials were preheated to 37 $^{\circ}$ C in an oven. Solubility experiments were conducted in triplicate (n = 3).

In vitro release kinetics of RSV from NPs was carried out in the aforementioned media, simulated gastric (pH 1.2) and intestinal (pH 6.8) fluids without enzymes. 1 mL of RSV native crystals suspension, RSV nanocores and each of considered LbL RSV nanoformulations were transferred into dialysis membrane devices (Spectra/Por Float-A-Lyzer[®] G2, 3.5 kDa MWCO), which were vertically suspended in enzyme-free release media, specifically in 8 mL of SGF for 2 h followed by the transition to SIF up to the time point 24 h, maintaining the temperature at 37 $^{\circ}$ C and 200 rpm stirring during the whole experiment. At the allotted time points, incubation medium samples were collected, which was immediately replaced with the same volume of fresh incubation medium. The amount of released RSV was quantified by HPLC-DAD using the aforementioned conditions. Those studies were performed in triplicate (n = 3).

3.3.2.8. *In vitro* cytotoxicity assay

Cytotoxicity of developed nanoformulations was performed in Caco-2 cells (human intestinal epithelial cells), which were purchased from European Collection of Authenticated Cell Cultures (ECACC), through the MTT assay (Mosmann 1983). This cell line was cultured in DMEM (high glucose) supplemented with penicillin 100 U/mL, streptomycin 100 µg/mL and 10% (v/v) inactivated FBS, at 37 °C in a humidified atmosphere of 95% air and 5% CO₂. Briefly, human intestinal epithelial cells were cultured in a density of 0.1x10⁶ cells/well in 96-well microplates with a final volume of 200 µL. After 24 hours, prior to the addition of the samples, the medium was completely removed and 100 µL of fresh complete medium was added. Serial dilutions of the samples were prepared in incomplete DMEM's (serum free) to a final concentration in the wells ranging between 11.7 µg/mL and 1500 µg/mL. 100 µL of each sample was added and incubated with the cells for 24 h, at 37 °C and 5% CO₂. After 24h, 20 µL of a MTT solution (5 mg/mL in PBS) was added per well and cells were further incubated during 3 hours at 37 °C in a humidified atmosphere of 95% air and 5% CO₂. After this time-period of incubation with MTT, the supernatants were discarded and 100 µL of DMSO was added to each well. Quantification of formazan crystals was performed using an ELISA microplate reader at 570 nm with a reference wavelength of 620 nm. Three independent experiments were performed with the formulations. The results were expressed as percentage of MTT reduction relatively to control (cells in culture without the samples to test).

3.3.3. Statistical analysis

Statistical analysis was conducted using SPSS Statistics version 20.0; for curve fitting, Origin Pro Software was used. Data concerning PE concentration *versus* zeta potential were fitted to one of two models, specifically an exponential response curve (Equation 3.2):

$$y = y_0 + A_1 \cdot e^{\frac{x}{t_1}},$$

where y_0 represents the plateau for higher PE concentrations, $y_0 + A_1$ represents baseline zeta potential (no PE added) and t_1 is a kinetic parameter. Other model used to fit the data was a sigmoidal response curve (Boltzmann model) (Equation 3.3):

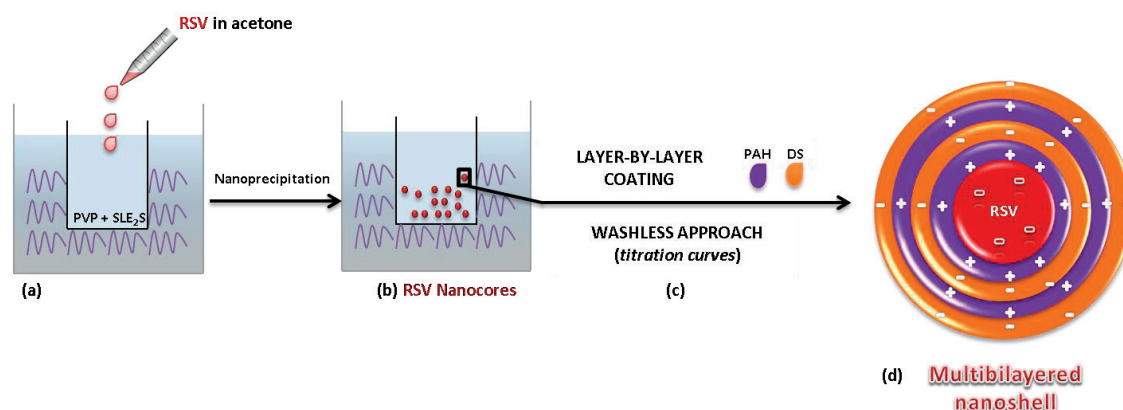
$$y = A_2 + \frac{A_1 - A_2}{1 + e^{\frac{x - x_0}{dx}}},$$

where A_1 and A_2 represent the upper and lower asymptotes, respectively. In order to investigate the stability studies, particle size and zeta potential were analyzed across time, and a

Friedman's non-parametric test for paired samples was used. Zeta potential and particle size were compared between NPs with different number of coating bilayers by using Kruskal-Wallis' non-parametric test, with pairwise comparisons using Bonferroni correction. For *in vitro* release profiles at pH 6.8, data was fitted to the aforementioned exponential model. Cell viability results were analyzed using two-way ANOVA, with a Dunnett's multiple comparisons test by using GraphPad Prism, version 6.00 (GraphPad Software, San Diego, CA, USA). A significance of 0.05 was considered for all comparisons.

3.4. Results and discussion

The schematic for obtaining NPs using electrostatic LbL self-assembly is depicted in **Figure 3.1**. The obtainment of well-dispersed RSV nanocores constituted the first and the key stage in the production of LbL-coated RSV nanosuspensions (**Figure 3.1a-b**). Those were obtained herein by nanoprecipitation (**Figure 3.1b**), a bottom-up approach, which was carried out by the addition of a concentrated RSV solution in acetone to an aqueous solution of surfactants (PVP 17 PF and SLE₂S) (**Figure 3.1a**). Afterwards, in the second main stage, those RSV nanocores provided a template for the LbL PE shell attachment, as a result of the application of the LbL self-assembly technology (**Figure 3.1c**). This technology relied upon the sequential addition of oppositely charged PEs, which accounted for colloidal stability. Necessary PE concentrations for each PE coating layer were accurately assessed by the use of titration curves, as exhibited in **Figure 3.2**. The use of the essential concentrations solely for each layer accomplishment avoided the use of PEs in excess, thus avoiding PE washing stages between the addition of subsequent layers. This procedure is called washless approach and constitutes a recent and valuable development over the traditional LbL assembly technique (Santos, Pattekari *et al.* 2015). The whole process was carried out under sonication, preventing NPs from aggregation phenomena. Thereby, a bottom-up approach using a washless LbL technique conducted successfully to the production of PAH/DS-based multilayered NPs encapsulating RSV (**Figure 3.1d**). Such a technique gave origin to potential oral RSV delivery systems and it is thoroughly described and characterized in the following sections.



WASHLESS BOTTOM-UP LAYER-BY-LAYER POLYELECTROLYTE ASSEMBLY

Figure 3.1: Schematic presentation of RSV-loaded LbL NPs preparation using a washless bottom-up LbL PE assembly.

RSV native microcrystals are firstly dissolved in acetone, being added next to an aqueous solution of PVP and SLE₂S under ultrasonication (a) which leads to the formation of RSV nanocores (b). Afterwards, the adsorption polycation/polyanion bilayer cycles by a LbL fashion coupled to a washless approach (c) origins a tuned multilayered LbL nanoshell (d).

[DS – dextran sulfate; LbL – Layer-by-Layer; NP – nanoparticle; PAH – polyallylamine hydrochloride; PE – polyelectrolyte; PVP – polyvinylpyrrolidone; RSV – resveratrol; SLE₂S – sodium lauryl ether sulfate]

3.4.1. Layer-by-Layer resveratrol nanoparticles preparation

3.4.1.1. Polyelectrolyte titrations – washless approach

RSV nanocores were obtained by nanoprecipitation with 115.7 ± 6.1 nm of particle size, 0.124 of PDI and a surface charge of -21.6 ± 0.4 mV, as depicted in **Table 3.1**.

Table 3.1: The particle size, polydispersity index, zeta potential and encapsulation efficiency of the studied nanoformulations: RSV nanocores and LbL NPs. Data represent mean \pm SD, n = 3.

| Formulation | Particle Size (nm) | Polydispersity Index (PDI) | Zeta Potential (mV) | Encapsulation Efficiency (%) |
|---------------------------------|--------------------|----------------------------|---------------------|------------------------------|
| RSV nanocores | 115.7 ± 6.1 | 0.124 | -21.6 ± 0.4 | 91.6 ± 1.6 |
| RSV-(PAH/DS) _{2.5} NPs | 177.7 ± 7.2 | 0.128 | $+28.5 \pm 0.2$ | 92.0 ± 1.2 |
| RSV-(PAH/DS) _{5.5} NPs | 215.3 ± 2.3 | 0.122 | $+29.5 \pm 0.4$ | 91.7 ± 2.7 |
| RSV-(PAH/DS) _{7.5} NPs | 218.7 ± 2.9 | 0.148 | $+29.0 \pm 1.5$ | 92.2 ± 1.7 |

[DS – dextran sulfate; LbL – Layer-by-Layer; NP – nanoparticle; PAH – polyallylamine hydrochloride; PDI – polydispersity index; RSV – resveratrol; SD – standard deviation]

The addition of the RSV concentrated solvent solution to the anti-solvent aqueous solution containing surfactants triggered a visual change of the batches from clear to an opalescent physical aspect, according to the occurrence of light scattering by dispersed NPs, the so-called

Tyndall effect. Such effect supported the obtainment of low-sized nanostructures. In this process, the adsorption of surfactants played the key role of crystal growth prevention, promoting the stabilization of the structures in suspension, and thereby ensuring their nanosize dimensions (Pattekari, Zheng *et al.* 2011, Parekh, Pattekari *et al.* 2014). The use of a combination of non-ionic surfactant with an ionic surfactant comprehended, respectively, the polymeric PVP, which prevented the crystallization of the low water-soluble RSV, imparting steric stabilization; and the anionic SLE₂S, that was responsible for the negative surface charge provision (Itoh, Pongpeerapat *et al.* 2003), offering electrostatic stabilization. This way, given that the LbL assembly process is driven essentially by electrostatic interactions, the intrinsic magnitude charge presented on the surface of RSV nanocores provided, thus, means for assembly the LbL PE shell using these drug-based structures as the anchoring nano-platform. **Figure 3.2a** pertains to the titration of the surface of RSV nanocores by the first added PE towards to the obtainment of the first coating layer. The first point of **Figure 3.2a** corresponds to RSV nanocores in the complete absence of PEs (PAH and DS), whose negative charge dictated that the charge of the first PE to be added. Owing to such, the polycation PAH was the first used PE (**Figure 3.2a**), followed by the polyanion DS (**Figure 3.2b**), and so forth. This way, the adsorption of the oppositely charged PE was repeated cyclically during the whole LbL assembly process until the deposition of the desired number layers.

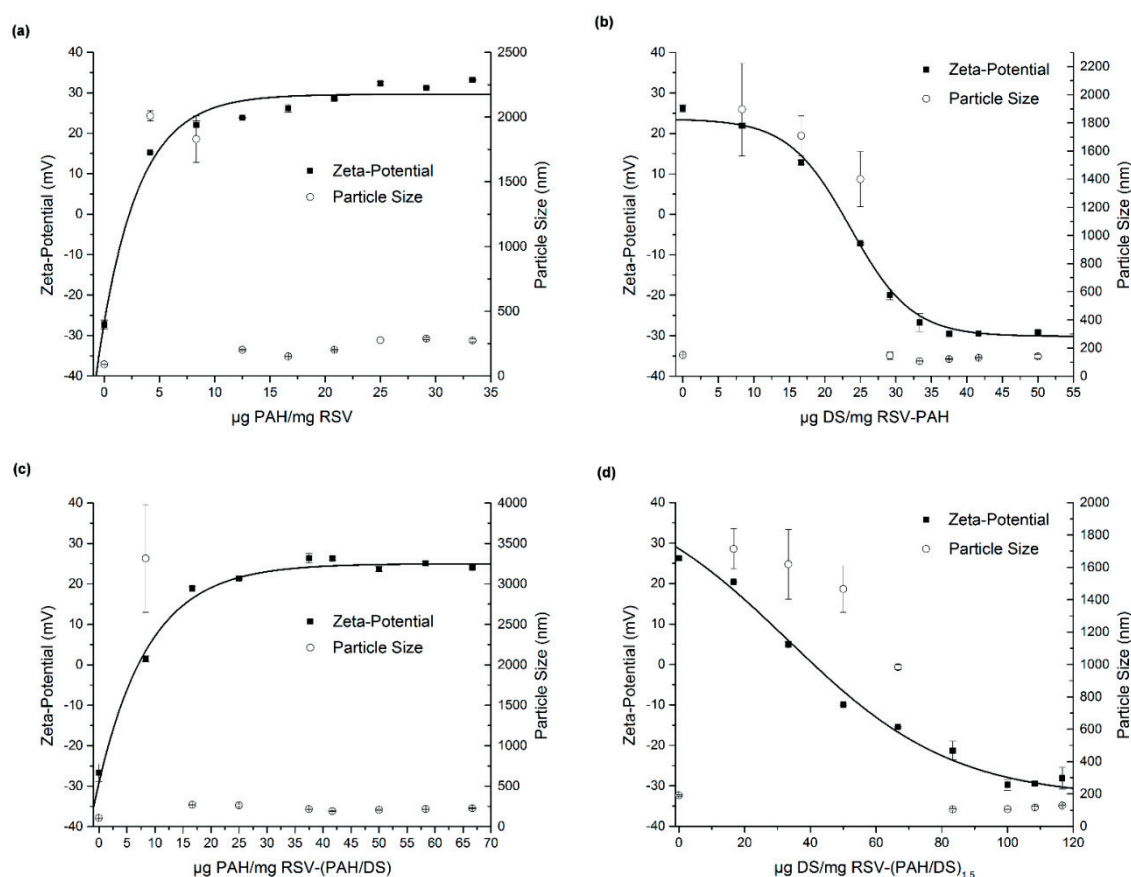


Figure 3.2: Zeta potential and particle size measurements against the PE concentration for 0.5 mg/mL RSV nanocores during PE titration procedures. Four sequential titrations referring to a polycation or a polyanion deposition are depicted in the stepwise addition of: **(a)** PAH to RSV nanocores, **(b)** DS to RSV-PAH NPs, **(c)** PAH to RSV-(PAH/DS) NPs, and **(d)** DS to RSV-(PAH/DS)_{1.5} NPs.

[DS – dextran sulfate; LbL – Layer-by-Layer; PAH – polyallylamine hydrochloride; PE – polyelectrolyte; RSV – resveratrol; NP – nanoparticle]

Attempts to use exclusively biopolymers as PEs were carried out due their biologically pertinent functionalities (Morton, Poon *et al.* 2013). Moreover, the use of low molecular weight PEs (inferior to 65 kDa) was imposed in parallel for the operation of LbL nanoassembly, since nano-scaled nanocores are characterized by a limited space for PE chain adsorption in comparison with microparticles (Shutava, Pattekari *et al.* 2012). Towards this aim, the use of the chitosan polycation with the DS polyanion, both with low molecular weights, was firstly screened. However, NPs endowed with this composition evidenced colloidal instability after the adsorption of 2.5 bilayers, by the prompt formation of irreversible aggregates (particle size higher than 1000 nm), excluding their utility. In fact, this initial investigation regarding the selection of the PE pair is of paramount importance after the deposition of a minimum of 2-3 bilayers towards the formation of robust LbL architectures with desired features, capable of maintaining the colloidal stability upon the assembly of further PE bilayers if required (Morton, Poon *et al.* 2013, Polomska, Gauthier *et al.* 2017). Facing the referred constraint, PAH was examined as the

polycation during the LbL process, as it was able to promote a linear growth of the LbL shell in our previous work (Santos, Pattekari *et al.* 2015), while maintaining DS as the polyanion. These investigations revealed that the use of PAH polycation and DS polyanion exhibited a good performance in the obtainment of LbL-coated NPs of RSV, as it is thoroughly exposed below, constituting the selected PE pair or bilayer.

Each PE layer of the LbL shell was quantitatively introduced, according to the determination of the sufficient inherent PE concentration to saturate the surface. Those assessments were accomplished by tracing PE titration curves (**Figure 3.2**), in which a range of PE concentrations, resulting from a stepwise PE addition to the system, was carefully examined for each PE layer deposition by the simultaneous control of zeta potential and particle size values. The complete PE adsorption was indicated by the recharging point of each titration curve, which corresponded, in practice, to the initiating point of the plateau of the curve. Such point is recognized as the adsorption saturation point, in which the adsorbed PE amount stands constant, as the result of the surface charge saturation (Sadeghpour, Seyrek *et al.* 2011). This observation constituted the prerequisite to advance to the next PE layer addition. This way, it is possible observe in **Figure 3.2a**, the titration of RSV nanocores with polycation PAH, that the plateau starts at 16.7 μg PAH/ mg RSV. Initial negative surface charge of RSV nanocores has been converted to positive after the PAH coating layer deposition upon RSV nanocores. The strongly positive obtained charge conferred colloidal stability, avoiding aggregation, which had been fundamental to proceed the LbL shell construction by the consecutive deposition of additional coating PE layers. **Figure 3.2b** relates to the second titration curve, in which DS was added to RSV-PAH NPs. The resulting plateau value corresponded to 33.3 μg DS/ mg RSV, assisting to a charge reversal from positive to a negative value. Concerning to the third titration, **Figure 3.2c**, in which PAH was added to RSV-PAH/DS NPs, the plateau has started at 41.7 μg PAH/ mg RSV. In the fourth titration, **Figure 3.2d**, the determined PE quantity corresponded to 100.0 μg DS/ mg RSV, arising from the addition of DS to RSV-(PAH/DS)_{1.5} NPs. Furthermore, beyond the careful analysis of zeta potential, all titration profiles were also coupled with particle size control, being their correlation of worth noting. We are able to verify that the attainment of the plateau of the titration curves has been accompanied by a stabilization of the particle size values into the nanoscale, emphasizing the key role of the proper PE covering of the surface on the obtainment of sufficient colloidal stability.

In point of fact, for each PE titration procedure, initially, the addition of a small amount of a PE to the oppositely charged NPs suspension leads to the adsorption of the PE upon the NPs

surface. This event initiates the neutralization of the surface charges, consequently reducing the stability of the nanosuspension. With continuous PE addition, the nanosuspension becomes firstly unstable, followed by the reversal of the surface charge at the isoelectric point and, in the last stage of the titration procedure, we assist to the suspension restabilization. Prompt aggregation occurs near the isoelectric point, where the zeta potential and, thus, the repulsion between particles are neutralized. This occurrence triggers the establishment of attractive van der Waals forces, which are responsible for a parallel steep peak in the particle size values (**Figure 3.2**). Accordingly, the recorded PDI values were also shown to be the highest at the isoelectric point due to the formation of heterogeneous sized clusters arisen from the aggregation phenomena. However, from the isoelectric point onwards, the restabilization of the nanosuspension occurs as a consequence of the repulsive forces established between the electrical bilayers upon the addition of more PE to the system (Sadeghpour, Seyrek *et al.* 2011), which is in accordance with an overcharging process (Nayef, Castiello *et al.* 2017). During this event, an arrangement of the PEs occurs upon the surface of the NP, enabling its neutral charge to paradoxically attract more oppositely charged PE up to the adsorption saturation point, in which no more PE is adsorbed to the surface, remaining in solution. This corresponds graphically to the attainment of the onset point of the titration, in which NPs acquire anew sufficient surface charge to repulse each other and maintain their colloidal stability, depicted by the stabilization of particle size along with zeta potential values (**Figure 3.2**). In addition, it is known that if more PE is after all added to the system, far beyond the PE plateau concentration, irreversible coagulation of PEs and NPs ends up to take place again (Nayef, Castiello *et al.* 2017). A schematic titration curve depicting the aforementioned characteristic distinct stages is advertised in **Figure 3.3**, in this case beyond the positively charged PE addition upon a negatively charge colloidal surface.

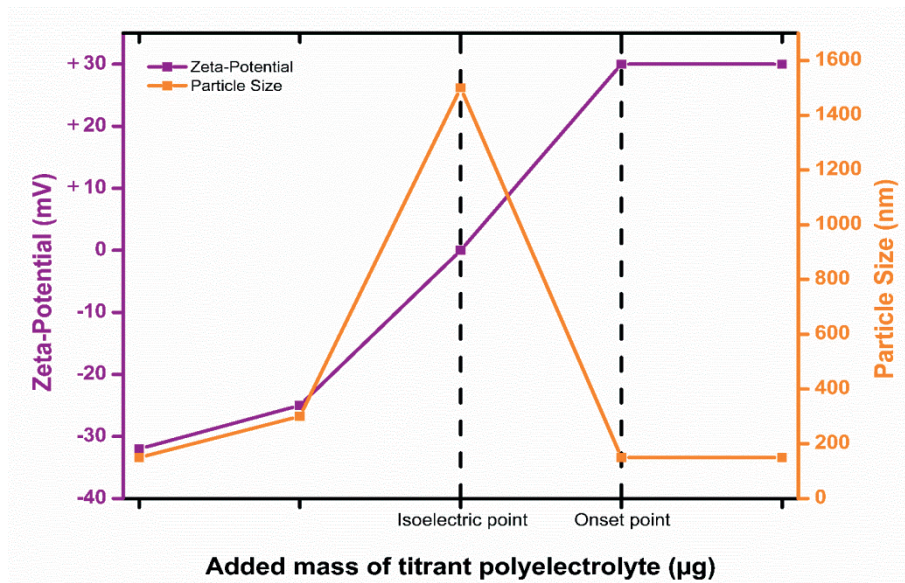


Figure 3.3: Diagram representing the distinct stages of a typical PE titration procedure, arising from the addition of a positively charged PE upon a negatively charged colloidal surface, emphasizing the isoelectric point and the onset point of the titration.

All the depicted stages and labelled points evidence the hypothetical oscillation of zeta potential (purple) and particle size (orange) values in the course of the PE titration procedure.

[PE – polyelectrolyte]

The examination of the titration curves profiles pinpoints additionally the existence of differences regarding the use of PAH and DS. As a matter of fact, with respect to PAH adsorption, an increasing impact on the zeta potential together with a more gradual plateau onset was found, which is in accordance with an exponential fitting model ($r^2 > 0.97$, **Figure 3.a**; $r^2 > 0.93$, **Figure 3.2c**). Regarding DS, this PE originated a more evident plateau onset point, coming closer to a sigmoid fitting model ($r^2 > 0.99$, **Figure 3.2b**; $r^2 > 0.99$, **Figure 3.2d**). Besides solely the first four titrations are herein exhibited, such behaviors were observed and coherent during the whole process of the LbL shell attachment, and those may be justified with regard to differences in charge density of the used PEs (Morton, Poon *et al.* 2013), as well as their conformation in solution (Choi, Kim *et al.* 2008).

PAH exhibits a high number of molecular loops and tails, which can have contributed to the formation of thicker layers, capable of hiding negatively charged patches (Bantchev, Lu *et al.* 2009). In addition, using PAH as the outermost layer of the shell enabled the adhesion of its strongly positively charged molecules to the precedent layers, which, along with their concomitant protrusion into the aqueous phase, promoted a raise of its density and charge. These phenomena impacted directly on the zeta potential magnitudes, as it is possible to verify in **Figure 3.4a**, which depicts higher values when using PAH in comparison to DS. Nevertheless,

the same phenomenon contributed in parallel for the absence of a total surface saturation, which is responsible for the observed exponential behavior of corresponding titration curve profiles, **Figure 3.2a** and **Figure 3.2c**.

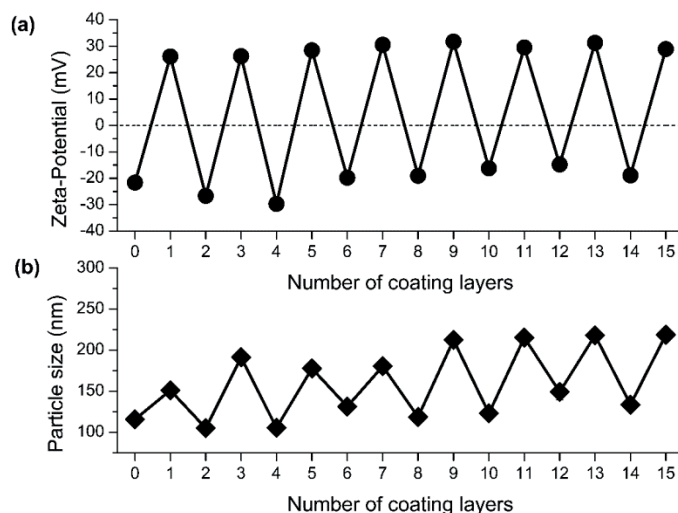


Figure 3.4: Zeta potential **(a)** and particle size **(b)** measurements of RSV nanocores and RSV-loaded LbL NPs with 2.5, 5.5 and 7.5 PAH/DS bilayers during the sequential build-up of the LbL shell, by the developed bottom-up and washless approach.

[DS – dextran sulfate; LbL – Layer-by-Layer; NP – nanoparticle; PAH – polyallylamine hydrochloride; RSV – resveratrol]

Titration curves resulting of the DS addition upon positive surfaces, in turn, exhibited a small influence on the zeta potential magnitudes at the outset. This was presumably a consequence of the adsorption of DS inside the tails and loops of PAH (Bantchev, Lu *et al.* 2009). The formation of negative patches on the surface may only has started when those tails and loops were surpassed, and the accomplishment of the surface coverage was revealed, in contrast to the PAH behaviour, by a marked change in zeta potential. Those events were additionally related to the obtainment of thinner and more encompassed PE coating layers by the washless approach, which consequently were responsible for a higher degree of chain interpenetration (Losche, Schmitt *et al.* 1998).

Even though titration curves were depicted herein only regarding the first four layers, as referred, those were carried out for each layer of the shell as well. LbL NPs covered with 2.5 PE bilayers was the simplest optimized considered nanoformulation. In order to ensure the feasibility of this nanoformulation as a viable platform to construct more complex nanoformulations, comprising more PE attached layers on the shell, its inherent physical stability was analysed for 30 days. Those NPs were shown to be stable for at least one week at room temperature, as evidenced in **Figure 3.5b**, revealing sufficient integrity to evolve further into a

more complex LbL-based construct. This way, a progressive construction of the LbL shell without the addition of PE excesses, by the application of a PE washless approach, was carried out up to the achievement of the most complex nanoformulation characterized by 7.5 PE bilayers (RSV-(PAH/DS)_{7.5}). It is worth noting that, during the development of those structures, the deposition of the next layer was always performed after the proper assessment of the PE concentration of the immediately preceding PE layer. This way, RSV LbL-coated NPs were obtained under this procedure with homogeneous particle size distributions at the nanoscale along with high zeta potential values, ensuring no excesses of PE during the assembly of the consecutive layers adsorption. Besides RSV nanocores, three LbL nanoformulations, comprising 2.5, 5.5 and 7.5 bilayers of PAH/DS in the LbL shell were considered for the present work and are analyzed below.

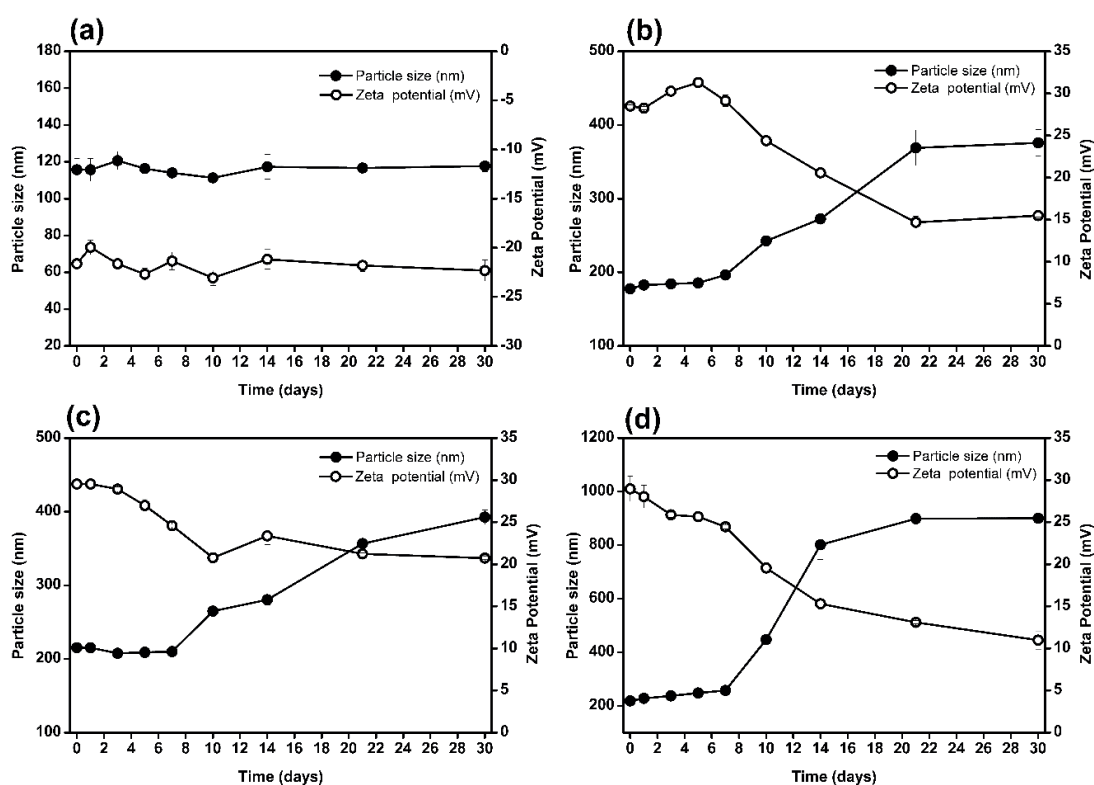


Figure 3.5: Colloidal stability of (a) RSV nanocores and RSV-loaded LbL NPs with (b) 2.5, (c) 5.5 and (d) 7.5 PAH/DS bilayers. The particle size (●) and zeta potential (○) variations were assessed during 30 days at 25 °C.

[DS – dextran sulfate; LbL – Layer-by-Layer; NP – nanoparticle; PAH – polyallylamine hydrochloride; RSV – resveratrol]

3.4.1.2. Zeta potential and particle size

Characterization of obtained LbL NPs in terms of zeta potential and particle size during the entire LbL assembly process is depicted in **Figure 3.4**.

As far as the zeta potential magnitudes are concerned (**Figure 3.4a**), the adsorption of PAH to the surface of negatively charged RSV nanocores (-21.6 ± 0.4 mV) promoted a surface charge reversal to a higher positive surface charge ($+26.2 \pm 1.0$ mV). These results suggested for an improvement of the colloidal stability of RSV nanocores after the attachment of the first PE of the LbL shell, a PAH coating layer. In the next LbL assembly stage, the adsorption of DS to RSV-PAH LbL NPs promoted again the reversal of the surface charge, this time into negative values (-26.7 ± 2.2 mV). This iterative adsorption of PAH and DS proceeded up to the deposition of 7.5 PE bilayers, corresponding the latter, thus, to the highest level of LbL-decoration of the surface of initial RSV nanocores developed in this work. The depicted reversion of the zeta potential characteristic of each PE deposition stage confirmed alternated surface NPs charge recharging, and, thus, the assembly occurrence on the surface. Such stepwise fashion evidence constitutes the driving force of this technology, emphasizing the success of each layer PE deposition, and, thus, the obtainment of LbL-coated NPs.

The examination of the **Figure 3.4a** also brings out a slight decrease of zeta potential magnitudes that has taken place from 2.5 bilayers deposition onwards, mainly regarding the case of DS layers. This may have occurred due to partial PE coating of those external layers, along with the establishment of secondary interactions between different deposited PE layers, accounting to a reduction of the surface charge density (Diez-Pascual, Wong 2010). In essence, upon the presence of some PE layers, the conformation of the weak PE PAH transits from an extended to a coiled status. Such coiled conformation is associated with the obtainment of thicker PAH layers, involving the existence of a lower degree of surface contact available for the attachment of the next DS-based PE layer, which may have impacted in the reduction of the zeta potential values of the ultimate layers composed of DS (Ngankam, Van Tassel 2005, Nayef, Castiello *et al.* 2017).

In the light of the higher exhibited zeta potential magnitudes conferred by PAH layers deposition (ca. +30 mV) compared to the ones referring to DS (ca. -20 mV), PAH was the selected PE to constitute the outermost coating of the LbL attached shell, conferring, thereby, superior physical stability to the system. This way, strongly charged LbL-coated NPs were effectively able to repulse, maintaining the colloidal stability.

In parallel, the analysis of particle size (**Figure 3.4b**) during the LbL assembly process confirmed the obtainment of homogeneous particle size populations, varying from ca. 116 nm for RSV nanocores to ca. 220 nm for 7.5 bilayers-coated LbL NPs, together with low mean PDI values, oscillating between 0.12 and 0.15, respectively. These results pointed out for the uniformity of LbL deposition by the presence of monodisperse NPs populations devoid of significant aggregation, as it is characteristic for LbL NPs prepared by this technique (Lvov, Pattekari *et al.* 2011, Shutava, Pattekari *et al.* 2012, Santos, Pattekari *et al.* 2015). Meanwhile, it is possible to see that as the LbL shell grows an oscillation of the particle size values occur depending on the used PE. In fact, DS-terminated NPs exhibited lower particle size values (ca. 100-130 nm) in contrast to the higher particle size values obtained for PAH-terminated NPs (ca. 150-220 nm). This enhancement in the particle size was a consequence of the establishment of interactions of the weak PE PAH with the interior of the LbL system or even by the diffusion of PAH towards also the interior, contributing to the enhancement of the film thickness (De Villiers, Lvov 2011). Interestingly, this phenomenon of the increase in particle size after the adsorption of PAH was found to be reversible by the addition of DS. This stems from the fact that PAH is a weak PE, which, besides its suppose inherent high charge in solution, gives origin to layers bearing only slight surface charge values. This leads, thus, to aggregation phenomena when using it as the outermost layer constituent. The deposition of a strong PE, as DS, in the following layer reduces the aggregation, by redispersion, leading to lower particle size values (Shutava, Balkundi *et al.* 2009). However, it is worth pointing out that the reduced particle size promoted by the use of DS when used as the outermost layer of the LbL shell has not conferred higher stability to these constructs. As a matter of fact, the monitoring of the physical stability during the development of nanoformulations revealed that LbL shells of NPs finished with DS revealed prompt aggregation, visible at naked eye, in less than 24 h. By the contrary, the NPs endowed with PAH as the outermost layer were stable over time (at least for 7 days). Given these results, PAH was selected to constitute the outermost layer of the LbL architecture for all the considered LbL nanoformulations, due to its conferred superior colloidal stability along with the obtainment of proper particle size distributions into the nanoscale, precisely with a particle size below 220 nm and very good PDIs, all below 0.15.

3.4.2. Nanoparticle imaging

The morphology and the particle size of RSV crystals and all considered nanoformulations were assessed by SEM, TEM and confocal microscopy (**Figure 3.6**). RSV native microcrystals and RSV-(PAH/DS)_{5.5} NPs are advertised, respectively, in **Figure 3.6a** and **Figure 3.6b**. It is clear, through

these SEM images, the reduction of the typical needle-like shaped RSV native microcrystals of ca. 10-50 μm length to the nanorange (ca. 200 nm), by the obtainment of well-dispersed square-like shaped LbL NPs.

TEM analysis confirmed these particle size and morphological results, as we can see in **Figure 3.6c**. Furthermore, TEM was also used to confirm the successful attachment of the LbL coating shell. This way, TEM analysis of the LbL NPs (**Figure 3.6c**) revealed the existence of a pronounced core surrounded by a less pronounced nebulous irregular outer halo, corresponding, respectively, to the RSV nanocore covered with the LbL coating shell. Such visual distinction was attributed to the different electron density of each material, supporting the presence of the LbL shells upon the nanocore surface during the LbL assembly process (Parekh, Pattekari *et al.* 2014).

The investigation of the LbL shell attachment was assessed by confocal microscopy as well. FITC-labelled PAH was used to prepare fluorescent LbL NPs, as it is depicted in **Figure 3.6d**. Besides some lack of resolution offered by this technique (ca. 100 nm), which does not enable for detailed NP structure assessment, it is possible to see dispersed green fluorescent bright spots around 200 nm. The depicted high green fluorescent color is attributed to the FITC labelling, supporting once more the success of the attachment of the fluorescent PAH upon the surface of RSV nanocores, and ultimately the success of this coating nanotechnology.

Overall, the nanoscale dimensions evaluated for the nanoformulations by TEM, SEM and confocal microscopy were in line with those obtained by DLS, as depicted in **Table 3.1**.

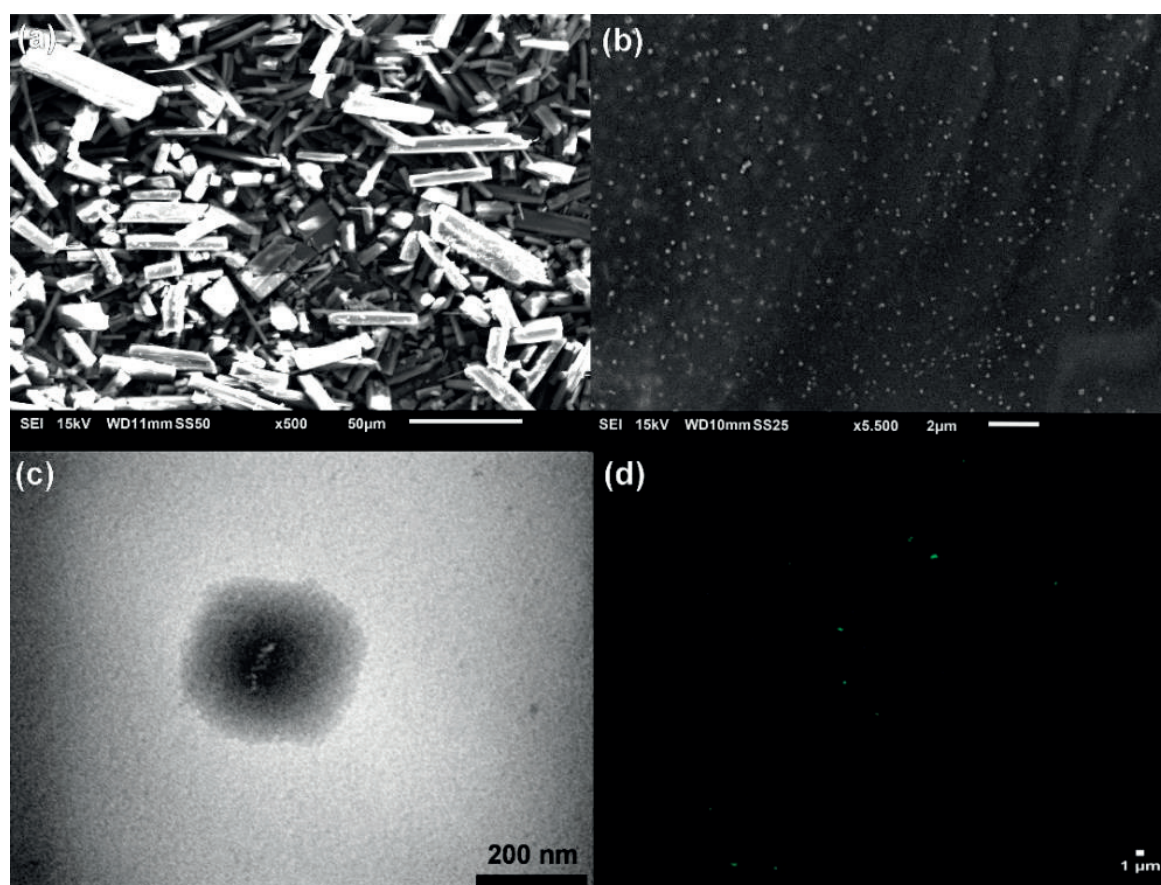


Figure 3.6: Representative image of **(a)** RSV native micrometer-sized crystals (x500) evaluated by SEM; RSV LbL NPs with a RSV-(PAH/DS)_{5.5} coating shell evidenced by **(b)** SEM (x5500) and **(c)** TEM (x98000). Confocal fluorescent image of RSV-(PAH/DS)_{5.5} NPs coated with FITC-labelled PAH **(d)**.

[DS – dextran sulfate; FITC – fluorescein isothiocyanate; LbL – Layer-by-Layer; NP – nanoparticle; PAH – polyallylamine hydrochloride; RSV – resveratrol; SEM – scanning electron microscopy; TEM – transmission electron microscopy]

3.4.3. Encapsulation efficiency

The encapsulation efficiency of a drug nanocarrier assumes particular importance for drug delivery systems performance. The determination of this parameter revealed that a very high percentage of RSV, above 90% for all the nanoformulations, was encapsulated using this procedure, together with the fact that the number of LbL coatings did not impacted significantly on it (**Table 3.1**). This suggested that the key process stage of the present nanotechnology in terms of drug encapsulation concerns to the initial nanoprecipitation of RSV into RSV nanocores. As a matter of fact, nanoprecipitation is recognized to enable the formation of NPs with high encapsulation efficiency values using low water-soluble drugs, as RSV (Singh, Pai 2014b), which is in line with our previous findings reporting lower encapsulation efficiency values (ca. 72-78%) when using the top-down approach (Santos, Pattekari *et al.* 2015). Beyond the successful

nanoprecipitation of RSV nanocores, the attachment of the LbL shell decorated the surface of the formers with no influence on the encapsulation efficiency of the drug. The main losses attributed to this process, even insignificant, were due to the vigorous sonication forces, which provoked the occurrence of splashed out formulation during the manufacturing process. Therefore, one can conclude that the present nanoformulations enabled the successful nanoencapsulation of RSV.

3.4.4. Stability studies

3.4.4.1. Colloidal stability

The colloidal stability of the RSV nanocores and LbL coated NPs with 2.5, 5.5 and 7.5 PE bilayers was assessed to investigate the impact of storage conditions during one month at room temperature on their physicochemical properties, as depicted in **Figure 3.5**. Under these conditions, RSV nanocores (**Figure 3.5a**) evidenced no significant changes neither in terms of particle size or zeta potential over the experimental time frame. Those results clearly elucidate about the high colloidal stability of RSV nanocores, which is due to the combined effect of steric and electrostatic stabilization capable of promoting a long-term stability (Singh, Makadia *et al.* 2017). It is interesting to observe that the zeta potential of these nanocores presents a magnitude close to -21 mV (**Table 3.1**), which is not considered an extremely high magnitude. The high stability of these structures is due to the effective combination of steric and electrostatic stabilizers adsorbed on the surface of nanocores that ensure the high colloidal stability. As a matter of fact, when using such type of stabilizers combination, an absolute zeta potential magnitude ca. to 20 mV is considered sufficient to obtain a stable formulation (Wu, Zhang *et al.* 2011), assumption that is absolutely in line with the results presented herein.

For the case of the LbL nanoformulations, namely with 2.5 (RSV-(PAH/DS)_{2.5} NPs) (**Figure 3.5b**), 5.5 (RSV-(PAH/DS)_{5.5} NPs) (**Figure 3.5c**) and 7.5 (RSV-(PAH/DS)_{7.5} NPs) (**Figure 3.5d**) PE bilayers, no changes regarding the particle size and zeta potential values were depicted during the first 7 days. Nonetheless, after this time point, the particle size started suffering an enhancement, along with a parallel reduction on zeta potential values, according to the occurrence of aggregation phenomena. Such detected events were more noticeable for the most complex nanoformulation endowed with 7.5 PE bilayers (RSV-(PAH/DS)_{7.5} NPs), whose particle size values were significantly different in comparison to the remain LbL nanoformulations, with 2.5 (RSV-(PAH/DS)_{2.5} NPs) and 5.5 (RSV-(PAH/DS)_{5.5} NPs) PE bilayers. These results were ascribed to the increase of the complexity of the LbL shell, which may has further fostered the establishment of

bridging interactions between neighbouring NPs in suspension, leading to destabilization. Regarding the LbL nanoformulations with 2.5 and 5.5 PE bilayers, minor variations in particle size and zeta potential were determined for the same period, since lower quantities of PE are present in comparison to the nanoformulation counterpart endowed with 7.5 PE bilayers. Such results allow the conclusion that aqueous LbL RSV-(PAH/DS) NPs are physically stable during 7 days at room temperature. Beyond that period, colloidal stability has proven to decline, mainly for the more complex LbL shells. The data obtained are broadly consistent to our previous results, where IBF NPs coated with the PE pair PAH/PSS evidenced a decrease in the colloidal stability with the increase of the complexity of the LbL shell, which was pronounced after a stable similar time-period at room temperature (Santos, Pattekari *et al.* 2015). Moreover, such behavior was already observed when studying LbL NPs coated with heparin and PLB16-5 (block-copolymers of poly-L-lysine with polyethylene glycol) (Parekh, Pattekari *et al.* 2014). Therefore, on the whole, the present NPs are considered physically stable due to the electrostatic and steric repulsion conferred by the stabilizers together with the chemical nature of the polymeric LbL architecture.

3.4.4.2. Chemical stability

RSV, which exhibits extreme photosensitivity and propensity for oxidative degradation, was shown to remain stable after the nanoencapsulation process. We were able to conclude this, since typical HPLC-DAD chromatograms of the standard RSV and those ones referring to the nanoformulations (nanoencapsulated RSV) evidenced the same retention time in the presence of the exact same chromatographic conditions. Moreover, the analysis of the UV-Vis spectra revealed the same pattern for the both cases, exhibiting the characteristic absorption maximum peak of RSV at 306 nm (Trela, Waterhouse 1996). This indicates that the two spectra are homologous, which are in accordance with the literature. Besides, the absence of new peaks indicators of the presence of new chemical entities, confirmed the absence of chemical alterations. For example, an eventual transformation of *trans*-RSV into *cis*-RSV would lead to a chromatogram containing an extra peak (Zupancic, Lavric *et al.* 2015). Taken together, these evidences demonstrated that nanoformulations successfully avoided the chemical degradation of RSV, protecting it from the contact with the dissolved oxygen, contributing, along with the conferred colloidal stability, to the overall storage stability of the present NPs suspended in water.

3.4.5. *In vitro* release studies

In vitro release studies simulating the GI transit of RSV native crystals (nonencapsulated RSV), RSV nanocores and LbL NPs coated with 2.5, 5.5 and 7.5 bilayers of PAH/DS were performed at body temperature in simulated gastric fluid followed by simulated intestinal fluid without enzymes (**Figure 3.7**). After 1 h in simulated gastric pH, differences among the different profiles were encountered. Regarding **Figure 3.7**, 2.5-bilayered coated NPs and RSV nanocores exhibited a slightly higher dissolution rate in relation to RSV crystals and the most complex LbL nanoformulations, specifically 5.5 and 7.5-bilayered coated NPs. This result pinpoints, thus, an impact of the shell wall thickness on RSV delayed dissolution in this medium. On the contrary, in a similar way to RSV nanocores which do not present PE coatings in their composition, 2.5-bilayered coated NPs were shown to exhibit an insufficient shell thickness to promote a RSV release delay in the same extension as the most complex LbL nanoformulations. Concerning RSV crystals, their significantly reduced dissolution stems from the fact that RSV is a weakly acidic drug (Zupancic, Lavric *et al.* 2015), evidencing a pH-dependent solubility, which, together with their native large micrometer-sized dimension, strongly limit its dissolution in the acidic regime. It is also worth noting that solely minor encountered RSV released amounts were found to be released for LbL nanoformulations in this medium, corresponding all to values below 20%. This RSV released percentage may have been assigned to the presence of PAH in the LbL shell. In fact, according to the pKa of PAH, at simulated gastric pH this PE may have been destabilized, which may have affected the integrity of the membrane permeability, given the formation of pores, ultimately enabling the RSV release from the LbL architecture (Antipov, Sukhorukov *et al.* 2002). In addition, when comparing to our previous results where PSS was applied as the polyanion also together with PAH as the polycation of the LbL shell (Santos, Pattekari *et al.* 2015), besides promoting a more regular release pattern, DS also prevented the premature release of RSV providing a superior retention capacity than PSS at gastric pH. This outcome predicts a lower RSV release in the stomach and thus a superior availability to absorption in the intestine, being in agreement with the assigned characteristics of stability and gastric protection exhibited by DS as a constituent of drug delivery systems intended for the oral route (Sarmiento, Ribeiro *et al.* 2007, Santos, Cunha *et al.* 2013). Despite this, after 2 hours of *in vitro* simulated gastric incubation, most RSV remained associated to LbL NPs (> 80%), indicating that these systems promoted a good gastric resistance, namely for 5.5- and 7.5-bilayered coated NPs, emphasizing the important role of the LbL shell on RSV retention under these conditions.

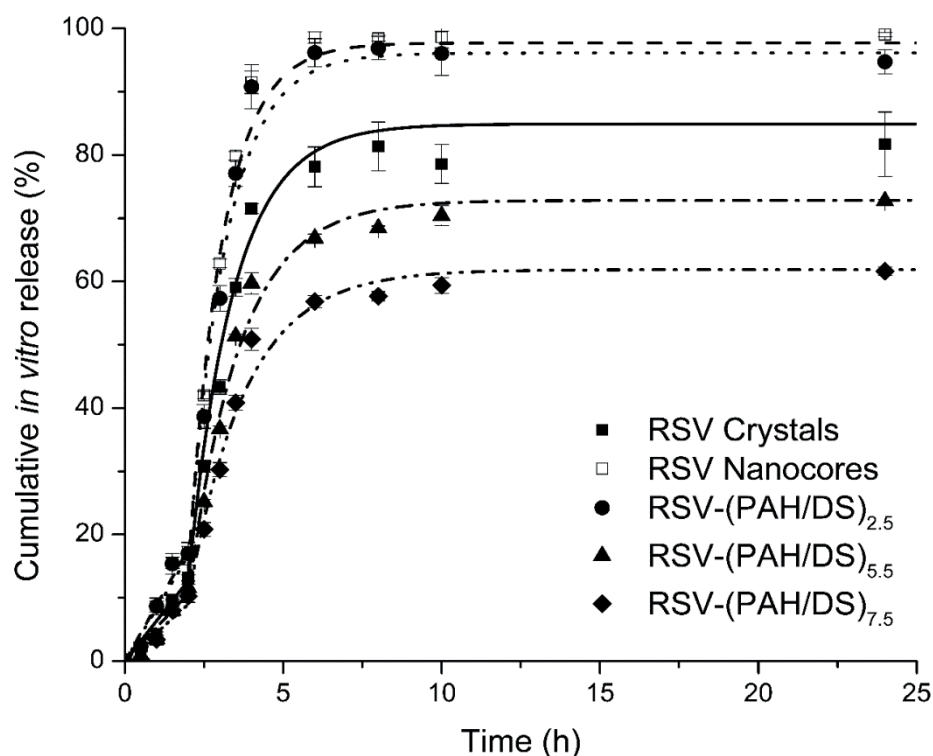


Figure 3.7: *In vitro* RSV release studies from non-encapsulated native crystals of RSV (■), RSV nanocores (□), and RSV-loaded LbL NPs prepared with 2.5 (●), 5.5 (▲) and 7.5 (◆) bilayered coatings of PAH/PSS in (a) simulated gastric pH 1.2 fluid and (b) simulated intestinal pH 6.8 fluid in *sink* conditions at 37 °C. Data represent mean ± SD, n = 3.

[DS – dextran sulfate; LbL – Layer-by-Layer; NP – nanoparticle; PAH – polyallylamine hydrochloride; RSV – resveratrol]

Following a pH change to 6.8, a biphasic release pattern was observed for all the studied profiles, characterized by an initial rapid release during the first 1.5 hours, which is attributed to the diffusion of RSV molecules adsorbed at the surface of the NPs, followed by a controlled release up to the attainment of the plateau at 6 h, meaning for no significant alterations until the end of the study (24 h). In essence, under these pH conditions, the charge density of PAH was reduced triggering an excess of negative charges in the PAH/DS shells, due to the presence of the strongly negative charged DS; consequently, the PE chains repelled each other, thereby provoking the swelling of the multilayer LbL shell, and, thus, the release of the RSV. These results showed a very good fit with the exponential kinetic model ($r^2 > 0.99$), suggesting an apparent first-order behavior. Moreover, the striking feature of this release profiles lies in the release rate of RSV from the studied formulations that was found to be delayed with increasing the number of coating PE bilayers of the LbL shell. At 4 hours, e.g., attention is drawn to only 51% of released RSV from 7.5-bilayers coated NPs as compared with 60% of released RSV from the 5.5-bilayers and 91% from the 2.5-bilayers samples. This effect was ascribed to the enhancement of the LbL

shell wall thickness, which may have conducted to the higher diffusional resistance offered by the coating shell materials to the molecules of RSV and, thus, triggered a RSV release delay from the drug core through the LbL net-like architecture (Sanna, Roggio *et al.* 2012). Apart from the decrease in the RSV release rate, a reduction of the evidenced early RSV burst release was also accomplished by using those structures. These findings are strongly consistent to additional data from the literature using additional low water-soluble drugs, as paclitaxel (Agarwal, Lvov *et al.* 2008, Pattekari, Zheng *et al.* 2011, Polomska, Gauthier *et al.* 2017), tamoxifen (Agarwal, Lvov *et al.* 2008), also including our previous studies with IBF (Santos, Pattekari *et al.* 2015). In point of fact, drug dissolution rate was shown to decrease just linearly with the enhancement of the shell thickness by the same token as the presented NPs herein, emphasizing a clear function of modified drug release attributed to LbL-coated NPs. This way, in one study using paclitaxel- and tamoxifen-loaded LbL NPs, the authors emphasized an easy control of the tamoxifen and paclitaxel release rates by changing the coating thickness of, respectively, PDDA/PSS and PAH/PSS-based LbL shells, reporting a slower drug release rate with the increase of the number of the PE assembled bilayers (Agarwal, Lvov *et al.* 2008). The same has been reported recently by others using paclitaxel-loaded PLR/PSS-PEG NPs (Polomska, Gauthier *et al.* 2017). In another study, in a matter of 8 hours, paclitaxel-loaded PAH/BSA NPs revealed a reduction in the drug release rate from ca. 80% using an half PE bilayer to ca. 40% using three coating bilayers (Pattekari, Zheng *et al.* 2011). Regarding our previous studies using IBF-loaded PAH/PSS NPs, after 2 h under simulated intestinal conditions ca. 51% of IBF was released from 7.5-bilayered LbL NPs in comparison to ca. 60% from the 5.5-bilayered LbL NPs and to ca. 89% released from 2.5-bilayered LbL NPs (Santos, Pattekari *et al.* 2015).

The analysis of the profiles also depicts a non-complete drug release from LbL PE bilayered shells concerning the most complex LbL nanoformulations, accordingly to evidence reported before (Shutava, Pattekari *et al.* 2012, Santos, Pattekari *et al.* 2015). Such effect may have happened due to the establishment of stronger electrostatic-based PE web forces surrounding the RSV nanocore, in contrast to the less complex LbL nanoformulations. In fact, the enhancement of the complexity of the LbL shell offered resistance to the diffusion of RSV to the exterior, which, in one hand contributed to a controlled release profile as referred, but, in another hand, was responsible for a non-complete RSV release. Furthermore, the presence of the biosynthetic PE PAH, which is biocompatible but it is not biodegradable, may have impacted as well on this output (Palama, Musaro *et al.* 2011).

Comparing the curves of the studied samples, no differences were detected between 2.5-bilayered coated NPs, the simplest LbL nanoformulation, and RSV nanocores profiles. In fact, those curves are almost superposable and, likewise the observed behavior in simulated gastric conditions, these nanoformulations led to a slightly RSV faster release compared to non-encapsulated RSV crystals and also 5.5- and 7.5-bilayered NPs. This behavior stems from the fact that RSV nanocores and 2.5-bilayered coated NPs present an insufficient LbL shell thickness, which did not allow for a significant RSV release delay. These data supported the results obtained before with paclitaxel-loaded PLL/heparin coating shells, in which the drug release rate was found to have no differences among the corresponding LbL shells composed with less than 3.5 bilayers (Shutava, Pattekari *et al.* 2012). In addition, when comparing specifically with RSV native crystals, 2.5-bilayered coated NPs, and also RSV nanocores, exhibited a faster RSV release profile because of their NPs small size compared to the micrometer size and the low solubility of the former under tested conditions. Owing to the characteristic small size of NPs, the surface area was highly superior between both 2.5-bilayered coated NPs and RSV nanocores and the release medium in relation to RSV native crystals. As a matter of fact, in agreement with the Kelvin equation the enhancement of the curvature of the particle surface leads to an increase of the drug dissolution pressure, being the solubility strongly enhanced with the reduction of the particle size into the nanoscale (Junghanns, Muller 2008). Moreover, according to Noyes-Whitney equation (He, Han *et al.* 2017), the enhancement of the solubility (designed also as saturation solubility) causes an increase in the dissolution rate of RSV. These data emphasize the key role of the optimization of the LbL shell towards the obtainment of a proper shell thickness.

This way, our results offer overwhelming evidence for a pH-dependent drug release pattern for PAH/DS-based LbL NPs. In addition, a controlled RSV release from PAH/DS-based LbL NPs was also found, essentially in simulated intestinal medium, which in turn emphasized the obtainment of a significant drug entrapment within the NPs. This underpinned, thus, the results of the encapsulation efficiency values assessment (section 3.3.3). The exhibited particle size values of the LbL structures around 200 nm is considered optimal for the uptake and transport by M cells (des Rieux, Fievez *et al.* 2007), whose, together with their exhibited modified *in vitro* drug release characteristics, constitute strong indicators for the feasibility of these nanoscale-designed structures as a promising oral RSV carrier intended for the oral route.

3.4.6. *In vitro* cytotoxicity assay

In vitro cytotoxicity assessment plays a key role in the safety investigation of a pharmaceutical formulation. The assessment of the cytotoxicity can be performed previous to animals testing by

the MTT assay (Mosmann 1983). This assay, which has been selected given that is one of the well-established cell viability assays, evaluates the mitochondrial function as a measurement of cell viability, allowing the detection of dead cells before the loss of their integrity and shape (Jose, Anju *et al.* 2014). Caco-2 cells were used in the light of the intended oral administration of the present nanoformulations. On account of the exposed motives, the potential cytotoxicity of RSV native crystals, RSV nanocores and RSV-loaded PAH/DS LbL NPs with distinctic number of coating bilayers (2.5, 5.5 and 7.5) was assessed by evaluating the viability of the Caco-2 cells by exposure to NPs formulations (**Figure 3.8**).

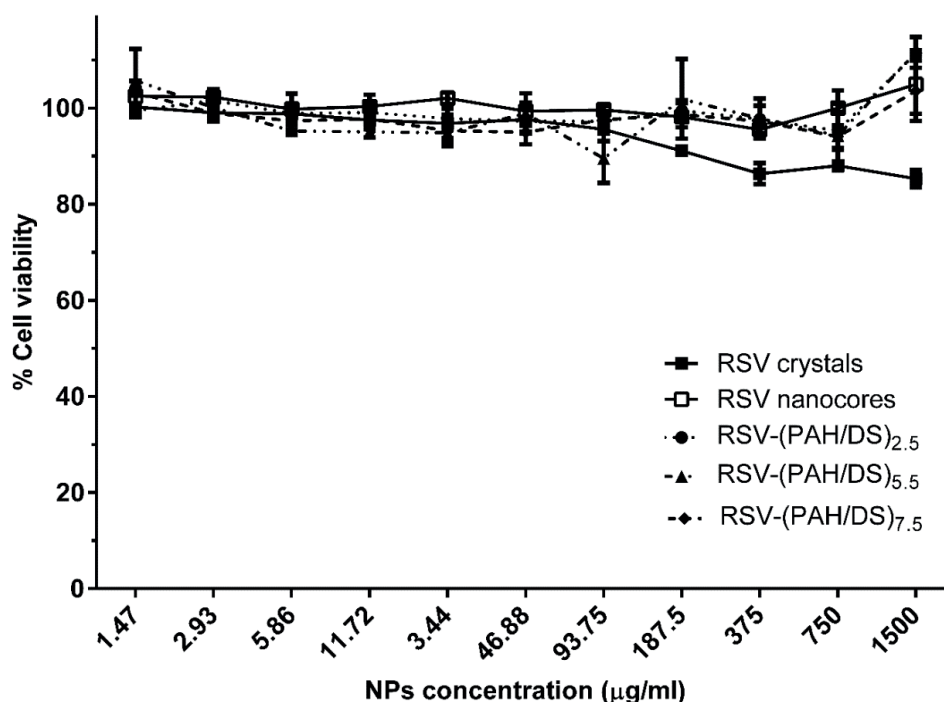


Figure 3.8: Cell viability of Caco-2 cells after 24h of incubation with RSV native crystals (■), RSV nanocores (□) and RSV-loaded LbL NPs coated with 2.5 (●), 5.5 (▲) and 7.5 (◆) PAH/DS bilayers for concentrations varying from 11.7 µg/mL to 1500 µg/mL. Cell viability of each sample was assessed by MTT assay. Data are shown as mean ± S.E.M (n = 3).

[DS– dextran sulfate; LbL – Layer-by-Layer; MTT – 3-(4,5-dimethylthiazol-2-yl)-2,5-diphenyltetrazolium bromide; NP– nanoparticle; PAH– polyallylamine hydrochloride; RSV – resveratrol]

The analysis of the cytotoxicity profiles showed that the cell viability was constant on 100%, with no statistical differences between tested samples along the large concentration range, excluding at the highest tested concentration. At that concentration level (1500 µg/mL), all the nanoformulations evidenced higher viability in relation to RSV native crystals, whose viability was shown to slightly decrease. The clearly high viability values concerning to all the nanoformulations were probably ascribed to the electrostatically induced repulsive forces established between NPs, which conducted to NPs suspension stability under the *in vitro* testing

used conditions, fostering NPs-cell interplay (Horie, Nishio *et al.* 2010). Regarding the encountered differences at 1500 $\mu\text{g}/\text{mL}$ concentration, those suggest that, even in a fairly small extension due to the high cell viability values above 80%, native RSV crystals have probably induced some loss of cell viability, accordingly to its concentration dependent-manner cytotoxicity (Rocha, Marques *et al.* 2017). This event did not effectively occur when the RSV is encapsulated within NPs, which emphasizes the protection effect conferred by NPs to the cells, particularly in the case of high RSV concentrations.

From these results, one can observe that RSV nanocores offered no toxicity to the cells under the tested conditions. This indicates that PVP and SLE₂S, located at the RSV nanocores surface, were thus found to promote non-toxicity in the used concentrations. Regarding the LbL coated NPs, a coherent non-toxic behavior was determined along the tested range, regardless of the composition of the LbL shell of the LbL-coated nanoformulations. These data were in line with previous studies reporting no additional cytotoxicity attributed to the presence of the LbL construct, as verified for PSS/PLR-PEG (Polomska, Gauthier *et al.* 2017) and chitosan/DS-PEG (Yu, Pishko 2011) shells. In addition, in our previous work using IBF-loaded PAH/PSS LbL NPs, the cell viability of Caco-2 cells was found to decrease from the high 187.5 $\mu\text{g}/\text{mL}$ concentration onwards for the LbL nanoformulations (Santos, Pattekari *et al.* 2015). In fact, comparing to the use of the synthetic PE PSS, the PE DS present in the LbL shells developed herein, is a biocompatible and a biodegradable PE (Palama, Musaro *et al.* 2011). This feature may have been responsible for the higher viability values in the same concentration range, which may have been responsible for the improved cytotoxicity profile. Nonetheless, considering the whole tested concentration range, those PAH/PSS shells were found to be non-toxic as well in a large range of concentrations (Santos, Pattekari *et al.* 2015), supporting the recognized non-toxicity of the LbL shells.

This way, all the nanoformulations evaluated in the tested concentrations presented a percentage of viability above 90%, revealing a very good cytotoxicity profile. Those results point towards an *in vitro* cytocompatibility of the tested nanoformulations with the cells, clearly indicating that the decoration of the surface of the NPs with LbL do not provoke any impact on the viability of this cell culture system under the performed conditions. Moreover, the positive surface charge evidenced by the PAH/DS LbL developed nanoformulations constitutes an important feature with biological impact, since the internalization of those NPs will be certainly favoured by nonspecific adsorptive endocytosis, facing the negatively surface charge cell plasma membrane (Palama, Musaro *et al.* 2011). These results explicitly evidenced that those novel

PAH/DS LbL nanoformulations constitute safe and promising nanocarriers for RSV delivery, thereby allowing further *in vitro/in vivo* implementations.

3.5. Conclusions

LbL NPs pose a desired category of materials owing to their modular and multifunctional merits, which are vital for the powerful next-generation nanomedicines breakthrough. In this work, we developed and characterized, for the first time, RSV-loaded PAH/DS-composed LbL NPs, with PE shells comprised with 2.5, 5.5 and 7.5 bilayers, by using a bottom-up approach combined with a washless LbL self-assembly nanotechnology. Thanks to the great strength of the LbL platforms of producing various material systems, we were able to nanoencapsulate RSV by performing LbL NPs by the use of strongly charged PEs organized into the three distinct multilayered LbL nanoshells. The application of a washless approach by the use of PE titration curves enabled the use of solely the sufficient amounts of PEs, handling cumbersome, time-consuming and costly intermediate washing steps pertaining to the conventional PE washings approach. By means of this washless approach, the maximum colloidal stability was ensured for each coating layer, which were determined to be fully saturated in the assessed onset points. Owing to such, a larger flexibility was provided regarding the possible number of bilayers to be assembled, along with a yield process maximization. We performed, thus, a simple washless procedure, which demands no sophisticated equipments and reduced energy expense, attributing promising scaling-up prospects to the LbL nanotechnology.

This way, the achievement of a tunable LbL shell enabled the structural control in the particle size and surface charge, assisting to well dispersed nanosuspensions with narrow particle size distributions, while promoting the obtainment of high encapsulation efficiency values and an excellent cytocompatibility. Those NPs promoted both colloidal and chemical protection to the nanoencapsulated RSV, which points to an enhancement of its therapeutic effects by instability minimizing. In addition to these gains, the RSV release rate from RSV-loaded PAH/DS-stabilized LbL NPs was found to be controlled by varying the number of PEs bilayers of the shell. Moreover, the use of the PAH/DS-composed shell showed to significantly retain RSV in simulated stomach conditions, being the present technique proposed to formulate a viable oral delivery system for RSV. The higher gastroretention found in the present study while using DS predicts also for a higher availability of RSV for absorption in the intestine comparing to the use of solely synthetic PEs, as PSS.

In the light of the present report, relevant features were successfully assigned for improved RSV oral delivery by the use of RSV-loaded LbL NPs. The LbL nanotechnology implemented upon RSV nanocores template by a washless approach is poised to perform promising advances in the

delivery of RSV, by the fabrication of effective oral nanoformulations for this prominent bioactive polyphenol with potential health-improvement properties.

References

- Agarwal, A., Lvov, Y., Sawant, R., Torchilin, V. Stable nanocolloids of poorly soluble drugs with high drug content prepared using the combination of sonication and layer-by-layer technology. *J Control Release* **128**, 255-260 (2008).
- Amri, A., Chaumeil, J. C., Sfar, S., Charrueau, C. Administration of resveratrol: What formulation solutions to bioavailability limitations?. *J Control Release* **158**, 182-193 (2012).
- Antipov, A. A., Sukhorukov, G. B., Leporatti, S., Radtchenko, I. L., Donath, E., Mohwald, H. Polyelectrolyte multilayer capsule permeability control. *Colloids Surf, A* **198**, 535-541 (2002).
- Bantchev, G., Lu, Z., Lvov, Y. Layer-by-layer nanoshell assembly on colloids through simplified washless process. *J Nanosci Nanotechnol* **9**, 396-403 (2009).
- Bonkowski, M. S., Sinclair, D. A. Slowing ageing by design: the rise of NAD⁺ and sirtuin-activating compounds. *Nat Rev Mol Cell Biol* **17**, 679-690 (2016).
- Charytoniuk, T., Drygalski, K., Konstantynowicz-Nowicka, K., Berk, K., Chabowski, A. Alternative treatment methods attenuate the development of NAFLD: A review of resveratrol molecular mechanisms and clinical trials. *Nutrition* **34**, 108-117 (2017).
- Choi, Y. W., Kim, K., Kim, J. Y., Lee, Y., Sohn, D. Adsorption mechanism of a weak polyelectrolyte, PAH, onto carboxylate PS particles. *Colloids Surf, A* **315**, 7-12 (2008).
- Correa, S., Choi, K. Y., Dreaden, E. C., Renggli, K., Shi, A., Gu, L., *et al.* Highly scalable, closed-loop synthesis of drug-loaded, layer-by-layer nanoparticles. *Adv Funct Mater* **26**, 991-1003 (2016).
- De Villiers, M. M., Lvov, Y. M. Layer-by-layer self-assembled nanoshells for drug delivery. *Adv Drug Deliv Rev* **63**, 699-700 (2011).
- De Villiers, M. M., Otto, D. P., Strydom, S. J., Lvov, Y. M. Introduction to nanocoatings produced by layer-by-layer (LbL) self-assembly. *Adv Drug Deliv Rev* **63**, 701-715 (2011).
- Deng, Z. J., Morton, S. W., Ben-Akiva, E., Dreaden, E. C., Shopsowitz, K. E., Hammond, P. T. Layer-by-layer nanoparticles for systemic codelivery of an anticancer drug and siRNA for potential triple-negative breast cancer treatment. *ACS Nano* **7**, 9571-9584 (2013).

- Des Rieux, A., Fievez, V., Momtaz, M., Detrembleur, C., Alonso-Sande, M., Van Gelder, J., *et al.* Helodermin-loaded nanoparticles: characterization and transport across an *in vitro* model of the follicle-associated epithelium. *J Control Release* **118**, 294-302 (2007).
- Diez-Pascual, A. M., Wong, J. E. Effect of layer-by-layer confinement of polypeptides and polysaccharides onto thermoresponsive microgels: a comparative study. *J Colloid Interface Sci* **347**, 79-89 (2010).
- Ethemoglu, M. S., Seker, F. B., Akkaya, H., Kilic, E., Aslan, I., Erdogan, C. S., *et al.* Anticonvulsant activity of resveratrol-loaded liposomes *in vivo*. *Neuroscience* **357**, 12-19 (2017).
- Gordon, B. S., Delgado Diaz, D. C., Kostek, M. C. Resveratrol decreases inflammation and increases utrophin gene expression in the mdx mouse model of Duchenne muscular dystrophy. *Clin Nutr* **32**, 104-111 (2013).
- Gu, L., Deng, J. Z., Roy, S., Hammond, P. T. A combination RNAi-Chemotherapy Layer-by-Layer nanoparticle for systemic targeting of KRAS/P53 with cisplatin to treat non-small cell lung cancer. *Clin Cancer Res* **23** (2017).
- He, J. L., Han, Y., Xu, G. J., Yin, L. F., Neubi, M. N., Zhou, J. P., *et al.* Preparation and evaluation of celecoxib nanosuspensions for bioavailability enhancement. *RSC Adv* **7**, 13053-13064 (2017).
- Hiller, S., Leporatti, S., Schnäckel, A., Typlt, E., Donath, E. Protamine assembled in multilayers on colloidal particles can be exchanged and released. *Biomacromolecules* **5**, 1580-1587 (2004).
- Horie, M., Nishio, K., Kato, H., Shinohara, N., Nakamura, A., Fujita, K., *et al.* *In vitro* evaluation of cellular responses induced by stable fullerene C60 medium dispersion. *J Biochem* **148**, 289-298 (2010).
- ISO13321. Methods for determination of particle size distribution part 8: photon correlation spectroscopy, International Organisation for Standardisation (ISO) (1996).
- ISO22412. Particle Size Analysis — Dynamic Light Scattering, International Organisation for Standardisation (ISO) (2008).
- Itoh, K., Pongpeerapat, A., Tozuka, Y., Oguchi, T., Yamamoto, K. Nanoparticle formation of poorly water-soluble drugs from ternary ground mixtures with PVP and SDS. *Chem Pharm Bull (Tokyo)* **51**, 171-174 (2003).

- Joraholmen, M. W., Skalko-Basnet, N., Acharya, G., Basnet, P. Resveratrol-loaded liposomes for topical treatment of the vaginal inflammation and infections. *Eur J Pharm Sci* **79**, 112-121 (2015).
- Jose, S., Anju, S. S., Cinu, T. A., Aleykutty, N. A., Thomas, S., Souto, E. B. In vivo pharmacokinetics and biodistribution of resveratrol-loaded solid lipid nanoparticles for brain delivery. *Int J Pharm* **474**, 6-13 (2014).
- Junghanns, J. U., Muller, R. H. Nanocrystal technology, drug delivery and clinical applications. *Int J Nanomedicine* **3**, 295-309 (2008).
- Losche, M., Schmitt, J., Decher, G., Bouwman, W. G., Kjaer, K. Detailed structure of molecularly thin polyelectrolyte multilayer films on solid substrates as revealed by neutron reflectometry. *Macromolecules* **31**, 8893-8906 (1998).
- Lvov, Y. M., Pattekari, P., Zhang, X., Torchilin, V. Converting poorly soluble materials into stable aqueous nanocolloids. *Langmuir* **27**, 1212-1217 (2011).
- Mantegna, S., Binello, A., Boffa, L., Giorgis, M., Cena, C., Cravotto, G. A one-pot ultrasound-assisted water extraction/cyclodextrin encapsulation of resveratrol from *Polygonum cuspidatum*. *Food Chem* **130**, 746-750 (2012).
- Morton, S. W., Poon, Z., Hammond, P. T. The architecture and biological performance of drug-loaded LbL nanoparticles. *Biomaterials* **34**, 5328-5335 (2013).
- Mosmann, T. Rapid colorimetric assay for cellular growth and survival: application to proliferation and cytotoxicity assays. *J Immunol Methods* **65**, 55-63 (1983).
- Nayef, L., Castiello, R., Tabrizian, M. Washless method enables multilayer coating of an aggregation-prone nanoparticulate drug delivery system with enhanced yields, colloidal stability, and scalability. *Macromol Biosci* **17** (2017).
- Ngankam, A. P., Van Tassel, P. R. In situ layer-by-layer film formation kinetics under an applied voltage measured by optical waveguide lightmode spectroscopy. *Langmuir* **21**, 5865-5871 (2005).
- Palama, I. E., Musaro, M., Coluccia, A. M., D'Amone, S., Gigli, G. Cell uptake and validation of novel pectins for biomedical applications. *J Drug Deliv* **2011**, 203676 (2011).

- Parekh, G., Pattekari, P., Joshi, C., Shutava, T., DeCoster, M., Levchenko, T., *et al.* Layer-by-layer nanoencapsulation of camptothecin with improved activity. *Int J Pharm* **465**, 218-227 (2014).
- Pattekari, P., Zheng, Z., Zhang, X., Levchenko, T., Torchilin, V., Lvov, Y. Top-down and bottom-up approaches in production of aqueous nanocolloids of low solubility drug paclitaxel. *Phys Chem Chem Phys* **13**, 9014-9019 (2011).
- Polomska, A., Gauthier, M. A., Leroux, J. C. *In vitro* and *in vivo* evaluation of PEGylated layer-by-layer polyelectrolyte-coated paclitaxel nanocrystals. *Small* **13** (2017).
- Ramalingam, P., Ko, Y. T. Improved oral delivery of resveratrol from N-trimethyl chitosan-g-palmitic acid surface-modified solid lipid nanoparticles. *Colloids Surf B Biointerfaces* **139**, 52-61 (2016).
- Rauf, A., Imran, M., Butt, M. S., Nadeem, M., Peters, D. G., Mubarak, M. S. Resveratrol as an anticancer agent: a review. *Crit Rev Food Sci Nutr* 1-20 (2016).
- Rocha, V., Marques, C., Figueiredo, J. L., Gaio, A. R., Costa, P. C., Sousa Lobo, J. M., *et al.* *In vitro* cytotoxicity evaluation of resveratrol-loaded nanoparticles: Focus on the challenges of *in vitro* methodologies. *Food Chem Toxicol* **103**, 214-222 (2017).
- Sadeghpour, A., Seyrek, E., Szilagyi, I., Hierrezuelo, J., Borkovec, M. Influence of the degree of ionization and molecular mass of weak polyelectrolytes on charging and stability behavior of oppositely charged colloidal particles. *Langmuir* **27**, 9270-9276 (2011).
- Sanna, V., Roggio, A. M., Siliani, S., Piccinini, M., Marceddu, S., Mariani, A., *et al.* Development of novel cationic chitosan-and anionic alginate-coated poly(D,L-lactide-co-glycolide) nanoparticles for controlled release and light protection of resveratrol. *Int J Nanomedicine* **7**, 5501-5516 (2012).
- Sanna, V., Siddiqui, I. A., Sechi, M., Mukhtar, H. Resveratrol-loaded nanoparticles based on poly(epsilon-caprolactone) and poly(D,L-lactic-co-glycolic acid)-poly(ethylene glycol) blend for prostate cancer treatment. *Mol Pharm* **10**, 3871-3881 (2013).
- Santos, A. C., Cunha, J., Veiga, F., Cordeiro-da-Silva, A., Ribeiro, A. J. Ultrasonication of insulin-loaded microgel particles produced by internal gelation: impact on particle's size and insulin bioactivity. *Carbohydr Polym* **98**, 1397-1408 (2013).

- Santos, A. C., Pattekari, P., Jesus, S., Veiga, F., Lvov, Y., Ribeiro, A. J. Sonication-assisted layer-by-layer assembly for low solubility drug nanoformulation. *ACS Appl Mater Interfaces* **7**, 11972-11983 (2015).
- Santos, A. C., Veiga, F., Ribeiro, A. J. New delivery systems to improve the bioavailability of resveratrol. *Expert Opin Drug Deliv* **8**, 973-990 (2011).
- Sarmiento, B., Ribeiro, A., Veiga, F., Ferreira, D., Neufeld, R. Oral bioavailability of insulin contained in polysaccharide nanoparticles. *Biomacromolecules* **8**, 3054-3060 (2007).
- Shutava, T. G., Balkundi, S. S., Vangala, P., Steffan, J. J., Bigelow, R. L., Cardelli, J. A., *et al.* Layer-by-layer-coated gelatin nanoparticles as a vehicle for delivery of natural polyphenols. *ACS Nano* **3**, 1877-1885 (2009).
- Shutava, T. G., Pattekari, P. P., Arapov, K. A., Torchilin, V. P., Lvov, Y. M. Architectural layer-by-layer assembly of drug nanocapsules with PEGylated polyelectrolytes. *Soft Matter* **8**, 9418-9427 (2012).
- Singh, G., Pai, R. S. Optimized PLGA nanoparticle platform for orally dosed trans-resveratrol with enhanced bioavailability potential. *Expert Opin Drug Deliv* **11**, 647-659 (2014a).
- Singh, G., Pai, R. S. *In-vitro/in-vivo* characterization of trans-resveratrol-loaded nanoparticulate drug delivery system for oral administration. *J Pharm Pharmacol* **66**, 1062-1076 (2014b).
- Singh, S. K., Makadia, V., Sharma, S., Rashid, M., Shahi, S., Mishra, P. R., *et al.* Preparation and *in-vitro/in-vivo* characterization of trans-resveratrol nanocrystals for oral administration. *Drug Deliv Transl Res* **7**, 395-407 (2017).
- Summerlin, N., Soo, E., Thakur, S., Qu, Z., Jambhrunkar, S., Popat, A. Resveratrol nanoformulations: challenges and opportunities. *Int J Pharm* **479**, 282-290 (2015).
- Sung, M. M., Byrne, N. J., Robertson, I. M., Kim, T. T., Samokhvalov, V., Levasseur, J., *et al.* Resveratrol improves exercise performance and skeletal muscle oxidative capacity in heart failure. *Am J Physiol Heart Circ Physiol* **312**, H842-H853 (2017).
- Trela, B. C., Waterhouse, A. L. Resveratrol: isomeric molar absorptivities and stability. *J Agric Food Chem* **44**, 1253-1257 (1996).

- Venuti, V., Cannava, C., Cristiano, M. C., Fresta, M., Majolino, D., Paolino, D., *et al.* A characterization study of resveratrol/sulfobutyl ether-beta-cyclodextrin inclusion complex and in vitro anticancer activity. *Colloids Surf B Biointerfaces* **115**, 22-28 (2014).
- Wu, L., Zhang, J., Watanabe, W. Physical and chemical stability of drug nanoparticles. *Adv Drug Deliv Rev* **63**, 456-469 (2011).
- Yadav, A., Sunkaria, A., Singhal, N., Sandhir, R. Resveratrol loaded solid lipid nanoparticles attenuate mitochondrial oxidative stress in vascular dementia by activating Nrf2/HO-1 pathway. *Neurochem Int* (2017).
- Yu, X., Pishko, M. V. Nanoparticle-based biocompatible and targeted drug delivery: characterization and *in vitro* studies. *Biomacromolecules* **12**, 3205-3212 (2011).
- Zupancic, S., Lavric, Z., Kristl, J. Stability and solubility of trans-resveratrol are strongly influenced by pH and temperature. *Eur J Pharm Biopharm* **93**, 196-204 (2015).

Chapter 4

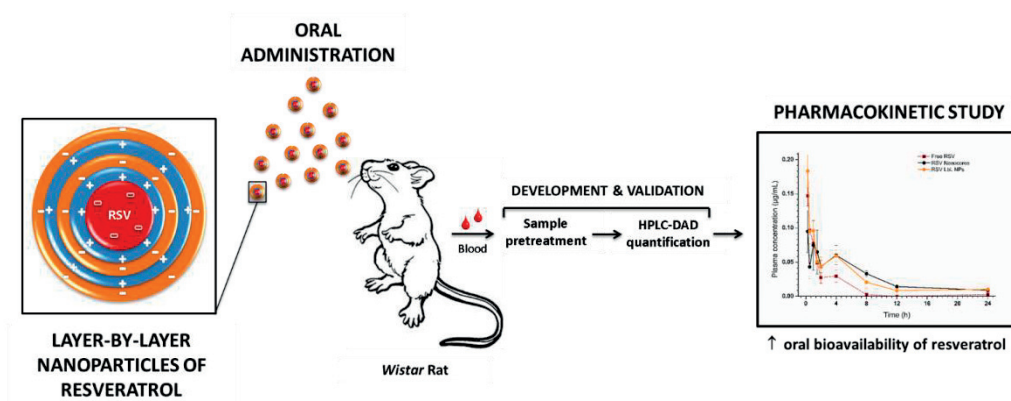
Pharmacokinetic applicability of a liquid chromatographic method for first-time orally administered resveratrol-loaded Layer-by-Layer nanoparticles to rats

4.1. Abstract

Resveratrol (RSV) is a plant-derived polyphenol endowed with a broad-spectrum of promising therapeutic activities. The applicability of RSV *in vivo* has, however, limited success so far, largely due to inefficient systemic delivery resulting from its low water solubility. Layer-by-Layer (LbL) nanotechnology constitutes an innovative formulation strategy to address this concern, which is based on the design of tunable onion-like multilayered nanoarchitectures upon the surface of low soluble drug nanocores, as RSV. The purpose of this study was the investigation of the bioavailability of a LbL nanoformulation composed of 5.5 bilayers of polyallylamine hydrochloride (PAH) and dextran sulfate (DS) (LbL nanoparticles (NPs)) by pharmacokinetic studies following oral dosing to *Wistar* rats (20 mg/kg). The systemic exposure of LbL NPs was compared to the respective nanoformulation without LbL coatings (RSV nanocores) and the free RSV suspension. Results demonstrated that both LbL NPs and RSV nanocores significantly enhanced, respectively, 1.76-fold and 2.74-fold the systemic exposure of RSV compared to free RSV suspension, emphasizing their biopharmaceutical advantage. Surprisingly, besides the modified drug release potential of the LbL NPs, those exhibited a slight lower systemic exposure (0.36-fold) in comparison to non-LbL modified RSV nanocores. Those results were justified to the sole composition of the LbL shell by electrostatic interactions, requiring further research towards the application of stronger interactions. For this study, due to the key role of the bioanalytical method in the *in vivo* data acquisition, a rapid, selective, and sensitive HPLC–DAD method has been successfully optimized and fully validated to confidently quantify RSV levels in rat plasma matrix, together with the optimization of the sample preparation procedure. Moreover, the chemical stability of RSV was assured for 24 h in simulated gastric and intestinal fluids with enzymes. Overall, our findings suggest that LbL NPs should be of great attention, representing a potential drug delivery system for RSV in the vanguard of the application of RSV not solely as a supplement but as a therapeutic drug.

Keywords: resveratrol; Layer-by-Layer self-assembly; nanoparticle; oral delivery; pharmacokinetic; validation; bioavailability; *in vivo*; rat; HPLC.

Graphical abstract



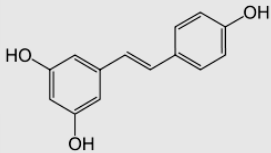
RSV-loaded LbL NPs to Wistar rats enhance, after oral administration, the bioavailability of RSV, which was investigated using an HPLC–DAD optimized and fully validated method.

[HPLC-DAD – high-performance liquid chromatography - diode array detection; LbL – Layer-by-Layer; NP – nanoparticle; RSV – resveratrol]

4.2. Introduction

Resveratrol (RSV), 3,5,4'-trihydroxystilbene, has attracted remarkable attention worldwide by scientists and health professionals over the past two decades (Santos, Veiga *et al.* 2011, Amri, Chaumeil *et al.* 2012, Bonkowski, Sinclair 2016). This compound is a naturally occurring polyphenol, more specifically a non-flavonoid stilbene, present in several higher plant species and especially abundant in the skin of red grapes and in *Polygonum cuspidatum*. The chemical structure and relevant characteristics of RSV are depicted in **Table 4.1**. RSV has been qualified as a phytoalexin, due to its particular feature of being synthesized by plants under environmental stress, as injury, fungal attack and UV irradiation. RSV exists as *cis* and *trans* structural isoforms, which exhibit significantly different activity profiles. The most abundant and commonly used isoform is *trans*-RSV, to which the major pharmacological activities are assigned (Santos, Veiga *et al.* 2011). A great body of evidence supports the variety of beneficial multi-target biological and pharmacological effects of *trans*-RSV, including anticancer activity (Rauf, Imran *et al.* 2016), cardioprotection (Sung, Byrne *et al.* 2017), neuroprotection (Ethemoglu, Seker *et al.* 2017), antidiabetic outcomes and sirtuin activation capacity (Bonkowski, Sinclair 2016), which are directly associated with its antioxidant and anti-inflammatory properties (Santos, Veiga *et al.* 2011). However, this promising dietary phytochemical shows instability in physiological media and it belongs additionally to the Biopharmaceutical Classification System (BCS) II class, exhibiting a poor physicochemical and biopharmaceutical profile, characterized by a low water solubility (Amri, Chaumeil *et al.* 2012). In addition to this concern, RSV suffers a large phase II metabolism in the gastrointestinal (GI) tract. Those characteristics are responsible for a dissolution-limited absorption and a low bioavailability *in vivo*, which largely compromise RSV demanded therapeutic activities as well as inherent clinical development (Santos, Veiga *et al.* 2011, Singh, Pai 2014a, Singh, Pai 2015). These aforementioned pharmacokinetic limitations of RSV call, thus, for the development of drug delivery systems capable of improving the pharmacokinetics profile, and, ultimately, enhancing its bioavailability *in vivo*. Innovative formulation strategies to tackle this challenge consist in the use of nanotechnology, which has been showing meritorious potentials, along which Layer-by-Layer (LbL) self-assembly nanoparticles (NPs) is hereinafter pointed out.

Table 4.1: Chemical structure and relevant physicochemical and biological properties characteristics of RSV to take into account while designing a drug delivery system.

| Resveratrol | | | |
|---|---------------------|--|-------------------------------------|
| Chemical structure | Characteristics | | References |
|  | CAS | 501-36-0 | (Amri, Chaumeil <i>et al.</i> 2012) |
| | Molecular formula | C ₁₄ H ₁₂ O ₃ | (Santos, Veiga <i>et al.</i> 2011) |
| | Melting point | 253 – 255 °C | (Amri, Chaumeil <i>et al.</i> 2012) |
| | logP _{o/w} | 3.1 | (Robinson, Mock <i>et al.</i> 2015) |
| | Water solubility | ca. 0.03 g/L “Practically insoluble” | (Amri, Chaumeil <i>et al.</i> 2012) |
| | pK _a 1 | 8.8 | (Robinson, Mock <i>et al.</i> 2015) |
| | pK _a 2 | 9.8 | |
| | pK _a 3 | 11.4 | |
| Plasma half-life | ca. 8 – 14 min | (Singh, Pai 2014b) | |

[CAS – chemical abstracts service registry number; logP_{o/w}, 1 – octanol/water partition coefficient; RSV – resveratrol]

LbL self-assembly consists in the sequential and hierarchically assembly of oppositely charged polyelectrolytes (PEs), established with nanometer scale precision, directly onto charged drug NPs surface (De Villiers, Otto *et al.* 2011, Polomska, Leroux *et al.* 2017). Modular nanocapsule-type structures arise from this technology, which consist, in essence, of a drug nanocore coated with a multilayered PE shell. Several distinct components may be included into a LbL construct, including synthetic PEs as poly(allylamine hydrochloride) (PAH), poly(styrene sulfonate) (PSS), poly(diallyldimethylammonium chloride) (PDDA), or naturally derived ones such as bovine serum albumin (BSA), protamine sulfate (PS), chitosan, alginate, poly-L-lysine (PLL), poly(ethylenimine) (PEI) and heparin (De Villiers, Otto *et al.* 2011, Lvov, Pattekari *et al.* 2011, Shutava, Pattekari *et al.* 2012, Santos, Pattekari *et al.* 2015). Each multilayer nanofilm contains a set number of PEs pairs or bilayers, which are driven mainly by electrostatic interactions (De Villiers, Otto *et al.* 2011). Owing to such versatility, LbL NPs are considered powerful platforms with recognized synergistic capacities, combining the successful encapsulation of low soluble drugs along with colloidal stability conferred by steric and electrostatic repulsions, as well as drug degradation prevention (Lvov, Pattekari *et al.* 2011, Shutava, Lvov 2012, Shutava, Pattekari *et al.* 2012, Polomska, Leroux *et al.* 2017). The tuned and thickness design of the LbL architecture

nanocoating shell enables additionally for the controlled release of low soluble drugs (Parekh, Pattekari *et al.* 2014, Santos, Pattekari *et al.* 2015, Polomska, Gauthier *et al.* 2017), presenting itself as a powerful tool for the increase of the *in vivo* bioavailability of this class of drugs, where RSV belongs. Herein, two different RSV-loaded nanoformulations were considered as vehicles for the oral administration of RSV. Those included LbL NPs composed of PAH as the polycation and dextran sulfate (DS) as the polyanion as PEs of the 5.5-bilayered LbL shell; and RSV-nanocores, i.e., simple RSV template NPs, without adsorbed LbL coatings. This multilayered 5.5-bilayered shell was obtained by a washless approach, by the use of sufficient PE concentrations for each coating layer, avoiding intermediate washings, as previously carried out in our recent work (Santos, Pattekari *et al.* 2015).

The objective of the present work was to investigate the bioavailability of RSV when encapsulated into LbL NPs and compare the outcomes with those obtained with simple RSV-nanocores after oral administration to *Wistar* rats. *In vivo* pharmacokinetic studies in *Wistar* rats were conducted by making use of a simple, sensitive and selective HPLC-DAD bioanalytical method for the determination of RSV in rat plasma matrix. This method has been successfully developed and fully validated, supporting a reliable and accurate assessment of the *in vivo* bioavailability of the NPs. Additionally, the present work included the performance of RSV stability studies under physiological GI conditions in order to mimic *in vivo* conditions and predict about RSV chemical stability. Hence, with this study, we aimed to understand deeply about the *in vivo* bioavailability of RSV promoted by its LbL NPs' encapsulation, in the light of the scarcity of studies available regarding the potential of this promising nanotechnology regarding *in vivo* oral administration.

4.3. Materials and methods

4.3.1. Materials

PAH (M_w ca. 15 kDa), DS (M_w ca. 5 kDa), poly(ethylene glycol) (PEG, M_w ca. 35 kDa) and carbamazepine, used as internal standard (IS) to determine RSV in plasma, were obtained from Sigma-Aldrich (Steinheim, Germany). RSV was purchased from Abatra Technology Co., Ltd. - Xi'an, China. Polyvinylpyrrolidone (PVP 17 PF, 7-11 kDa) was kindly supplied from BASF - The Chemical Company (Ludwigshafen, Germany) and sodium lauryl ether sulphate (Texapon® NSO, SLE₂S, 28% (w/w); Cognis) was provided by the Department of Chemistry of the University of Coimbra.

Methanol of HPLC grade was supplied by Chem-Lab NV (Zedelgem, Belgium). Acetonitrile of HPLC grade and acetic acid glacial were purchased from Carlo Erba, Reagents S.A.S. (Milan, Italy). Ethyl acetate and chloroform were obtained, respectively, from Fisher Scientific (Loughborough, UK) and Merck KGaA (Darmstadt, Germany), while *ortho*-phosphoric acid was acquired from Sigma-Aldrich (Steinheim, Germany). Potassium dihydrogen phosphate and dipotassium hydrogen phosphate trihydrate were purchased as well from Merck KGaA (Darmstadt, Germany). Extra pure acetone and hydrochloric acid 37% were obtained from Sharlau (Barcelona, Spain). Carboxymethylcellulose (CMC) sodium salt, used as the suspending RSV vehicle, was purchased from BDH Chemicals (Poole, UK). SnakeSkin™ Dialysis Tubing 3,500 molecular weight cut-off (MWCO) was purchased from ThermoFisher Scientific Inc. (Waltham, USA). Ultra-pure water (18.2 MΩ·cm at 25 °C) used was obtained from a Milli-Q ultra-pure water system from Millipore (Milford, MA, USA). All other reagents were of analytical grade and were used as received.

4.3.2. Methods

4.3.2.1. Resveratrol stability studies under physiological gastrointestinal conditions

4.3.2.1.1. Resveratrol solubility

Excess of RSV powder (4 mg) was added, separately, to 4 mL of simulated gastric fluid (SGF) and simulated intestinal fluid (SIF) with, respectively, pepsin and pancreatin enzymes (Portuguese Pharmacopoeia IX) into scintillation vials, and it was kept under magnetic stirring at 100 rpm for 24 h in a shaking water bath protected from light. After 12 h and 24 h, ca. 0.4 mL aliquots were collected and immediately centrifuged at 20000 g and 25 °C for 5 min (Centrifuge 5430 R,

Eppendorf, Hamburg, Germany). The supernatant was filtered through a 0.45 µm syringe filter (GHP Acrodisc, Pall Gelman Laboratory) to remove the excess of non-dissolved RSV. The solubility experiments were carried out in triplicate (n = 3). Filtered samples were assayed for RSV by HPLC after proper dilution in mobile phase.

The RSV assay was performed using a reversed-phase LiChrospher® 100 C₁₈ column, with 5 µm particle size, 3 mm internal diameter and 125 mm length, with a pre-column, acquired from MZ-Analysentechnik GmbH (Mainz, Germany). The analysis was carried out by a Shimadzu apparatus (Kyoto, Japan) equipped with a LC-20AD quaternary pump, a DGU-20A5 degasser unit, a SIL-20 AHT auto-sampler unit, a CTO-10AS oven and an UV/VIS photodiode array detector (SPD-M20A). Data acquisition and instrumentation control were enabled through the use of Shimadzu LC-solution version 1.25 software. The mobile phase mixture consisted of water at pH 2.5, adjusted with *ortho*-phosphoric acid (A) and methanol (B). The chromatographic separation was performed using a two-stage linear gradient: from 70% to 37% A in 10 min, and 3 min to achieve 70% A to restore the initial conditions. The total gradient run time was 13 min, with a flow rate of 1.0 mL/min, an injection volume of 20 µL and a temperature of 25 °C. Chromatographic separations were monitored at 306 nm. The mobile phase was filtered through a 0.45 µm filter and degassed ultrasonically for 30 min before use.

4.3.2.1.2. Chemical resveratrol stability

An aliquot of freshly prepared 1 mg/mL RSV stock solution was added to SGF and SIF in the presence of enzymes into scintillation vials to achieve a final concentration of 10 µg/mL. The mixtures were vortexed for 30 s, and vials were kept at 37 °C and 100 rpm in a shaking water bath restricted from light. Ca. 200 µL of sample aliquots were taken at multiple time points, accordingly to the *in vivo* study described below, specifically at 0.25, 0.5, 1, 1.5, 2, 4, 8, 12 and 24 h. Immediately following, samples were centrifuged at 20,000 g and 25 °C for 5 min and diluted properly in the mobile phase to be assayed by HPLC as described above. SGF and SIF solutions without RSV were used as blanks. Percentage stability was determined based on chromatographic peak area of the samples and that of 0 h (freshly prepared and injected) samples. A ratio range between stability and initial samples of 85-115% was undertaken as the stability criterion. Chromatograms were additionally analysed for the presence of extra peaks. Stability experiments were performed in triplicate (n = 3).

4.3.2.2. Formulation of Layer-by-Layer nanoparticles

Pure RSV powder was dissolved in extra pure acetone at 20 mg/mL. 60 μ L of this drug concentrated solution was added to an aqueous solution of 1 mg/mL PVP 17 PF and 0.005 mg/mL SLE₂S with pH 3.5, maintained under sonication by an ultrasound bath sonicator (Bandelin Sonorex Super; Bandelin, Berlin, Germany), for the obtainment of initial RSV nanocores. For the preparation of LbL-coated NPs, small aliquots of cationic PAH and anionic DS 1-4 mg/mL were added sequentially to RSV nanodispersion under constant sonication up to 5.5 bilayers deposition over the period of 20-50 min. The amount of PE needed to recharge and coat the surface of NPs was assessed for each layer assembly by PEs titrations achieved by a careful zeta-potential process monitoring (Santos, Pattekari *et al.* 2015). Zeta potential was measured by using electrophoretic light scattering (ELS) with a Zetasizer Nano ZS apparatus (Malvern Instruments Ltd.; Malvern, Worcestershire, UK). The samples were inserted in a folded capillary electrophoresis cell at pH 3.5. The same apparatus was also used to measure mean particle size and polydispersity index (PDI), which were monitored by dynamic light scattering (DLS) at a backscatter angle of 173°. All results were obtained by the mean of three measurements with automatic measurement duration at 25 °C.

4.3.2.3. Concentration of the Nanoparticles for *in vivo* administration

A volume equivalent to 10 batches of nanoformulations was sealed in a dialysis membrane bag (SnakeSkin™ Dialysis Tubing 3,500 molecular weight cut-off (MWCO)) and dialysed against a volume of 2 L of PEG solution at a high concentration of 20% (w/v) in water, at 2 – 8 °C. At the end of the dialysis, the concentrated nanodispersion was recovered from the dialysis bag and quantified. The final RSV concentration was assessed by HPLC, using the aforementioned chromatographic conditions, after sample extraction by dissolution in mobile phase mixture and appropriate dilution. In order to uniformize the RSV content of nanoformulations to 2 mg/mL, a proper dilution was ultimately applied using water pH 3.5. Each experiment was conducted in triplicate (n = 3).

Additional strategies were carried out towards the concentration of the nanoformulations, even though those were not considered for subsequent experiments. In this way, lyophilization was applied to obtain powdered samples, by freezing the aqueous nanoformulations at – 80 °C and lyophilizing in a freeze-dryer (Lyph-lock 6 apparatus, Labconco) for 24 h. The ultrafiltration-centrifugation approach was exploited as well through ultrafiltration-centrifugation devices, including Vivaspin® 2, 3 kDa MWCO, Sartorius, Germany; Vivaspin® 4, 10 kDa MWCO, Sartorius, Germany; and Amicon® Ultra-15, 50 kDa MWCO, Millipore, Germany. Nanoformulation samples

were placed into the sample compartment of each device, followed by application of variable centrifugation forces and time periods at 4 °C in order to concentrate suspensions as a consequence of the passage of water to the filtrate compartment.

4.3.2.4. Development and validation of the HPLC-DAD bioanalytical method

4.3.2.4.1. Preparation of stock solutions, calibration standards and quality control samples

An initial standard stock solution of RSV (1 mg/mL) was prepared by dissolving the suitable amount of this compound in mobile phase–methanol (67:33, v/v). This stock solution was properly diluted with mobile phase forthwith for the obtainment of the first intermediate solution of 200 µg/mL, which was ultimately diluted to obtain the last intermediate solution of 10 µg/mL. The latter intermediate solution was ultimately diluted to obtain six spiking working solutions with final concentrations of 0.20, 0.30, 0.50, 1.00, 2.00 and 5.00 µg/mL. Each of the previous working solutions was daily used for spiking blank rat plasma aiming the obtainment of six calibration standards in the following concentration range: 0.02 – 0.50 µg/mL.

Quality control (QC) samples at three representative concentration levels (low (QC1), medium (QC2) and high (QC3)) of the whole calibration range were independently prepared in the same biological matrix. To obtain these QCs, aliquots of blank rat plasma were spiked with QC1 (0.40 µg/mL), QC2 (1.50 µg/mL) and QC3 (4.50 µg/mL) spiking working solutions to obtain final plasma concentrations of 0.04, 0.15 and 0.45 µg/mL, respectively.

A stock initial solution of the IS was additionally prepared in methanol at 1 mg/mL, and it was properly diluted with mobile phase to prepare a spiking working solution of 100 µg/mL.

All stock and working spiking solutions were stored at 4 °C and restricted from light. For spiking purposes, 10 µL of each working solution (applicable both for RSV and IS) was used to spike each of the 100 µL aliquots of blank rat plasma.

4.3.2.4.2. Obtainment of blank rat plasma

For the obtainment of the blank rat plasma matrix required for the validation process, rats were anesthetized with inhaled isoflurane and, subsequently, decapitated. The blood samples were immediately collected into heparinized tubes. These blood samples were next centrifuged at 1514 g and 4 °C for 10 min to harvest the plasma supernatants, which were stored at -80 °C until

further use. All the animal experiments were carried out in conformity with the respective regulations, as exposed in the next section 4.2.2.5.1.

4.3.2.4.3. Sample preparation procedure

The optimized sample pre-treatment protocol was adapted from (Singh, Pai 2014) and comprised two consecutive main steps: protein precipitation and liquid-liquid extraction (LLE). After being thawed at room temperature, rat plasma samples were centrifuged at 20,000 g and 4 °C for 2 min to settle down possible matter in suspension. An aliquot of 100 µL of plasma was spiked with 10 µL of the corresponding spiking working RSV solution and with 10 µL of the spiking working IS solution (CBZ, 100 µg/mL) in a 1.5-mL tube. This mixture was vortexed for 1 min. Afterwards, the previous sample was acidified with 20 µL of 0.1 M HCl and vortexed for 15 s. Finally, 100 µL of acetonitrile was added, and the sample was vortexed for 1 min, in order to precipitate plasma proteins. After this, the tube was centrifuged at 20,000 g and 4° C for 20 min, to enable the LLE of the analyte and the IS, and the upper organic layer was cautiously transferred to a glass tube. The organic sample was evaporated to dryness under a gentle nitrogen stream at 50 °C for 15 min by using a sample concentrator (SBHCONC/1, Stuart, Staffs, UK). The obtained residue was further reconstituted with 100 µL of mobile phase. This sample was firstly vortexed for 1 min, next sonicated for 2 min, and ultimately centrifuged at 20,000 g and 4 °C for 10 min. At last, 40 µL of the obtained supernatant was injected into the chromatographic system.

4.3.2.4.4. HPLC-DAD instrumentation and analytical conditions

The chromatographic separation was conducted with the HPLC-DAD apparatus and software previously described in section 4.2.2.1.1. The optimized chromatographic separation of RSV and IS in plasma matrices was accomplished in 15 min at 30 °C on the reversed-phase LiChrospher® 100 C₁₈ column, described before as well. An isocratic elution mode was used at a constant flow rate of 1.0 mL/min with a mobile phase consisting of potassium dihydrogen phosphate buffer (adjusted to pH 3.8 with acetic acid 3%; 10 mM)–methanol–acetonitrile (60:35:5, v/v/v). The wavelength detection was set at 320 nm and an injection sample volume of 40 µL was used for all standards and samples. The mobile phase was filtered through a 0.45 µm filter and degassed ultrasonically for 30 min before being used.

4.3.2.4.5. Validation of the HPLC method

A full method validation was carried out in accordance with the international recommendations for bioanalytical method validation (US Food and Drug Administration 2001, European Medicines Agency 2011, US Food and Drug Administration 2013), just as on additional guiding principles (Shah, Midha *et al.* 2000, Nowatzke, Woolf 2007), with regard to the acceptance criteria established for selectivity, linearity, limits of quantification and detection, precision, accuracy, recovery and stability.

4.3.2.4.5.1. Selectivity

The method selectivity was assessed through the analysis of the potential chromatographic interference of matrix endogenous substances at the retention times of RSV and IS, using blank rat plasma samples obtained from six different subjects. To that end, blank samples resulting-chromatograms were compared with those acquired from samples spiked with RSV and IS.

4.3.2.4.5.2. Linearity

The method linearity was evaluated for RSV within the plasma concentration range of 0.02 – 0.50 µg/mL. Calibration curves were prepared using spiked plasma calibration standards at six different RSV concentrations levels, on five separate working days (n = 5). These calibration curves were obtained by plotting RSV-IS peak area ratio (y) versus the corresponding plasma nominal concentrations (x, µg/mL), fitted to $y = mx + c$ (regression linear model). Data were subjected to a weighted linear regression analysis using $1/x^2$ as weighting factor. The latter allowed for the best found linear fit, as indicated by the lowest value of the sum of the absolute percentage relative error generated by this model (Almeida, Castel-Branco *et al.* 2002).

4.3.2.4.5.3. Limits of quantification and detection

The limit of quantification (LOQ) of RSV was specified as the lowest standard concentration on the calibration curve capable of being determined with adequate precision (coefficient of variation (CV) ≤ 20%) and accuracy (bias within ± 20% - where bias is expressed as the percentage of deviation from nominal concentration). This concentration level was defined by both intra- and inter-daily analysis of plasma samples (n = 5), considering absolute deviations ≤ 20% for both CV and bias as acceptable values. The limit of detection (LOD) was defined as the concentration which yields a signal-to-noise ratio of 3:1. The procedure of LOD determination consisted in the analysis of spiked rat plasma samples with known concentrations following successive dilutions.

4.3.2.4.5.4. Precision and accuracy

Inter-day precision and accuracy were assessed by the analysis of QC samples (QC1, QC2 and QC3) on five consecutive days (n = 5), while the intra-day precision and accuracy were assessed by the investigation of five QC samples groups in just one day (n = 5). Precision was considered as acceptable for CV ≤ 15%, whereas accuracy was validated for bias ± 15%.

4.3.2.4.5.5. Recovery

The absolute recovery of RSV from rat plasma samples processed with the previously exposed sample preparation treatment was studied at the three considered QC samples concentration levels. These values were obtained in percentage by comparison between RSV-IS peak area ratio from treated QC plasma samples and the ratio resulting from direct injections of non-treated RSV and IS corresponding solutions at the same nominal concentrations (n = 5). Likewise, the same calculations were made regarding absolute recovery of IS between extracted samples and non-extracted solutions, using the same concentration level of that used in sample analysis.

4.3.2.4.5.6. Stability

RSV stability in rat plasma (including short-term, long-term, freeze-thaw cycles and post-preparative stabilities) was investigated using the low and high QC concentration levels (QC1 and QC3), comparing the recuperation of RSV obtained in samples analyzed before (reference samples) and those after being submitted to the stability analysis conditions (stability samples). A ratio range between stability and reference samples of 85-115% was assumed as the stability criterion (n = 5). Briefly, short-term and long-term stability were assessed at room temperature for 2 h and at -80 °C for up to 30 days, towards the simulation of sample handling and storage time of processed samples in the refrigerator and freezer prior to analysis, respectively (n = 5). The effect of three freeze-thaw cycles on the stability of RSV in rat plasma samples was evaluated as well. Aliquots of spiked plasma samples were stored at -80 °C for 24 h, thawed unassisted at room temperature and, after complete thawing, samples were refrozen anew using the same conditions until three cycles are complete. The post-preparative stability of RSV and IS on processed samples was additionally investigated, by submitting the reconstituted sample extracts under usual storage conditions before injection (4 °C for 8 h).

4.3.2.5. *In vivo* pharmacokinetic studies in rat

The *in vivo* study was performed to evaluate the impact of the nanoformulations in the bioavailability of resveratrol after oral administrations.

4.3.2.5.1. Animals

Healthy adult male *Wistar* Han rats (CrI:WI (Han) with 275-300 g were acquired from Charles River Laboratories (L'Arbresle, France). Animals were housed in local animal facilities under controlled environmental conditions (12 h light /dark cycle; temperature 22 ± 1 °C; relative humidity $50 \pm 5\%$), with access to pellet rodent diet and tap water *ad libitum* for 7 days before *in vivo* experiments began. All animal-involved experiments were premeditated and conducted with strict compliance to the international legislation of the European Directive 2010/63/EU (European Parliament and Council of the European Union, 2010), concerning the protection of animals used for scientific intentions. The applied experimental procedures were, in turn, reviewed by the Portuguese Veterinary General Division.

4.3.2.5.2. Pharmacokinetic study – oral administration

The pharmacokinetic study involved the administration of the considered formulations by the oral route. Rats were randomly distributed among four groups: group A (n = 3) received free RSV dispersed in 0.5% CMC (Das, Lin *et al.* 2008); group B (n = 5) received RSV nanocores; group C (n = 3) received RSV LbL-coated NPs; and group D (n = 2) received RSV LbL-coated NPs formulation excipients.

On the day before the study, rats were anesthetized with sodium pentobarbital intraperitoneal (60 mg/kg) to cannulate the lateral tail vein of each rat, by insertion of an Introcan Certo IV indwelling cannula (22 G; 0.9 x 2.5 mm). This procedure was conducted to allow the collection of serial blood samples. The animals were maintained in a heated environment to keep the body temperature and fully recovered from anesthesia overnight. These rats were fasted 12 h prior to administration, while water was allowed to drink freely. All the animals groups received an oral single dose equivalent to 20 mg of RSV per kg of animal weight (Singh, Pai 2014, Singh, Ahmad *et al.* 2016, Singh, Makadia *et al.* 2017) by a gavage needle at a level of 1 mL of RSV formulation per 100 g body weight (Mathot, Van Beijsterveldt *et al.* 2006). Serial blood samples of ca. 0.2 mL were withdrawn, via the cannula, into heparinized tubes at several pre-defined post-dose time points: 0.15, 0.5, 1, 1.5, 2, 4, 8, 12 and 24 h. Food access was allowed after 4 h post-dose. 0.5 mL heparin-saline (10 I.U./mL) was flushed slowly through the cannula after blood collection at 1.5 and 8 h post-dose to replace biological fluids. After collection, blood samples were immediately centrifuged at 1415 g and 4 °C for 10 min to harvest the plasma supernatants that were stored, ultimately, at deep freezer (–80 °C) until RSV extraction and HPLC-DAD analysis.

4.3.2.5.3. Pharmacokinetic analysis

The pharmacokinetic parameters maximum concentration of RSV in plasma (C_{\max}) and the corresponding time to achieve C_{\max} (t_{\max}) were recorded directly from the measured data. The remaining parameters were calculated by a non-compartmental pharmacokinetic analysis using the mean plasma concentration values ($n = 3-5$) determined for each time point, employing the Phoenix® WinNonlin® Version 6.4 software (Pharsight Co., Mountain View, CA, USA). The previous referred parameters consisted in: the plasma exposure (AUC), i.e., the area under the drug plasma concentration–time curve, which is determined from time zero to the last measurable drug concentration (AUC_{0-t}), that was calculated using the linear trapezoidal rule; the AUC from 0 h to infinity ($AUC_{0-\infty}$), which was calculated from $AUC_{0-t} + (C_{\text{last}}/k_{\text{el}})$, in which C_{last} consists in the last quantifiable drug plasma concentration and k_{el} (or k) pertains to the apparent elimination rate constant obtained by log–linear regression of the terminal segment of the drug plasma concentration–time profile; the percentage of AUC extrapolated from tlast to infinity [$AUC_{\text{extrap}}(\%)$], being tlast the time pertaining to the C_{last} ; the apparent terminal elimination half-life ($t_{1/2}$), and, at last, the mean residence time (MRT).

4.3.2.6. Statistical analysis

Statistical analysis was performed using SPSS Statistics version 21.0. In order to assess RSV stability under SGF and SIF with enzymes, the percentage of remaining drug for each time point was compared to a standardised value (115%) using one-sample t-test. Comparisons across time-points for each incubation medium were performed using Friedman’s non parametric test. Regarding the pharmacokinetics (PK) study, plasma concentrations between formulations were compared using Kruskal-Wallis’ non parametric test, with pairwise comparisons using Bonferroni correction. Comparisons across time-points for each formulation were performed using Friedman’s non parametric test. An analysis of variance (ANOVA) was used for the comparison of C_{\max} and $AUC_{0-\infty}$ between formulations. The test procedure was analogous to bioequivalence testing (conceptually). Following log-transformation of the data, the geometric mean ratio (GMR) and the corresponding 90% confidence intervals (CIs) were calculated. Comparison between formulations was done by the interpretation of the obtained GMR and the 90% CI (when the 90% CI did not include the unit, a statistical significant difference was assumed between formulations). The Kruskal-Wallis test was used to look for differences in t_{\max} between formulations.

4.4. Results and discussion

4.4.1. Resveratrol stability studies under physiological gastrointestinal conditions

Chemical stability of RSV under GI tract conditions was investigated by using SGF and SIF buffers in the presence of enzymes, pepsin and pancreatin, respectively. Samples were kept at 37 °C and under continuously stirring, as an attempt to mimic the physiological conditions (temperature and motility) found after *in vivo* oral administration. All experiments were additionally protected from light to avoid RSV photodegradation. In order to meet the aim, the solubility of RSV under the chosen conditions was firstly assessed to assure the complete dissolution of RSV under the performed conditions of the stability studies. This way, the determined solubility values for RSV in SGF and SIF with enzymes were $55.73 \pm 6.12 \mu\text{g/mL}$ and $57.57 \pm 1.46 \mu\text{g/mL}$, respectively. Reports exist in the literature regarding RSV solubility at different pH values (Li, Wegiel *et al.* 2013, Zupancic, Lavric *et al.* 2015). However, as far as we know, this is the first time the solubility of RSV is determined in the co-presence of these enzymes and without surfactants. No differences were effectively detected for RSV solubility values among the two studied media. Moreover, these values, along with the absence of differences in solubility among the media, were shown to be fairly similar to the ones obtained recently for the same pH values of buffered media (ca. $60 \mu\text{g/mL}$), but in the absence of enzymes (Zupancic, Lavric *et al.* 2015). This suggests, thus, that presence of enzymes do not influence the solubility of RSV.

Thereafter, the stability of RSV after 24 h under these aforementioned simulated physiological gastric and intestinal conditions was evaluated and the results are depicted in **Figure 4.1**. No statistical differences were detected between the reference RSV sample (which corresponds to zero time) and the samples incubated in SGF and SIF with enzymes during the 24 h study. All obtained values were maintained into the range criterion of 85-115%, revealing for no significant RSV degradation. These conclusions were experimentally supported by the same RSV chromatographic pattern, i.e., the same retention time, the absence of extra peaks in all the analyzed chromatograms, and the maintenance of 100% of the peak areas which accounted for the whole initial RSV quantity, confirming the RSV stability. A large body of evidence exists regarding the higher instability of RSV at higher pH values in contrast to its relative stability under acidic conditions (Trela, Waterhouse 1996, Robinson, Mock *et al.* 2015, Zupancic, Lavric *et al.* 2015). In fact, RSV degradation initiates to enhance exponentially for pH values above 6.8, but this behavior is described for longer time-periods, as a few days (Zupancic, Lavric *et al.* 2015), which were not achieved during our study, assuring thus the RSV chemical stability. These

studies confirmed, thus, the feasibility of further *in vivo* studies prosecution following the oral free- and formulated- RSV administration during a 24 h-time period.

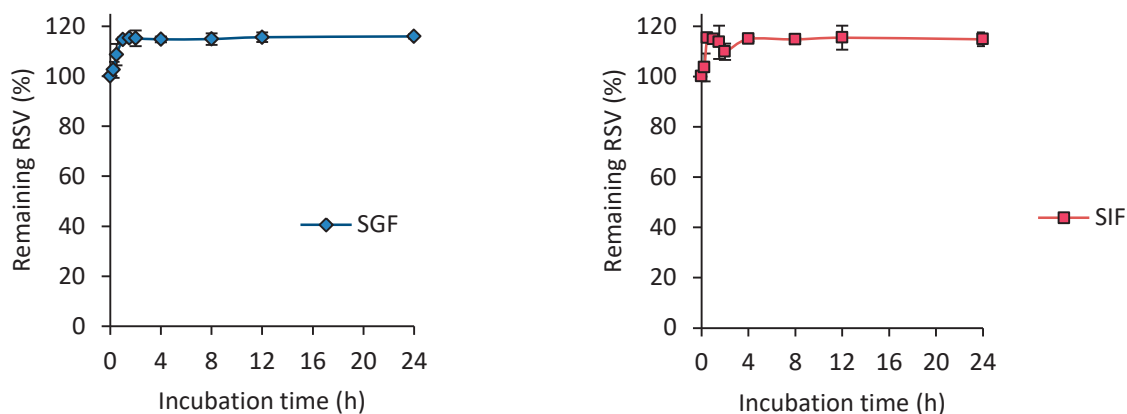


Figure 4.1: Chemical stability of RSV in SGF (a) and SIF (b) with enzymes at 37 °C. The levels of RSV were monitored up to 24 h under the previous conditions. Results are expressed as the percentage of initial RSV \pm SD (n = 3).

[RSV – resveratrol; SD – standard deviation; SGF – simulated gastric fluid; SIF – simulated intestinal fluid]

4.4.2. Optimization of the concentration of the nanoparticles for *in vivo* administration

The initial concentration of RSV in both nanoformulations was ca. 0.5 mg/mL. This concentration was found to be below the acceptable concentration range, facing the maximum volume possible to be administered orally to the animals (10 mL/kg) together with the required doses to reach quantifiable RSV plasma levels after *in vivo* oral administration (above 15 mg/kg) (Das, Lin *et al.* 2008, Singh, Pai 2014a, Singh, Pai 2014b, Singh, Pai 2014c, Penalva, Esparza *et al.* 2015 Singh, Ahmad *et al.* 2016). This critical concern imposed a concentration step of the considered nanosuspensions prior to *in vivo* administration, which was optimized regarding the closest maintenance to the initial exhibited characteristics of the NPs.

Several methods are described in the literature to concentrate NPs in water suspensions (Vauthier, Cabane *et al.* 2008). The first tested method consisted in lyophilization, a common used technological strategy for this purpose. However, this method was not considered for our studies, since both nanoformulations were shown to be not stable after water reconstitution, due to detected strong aggregation phenomena even in the presence of cryoprotectants (trehalose and mannitol). Thereby, our next attempts to concentrate the present nanosuspensions in a confined volume consisted in the use of ultrafiltration-centrifugation and dialysis methods.

The use of ultrafiltration-centrifugation devices (Vivaspin 4, 10 kDa MWCO, Sartorius) allowed for the ultrafiltration-centrifugation of the nanosuspensions. Significant deposition was verified initially upon the surface of the filter, which triggered the formation of compact nanosuspensions-based films when using higher centrifugation forces (4000 g). The recovery of these films by the addition of water for reconstitution was only partially successful, entailing for significant losses. Attempts were made to avoid this occurrence targeting a compromise between the reduction of the centrifugation force and the ultrafiltration-centrifugation time increase. However, not only it was not still possible to accomplish a fully nanosuspensions-based film redispersion, leading to large process losses; but also large aggregates were detected in the recovered nanosuspensions. The influence of a higher filter MWCO, more precisely by using a 50 kDa device, was additionally investigated, but great losses upon the filter still occurred, factors that eliminated this strategy as a valid option.

The third tested method consisted in the dialysis of the nanoformulations against a concentrated polymeric aqueous solution of PEG, the counter-dialysis medium. The initial characteristics of mean particle size, PDI and zeta-potential of LbL NPs were, respectively, 215.3 ± 2.3 nm, 0.122 and $+29.5 \pm 0.4$ mV; while the mean particle size, PDI and zeta potential of RSV nanocores were, respectively 115.7 ± 6.1 nm, 0.124 and -21.6 ± 0.4 mV. After the dialysis, a preservation of the particle size distributions (mean particle size, PDI and zeta-potential of concentrated LbL NPs, respectively, 243.5 ± 3.3 nm, 0.147 and $+26.4 \pm 0.4$ mV; mean particle size, PDI and zeta-potential of concentrated RSV nanocores, respectively, 135.7 ± 1.5 nm, 0.135 and -20.5 ± 0.071 mV) in relation to the initial non-concentrated nanoformulations was observed for the both cases. These results indicated for the maintenance of the characteristics of both nanoformulations at a higher concentration and, subsequently, for their colloidal stability. Thus, contrarily to the aforementioned concentration methods, dialysis was capable of avoiding aggregation phenomena. In fact, the application of an osmotic stress on nanoformulations triggered the displacement of the contained-dialysis bag water molecules towards the PEG-based outside counter-dialysis medium until equilibrium was attained from both sides of the dialysis membrane. This way, as the concentration process occurred near equilibrium, the aggregation phenomena were avoided. Our results were in agreement with previous reports, reinforcing the advantage of the dialysis particularly in the case of nanocapsules concentration, as like as the LbL NPs, considered as fragile structures (Vauthier, Cabane *et al.* 2008). Apart from these advantages, this method is fairly simple and does not demand for advanced equipment. The final RSV nanoformulations concentration was, this way, successfully increased 4-fold,

obtaining a final concentration around 2 mg/mL as pretended. The obtainment of this concentration enabled the administration of 20 mg/kg dose to the animals.

4.4.3. Development and validation of the HPLC-DAD bioanalytical method

4.4.3.1. Development and optimization of chromatographic method

Facing the stringent bioanalytical requirements necessary for pharmacokinetic studies, a chromatographic method was developed, optimized and ultimately fully validated. The main goal to be attained was to accurately quantify RSV, imposing, thus, the practical need to establish the best chromatographic conditions to achieve the best separation of RSV and the IS from rat plasma samples, whilst allowing for the lowest detection and quantification limits, by using low sample volumes, and during the shortest running time. Besides, the development of a straightforward HPLC method based on an isocratic elution was also desired.

Facing the complexity of the rat plasma matrix, a proper sample preparation procedure is demanded, and an IS is naturally required in order to minimize any differences resulting from that procedure. The selection of the adequate IS consisted in the test of some compounds including catechin, caffeine and carbamazepine. This latter was chosen as the IS as it exhibited the most appropriate retention time and it, as well, displayed chromatographic behavior and absolute recovery values close to those displayed by RSV.

In the early stages, used mobile phase conditions consisted on those used previously for additional quantifications related to procedures as the stability studies and the optimization of the NPs concentration, as described in section 4.2.2.1.1. This first mobile phase was constituted by a mixture of water pH 2.5, adjusted with *ortho*-phosphoric acid (A) and methanol (B). The inherent chromatographic separation was performed using a two-stage linear gradient during a total time of 13 min. A flow rate of 1.0 mL/min, an injection volume of 20 μ L and a temperature of 25 °C were used, and chromatographic separations were monitored at 306 nm. However, besides the presence of interfering plasma substances at the retention time of RSV, the obtained LOQ in plasma (1.25 μ g/mL) was found to be insufficient to *in vivo* quantification purposes. Regarding the available literature, the chromatographic conditions of Singh *et al.* (Singh, Pai 2014b) were adopted due to the lower reported LOQ. This mobile phase was constituted by a mixture of methanol – potassium dihydrogen phosphate buffer (adjusted to pH 3.8 with acetic acid 3%; 10 mM), 70:30 (v/v). Initial chromatographic conditions consisted in the use of a 1 mL/min constant flow rate in an isocratic mode, 20 μ L of injection volume, a temperature of

30 °C, and a detection wavelength of 306 nm. Very low values for the retention times of RSV and IS were obtained for these conditions 0 (<2.5 min), depicted in **Table 4.2**, however these coincided with the elution of the plasma interfering substances. The **Table 4.2** summarizes the characteristics of chromatographic RSV and IS peaks, including the retention times, areas, heights and tailing factors, which are graphically presented in **Figure 4.2**. The separation of these matrix substances from the analytes was achieved by the progressive reduction of the methanol proportion in the mobile phase (70% to 40%), corresponding to conditions 0 to 3, as depicted in **Figure 4.2**. As expected, when the proportion of the organic phase (methanol) decreased, the retention times were enhanced, together with consequent peak broadening and, thus, a reduction of peak areas and heights, in accordance with respective tailing factors above 1.4. So, the poor peaks resolution in regard to both shape and symmetry obtained by these conditions claimed for the incorporation of acetonitrile in the mixture.

Different proportions of methanol were, thus, investigated, maintaining acetonitrile at 5% in the mobile phase mixture, which correspond to conditions 4 to 9, in **Figure 4.2** and **Table 4.2**. Obtained results demonstrated that the presence of acetonitrile allowed for the obtainment of sharpened and symmetric peaks for both RSV and IS, while the reduction of the methanol proportion allowed the increase of their retention times and, thus, the full separation from the plasma interfering compounds. Conditions 6, also depicted in **Table 4.2**, were suggested initially to be the best option, since the transition to conditions 7 started to enhance excessively the retention times. However, in an attempt to better optimize the retention times of RSV between 4.9 min (conditions 6) and 8.8 min (conditions 7), additional factors were tested. This way, considering conditions 7, the proportion of acetonitrile (from 5 to 8%, respectively corresponding to conditions 10 and 11), and the effect of the enhancement of the run temperature (from 30 to 40 °C, respectively corresponding to conditions 10 and 11) were investigated. Under these four latter conditions, in fact, RSV and IS peaks exhibited higher resolution, evidenced by their relatively lower tailing factors, and had been approached in term of retention times, thereby shortening the run analysis. However, in comparison with conditions 7 (using 5% of acetonitrile and at 30 °C), these operating conditions represented a lower relationship between the resolution, peak shape and run time parameters, offering no significant advantages.

Therefore, due to the better compromise in relation to all the necessary chromatographic parameters, conditions 6, corresponding to a mixture of potassium dihydrogen phosphate buffer (adjusted to pH 3.8 with acetic acid 3%; 10 mM)–methanol–acetonitrile in the proportion of

60.35:5 (v/v/v), were selected as the optimal mobile phase mixture. The analysis was performed at 30 °C and the flow rate was maintained at 1 mL/min, as it allowed the good compromise between the chromatographic separation and the areas, heights and peak tailing factors of RSV and IS. These analytical conditions allowed the elution of RSV at 4.9 min, being the IS the last-eluting compound, with a retention time of ca. 12 min, accomplished in a run time of 15 min (Figure 4.2).

Table 4.2: Values of R_t , area, height, and T_f for each chromatogram of RSV (20 µg/mL) and IS (20 µg/mL), by using different mobile phase compositions (methanol – potassium dihydrogen phosphate buffer (adjusted to pH 3.8 with acetic acid 3%; 10 mM) – acetonitrile (v/v/v)).

| Conditions | Mobile phase composition (methanol / buffer solution* / acetonitrile (v/v/v)) | RSV R_t (min) | RSV Area | RSV Height | RSV T_f^{**} | IS R_t (min) | IS Area | IS Height | IS T_f^{**} |
|------------|---|-----------------|----------|------------|----------------|----------------|---------|-----------|---------------|
| 0 | 70:30:0 | 1.4 | 5997398 | 752445 | 1.48 | 2.2 | 1163880 | 108751 | 1.41 |
| 1 | 50:50:0 | 2.7 | 5766867 | 364955 | 1.53 | 6.4 | 1151557 | 40556 | 1.42 |
| 2 | 45:55:0 | 4.0 | 5746257 | 249257 | 1.42 | 10.6 | 1142784 | 24956 | 1.40 |
| 3 | 40:60:0 | 6.3 | 5722028 | 168824 | 1.45 | 15.9 | 1131982 | 21027 | 1.41 |
| 4 | 45:50:5 | 2.9 | 6791562 | 412469 | 1.49 | 6.7 | 1336096 | 47400 | 1.36 |
| 5 | 40:55:5 | 4.4 | 7764046 | 306504 | 1.44 | 9.9 | 1522755 | 32094 | 1.40 |
| 6 | 35:60:5 | 4.9 | 5661522 | 202280 | 1.37 | 12.2 | 1139082 | 19271 | 1.33 |
| 7 | 30:65:5 | 8.8 | 5647810 | 125915 | 1.28 | 24.5 | 1129823 | 11360 | 1.26 |
| 8 | 28:67:5 | 10.9 | 5650399 | 105368 | 1.28 | 30.6 | 1120091 | 9314 | 1.28 |
| 9 | 25:70:5 | 16.0 | 5644327 | 76488 | 1.33 | 44.7 | 1099873 | 6590 | 1.34 |
| 10 | 30:64:6 | 7.6 | 5605839 | 140362 | 1.23 | 20.9 | 1114885 | 12556 | 1.19 |
| 11 | 30:62:8 | 5.8 | 5605281 | 181556 | 1.25 | 15.7 | 1126196 | 16903 | 1.19 |
| 12 | 30:65:5 (40 °C) | 6.4 | 5611787 | 168646 | 1.28 | 19.7 | 1118769 | 14479 | 1.22 |
| 13 | 30:64:6 (40 °C) | 5.6 | 5608275 | 189575 | 1.24 | 17.1 | 1079413 | 15660 | 1.18 |

* Potassium dihydrogen phosphate buffer (adjusted to pH 3.8 with acetic acid 3%; 10 mM).

** Calculated as the ratio between W and $2f$ (W is the peak width at 5% of the peak height; f is the distance between the maximum and the leading edge of the peak).

[IS – internal standard; RSV – resveratrol; R_t – retention time; SD – standard deviation; SGF – simulated gastric fluid; SIF – simulated intestinal fluid; T_f – tailing factor]

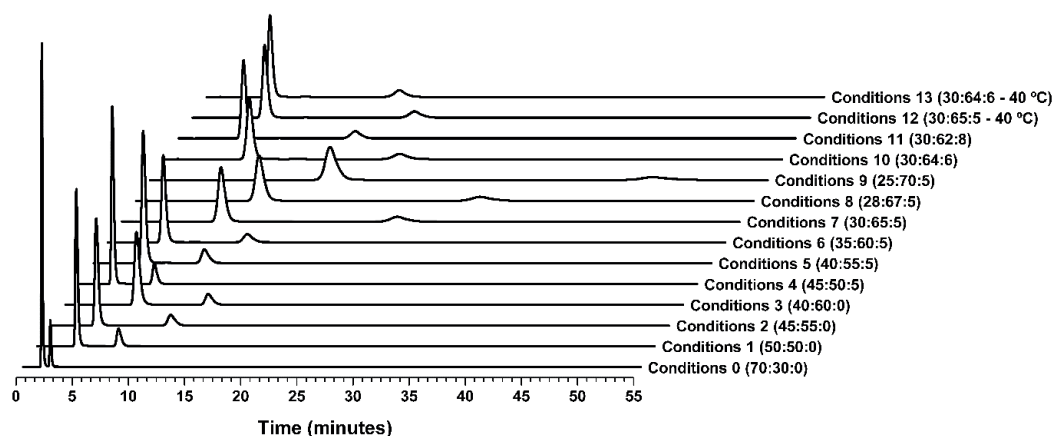


Figure 4.2: Chromatograms of RSV and IS, respectively, from left to right, both at 20 µg/mL, resulting from the use of different mobile phase mixture compositions, containing methanol – potassium dihydrogen phosphate buffer (adjusted to pH 3.8 with acetic acid 3%; 10 mM) – acetonitrile, (v/v/v).

[IS – internal standard; RSV – resveratrol]

4.4.3.2. Sample preparation procedure

The use of a sample preparation procedure is imperative for plasma-derived *in vivo* samples in order to provide a suitable sample for HPLC analysis. Considering the required multiple blood samples collection within marked short time-intervals associated with the present *in vivo* study, limited available blood sample volumes for analysis was forcefully implicit. This constraint called for the development of a simple sample preparation procedure with the minimal sample treatment.

The first aim of this procedure optimization was to maximize the removal of matrix endogenous substances and the extraction of RSV and IS from the plasma samples. A simple and rapid protein precipitation followed LLE procedure was adopted. Protein precipitation was firstly performed to eliminate RSV plasma protein binding, in the face of its high propensity (98%) for this occurrence (Robinson, Mock *et al.* 2015). LLE was simultaneously applied for the extraction and isolation of RSV and IS from the plasma matrix to the organic phase. The latter was selected as it offers several noteworthy gains over to additional extraction procedures, namely its simplicity, high extraction efficiencies and recoveries, less time-consuming, lower associated costs and small required sample volumes (Ramalingam, Ko 2016).

The sample preparation procedure is dictated not only by the analytical method but also by the characteristics of the analyte(s). Thus, distinct types and proportions of organic solvents were evaluated, including acetonitrile, chloroform and ethyl acetate. The use of chloroform or ethyl acetate was not favorable due to the need of multiple steps of LLE extraction and the need of

higher organic solvents volumes. Moreover, in particular for the use of chloroform, apart from its toxicity, additional handling difficulties arose due to its higher density in comparison to water. This way, acetonitrile yielded the higher recovery values, both for RSV and IS, like reported by (Singh, Pai 2014b). In addition, some adaptations were made to improve the efficiency of the extraction and recovery procedure. Firstly, significant gains in RSV recovery were pinpointed when vortexing was carried out immediately after the working solution spiking plasma procedure in comparison to the absence of this step. A vortexing step was thus implemented for 1 min after both RSV and IS plasma spiking, significantly favoring the dissolution of RSV in the plasma matrix.

The influence of the pH was additionally evaluated by the addition of phosphate buffered solution (PBS) pH 6 and 7.4, potassium hydroxide (KOH) 0.2 M or hydrochloric acid (HCl) at both 10 and 20% (w/v). The acidification of the sample mixture, by the use of 20% HCl by a single addition, was shown to promote the best recovery values. In essence, at acidic pH, the weak acid RSV molecule lies in its non-ionized form, resulting in the enhancement of the extraction of RSV in the organic phase. Thereafter, the detection wavelength value was optimized as well in view of minimizing the plasma endogenous interferences eluted close to RSV retention time while assuring for sufficient signal intensity. The value of 306 nm was chosen initially due to the maximum absorption peak for RSV at this wavelength. However, the UV screening spectra revealed that the closest eluted interferences to the RSV peak were not detected at 320 nm. Moreover, the IS showed higher absorbance at this wavelength value, without no significant impact in terms of RSV absorbance. In view of these test results, 320 nm was selected, thus, for the analysis due to the best compromise achieved regarding sensitivity and selectivity. The injection volume was tested as well in order to improve the sensitivity. Injection volumes of 20 and 40 μ L were evaluated, allowing a signal area enhancement of ca. 2-fold for the latter, as expected. The injection volume selected was, thus, 40 μ L, promoting an enhancement of the method sensitivity.

Therefore, as a result of these investigations, a single-step of plasma protein precipitation and LLE by using just acetonitrile as the organic phase has been successfully applied, avoiding the use of additional expensive approaches, as, e.g., the solid-phase extraction.

4.4.3.3. Validation

A thorough and complete validation of the assay method for RSV was performed in rat plasma in order to enhance the method confidence facing its applicability in further PK studies.

4.4.3.3.1. Specificity, calibration, linearity, LOQ and LOD

The chromatographic separation of RSV and carbamazepine, used as the IS, in spiked rat plasma samples was successfully attained by using the abovementioned chromatographic protocol. Using this protocol, RSV eluted after 4.9 min and IS after 12.2 min. Representative chromatograms of blank and spiked rat plasma samples are presented in **Figure 4.3**.

The selectivity of the protocol in plasma was assessed and confirmed using the previously referred sample pre-treatment protocol and chromatographic conditions. The analysis of blank plasma from six different rats demonstrated the absence of interfering peaks from matrix endogenous compounds located at the retention times of RSV and IS, thereby confirming that the method is specific.

The present method demonstrated linearity over the defined concentration range (0.02 – 0.50 µg/mL), along with a consistent correlation ($r^2 = 0.997$) between peak area ratios (RSV/IS) and the corresponding plasma concentrations (**Table 4.3**).

Data of intra- and inter-day accuracy and precision assessment are depicted in **Table 4.4**. The LOQ was experimentally set at 0.02 µg/mL for RSV with a substantial precision ($CV \leq 7.73\%$) and accuracy (bias ranged between 0.85 and 1.61). The LOD was defined at the concentration 0.015 µg/mL.

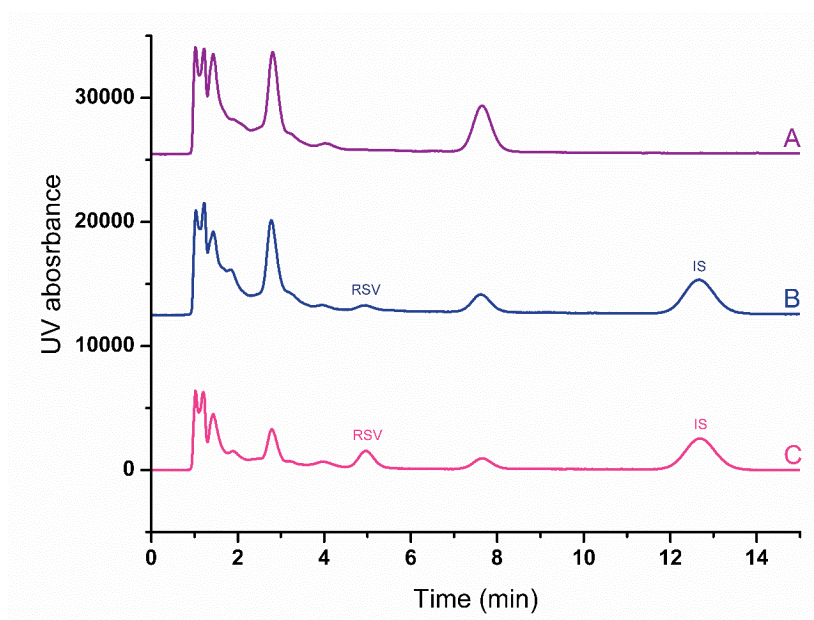


Figure 4.3: Typical chromatograms of extracted rat plasma: **(A)** blank plasma; **(B)** plasma spiked with the IS and analyte RSV at LOQ concentration; **(C)** plasma spiked with IS and the analyte RSV at the intermediate concentration of the calibration range.

[IS – internal standard; LOQ – limit of quantification; RSV – resveratrol]

Table 4.3: Calibration parameters (mean values) of the developed HPLC-DAD method employed for the quantification of RSV in rat plasma.

| CALIBRATION PARAMETERS | | | |
|------------------------|-----------------------------|------------------------|-------|
| Analyte | Concentration range (µg/mL) | Regression Equation* | r^2 |
| RSV | 0.02 – 0.50 | $y = 2.1412x - 0.0122$ | 0.997 |

* Regression equation is given by $y = mx + b$, where y represents RSV-IS peak ratio (expressed in arbitrary area units); x represents analyte concentration (expressed in µg/mL), $n = 5$.

r^2 , coefficient of determination.

[HPLC-DAD – high-performance liquid chromatography - diode array detection; RSV – resveratrol]

Table 4.4: Inter- and intra-day precision (% CV) and accuracy (% Bias) of RSV in rat plasma samples at the LOQ, low (QC1), medium (QC2) and high (QC3) concentrations of the calibration ranges.

| LOQ, QC1, QC2 and QC3 samples | | | | | | | | |
|-------------------------------|--------|-------------------------------|-------------------------------------|-------|--------|-------------------------------------|------|--------|
| | | | Inter-day | | | Intra-day | | |
| Analyte | Sample | Nominal concentration (µg/mL) | Experimental concentration* (µg/mL) | % CV | % Bias | Experimental concentration* (µg/mL) | % CV | % Bias |
| RSV | LOQ | 0.02 | 0.020 ± 0.002 | 7.73 | 1.61 | 0.020 ± 0.003 | 2.66 | 0.85 |
| | QC1 | 0.04 | 0.043 ± 0.004 | 10.29 | 8.14 | 0.036 ± 0.003 | 8.98 | -9.46 |
| | QC2 | 0.15 | 0.146 ± 0.011 | 7.76 | -2.56 | 0.130 ± 0.007 | 6.04 | -13.13 |
| | QC3 | 0.45 | 0.432 ± 0.022 | 5.36 | -4.07 | 0.434 ± 0.007 | 1.66 | -3.47 |

* Mean ± SD, $n = 5$.

[Bias – deviation from nominal value; CV – coefficient of variation; LOQ - limit of quantification; QC1 – low quality control; QC2 – medium quality control; QC3 – high quality control; RSV – resveratrol; SD – standard deviation]

4.4.3.3.2. Precision and accuracy

The data of intra- and inter-day accuracy (bias) obtained from the three QC samples were comprised in the interval -13.13% and 8.14%, and the precision levels (CV) were below 10.29%. All the obtained results (LOQ and the three concentration investigated levels) fulfilled the acceptance criteria of the aforementioned guidelines, since neither CV nor bias surpassed 15% values, according to the recommendations. This way, these results attest clearly the accuracy, precision and reproducibility of the sample pre-treatment and the HPLC-DAD applied and developed protocols.

4.4.3.3.3. Recovery and matrix effects

The data related to the determined overall absolute recoveries of the three QC considered levels related to the methods developed herein are depicted in **Table 4.5**. These values ranged from 92.72% to 104.47%, and CV values were lower than 10.92%. The mean recovery of the IS in plasma was 79.13% and the CV was found to be 4.50% (n = 15). The obtained high percentages of recovery together with the low CV values definitely prove that the sample pre-treatment and the following HPLC-DAD applied methods exhibit consistency, precision and reproducibility. We developed and validated, thus, a method with high recovery RSV yields (> 92.72%), even in the presence of a LLE protocol, which is often related to the obtainment of lower recovery values (Goncalves, Alves *et al.* 2016).

Table 4.5: Absolute recovery of RSV from rat plasma using the optimized sample pre-treatment and extraction protocol, by using the low (QC1), medium (QC2) and high (QC3) concentrations of the calibration ranges.

| Absolute recovery | | | | |
|-------------------|--------|---|------------------------|------------------|
| Analyte | Sample | Nominal concentration ($\mu\text{g}/\text{mL}$) | Absolute recovery* (%) | Precision (% CV) |
| RSV | QC1 | 0.04 | 104.47 \pm 11.41 | 10.92 |
| | QC2 | 0.15 | 92.72 \pm 4.12 | 4.44 |
| | QC3 | 0.45 | 102.66 \pm 4.00 | 3.89 |

* Mean \pm SD, n = 5.

[CV – coefficient of variation; QC1 – low quality control; QC2 – medium quality control; QC3 – high quality control; RSV – resveratrol; SD – standard deviation]

4.4.3.3.4. Stability

The stability of RSV was studied for the low and the high QC levels under the aforementioned conditions (section 4.2.2.4.5.6), which were set according to the feasible conditions to be met during the analytical processing and sample storage. The obtained data are present in **Table 4.6**. As it is possible to infer, RSV was demonstrated to be stable in unprocessed plasma samples for up to 2 h at room temperature, for 1 month at $-80\text{ }^{\circ}\text{C}$ and after the processing of three freeze-thaw cycles. The stability of RSV in mobile phase was also demonstrated for up to 8 h at $4\text{ }^{\circ}\text{C}$. Thereby, no significant RSV degradation took place under the performed conditions both in unprocessed and in processed plasma samples.

Table 4.6: Stability (values in percentage) of RSV under different conditions of sample handling and storage.

| Stability conditions | | | | | | |
|----------------------|--------|-------------------------------|-----------------------|------------------|----------------------------|--------------|
| | | | Rat plasma | | | Mobile phase |
| Analyte | Sample | Nominal concentration (µg/mL) | Room temperature, 2 h | - 80 °C, 30 days | Freeze/thaw (three cycles) | 4 °C, 8 h |
| RSV | QC1 | 0.04 | 89.47 | 97.56 | 87.87 | 87.62 |
| | QC3 | 0.45 | 95.98 | 86.46 | 92.61 | 93.35 |

n = 5.

[QC1 – low quality control; QC3 – high quality control; RSV – resveratrol]

4.4.4. Evaluation of the bioavailability of nanoparticles – pharmacokinetic study

This work was carried out to investigate and compare plasma PK and disposition of RSV arising out of the administration of a single oral dose of free RSV suspension, RSV nanocores and RSV LbL NPs (comprising 5.5 bilayers of PEs) to *Wistar* rats, in order to infer about the potential role of the LbL nanotechnology in the bioavailability of RSV. Representative chromatograms are shown in **Figure 4.4**.

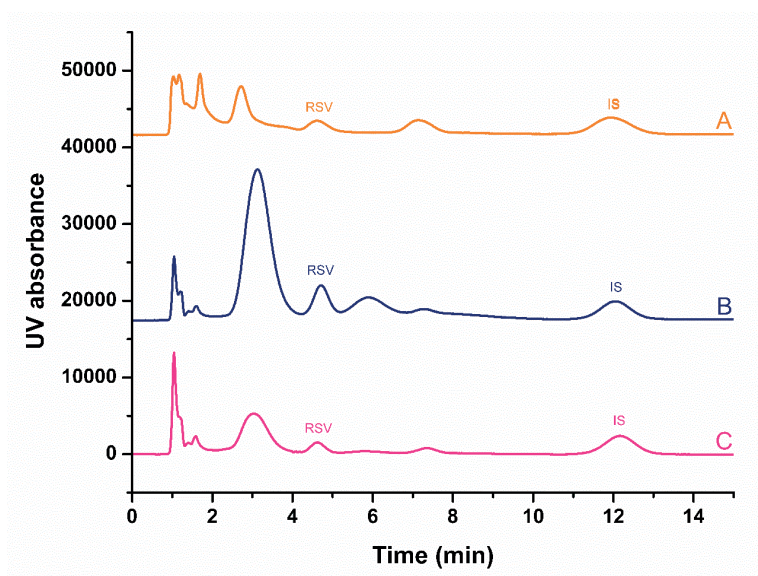


Figure 4.4: Representative chromatograms of plasma samples obtained from rats treated with: **(A)** free RSV; **(B)** RSV nanocores and **(C)** RSV-loaded LbL NPs after oral administration.

[IS – internal standard; LbL – Layer-by-Layer; NP – nanoparticle; RSV – resveratrol]

The rat was selected as the animal model to perform these studies not only because of the reduced involved costs and the convenience of handling, but also because it has been frequently employed to examine the PK of RSV over the last years (Das, Lin *et al.* 2008, Frozza, Bernardi *et al.* 2010, Jose, Anju *et al.* 2014, Penalva, Esparza *et al.* 2015, Zhou, Zhou *et al.* 2015, Singh, Ahmad *et al.* 2016, Zu, Zhang *et al.* 2016). In addition, the dose of 20 mg/kg was considered as adequate on the basis of reported doses ranges in the literature concerning RSV-loaded NPs administered by the oral route (Das, Lin *et al.* 2008, Singh, Pai 2014b, Penalva, Esparza *et al.* 2015, Singh, Pai 2015, Singh, Ahmad *et al.* 2016).

The obtained concentration-time profiles of RSV, the corresponding calculated PK parameters, as well as the comparative analysis of PK parameters are illustrated in **Figure 4.5**, **Table 4.7** and **Table 4.8**, respectively. The free RSV suspension was used as a control to compare PK behavior and parameters with that of the two studied nanoformulations.

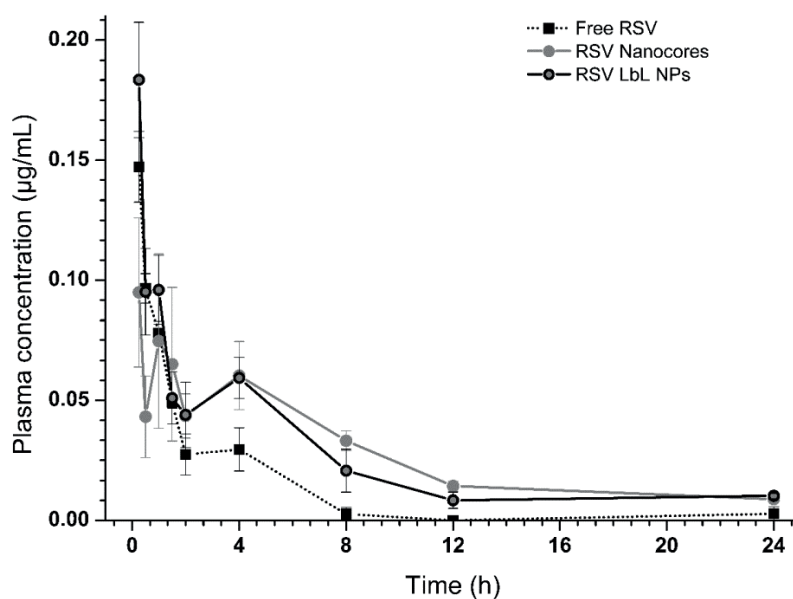


Figure 4.5: Concentration-time profiles of RSV following oral free RSV (■), nanocores (●) and RSV LbL NPs (●) administration (20 mg/kg) to rats. Symbols represent the mean values \pm S.E.M. of three to five determinations per time point ($n = 3-5$).

[LbL – Layer-by-Layer; NP – nanoparticle; RSV – resveratrol; S.E.M. – standard error of the mean]

Table 4.7: Mean pharmacokinetic parameters of RSV in plasma after single oral administration of free RSV suspension, nanocores and LbL NPs to rats in the dose of 20 mg/kg.

| Oral Administration | | | |
|-----------------------------|---------------------|------------------|------------------|
| Pharmacokinetic parameters* | Free RSV suspension | Nanocores | LbL NPs |
| t_{max} (h) | 0.25 (0.25-0.25) | 1.00 (0.25-4.00) | 0.25 (0.25-0.25) |
| C_{max} (ng/mL) | 147.33 ± 25.81 | 109.40 ± 50.73 | 183.50 ± 41.91 |
| AUC_{0-t} (ng.h/mL) | 224.67 ± 59.97 | 625.00 ± 185.29 | 607.00 ± 172.05 |
| $AUC_{0-\infty}$ (ng.h/mL) | 250.67 ± 66.04 | 711.60 ± 182.94 | 652.50 ± 181.72 |
| AUC_{extrap} (%) | 10.11 ± 6.32 | 12.96 ± 6.04 | 7.04 ± 1.06 |
| k_e (h ⁻¹) | 0.83 ± 0.48 | 0.11 ± 0.05 | 0.23 ± 0.03 |
| $t_{1/2}$ (h) | 1.17 ± 0.90 | 6.99 ± 2.41 | 3.12 ± 0.40 |
| MRT (h) | 1.79 ± 0.81 | 7.75 ± 0.99 | 6.82 ± 0.24 |

*Parameters values are expressed as mean ± SD, except t_{max} values which are expressed as median (range). These parameters were estimated using the mean concentration-time curves obtained from three to five different animals per time point (n = 3-5).

[AUC_{0-t} – area under the concentration time-curve from time zero to the last measurable drug concentration; $AUC_{0-\infty}$ – area under the concentration time-curve from time zero to infinity; AUC_{extrap} – area under the concentration time-curve extrapolated from the time of the last measurable concentration to infinity; C_{max} – maximum concentration; k_e – apparent elimination rate constant; LbL – Layer-by-Layer; RSV – resveratrol; SD – standard deviation; t_{max} – time to achieve the maximum concentration; $t_{1/2}$ – apparent terminal elimination half-life; MRT – mean residence time; NP – nanoparticle]

Table 4.8: Point estimates and 90% confidence intervals for the comparison of the calculated pharmacokinetic parameters evaluated for the studied formulations (free RSV, nanocores and LbL NPs) administered to the animals.

| Comparison | C_{max} Point estimate (90%CI) | $AUC_{0-\infty}$ Point estimate (90%CI) |
|---------------------------------|-------------------------------------|--|
| Nanocores / Free RSV suspension | 0.93 (0.51 ; 1.69) | 2.74 (1.74 ; 4.32) |
| LbL NPs / Free RSV suspension | 1.09 (0.60 ; 1.99) | 1.76 (1.12 ; 2.78) |
| LbL NPs/Nanocores | 1.17 (0.68 ; 2.01) | 0.64 (0.42 ; 0.96) |

[$AUC_{0-\infty}$ – area under the concentration time-curve from time zero to infinity; CI – confidence interval; C_{max} – maximum concentration; LbL – Layer-by-Layer; NP – nanoparticle; RSV – resveratrol]

Regarding the administration of free RSV, as expected, quantifiable concentrations were detected just within the first 4 h. These values are in accordance with the literature, and clearly reveal the scarce bioavailability of free RSV suspension after oral administration. This result has been pointing towards the occurrence of an incomplete RSV oral absorption in rats (Penalva, Esparza *et al.* 2015, Singh, Pai 2015). Moreover, the low oral bioavailability of RSV is additionally attributed not only to the slower and partial dissolution of RSV in the GI tract (Amri, Chaumeil *et al.* 2012), which is characteristic of BCS class II drugs (Singh, Pai 2014b), but also due to a higher hepatic metabolization (forming RSV-glucuronides and RSV-sulfates) (Santos, Veiga *et al.* 2011, Amri, Chaumeil *et al.* 2012) and the passage to the enterohepatic circulation (Singh, Pai 2014b). In fact, as may be seen in all the three investigated concentration-time profiles herein, a first peak appears at 1 h, followed by a second peak at 4 h post-dosing. This behavior is due to the occurrence of the previously referred and well documented first-pass effect and enterohepatic circulation suffered by RSV after oral administration. Such a process consists in the reabsorption of a major part of secreted bile acids by the intestine, which returns to the liver via the portal circulation and so forth (Santos, Veiga *et al.* 2011, Singh, Pai 2014b). RSV and its conjugated metabolites undergo the first-pass metabolism and pass through the enterohepatic circulation, coming out in a plasma concentration-time profile with multiple peaks (Wenzel, Soldo *et al.* 2005, Singh, Pai 2015).

As far as the nanoformulations are concerned, it is worth noting that the systemic exposures of RSV after their oral administration were significantly higher in relation to the administration of free RSV suspension to rats. The $AUC_{0-\infty}$ of free RSV suspension, LbL NPs and nanocores was, respectively, 250.67 ± 66.04 , 652.50 ± 181.72 and 711.60 ± 182.94 ng.h/mL (**Table 4.7**), accounting for, respectively, 1.76-fold and 2.74-fold higher systemic exposure of RSV when technologically modified and administered in the form of LbL NPs and nanocores in relation to free RSV suspension (**Table 4.8**). These results reveal a remarkable improvement of the bioavailability of RSV. The examination of **Table 4.7** additionally displays that the oral administration of free RSV suspension resulted in an initial C_{max} of 147.33 ± 25.81 ng/mL at 0.25 h (t_{max}), which declined rapidly, as it is possible to see in **Figure 4.5**. In fact, even though no significant differences were found for the values of t_{max} and C_{max} among administered formulations, including free RSV suspension, it is noteworthy to pinpoint the notorious enhancement of the bioavailability extent of RSV provided by the nanoformulations, emphasizing their biopharmaceutical superiority. These results are consistent with our *in vitro* drug release experiments under SGF and SIF conditions using a model BCS II drug, which had predicted a higher dissolution rate for the nanoformulations in relation to the free drug

suspension and, thereby, had been quite indicative of their higher bioavailability potential (Santos, Pattekari *et al.* 2015). This performance is owed to the combined result of several factors. Firstly, both nanoformulations promoted an enhancement of the water solubility of RSV (Santos, Pattekari *et al.* 2015). Second, nanoformulations were shown to be stable in the stomach, maintaining the incorporation of RSV within the nanoformulations until reaching the intestine (Davidov-Pardo, Perez-Ciordia *et al.* 2015). Owing to such, the bioaccessibility of RSV (i.e., the available quantity of RSV for absorption in the intestine) has been improved, contributing, thus, for higher bioavailability. In addition to these gains, the small particle size of these formulations at nanoscale was indubitably a key technological factor, responsible for a large interfacial surface area and a reduced diffusion layer thickness, which lead to an improved dissolution in the GI tract, and thus to an improved diffusion across the membrane (Santos, Pattekari *et al.* 2015) which ultimately improved the systemic exposure of RSV. Additionally, this improvement of the bioavailability of the RSV is also pointed to an enhancement of the absorption rate promoted by the use of both nanoformulations. This assumption arises from similar results of enhanced bioavailability obtained for additional colloidal carriers, in which several methods of nanoencapsulation were shown to promote an absorption improvement of RSV, the attributed key factor to achieve this outcome. Poly(lactic-co-glycolic acid) (PLGA) NPs, prepared also by nanoprecipitation (Singh, Pai 2014b), and self-nanoemulsifying drug delivery systems (Singh, Pai 2015) accounted for a significant enhancement in the rate and extent of the bioavailability of RSV. These data were correlated to a detected increase in the absorptivity and permeability of those NPs via the Peyer's patches, evaluated through an *in situ* single-pass intestinal perfusion model in rats. Even more recently, *ex vivo* permeation studies conducted with an Ussing chamber model with rat intestinal epithelium corroborated the aforementioned findings, by the obtainment of higher intestinal permeation absorptive fluxes of RSV arising out of the use of self-nanoemulsifying drug delivery systems. The authors attributed the mechanism underlying the enhanced RSV permeation of the nanoformulations could be quite similar to the specific case of polymeric NPs (Mamadou, Charrueau *et al.* 2017), such as the present LbL NPs.

The structures of LbL NPs and nanocores, engineered at the nanoscale, promoted the extension of the $t_{1/2}$ (ca. 3-times and 6-times higher, respectively) and MRT (3.8-times and 4.3-times higher, respectively) parameters in relation to free RSV suspension as well, which confirms the prolonged drug residence and greater absorption period in the GI tract. Thereby, RSV released from nanoformulations remained in its unchanged form in rat plasma for nearly 4-times higher compared with free RSV suspension. These results are portrayed in the concentration-time profiles, in which plasma RSV levels for LbL NPs and nanocores are superior to those pertaining

to free RSV suspension. Specifically for the case of nanocores, significant differences were determined precisely at 8 and 12 h post-dosing, pointing to an extended absorption of RSV, assessed up to 12 h, in contrast to the short 4 h-concentration-time profile lasting of free RSV suspension (**Figure 4.5**).

Notwithstanding, according to the previously carried out *in vitro* drug release studies, LbL NPs would promote supposedly for higher bioavailability due to a controlled drug release pattern, responsible for a controlled absorption and distribution drug profiles, compared to a rapid and immediate (non-modified) release pattern promoted by their counterpart nanocores or the less complex nanoformulation (Santos, Pattekari *et al.* 2015). Interestingly, and contrary to expectations, LbL NPs exhibited an $AUC_{0-\infty}$ value 0.36-fold lower than the one found for nanocores (**Table 4.8**). This reveals that, despite the aforementioned marked enhancement of the systemic exposure promoted by the LbL NPs in relation to the administration of the free drug, a slight inferior systemic exposure was encountered when this nanoformulation was compared to its counterpart nanoformulation, the nanocores. Several reasons may have been responsible for these unforeseen results. The presence of a significant number of coating bilayers (5.5) at the surface of the LbL NPs may have been responsible for this evidence, as incomplete drug release was found by our group, in previous *in vitro* release studies using ibuprofen as a BCS class II drug model, for this kind of structures, which was shown to be more pronounced in line with the rise of the thickness of the LbL shell (Santos, Pattekari *et al.* 2015). Moreover, *in vivo* interactions are extremely cumbersome to control due to the collective influence of many parameters which can impact on the *in vivo* fate and behavior of NPs (Singh, Pai 2014b, Polomska, Gauthier *et al.* 2017). In such a context, this evidence we found is in agreement with previous recent findings, which point to the possibility of displacement of the LbL shell from the surface when in contact with biological components, eliminating its protective and controlled release attributes (Polomska, Gauthier *et al.* 2017). This way, we hypothesize that simple nanocores, devoid of coating layers, may have promoted for the complete dissolution and absorption of loaded RSV, avoiding the enzymatic metabolism, and thereby, prolonging systemic circulation. In fact, this kind of structures hold recognized properties of enhanced bioadhesion to the intestinal epithelium (Muller, Jacobs 2002), that may have extended the GI residence time (Penalva, Esparza *et al.* 2015). Those factors accounted probably for an improved absorption and, ultimately, a direct uptake by the intestinal cells, as previously investigated with similar structures loading a low soluble drug, namely nimodipine nanocrystals (Fu, Sun *et al.* 2013). This interpretation is additionally supported by recent results obtained with saquinavir nanocrystals stabilized with polymeric poly(styrene sulfonate) (PSS). The authors verified that

the oral absorption of this low soluble drug once loaded into the nanocrystals was significantly increased by the enhanced Caco-2 cellular uptake and transport. Those phenomena arose from enhanced drug dissolution and cellular uptake of nanocrystals in comparison with the coarse drug, resulting in a higher oral bioavailability in rats (He, Xia *et al.* 2015). It is worth noting by the same token the presence of SLE₂S and PVP 17 PF stabilizers at the surface of the nanocores, which may have additionally impacted in the bioavailability improvement. This effect was recently reported by the use of d- α -tocopherol polyethylene glycol 400 succinate (TPGS), pluronic F127 and lecithin as stabilizers at the surface of RSV-loaded nanocrystals (or nanocores), which were obtained by the use of sonication as well (Singh, Makadia *et al.* 2017). Moreover, the combination of an electrostatic (SLE₂S) and a steric (PVP 17 PF) stabilizer promoted probably even for a higher efficacy in the stabilization of the nanocrystals, which impacted certainly in the effective performance of those structures, as assessed for additional low soluble drug-based nanocrystals (Ma, Yang *et al.* 2017).

Besides the improvement in the bioavailability of RSV, we still assist, as it is characteristic for free RSV administration (Singh, Pai 2014b), to a concentration-time profile with two-peaks for the case of both nanoformulations as well. In fact, certain of the administered nanoformulations may have been under a supersaturable dissolution state in the fasted GI medium. Consequently, some released RSV molecules may have been, that way, in the dissolved molecular state, being transported across the intestinal membrane by passive diffusion and directed into the liver, where, at last, suffered metabolization (Fu, Sun *et al.* 2013). It is worth noting that the solubility of RSV in SIF with enzymes was found to be ca. 58 $\mu\text{g}/\text{mL}$, as previously referred in section 4.3.1. Given that the administered RSV dose to the animals was 20 mg/kg, if one consider a rat with 275 g and the small intestinal corresponding volume of ca. 1 mL (McConnell, Basit *et al.* 2008), the respective theoretically dissolved RSV maximum concentration in the small intestine shall correspond to 5.5 mg/mL. This value greatly exceeds the determined solubility of RSV in this medium, supporting the existence of a supersaturable dissolution state in the small intestine, which is related to the physicochemical characteristics of the drug. In addition, previous permeability *ex vivo* studies assessed with rat intestine evidenced that a self-microemulsifying drug delivery system bearing a RSV concentration of ca. 22 $\mu\text{g}/\text{mL}$ (corresponding to 0.1 mM) was not sufficient to promote an enhancement of the RSV intestinal permeability, in contrast to the use of a nanoformulation with a RSV concentration of 200 $\mu\text{g}/\text{mL}$ (corresponding to 0.9 mM) that has shown significantly higher RSV permeability in relation to the free drug solution (Seljak, Berginc *et al.* 2014). These data are consistent with recent output regarding another self-emulsifying drug delivery system, in which the rat small intestine permeability was found to be

higher for the nanoformulation again at 200 µg/mL (corresponding to 0.9 mM) (Mamadou, Charrueau *et al.* 2017). On the basis of these premises, we can state that the administrated dose of 20 mg/kg during this study did not limit the absorption of RSV associated to the nanoformulations in relation to its dissolution, which is in accordance with the use of this dose by others, as previously reported. Moreover, besides the concentration of RSV in SIF required for its oral absorption *in vivo* remains unknown, the value shall be greater than 22 µg/mL, or even greater than or equal than 200 µg/mL. In either possible case, the necessary concentration of RSV in SIF for its absorption may has been successfully attained *in vivo* by the use of the nanoformulations, emphasizing their significance in the enhancement of the solubility and dissolution of RSV in this aqueous medium, demanded for its absorption following oral administration.

The remaining part of the administered nanoformulations was possibly maintained as physical nanocores or LbL NPs, which may have been absorbed over mesenteric lymphatic transport facilitated by endocytosis, or even eventually by the M-cells, and afterwards drained to the mesenteric lymph duct, avoiding the first-pass metabolism and improving the bioavailability values in relation to the free drug. This assumption is in accordance to evidence encountered in a study that was carried out to investigate the intestinal membrane transporting mechanism of low soluble drug loaded-nanocrystals. The authors concluded that nanocrystals were subjected to macropinocytosis and caveolin-mediated endocytosis by enterocytes in the form of intact nanocrystals, thus surpassing the liver first-pass metabolism (Fu, Sun *et al.* 2013); and, thereby, that the enhancement of the aqueous solubility (Muller, Gohla *et al.* 2011) is far to be the sole leading factor for the bioavailability improvement promoted by those structures. In a technological standpoint, the particular particle size located at nanoscale allowed, indubitably, for the stated improvement of drug PK behavior (Muller, Gohla *et al.* 2011, Zu, Zhang *et al.* 2016).

Additionally, besides the plasma quantification of RSV, the plasma determination of the most commonly found *in vivo* RSV glucuronides and sulfates conjugates by the use of standards – most notably, *trans*-RSV-3,5-disulfate, *trans*-RSV-3-sulfate and *trans*-RSV-3-*O*-glucuronide (Santos, Veiga *et al.* 2011, Amri, Chaumeil *et al.* 2012)) – constitutes a potential approach, which should be envisaged in further studies entailing the oral bioavailability assessment of new drug delivery systems of RSV. Despite of certain difficulties associated with the obtainment and stability of those metabolites, the contribution of the enterohepatic circulation could be far better understood by the use of an effective bioanalytical method to quantify RSV metabolites.

In fact, aside from RSV in its unchanged form, potential therapeutic activity, as well as the possibility of acting as RSV prodrugs, have been likewise recognized for those metabolites (Baur, Sinclair 2006, Smoliga, Blanchard 2014, Penalva, Esparza *et al.* 2015), which thereby most likely contribute for the oral bioavailability and, ultimately, for the biological activity of the administered RSV dose.

However, in the light of the recognized capacities of controlled drug release and protection promoted by the LbL technology (Santos, Pattekari *et al.* 2015), it would be desirable to further improve the oral bioavailability *in vivo* conferred by the LbL NPs in relation to non-modified nanocores. In addition to this need, it would be desirable to avoid the presence of multiple peaks in the concentration-time profiles as well, which is assigned by the absence or mitigation of the first-pass effect and the enterohepatic circulation (Singh, Pai 2014b). Suggestions for the evolution of these systems are based on the development of suitable polymeric LbL coatings for *in vivo* oral administration, capable of: protecting RSV from degradation, precisely by the first-pass and the GI tract metabolisms; targeting the mesenteric lymph; controlling RSV release, as already accomplished by *in vitro* release studies (Santos, Pattekari *et al.* 2015); preventing particle-size enhancement or aggregation phenomena, keeping the nanoscale dimension *in vivo* to avoid the clearance by the M-cells and the macrophage system, and thereby enhancing the MRT.

Despite this, we can still state that our findings introduce relevant information about the oral administration of LbL NPs. We inquire whether technologies based exclusively on electrostatic interactions to maintain coating LbL architectures attached at the surface of drug nanocores are adequate to *in vivo* administration. The demonstrated increase of the bioavailability of RSV provided by these nanoformulations constitutes a strong indicator for the capacity of therapeutic effects of RSV achievement when encapsulated by these structures, which emphasizes their potential role as effective carriers for the oral delivery of RSV. Therefore, the administration of LbL NPs *in vivo* covers undoubtedly an undiscovered and promising area, calling for new research studies.

4.5. Conclusions

The novelty of the present work was the administration of LbL NPs orally to *Wistar* rats. As far as we know, this is the first report concerning pharmacokinetic assessment available for LbL polymeric NPs following the oral administration *in vivo*. The optimization and fully validation of the bioanalytical HPLC-DAD method was imposed for the obtainment of reliable RSV quantifications in rat plasma matrix samples. A simple, selective, sensitive and accurate chromatographic behavior with the minimal sample preparation procedure was thereby successfully achieved. This method has shown to promote a good peak resolution in a viable run time by using a plain isocratic program and a mobile phase composed mainly of the water phase (60%). Preliminary investigations related to GI impact on formulations revealed that RSV is stable under simulated gastric and intestinal conditions with enzymes for a 24 h time period. This assumption, together with additional *in vivo* studies regarding the oral route, suggested the feasibility of RSV quantification under these conditions for such a time period. In addition, the concentration of the nanoformulations was additionally imposed in order to achieve a proper dose to administer orally to the animals. We demonstrated that, among distinct tested methods, dialysis was shown to offer the best conditions concerning the maintenance of the colloidal stability of the considered nanoformulations to perform the *in vivo* study. These sample pretreatments and preliminary studies were shown to be crucial in the executability of the *in vivo* assessments.

The oral administration of RSV-loaded LbL NPs and RSV-loaded nanocores to *Wistar* rats at 20 mg/kg evidenced a remarkable enhancement of the systemic exposure for both nanoformulations. These results emphasize the efficacy of these structures as delivery vehicles for RSV regarding oral administration. However, RSV nanocores promoted a significantly slight higher systemic exposure of RSV in relation to the administration of RSV-loaded LbL NPs. This evidenced lack of differences among the two tested nanoformulations *in vivo* demands for further research. The occurrence of a possible LbL shell detachment from the surface of RSV nanocores may have taken place *in vivo*, due to some weaknesses related to the capacity of solely electrostatic interactions to maintain intact the whole LbL architecture, promoting destabilization. Henceforth, additional approaches – which may include a deep functionalization of the LbL shell and the establishment of covalent bonds as part of the LbL shell – may impact positively on the maintenance of the integrity and operation of these architectures, paving the way for improved LbL nanoformulations towards the oral administration of this valuable polyphenol with potential health-advancing effects.

References

- Almeida, A. M., Castel-Branco, M. M., Falcao, A. C. Linear regression for calibration lines revisited: weighting schemes for bioanalytical methods. *J Chromatogr B Analyt Technol Biomed Life Sci* **774**, 215-222 (2002).
- Amri, A., Chaumeil, J. C., Sfar, S., Charrueau, C. Administration of resveratrol: What formulation solutions to bioavailability limitations? *J Control Release* **158**, 182-193 (2012).
- Baur, J. A., Sinclair, D. A. Therapeutic potential of resveratrol: the *in vivo* evidence. *Nat Rev Drug Discov* **5**, 493-506 (2006).
- Bonkowski, M. S., Sinclair, D. A. Slowing ageing by design: the rise of NAD⁺ and sirtuin-activating compounds. *Nat Rev Mol Cell Biol* **17**, 679-690 (2016).
- Das, S., Lin, H. S., Ho, P. C., Ng, K. Y. The impact of aqueous solubility and dose on the pharmacokinetic profiles of resveratrol. *Pharm Res* **25**, 2593-2600 (2008).
- Davidov-Pardo, G., Perez-Ciordia, S., Marin-Arroyo, M. R., McClements, D. J. Improving resveratrol bioaccessibility using biopolymer nanoparticles and complexes: impact of protein-carbohydrate maillard conjugation. *J Agric Food Chem* **63**, 3915-3923 (2015).
- De Villiers, M. M., Otto, D. P., Strydom, S. J., Lvov, Y. M. Introduction to nanocoatings produced by layer-by-layer (LbL) self-assembly. *Adv Drug Deliv Rev* **63**, 701-715 (2011).
- Ethemoglu, M. S., Seker, F. B., Akkaya, H., Kilic, E., Aslan, I., Erdogan, C. S., *et al.* Anticonvulsant activity of resveratrol-loaded liposomes *in vivo*. *Neuroscience* **357**, 12-19 (2017).
- European Medicines Agency. Guideline on Bioanalytical Methods Validation. in: http://www.ema.europa.eu/docs/en_GB/document_library/Scientific_guideline/2011/08/WC500109686.pdf. Committee for Medicinal Products for Human Use and European Medicine Agency. London, *European Medicines Agency* (2011). Accessed in November 2017.
- Frozza, R. L., Bernardi, A., Paese, K., Hoppe, J. B., da Silva, T., Battastini, A. M., *et al.* Characterization of trans-resveratrol-loaded lipid-core nanocapsules and tissue distribution studies in rats. *J Biomed Nanotechnol* **6**, 694-703 (2010).

- Fu, Q., Sun, J., Ai, X., Zhang, P., Li, M., Wang, Y., *et al.* Nimodipine nanocrystals for oral bioavailability improvement: role of mesenteric lymph transport in the oral absorption. *Int J Pharm* **448**, 290-297 (2013).
- Goncalves, D., Alves, G., Fortuna, A., Soares-da-Silva, P., Falcao, A. Development of a liquid chromatography assay for the determination of opicapone and BIA 9-1079 in rat matrices. *Biomed Chromatogr* **30**, 312-322 (2016).
- He, Y., Xia, D. N., Li, Q. X., Tao, J. S., Gan, Y., Wang, C. Enhancement of cellular uptake, transport and oral absorption of protease inhibitor saquinavir by nanocrystal formulation. *Acta Pharmacol Sin* **36**, 1151-1160 (2015).
- Jose, S., Anju, S. S., Cinu, T. A., Aleykutty, N. A., Thomas, S., Souto, E. B. *In vivo* pharmacokinetics and biodistribution of resveratrol-loaded solid lipid nanoparticles for brain delivery. *Int J Pharm* **474**, 6-13 (2014).
- Li, B., Wegiel, L. A., Taylor, L. S., Edgar, K. J. Stability and solution concentration enhancement of resveratrol by solid dispersion in cellulose derivative matrices. *Cellulose* **20**, 1249-1260 (2013).
- Lvov, Y. M., Pattekari, P., Zhang, X., Torchilin, V. Converting poorly soluble materials into stable aqueous nanocolloids. *Langmuir* **27**, 1212-1217 (2011).
- Ma, J., Yang, Y., Sun, Y., Sun, J. Optimization, characterization and *in vitro/vivo* evaluation of azilsartan nanocrystals. *Asian J Pharm Sci (Amsterdam, Neth.)* **12**, 344-352 (2017).
- Mamadou, G., Charrueau, C., Dairou, J., Limas Nzouzi, N., Eto, B., Ponchel, G. Increased intestinal permeation and modulation of presystemic metabolism of resveratrol formulated into self-emulsifying drug delivery systems. *Int J Pharm* **521**, 150-155 (2017).
- Mathot, F., Van Beijsterveldt, L., Preat, V., Brewster, M., Arien, A. Intestinal uptake and biodistribution of novel polymeric micelles after oral administration. *J Control Release* **111**, 47-55 (2006).
- McConnell, E. L., Basit, A. W., Murdan, S. Measurements of rat and mouse gastrointestinal pH, fluid and lymphoid tissue, and implications for *in-vivo* experiments. *J Pharm Pharmacol* **60**, 63-70 (2008).
- Muller, R. H., Gohla, S., Keck, C. M. State of the art of nanocrystals--special features, production, nanotoxicology aspects and intracellular delivery. *Eur J Pharm Biopharm* **78**, 1-9 (2011).

- Muller, R. H., Jacobs, C. Buparvaquone mucoadhesive nanosuspension: preparation, optimisation and long-term stability. *Int J Pharm* **237**, 151-161 (2002).
- Nowatzke, W., Woolf, E. Best practices during bioanalytical method validation for the characterization of assay reagents and the evaluation of analyte stability in assay standards, quality controls, and study samples. *AAPS J* **9**, E117-122 (2007).
- Parekh, G., Pattekari, P., Joshi, C., Shutava, T., DeCoster, M., Levchenko, T., *et al.* Layer-by-layer nanoencapsulation of camptothecin with improved activity. *Int J Pharm* **465**, 218-227 (2014).
- Penalva, R., Esparza, I., Larraneta, E., Gonzalez-Navarro, C. J., Gamazo, C., Irache, J. M. Zein-based nanoparticles improve the oral bioavailability of resveratrol and its anti-inflammatory effects in a mouse model of endotoxic shock. *J Agric Food Chem* **63**, 5603-5611 (2015).
- Polomska, A., Gauthier, M. A., Leroux, J. C. *In vitro* and *in vivo* evaluation of PEGylated layer-by-layer polyelectrolyte-coated paclitaxel nanocrystals. *Small* **13** (2017).
- Polomska, A., Leroux, J. C., Brambilla, D. Layer-by-layer coating of solid drug cores: A versatile method to improve stability, control release and tune surface properties. *Macromol Biosci* **17** (2017).
- Ramalingam, P., Ko, Y. T. Validated LC-MS/MS method for simultaneous quantification of resveratrol levels in mouse plasma and brain and its application to pharmacokinetic and brain distribution studies. *J Pharm Biomed Anal* **119**, 71-75 (2016).
- Rauf, A., Imran, M., Butt, M. S., Nadeem, M., Peters, D. G., Mubarak, M. S. Resveratrol as an anticancer agent: a review. *Crit Rev Food Sci Nutr*, 1-20 (2016).
- Robinson, K., Mock, C., Liang, D. Pre-formulation studies of resveratrol. *Drug Dev Ind Pharm* **41**, 1464-1469 (2015).
- Santos, A. C., Pattekari, P., Jesus, S., Veiga, F., Lvov, Y., Ribeiro, A. J. Sonication-assisted layer-by-layer assembly for low solubility drug nanoformulation. *ACS Appl Mater Interfaces* **7**, 11972-11983 (2015).
- Santos, A. C., Veiga, F., Ribeiro, A. J. New delivery systems to improve the bioavailability of resveratrol. *Expert Opin Drug Deliv* **8**, 973-990 (2011).

- Seljak, K. B., Berginc, K., Trontelj, J., Zvonar, A., Kristl, A., Gasperlin, M. A self-microemulsifying drug delivery system to overcome intestinal resveratrol toxicity and presystemic metabolism. *J Pharm Sci* **103**, 3491-3500 (2014).
- Shah, V. P., Midha, K. K., Findlay, J. W., Hill, H. M., Hulse, J. D., McGilveray, I. J., *et al.* Bioanalytical method validation--a revisit with a decade of progress. *Pharm Res* **17**, 1551-1557 (2000).
- Shutava, T. G., Lvov, Y. M. Chapter 9: Encapsulation of natural polyphenols with antioxidant properties in polyelectrolyte capsules and nanoparticles. *Natural compounds as inducers of cell death: volume 1*. Diederich, M., Noworyta, K., Dordrecht, Springer: 215-235 (2012).
- Shutava, T. G., Pattekari, P. P., Arapov, K. A., Torchilin, V. P., Lvov, Y. M. Architectural layer-by-layer assembly of drug nanocapsules with PEGylated polyelectrolytes. *Soft Matter* **8**, 9418-9427 (2012).
- Singh, A., Ahmad, I., Ahmad, S., Iqbal, Z., Ahmad, F. J. A novel monolithic controlled delivery system of resveratrol for enhanced hepatoprotection: nanoformulation development, pharmacokinetics and pharmacodynamics. *Drug Dev Ind Pharm* **42**, 1524-1536 (2016).
- Singh, G., Pai, R. S. *In-vitro/in-vivo* characterization of trans-resveratrol-loaded nanoparticulate drug delivery system for oral administration. *J Pharm Pharmacol* **66**, 1062-1076 (2014a).
- Singh, G., Pai, R. S. Optimized PLGA nanoparticle platform for orally dosed trans-resveratrol with enhanced bioavailability potential. *Expert Opin Drug Deliv* **11**, 647-659 (2014b).
- Singh, G., Pai, R. S. *In vitro* and *in vivo* performance of supersaturable self-nanoemulsifying system of trans-resveratrol. *Artif Cells Nanomed Biotechnol* **44**, 510-516 (2014c).
- Singh, G., Pai, R. S. Trans-resveratrol self-nano-emulsifying drug delivery system (SNEDDS) with enhanced bioavailability potential: optimization, pharmacokinetics and *in situ* single pass intestinal perfusion (SPIP) studies. *Drug Deliv* **22**, 522-530 (2015).
- Singh, S. K., Makadia, V., Sharma, S., Rashid, M., Shahi, S., Mishra, P. R., *et al.* Preparation and *in-vitro/in-vivo* characterization of trans-resveratrol nanocrystals for oral administration. *Drug Deliv Transl Res* (2017).
- Smoliga, J. M., Blanchard, O. Enhancing the delivery of resveratrol in humans: if low bioavailability is the problem, what is the solution? *Molecules* **19**, 17154-17172 (2014).

- Sung, M. M., Byrne, N. J., Robertson, I. M., Kim, T. T., Samokhvalov, V., Levasseur, J., *et al.* Resveratrol improves exercise performance and skeletal muscle oxidative capacity in heart failure. *Am J Physiol Heart Circ Physiol* **312**, H842-H853 (2017).
- Trela, B. C., Waterhouse, A. L. Resveratrol: Isomeric molar absorptivities and stability. *J Agric Food Chem* **44**, 1253–1257 (1996).
- US Food and Drug Administration. Guidance for Industry: Bioanalytical method validation. in: <http://www.fda.gov/downloads/Drugs/GuidanceComplianceRegulatoryInformation/Guidances/ucm070107.pdf>. US Department of Health and Human Services, Food and Drug Administration, Center for Drug Evaluation and Research and Center for Veterinary Medicine (2001). Accessed in November 2017.
- US Food and Drug Administration. Guidance for Industry: Bioanalytical method validation. in: <https://www.fda.gov/downloads/drugs/guidances/ucm368107.pdf>. US Department of Health and Human Services, Food and Drug Administration, Center for Drug Evaluation and Research and Center for Veterinary Medicine (2013). Accessed in November 2017.
- Vauthier, C., Cabane, B., Labarre, D. How to concentrate nanoparticles and avoid aggregation? *Eur J Pharm Biopharm* **69**, 466-475 (2008).
- Wenzel, E., Soldo, T., Erbersdobler, H., Somoza, V. Bioactivity and metabolism of trans-resveratrol orally administered to Wistar rats. *Mol Nutr Food Res* **49**, 482-494 (2005).
- Zhou, J., Zhou, M., Yang, F. F., Liu, C. Y., Pan, R. L., Chang, Q., *et al.* Involvement of the inhibition of intestinal glucuronidation in enhancing the oral bioavailability of resveratrol by labrasol containing nanoemulsions. *Mol Pharm* **12**, 1084-1095 (2015).
- Zu, Y., Zhang, Y., Wang, W., Zhao, X., Han, X., Wang, K., *et al.* Preparation and *in vitro/in vivo* evaluation of resveratrol-loaded carboxymethyl chitosan nanoparticles. *Drug Deliv* **23**, 981-991 (2016).
- Zupancic, S., Lavric, Z., Kristl, J. Stability and solubility of trans-resveratrol are strongly influenced by pH and temperature. *Eur J Pharm Biopharm* **93**, 196-204 (2015).

Chapter 5

Concluding remarks and future perspectives

5.1. Concluding remarks

In this dissertation, we investigated a proposed technological solution to overcome the bottleneck associated with the administration of resveratrol (RSV) by the oral route, which constitutes, on the one hand, the preferred route of administration, but, in the other hand, unfortunately entails a matter of serious concern due to the poor pharmacokinetic profile of RSV. We hypothesized, thus, the use of RSV-loaded Layer-by-Layer nanoparticles (LbL NPs), platforms with growing interest in the domain of drug delivery, as a new technological strategy for surpassing the limitations of the available classical pharmaceutical dosage forms, towards the fabrication of an effective formulation.

Towards this aim, in the first part of this dissertation research work (**Chapter 2**), a sonication-assisted top-down approach, together with a washless LbL technique, was fully developed to tackle the issue of the nanoencapsulation of the poor water soluble model BCS II drug ibuprofen (IBF). For each saturated layer deposition, the polyelectrolyte (PE) sufficient concentration was assessed by tracing titration curves. Given the found IBF negative surface charge, the first layer of the nanoshell was constituted by the cationic PE polyallylamine hydrochloride (PAH), followed by the anionic PE polystyrene sulfonate (PSS). This PE pair sequence was performed up to the achievement of 2.5 (IBF-(PAH/PSS)_{2.5} NPs), 5.5 (IBF-(PAH/PSS)_{5.5} NPs) and 7.5 (IBF-(PAH/PSS)_{7.5} NPs) bilayer-composed nanoformulations. IBF LbL NPs coated with 7.5 bilayers of PAH/PSS evidenced 128 ± 38 nm of particle size, 0.24 of PDI, a high zeta potential value of $+32.7 \pm 0.6$ mV, with an IBF entrapment efficiency of $72 \pm 6\%$. Those nanoformulations were shown to be stable aqueous nanocolloids and biocompatible using Caco-2 cells. In addition, a controlled IBF release was accomplished from LbL NPs under simulated intestinal conditions (namely, from 5 h up to 7 days), according to the number of coating layers of the LbL nanoshell. From these results, we concluded that PAH/PSS-composed LbL NPs constituted a potential delivery system to improve the biopharmaceutical parameters of BCS II drugs, as the case of RSV.

This way, in a second stage (**Chapter 3**), we moved towards the nanoencapsulation of the desired RSV. Using the knowledge and principles acquired before by using the model drug IBF, we developed and characterized, for the first time, RSV-loaded PAH/DS-composed LbL NPs. Those NPs presented PE nanoshells comprised with 2.5, 5.5 and 7.5 bilayers, being obtained, this time, by using RSV nanoprecipitation (a bottom-up approach) followed by LbL self-assembly of PEs, led by a washless approach. The PEs used were the cationic PAH and the anionic dextran sulfate (DS). Each saturated PE layer deposition involved, once more, the rigorous PE concentration assessment by the use of titration curves, following a PE washless approach.

Aqueous RSV nanocores and RSV LbL nanoformulations with distinct number of PAH/DS bilayers were developed, including 2.5 (RSV-(PAH/DS)_{2.5} NPs), 5.5 (RSV-(PAH/DS)_{5.5} NPs) and 7.5 (RSV-(PAH/DS)_{7.5} NPs) bilayered nanoformulations. Homogenous particle size distributions at the sought-after nanoscale interval (ca. 116-220 nm; polydispersity index below 0.15), with good colloidal (zeta potential magnitudes ca. \pm 20-30 mV) and chemical stabilities, high encapsulation efficiencies (> 90%) together with an excellent cytocompatibility with Caco-2 cells (cell viability above 90%) were verified for all the studied nanoformulations. Importantly, LbL NPs promoted a controlled release of RSV pursuant to the number of PE bilayers under simulated gastrointestinal conditions, particularly in the simulated intestine medium, strongly emphasizing their biopharmaceutical advantage. Those findings manifestly pinpointed that LbL PAH/DS-based NPs constituted a promising nanodelivery system for the oral *in vivo* delivery of RSV.

In both of the previous works concerning the development of LbL NPs, we were able to conclude that, the great potential of the LbL self-assembly of producing various material systems enabled the successful nanoencapsulation of both BCS II drugs, IBF and RSV. This nanotechnology was shown to be a simple process, regarding the ease of application of the coatings, the minute used amounts of polymers, no special equipment requirement and no use of harsh chemicals or temperatures. Thereby, the solid drug nanocores are possible to be coated by a large variety of polymeric coatings, ranging from biopolymeric to synthetic polymeric materials, conferring several advantageous effects, together with a high level of versatility and applicability. Such platforms were achieved by the use of strongly charged PEs rigorously which were ordered into the distinct obtained multilayered LbL nanoshells. In addition, the choice of developing and using a washless PE approach, enabled the use of solely the sufficient amounts of PEs for each coating layer. Using this coating technology approach, we, thus, surpassed the conventional LbL-coating approach, avoiding cumbersome handling procedures as centrifugations, filtrations and intermediate PE washings, as well as time-consuming and costly intermediate PE washings steps. Furthermore, in addition to these gains, the maximum colloidal stability was assured for each PE coating layers, which were assessed to be entirely saturated in the determined onset points. As a result, a superior flexibility during the assembly process was enabled with regard to the possible number of bilayers to be assembled, together with a yield process maximization. We executed, thereby, a significantly much easier washless procedure, which did not required sophisticated equipment and reduced the energy expense, thus assigning promising scaling-up perspectives to the LbL nanotechnology.

Other collected merit of this work consisted in the application of the LbL self-assembly at nanoscale. As a matter of fact, we successfully evolved from a conventional LbL approach at microscale, which is already very well described in the literature for the case of well soluble drugs, to a nanoarchitectural LbL design of low soluble drug nanocolloids in a very good dispersed state. This goal was achieved by stabilization of the NPs with strongly charged and rigorously designed PE shells. Those tunable LbL shells allowed for structural control over particle size and surface charge, which led to the obtainment of well dispersed nanosuspensions with narrow particle size distributions, high encapsulation efficiency values and absence of *in vitro* toxicity. We were able to assist as well that NPs afforded both colloidal and chemical protection to the nanoencapsulated RSV, pinpointing an improvement of its beneficial effects by the instability minimization. In addition to these merits, the RSV release rate from RSV-loaded LbL NPs was found to be interestingly controlled by varying the number of PEs bilayers of the nanoshell. The versatility of those structures assumed particular interest, since the varying the composition of the shell we assisted to different *in vitro* drug release behaviors. In fact, a higher gastroretention was found while applying DS as polyanion in comparison to the use of solely synthetic PEs, as PSS, which predicted for a superior availability of RSV for absorption in the intestine using the PE pair combination PAH/DS rather than PAH/PSS. Facing these data, RSV-loaded PAH/DS LbL NPs were proposed to formulate a viable oral delivery system for RSV, and thus to be tested *in vivo*.

In the last stage of the research work of the present dissertation, the pharmacokinetic assessment of LbL polymeric NPs following the *in vivo* oral administration in Wistar rats was carried out, which, as far as we know, constitute the first report in the literature (**Chapter 4**). To tackle this challenge, the optimization and fully validation of the bioanalytical HPLC-DAD method was firstly required for the performance of reliable RSV quantifications in rat plasma samples. A simple, selective, sensitive and accurate chromatographic behavior together with the minimal sample preparation procedure was successfully attained. The developed chromatographic method enabled good peak resolutions in a viable run time, which were achieved by the use of a plain isocratic program and a mobile phase constituted predominantly of the water phase. In addition, investigations related to the gastrointestinal conditions impact on the nanoformulations evidenced that RSV was found to be stable under simulated gastric and intestinal conditions with enzymes (pepsin and pancreatin) for a 24 h time period. These results suggested the feasibility of RSV quantification under these conditions during such a time period. Furthermore, a concentration of the nanoformulations was demanded to obtain a proper dose for oral administration purposes to the animals. We concluded that, among the different tested

strategies to address this question, dialysis provided the best conditions, as confirmed by the colloidal stability maintenance of the nanoformulations. The aforementioned preliminary investigations and sample pretreatments were shown to be critical in the executability of the *in vivo* studies.

Those data were motivating to proceed from *in vitro* studies to a real *in vivo* configuration. This way, and last of all, the investigation of the bioavailability of the LbL nanoformulation composed of 5.5 bilayers of PAH and DS (RSV-(PAH/DS)_{5.5} NPs) by pharmacokinetic studies following oral dosing (20 mg/kg) was carried out in Wistar rats. In these studies the systemic exposure of this LbL nanoformulation was compared to the respective nanoformulation without LbL coatings (RSV nanocores) and the free RSV suspension. Results demonstrated that both LbL NPs and RSV nanocores remarkably enhanced, respectively, 1.76-fold and 2.74-fold the systemic exposure of RSV compared to free RSV suspension, highlighting their biopharmaceutical advantage. These results thus underlined the efficacy of these NPs as delivery vehicles for the oral administration of RSV, meeting the main objectives of this research work. However, and surprisingly, besides the modified drug release potential of the LbL NPs, those demonstrated a slight lower systemic exposure (0.36-fold) in comparison to non-LbL modified RSV nanocores. A possible LbL shell detachment from the surface of RSV nanocores may have occurred, facing the existence of solely electrostatic interactions to maintain intact the whole LbL architecture, which may have induced some degree of destabilization under *in vivo* environmental configurations.

Putting all the findings of this dissertation together, we are able to conclude that relevant technological and biopharmaceutical features were successfully achieved for improved RSV oral delivery by the development of novel RSV-loaded LbL NPs. The oral administration of LbL NPs to Wistar rats was performed for the first time, by using original nanoformulations as well, thus introducing new valuable scientific information in the field of LbL self-assembly specifically concerning the *in vivo* bioavailability behavior encountered under the biological environment of the oral route. This way, the performed research work successfully met the main initially proposed objectives, allowing us to state that the LbL NPs assume great relevance in the domain of pharmaceutical sciences, representing a potential drug delivery vehicle in the vanguard of the promising use of RSV.

5.2. Future perspectives

The attractive results carried out during the course of this dissertation undoubtedly provide novel insights into the potential intervention of the LbL nanotechnology for the encapsulation and delivery of the challenging RSV, which may positively impact on its clinical translation. The presented thesis research work lays the foundation and supplies a proof of concept that should be seized further on. In fact, promising findings and answers were successfully obtained, however some questions, which are presented next, should be addressed for further improvement of the developed LbL nanoformulations.

In fact, nowadays, for a variety of reasons, a commercial formulation of RSV developed for clinical proposal is still not available. First of all, the levels of RSV obtained in blood following its oral administration do not justify its therapeutic activities, raising doubts about a straight relationship between the activity and the RSV content claimed by formulations. Another justification, related to the previous, consists in the wide range of formulations which are being tested in various animal models, which make the comparison of results and, in consequence, the translational research very hard. Hence, a systematic organization of RSV formulations according to their mode of preparation, with clear discrimination of their RSV content, as well an improvement in the quality assurance and standardization of such formulations would make the task of comparing results easier, allowing to draw reliable conclusions. In addition, despite promising results in preclinical settings, the applicability of RSV to humans has met with only limited success, largely due to the inefficient systemic delivery of RSV and consequently to the low bioavailability. In fact, studies revealed that high doses of RSV may be insufficient to achieve therapeutic concentrations required to exert beneficial effects in humans. Therefore, to achieve an optimal response of RSV, new strategies are sought out both to enhance its bioavailability and to reduce its perceived toxicity. Nanotechnology represents nowadays one of the greatest growing areas of science and technology employed to surpass these goals, evidencing a burgeoning number of publications which propose NPs as auspicious candidates for successful RSV administration and delivery in the near future. In this context, sonication-assisted LbL polymer self-assembly, the selected nanotechnology to overpass RSV oral administration boundaries in this work, was shown to be successfully capable of encapsulating RSV at nanoscale, as expected. However, some questions, which are exposed below, remain to be solved.

Additional techniques able to reinforce the characterization of the LbL platforms should be endorsed, including: the quartz crystal microbalance, which provides evidence concerning the

stepwise-fashion growth of the LbL deposited film; and additional imaging techniques, as Cryo-scanning electron microscopy and Cryo-transmission electron microscopy to confirm visually the adsorption of the distinct layers of the LbL nanoshell.

New strategies or PEs should be applied to overcome harsh gastric environment and potentiate controlled drug release in the intestine to avoid RSV release in acidic medium. This will allow a maximization of the obtainment of desirable therapeutic effects after oral administration of the LbL nanoencapsulated drug with all the encapsulated drug released in the intestine. Strategies proposed to achieve this result consist in the use of a suitable gastro-resistant approach, like gelatinous gastro-resistant capsules or the use of an enteric coating polymer, preferably with a molecular weight lower than 65 kDa to prevent simultaneously and importantly the colloidal aggregation and thus the integrity of the nanoformulations.

Besides the present work has strengthened the knowledge of the behavior of LbL NPs after oral administration, additional pharmacokinetic studies, using other dosing schedules and study periods, as well as biodistribution studies are demanded to examine the real utility and functionality of these applications. Owing to a lack of relationship between the effective amount of RSV and/or its metabolites needed to perform a desired effect, appropriate techniques of extraction and quantification in samples collected during pharmacokinetic studies compared to the concentration of RSV initially administered are required. Some fundamental aspects of RSV's action need to be understood, since the evaluation of formulations and bioavailability, based on RSV levels, is not established if it constitutes a valid strategy. In fact, aside from RSV in its unchanged form, potential therapeutic activity, as well as the possibility of acting as RSV prodrugs, have been likewise recognized for those metabolites, which thereby most likely contribute for the oral bioavailability and, ultimately, for the biological activity of the administered RSV dose. So, besides the plasma quantification of RSV, the plasma determination of the most commonly found *in vivo* RSV glucuronides and sulfates conjugates by the use of standards – most notably, *trans*-RSV-3,5-disulfate, *trans*-RSV-3-sulfate and *trans*-RSV-3-O-glucuronide – constitutes probably a potential approach, which should be envisaged in further studies entailing the oral bioavailability assessment of new drug delivery systems of RSV. Despite of certain difficulties associated with the obtainment and stability of those metabolites, the contribution of the enterohepatic circulation could be far better understood by the use of an effective bioanalytical method to quantify RSV metabolites.

Moreover, *in vivo* interactions are extremely cumbersome to control due to the collective influence of many parameters which can impact on the *in vivo* fate and behavior of NPs and the

drug. Of particular interest is the study of RSV interactions with serum proteins, as they may compromise the RSV bioavailability, being their lack of quantification still a weakness of pharmacokinetics research. Moreover, established interactions and the stability of the polyelectrolyte LbL shells with and within biological media are of utmost importance, as they fully determine the biological fate and thus the inherent therapeutic outcomes. As a matter of fact, in the present pharmacokinetic study performed in this dissertation, RSV nanocores (devoid of LbL coatings) promoted a significantly slight higher systemic exposure of RSV regarding the administration of RSV-loaded LbL NPs. This way, in the light of the recognized capacities of controlled drug release and protection promoted by the LbL technology, it would be desirable to further improve the oral bioavailability *in vivo* conferred by the LbL NPs in relation to non-modified nanocores. Those results were assigned to the displacement of the LbL shell from the surface when in contact with biological components, which probably occurred as a consequence of the sole presence of electrostatic interactions to maintain the LbL architectures attached at the surface of drug nanocores. Henceforth, additional approaches should comprise the establishment of stronger interactions, by a deep functionalization of the LbL shell and the establishment of covalent bonds as part of the LbL shell. This may impact positively on the maintenance of the integrity and operation of these architectures, paving the way for improved LbL nanoformulations of RSV.

Future work should consider more frequently, and ideally on an exclusive basis, the use of biopolymers in the LbL systems due to their favorable biocompatibility and biodegradability, with special emphasis on pharma grade biopolymers, which arise from the novel advances on polymer science, evidencing more controlled and reproducible properties. The application of these kind of coatings may dictate the interactions of the NPs with tissues and cells of relevance, conferring superior *in vivo* performance. For example, PE with enhanced properties of enhanced bioadhesion to the intestinal epithelium may contribute to an extended GI residence time and an improved absorption and bioavailability.

Lastly, further investigation will need to be undertaken concerning the cellular uptake mechanisms and the intracellular fates of LbL NPs, as well as the potential toxicity and elimination routes of the LbL shells. The existence of these unknown factors implies an end-to-end analysis of the LbL shell role, regarding its physicochemical properties and architecture, on its biological performance to enable its future translation to the clinical with significant benefits concerning the delivery of RSV.